EFFECT OF FRAME SHAPE AND GEOMETRY ON THE GLOBAL BEHAVIOR OF RIGID AND HYBRID FRAME UNDER EARTHQUAKE EXCITATIONS

by

S. M. ASHFAQUL HOQ

Presented to the Faculty of the Graduate School of

The University of Texas at Arlington in Partial Fulfillment

of the Requirements

for the Degree of

MASTER OF SCIENCE IN CIVIL ENGINEERING

THE UNIVERSITY OF TEXAS AT ARLINGTON

May 2010

ACKNOWLEDGEMENTS

I would like to express my sincere gratitude to my thesis advisor, Dr. Ali Abolmaali, for his continuous help and guidance in the accomplishment of this work. I really appreciate Dr. Ali Abolmaali for his unrestricted personal guidance throughout this study, for bringing out the best of my ability. His kind supervision, encouragement, assistance and invaluable suggestion at all stages of the work made it possible to complete this work. The services he offered personally were a great help.

I would like to express my sincere thanks to Dr. John H. Matthys and Dr. Guillermo Ramirez, for their time to serve on my thesis committee and providing invaluable suggestions and advice.

I would like to thank Dr. Tri Le, Dobrinka Radulova, Mohammad Razavi and all my colleagues and friends for their moral support and helpful discussions.

Finally, I would like to express my heartfelt thanks to my parents and siblings for their unconditional love, support, encouragement and blessings to complete my masters program.

April 15, 2010

ABSTRACT

EFFECT OF FRAME SHAPE AND GEOMETRY ON THE GLOBAL BEHAVIOR OF RIGID AND HYBRID FRAME UNDER EARTHQUAKE EXCITATIONS

S.M.Ashfaqul Hoq, M.S.

The University of Texas at Arlington, 2010

Supervising Professor: Dr. Ali Abolmaali

The primary focus of this study is to present a shape which will improve building performance in earthquake excitations. The investigation started with a 3-, 9-, 12- and 20-story rectangular frame. The seismic performance is observed for different earthquake data with different frequency content. Then, the Rhombus Shape is introduced to compare with the Rectangular Shape frames, keeping the height-to-width ratio and loading the same. For the first part of the investigation, deflection and member forces are compared between rhombus and rectangular shape considering all connections rigid. In the second part of the study partially restrained connections are introduced in mid levels of the high rise frames to observe the redistribution pattern of internal forces. The results show that with all rigid connections, a rhombus shape performs better than a rectangular frame in most of the cases. Also, partially restrained connections which forms hybrid frame have more significant effects on the rectangular frame than the rhombus frame.

TABLE OF CONTENTS

APPENDIX

LIST OF ILLUSTRATIONS

LIST OF TABLES

Table Page

CHAPTER 1

INTRODUCTION

1.1 Introduction

Among different loads, earthquake is the most uncertain in nature. It develops under earth due to movement of the plate tectonics and that is the reason it cannot be predicted when and with how much energy it will be generated. Like other loads, it cannot be calculated precisely or forecasted with reasonable accuracy. Other than the earthquake, the structural response which is dynamic in nature is also quite unpredictable due to the variable associated such as soil properties, material and geometry of the structure, construction quality, location of the structure, magnitude and frequency of ground motion, epicenter, focal depth, etc. Due to the unpredictable nature of the load it has always been a challenging task for structural researchers and professionals to prepare any guideline for earthquake engineering.

Structural steel framing system evolved in an attempt to resist lateral forces. After 1906, it was highlighted that the buildings with steel frame performs better in earthquakes than the masonry structures (FEMA-355e). Prior to the San Francisco earthquake at this year there was no provision for earthquake in the building codes. After Santa Barbara earthquake in 1925, Uniform Building Code (UBC) was the first to include seismic provisions in 1927. In 1959 Structural Engineers Association of California (SEAOC) issued “lateral force recommendation” which was later adopted by the UBC in 1961. The key feature was the requirement of steel moment resisting frame for tall buildings over 160ft. American Institute of Steel Construction (AISC) includes seismic provisions in their 1992 specifications. With each major earthquake the building code is modified (FEMA-355e). At this point, it was believed that the steel moment resisting frames are adequate to dissipate earthquake energy with the presumed ductile behavior of its moment resisting connections. But, the Northridge earthquake in 1994 challenged this assumption when many beam-column connections failed in a brittle manner. This type of brittle failure causes little observable damage which raises the concern about undiscovered damage in past earthquakes. After Northridge, investigation has confirmed such type of damage in some buildings subjected to Loma Prieta (1989), Landers (1992), and Big Bear (1992) earthquake (FEMA-355f).

The significant amount of monetary losses in the Northridge and Loma Prieta earthquakes triggered the popularity of the performance based seismic design. Vision 2000 report by the SEAOC (1995) highlighted the fact of economic losses even in the moderate earthquakes. It was identified the need of a design and construction procedure which could control the damage to acceptable limits. These limits were same as those described in the FEMA-273 developed by the Applied Technology Council (ATC). The four performance levels labeled as Operational, Immediate Occupancy, Life Safety and Collapse Prevention were the state of the defined and observable damage in the structure.

Federal Emergency Management Agency published the FEMA-355f prepared by the SAC joint venture in September 2000, where it narrated performance prediction and evaluation technique for moment resisting frames along with the seismic hazard levels and analysis procedures. An important feature of this procedure was to state capacity and demand in terms of story drift. It should be mentioned that prior to the 1976 specifications there was no limits for lateral drift in seismic design.

FEMA-356 tabulated some typical drift values to describe the overall structural response. A steel moment frame with 5% transient or permanent drift will fall in the collapse prevention level. For life safety it was 2.5% transient and 1% permanent drift; for immediate occupancy it was 0.7% transient with negligible permanent drift. For braced steel frame these drift values were 2% transient or permanent, 1.5% transient and 0.5% permanent; 0.5% transient with negligible permanent for collapse prevention, life safety and immediate occupancy level respectively. But, these values were not drift limits requirements. Vision 2000 by the SEAOC imposed some drift limitations for steel moment frames as 2.5% transient or permanent drift for collapse prevention, 1.5% permanent and 0.5% transient for life safety level and 0.5% transient with no permanent drift for operational level. Also, the connection requirements according to the Seismic Provisions of AISC 2005 requires that beam to column connections be able to carry minimum 0.04 radians of inter story drift angle.

To keep the inter story drifts within the specified limits a rhombus shape was proposed as a seismic load resisting system in the first phase of this study instead of the popular rectilinear assemblage of beams and columns. The proposed shape is created from the rectangular moment frame by placing a rhombus with the same height and width as the rectangle frame. Then the pure rhombus shape is generated by removing all the members outside of it. A proposed 20-story rhombus frame with the corresponding rectangular frame is shown in Figure 1.1.

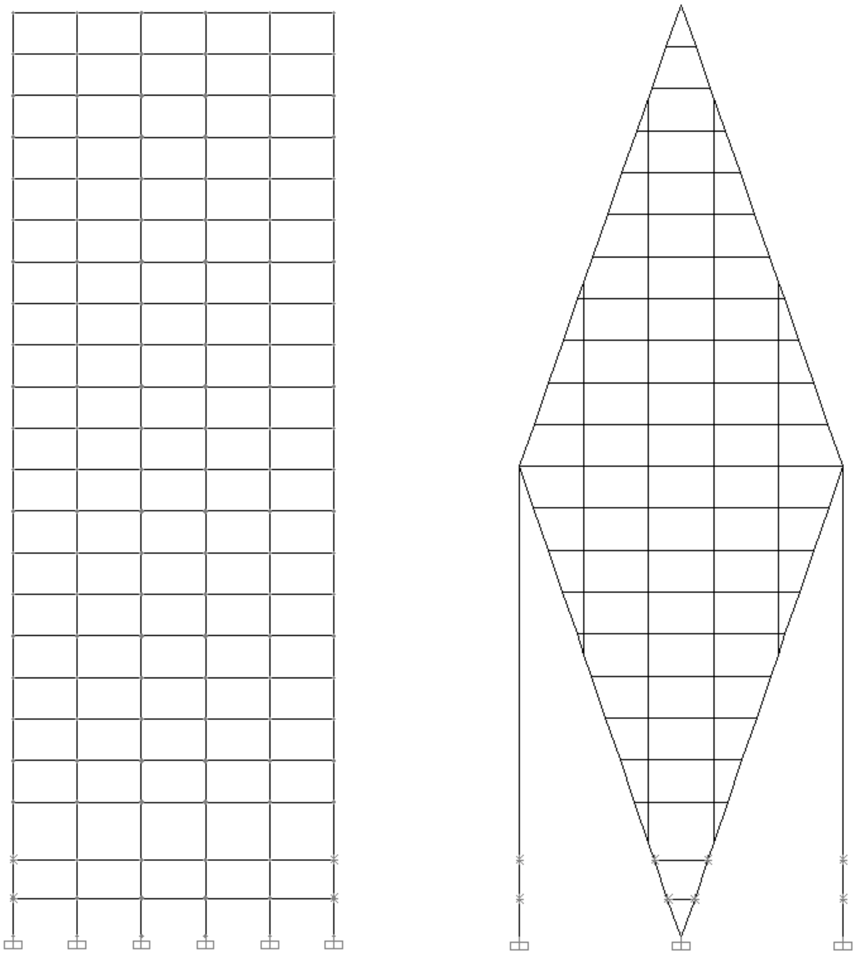

Figure 1.1 20-Story Rectangular frame and equivalent Rhombus shape

The idea behind this shape is to utilize the advantage of both the rectangular moment frames and concentrically braced frames. The first type of framing system uses the flexural stiffness of the members to gain lateral stiffness; while in the later type, internal axial stiffness of the diagonals are the main sources for lateral stiffness. Different framing systems are discussed briefly in the background section of this chapter.

To study the performance of the proposed rhombus shape, a wide range of steel frames are selected with different height-to-width ratios. These frames represent low-rise to high-rise buildings. Rhombus shape is compared with rectangular shape under different earthquake excitations. As low-rise buildings are usually vulnerable to high frequency earthquake and high-rise buildings are vulnerable to low frequency earthquake, four different earthquakes are selected with wide range of frequency content. These are Elcentro (1940), Northridge (1994), Parkfield (1966) and two data for Kocaeli (1999) earthquake.

In the second phase of this study the concept of eccentrically braced frame (EBF) is presented. The energy dissipation characteristic of the “link” of an EBF system is tried to be incorporated in the frame system in the form of semi-rigid connections. In this part of the study hybrid frames with rigid and semi-rigid connections are analyzed. The effect of semi-rigid connections on global behavior of the hybrid rectangular and rhombus frames are compared with the rigid frames. The eccentrically braced frame system and the semi-rigid connections are briefly discussed in the background section.

1.2 Background

1.2.1 Moment Frames (MFs)

Moment resisting frames are the rectangular assemblage of beams and columns. The beams are rigidly connected to the columns. Primarily the rigid frame action provides resistance to lateral forces which develops bending moments and shear forces in the frame members and joints. A moment frame cannot displace laterally without bending the beams and columns due to its rigid beam-column connections. The bending rigidity and strength of the frame members provide the lateral stiffness and strength for the entire structure. For several reasons steel moment resisting frames have been popular in high seismic regions. It is viewed as a highly ductile system among all the structural systems. Also, large force reduction factors are assigned to design earthquake forces in building codes. No bracing members are present to block the wall openings which provide architectural versatility for space utilization. But, compared to other braced systems moment frames generally required larger member sizes than those required only for strength alone to keep the lateral deflection within code approved drift limits. Again, the inherent flexibility of the system may introduce drift-induced nonstructural damage under earthquake excitation than with other stiffer braced systems. Even these perceptions regarding the expected performance of steel moment frames in energy dissipation under lateral loads was sacrificed after the 1994 Northridge earthquake when the steel moment frames did not perform as expected. Brittle failures occurred at beam-column connections which challenge the assumption of high ductility of the system (Michel Bruneau et al. 1998).

Moment frames are composed of beam, column, and panel zone. Panel zone is the portion of the column contained within the joint region at the intersection of beam and column. In traditional analysis moment frames are often modeled with dimensionless nodes which are the intersection of beam and column members. Such models do not consider panel zone. But ductile moment frames require explicit consideration of panel zone. Depending on the yield strength and the yield thresholds, the beam, column and even panel zone could contribute to the total plastic deformation at the joint. A structural component considerably weaker than the other framing into the joint will have to provide the needed plastic energy dissipation. Those structural components expected to dissipate hysteretic energy during an earthquake must be detailed to allow the development of large plastic rotations. Plastic rotation demand is typically obtained by inelastic response history analysis. Without considering panel zone plastic deformations it was expected that the largest plastic rotations in the beams are 0.02 radian (Tsai 1988, Popov and Tsai 1989). After the Northridge earthquake the required connection plastic rotation capacity was increased to 0.03 radian for new construction and for post earthquake modification of existing building it was 0.025 radian (SAC1995b).

1.2.2 Concentrically Braced Frames (CBFs)

The concentrically braced frame is a lateral force resisting system. It is an efficient frame system marked by its high elastic stiffness which is commonly used to resist wind or earthquake loadings. The system achieves high stiffness by its diagonal bracing members which resist lateral forces by using higher internal axial actions and relatively lower flexural actions. Diagonal bracings form the main units which provide lateral stiffness in a CBF system. Braces can be in the form of I-shaped sections, circular or rectangular tubes, double angle attached together to form a T-shaped section, solid T-shaped sections, single angles, channels and tension only rods and angles. Bracing members are commonly connected with other members of the framing system by welded or bolted gusset plates. The CBF design method generally focuses on dissipating energy in the braces such that the connection is designed to remain elastic at all times. To maximize the energy dissipation, the brace connections should be designed to be stronger than the bracing members they connect so that the bracing member can yield and buckle (Michel Bruneau et al. 1998). Some common CBF systems are shown in Figure 1.2.

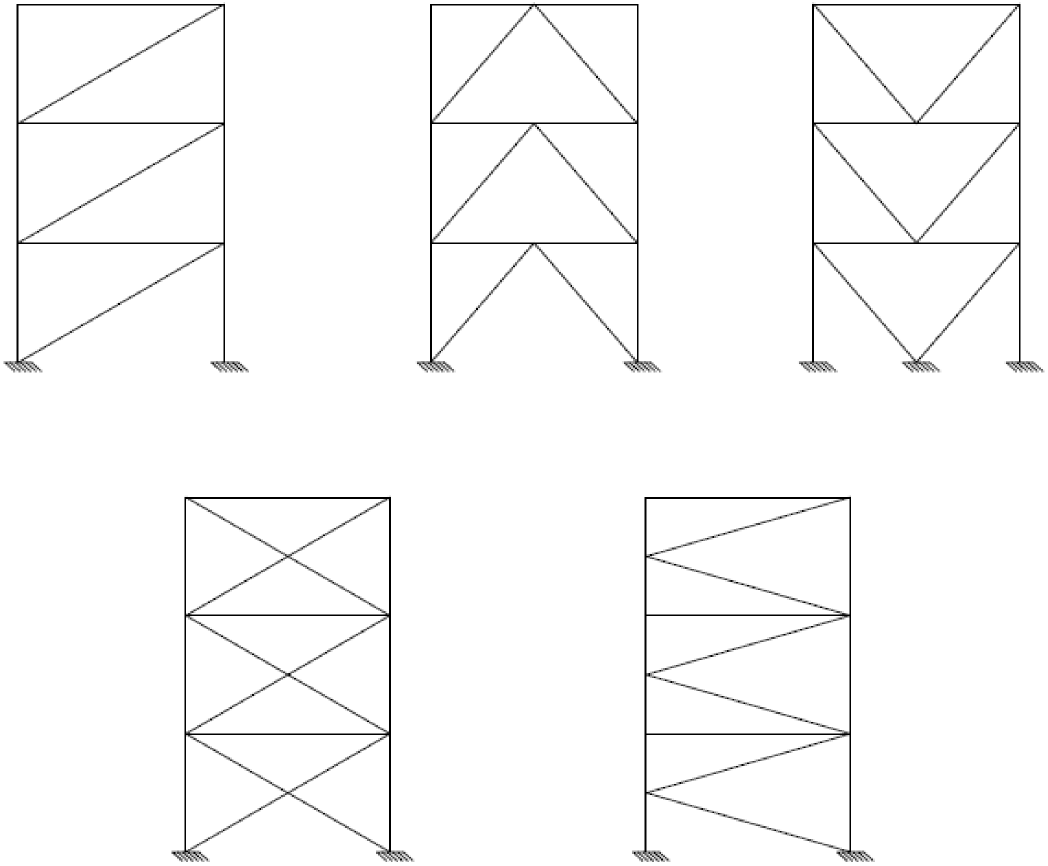

Figure 1.2 Typical CBF configurations

CBF systems are considered to be less ductile seismic resistant structure as compared to other systems due to failure of the bracing members under large cyclic displacements. These structures can experience large story drift after buckling of bracing members, which in turn may lead to fracture of bracing members. Recent analytical studies have shown that CBF system designed by conventional elastic design method can undergo severe damage under design level ground motions (Sabelli, 2000). Current seismic codes (ANSI, 2005a) has provisions to design ductile CBF which is also known as Special Concentrically Braced Frames (SCBFs).

1.2.3 Eccentrically Braced Frames (EBFs)

The eccentrically braced frame is a combination of concentrically braced frame and moment resisting frame. The EBF combines individual advantages of each frame and minimizes their respective disadvantages. It possesses high elastic stiffness, stable inelastic response under cyclic lateral loading and excellent ductility and energy dissipation capacity (Michel Bruneau et al. 1998). Eccentric braced frames utilize both the axial loading of braces and flexure of beam sections to resist the lateral forces. It addresses the need for a laterally stiff framing system with large energy dissipation capabilities under large seismic forces. The key distinguishing feature of an EBF is the isolated segment of a beam termed as "link." A typical EBF consists of a beam, one or two braces and columns. Its configuration is similar to other conventional braced frames with the exception that each brace must be eccentrically connected to the frame. Eccentric connection introduces shear and bending in the beam adjacent to brace. The short segment of the frame where those forces are concentrated is the "link." All inelastic activity is intended to be confined to the properly detailed link. Links act as structural fuses which dissipate seismic input energy without much degradation of strength and stiffness and thereby transfer less force to the adjacent columns, beams and braces. Common EBF arrangements are given in Figure 1.3.

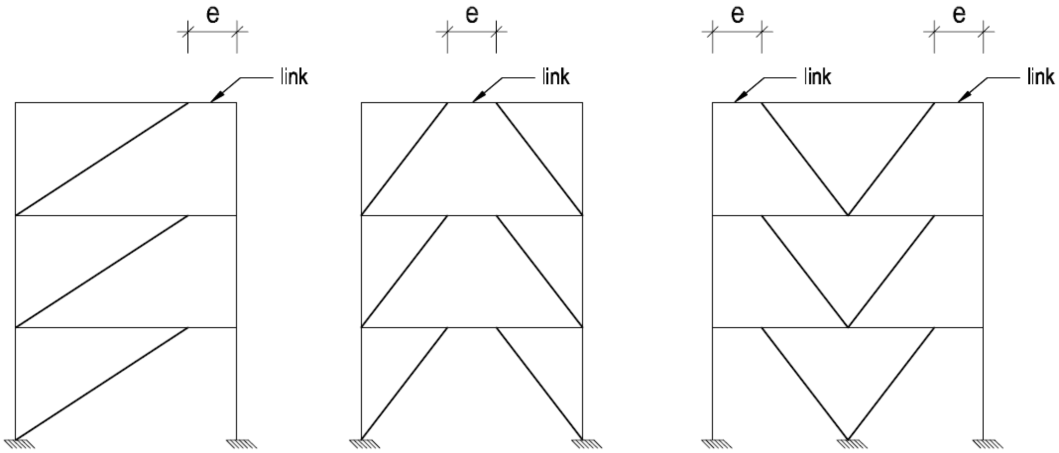

Figure 1.3 Typical EBF configurations

Lateral stiffness of the EBF is a function of the ratio of link length to the beam length. As the link becomes smaller the frame becomes stiffer approaches the stiffness of CBF. And as the link becomes longer the frame becomes more ductile approaching to the stiffness of a moment frame.

1.3 Literature review

PRE-NORTHRIDGE DESIGN

The presumed ductility of the discussed framing systems are dependent on the connection properties. The welded moment connections were popular in North American seismic regions before Northridge earthquake. By the 1960s the building industry was frequently using an alternative connection detail with a bolted web connection and fully welded flanges. To see the plastic behavior of these moment connections the first test was conducted in 1960s. Popov and Pinkney (1969) tested 24 beam column joints. Specimens with welded flanges and bolted connections showed superior inelastic behavior compared with the cover plated moment connection and the fully bolted moment connection due to the fact of slippage of the bolts which causes visible pinching of the hysteresis loops under cyclic loading (FEMA-355e) (Michel Bruneau et al. 1998).

In 1970s, welded flanges-bolted web connections with fully welded connections are compared (Popov and Stephen 1970) and the fully welded connection exhibited more ductile behavior. Four out of five bolted webs failed abruptly. Popov and Stephen (1972) also concluded that "The quality of workmanship and inspection is exceedingly important for the achievement of best results (Michel Bruneau et al. 1998)."

Popov et al. (1985) tested eight specimens. The test mainly emphasize on panel zone behavior with W18 beams. As per the authors, during the welding procedure: "the back-up plates for the welds on the beam flange-to-column flange connections were removed after the full-penetration flange welding was completed and small cosmetic welds appeared to have been added and ground off on the underside (FEMA-355e)."

The tests by Tsai and Popov (1987) and Tsai and Popov (1988) indicated some prequalified moment connections in ductile moment frames with W18 and W21 similar in depth to those tested by Popov and Stephen (1971), were not as ductile as expected. Before developing adequate plastic rotations, specimens with welded flanges-bolted web connections failed abruptly. Only four out of eight specimens achieve desirable beam plastic rotation. Authors realized about the quality control as an important factor (FEMA-355e)

Engelhardt and Husain (1993) conducted 8 tests to investigate the effect of the ratio of Z_f/Z on rotation capacity using W21 and W24 beams, where Z_f is the plastic modulus of the beam flanges and Z is the plastic modulus of the entire beam. They could not find any relation between Z_f/Z with amount of hysteretic behavior developed prior to failure. But, interestingly some of the specimens showed lack of ductility. This study also compared their results with past experimental data. Assuming that connections must have a beam plastic rotation capacity of 0.015 radian to survive under severe earthquake, they found none of the specimens could provide that amount (Michel Bruneau et al. 1998).

Before Northridge earthquake most of the beam-column connections in a moment resisting frames were detailed to be able to transfer plastic moment of the beams to the columns (Roeder and Foutch 1995). Thus, relatively lighter column and beam sizes were sufficient for those frames to resist seismic forces. With time many engineers concluded that it was economically advantageous to limit the number of bays in a frame designed as ductile moment frame. Prior to the Northridge earthquake even some engineers frequently designed building with only four single-bay ductile moment frames with two in each principal direction. This trend results with the loss in structural redundancy. In an addition these single-bay moment frames required considerably deeper beams and columns with thicker flanges than the multi-bay ones previously used to resist the same lateral forces. It provided an opportunity to investigate potential size effects (Michel Bruneau et al. 1998). Roeder and Foutch (1996) compiled all the test results for pre-northridge connections and found that the expected ductility decreases with the deeper sections. Bonowitz (1999a) found the same results from the tests conducted after Northridge earthquake (FEMA-355e)

POST-NORTHRIDGE DESIGN

Numerous factors have been identified which were potentially contributed to the poor seismic performance of the pre-Northridge steel moment connections. Failure happened due to different combinations of those factors: workmanship and inspection quality; weld design; fracture mechanics; base metal elevated yield stress; welds stress condition; stress concentrations; effect of triaxial stress conditions; loading rate; amd presence of composite floor slab (Michel Bruneau et al. 1998).

Numerous solutions to the moment frame connection problems have been proposed. Two key strategies have been developed to overcome the problem. One of them is to strengthening the connection and the other is weakening the beam ends which is framed into the connection. Both strategies effectively move the plastic hinges away from the face of the column (Michel Bruneau et al. 1998).

Satisfactory performance requires that a connection should be capable of developing a beam plastic rotation of 0.03 radian with a minimum strength equal to 80 percent of the plastic strength of the girder. These are the acceptance criteria suggested in

SAC interim guidelines (1995b). As the minimum requirement it was recommended that experimental validation of proposed connection be done with the qualification tests in compliance with the ATC-24 loading protocol (ATC1992).

SEMI-RIGID CONNECTIONS

A connection in a moment frame will termed as partially restrained if it contributes to a minimum 10% of the lateral deflection or the connections strength is less than the weaker element of connected members (FEMA-356). It is presumed that in the Northridge earthquake, partially restrained connections could result in a better performance to provide flexibility in the structure. Proper placing of semi-rigid connections along with the rigid connection could improve the performance of moment frames. Modeling process of semi-rigid connections in a beam column joint is described in Chapter 4.

Kasai et al. (1999) and Maison et al. (2000) studied the effect of semi-rigid connections within the SAC program. But, in those studies all the connections were considered as partially restrained (FEMA-355c). However, the knowledge about the effect of semi-rigid connections in a hybrid frame is limited. Built on the pioneer work of Radulova (2009), this research aims to study the seismic performance of fully rigid and hybrid rhombus and rectangular framing systems.

1.4 Objective of the Present Study

The objective of this study is to identify the effect of building shape on its seismic performance. Thus rhombus shape frames are selected based on engineering intuition and they were subjected to five earthquake records from four different frequency earthquake. The control frame was selected to be the rectangular frame based on the SAC Frame (FEMA-355) geometry. The aspect ratio and geometrical dimensions were varied to obtain their earthquake response which included lateral sway, inter-story drift and member forces. In the second phase of the study, high rise hybrid frames with rigid and semi-rigid connections are subjected to earthquake forces to identify the effect of semi-rigid connections on the global behavior of the frames.

1.5 Scope of the Study

The scope of this study was limited between Rhombus and Rectangular shape frames. For both rhombus and rectangular; three, nine, twelve and twenty story frames are modeled with all the connections being rigid. The frames are analyzed under 5 different seismic excitation records only. These are for Elcentro, Northridge, Parkfield and two records for Kocaeli earthquakes. The results compared between the two shapes includes lateral sway, inter story drifts and internal forces of the members. Semi-rigid connection property has been incorporated only on the 20-story frames. Bi-linear moment-rotation curve has been used to define semi-rigid connection properties. No ultimate moment provision has been considered in moment-rotation curves. To create the hybrid frames semi-rigid connections are placed only on the mid levels of the frames, based on Radulova (2009).

1.7 Organization of the Present Study

This study is organized as per objectives. Background about this research is narrated in Chapter 1. It includes previous earthquakes effects, seismic regulations, brief discussion on connections, different framing systems and objectives of the study. Chapter 2 describes about the different analysis procedures. In Chapter 3, the proposed rhombus frames are compared with the corresponding rectangular frames under different earthquake records. Modeling process of semi-rigid connection is described in Chapter 4. It also includes earthquake response of hybrid frames with rigid and semi-rigid connections. Comments and discussions on the results are described in Chapter 5 along with the recommendations for future work in this area.

CHAPTER 2

BACKGROUND ON FRAME ANALYSIS

2.1 Introduction

Structural analysis uses the laws of physics and mathematics to predict the performance and behavior of structures. Actual behavior of a structure is complicated, but different level of idealization could decrease the complexity. Here in this chapter the term analysis will mainly deal with the procedures and guidelines to obtain the member strength and deformation demands of a structure under seismic load. In the first part of this chapter different analysis methods proposed by Federal Emergency Management Agency (FEMA), National Earthquake Hazards Reduction Program (NEHRP) will be overviewed. Then general discussion on some analysis procedure will be given briefly and at last some solution techniques will be discussed.

2.2 Analysis Methods

Different degrees of complexity due to geometry of the structure along with the material behavior are associated in the structural response under seismic excitation. Depends on the needed accuracy different types of idealizations are proposed in the evaluation of structural response. FEMA-355f considered four elastic and three inelastic analysis procedures implemented by FEMA-273, NEHRP Guideline (1997) for performance evaluation of steel moment resisting frames.

2.2.1 Elastic Analysis Methods

The proposed elastic analysis procedures are equivalent lateral force and modal analysis by FEMA-302, FEMA-273 linear static and linear dynamic methods and linear time history analysis procedures (FEMA-355f).

In the equivalent lateral force method, base shear is calculated based on seismic response coefficient and total dead load with applicable portion of other loads. This base shear is distributed to different floor levels and the response will be calculated from the static analysis (FEMA-355f).

FEMA-273 linear static procedure uses the same background as the equivalent lateral load method to calculate the seismic load. Instead of design base shear this method brings in the term "pseudo lateral load" which is the final product after using different modification factors. The "pseudo lateral load" is selected in a way so that the response due to this load will be approximately same as from nonlinear time history analysis (FEMA-355f).

Linear time history procedure uses two methods in calculating structural response. In one method modal analysis and mode superposition is used which is explained later in this chapter. In another method this procedure uses direct integration technique in calculating seismic response. Some common integration techniques namely Newmark and Wilson methods are discussed at the end of this chapter.

2.2.2 Inelastic Analysis Methods

The considered inelastic analysis procedures are FEMA-273 nonlinear static procedure, capacity spectrum procedure (Skokan and Hart, 1999) and nonlinear time history analysis (FEMA-355f).

FEMA-273 nonlinear static procedure is also known as the static pushover analysis. In this method inelastic material behavior with P-Δ effects are included. These effects are briefly discussed later. In this method a target displacement is assigned at any point of the structure and then the structure is pushed with a increasing lateral load until the target displacement is achieved to that point or the structure collapses (FEMA-355f).

Capacity spectrum method is mainly applicable for reinforced concrete structures (ATC, 1996) and thus beyond the scope of this study. And the nonlinear time history analysis procedure is same as the linear time history analysis, only material nonlinearity along with the geometric effects should be considered in evaluation of structural response. Some key terms of these analysis procedures are explained in the following sections.

2.3 First Order Elastic Analysis

The first order elastic frame analysis considers the structural behavior as linear under any type of loading. This analysis method does not consider the geometric effects as member and the structural deflections (P-Δ and P-δ effects) as well as material nonlinearity. It assumes that the displacement will be very small and therefore the second order effects due to geometrical changes are ignored. And thus the stiffness matrix is constant for the members independent of applied axial forces. The deflection is proportional with the applied load, ie with increasing load the displacement will also increase which can be expressed as a straight line as shown in Figure 2.1.

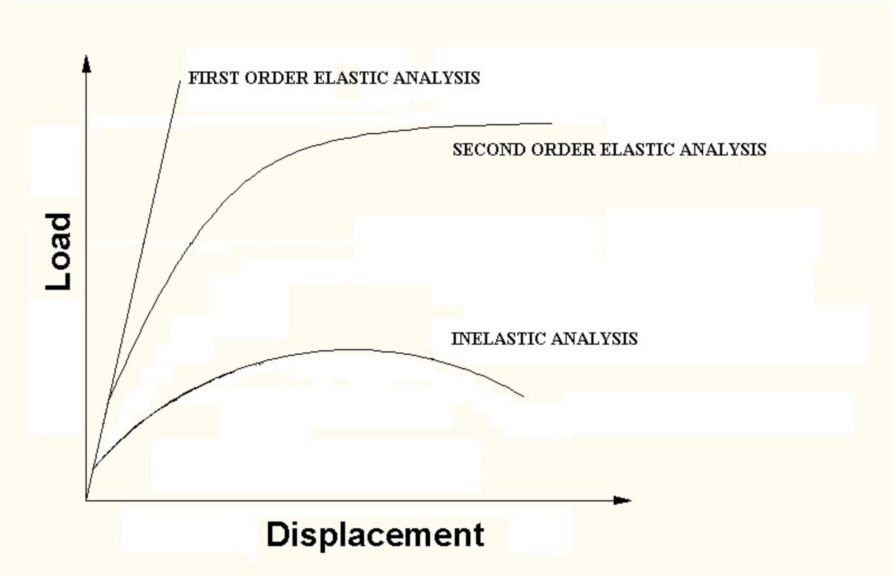

Figure 2.1 Generalised Load-Displacement curve for different types of analysis

The initial slopes of other types of analyses are coincided with it. It is because at lower loads the structures do not develop any secondary effects in geometry and material properties.

2.4 Second Order Elastic Analysis

Second order elastic analysis considers the geometric effects which are due to the member and structural deflections named as P-δ and P-Δ effects respectively. Structural response due to the second order elastic analysis is presented in the load-displacement curve shown in Figure 2.1. Initially it follows the path of linear analysis, but as the loading increased to produce sufficient geometric effect it starts to deviate from linear analysis to show the effect of geometric nonlinearity. Figure 2.2 shows P-δ and P-Δ effects, which is the cause for this geometric nonlinearity.

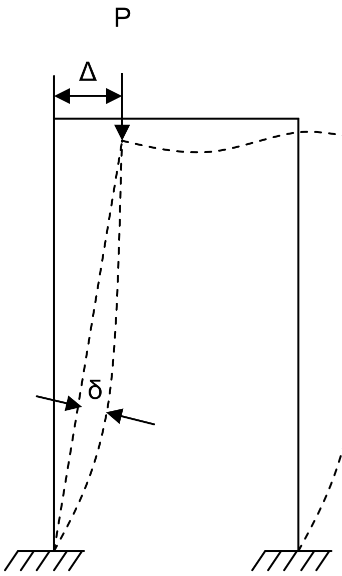

Figure 2.2 P-δ and P-Δ effects

These geometric effects produce higher internal forces due to axial loads. The stiffness matrix needs to be adjusted to reflect these effects and the corrections develop additional deflection. To account this problem the system reaches in equilibrium in an iterative process. As the stiffness matrix and thus the structural response are dependent on the deflected shape of the frame, principle of superposition is not applicable in second order elastic analysis. As material nonlinearity is not considered, this method over predicts the collapse load.

P-δ EFFECT

When a member deforms, it affects the stiffness of that member and additional moment will be developed in the member. This second order effect due to deflection along a member and the axial force is termed as P-δ effect.

P-Δ EFFECT

If a structure deflects significantly, then the original geometry of the structure cannot be used to formulate the transformation matrix due to change in nodal coordinates. This is known as P-Δ effect.

2.5 Inelastic Analysis

Material yielding and instability of structural members have significant effect to control the ultimate load. If the material nonlinearity is included in the second order elastic analysis, it would become the inelastic analysis. Nonlinearity in the inelastic analysis exists in two forms – geometric nonlinearity and material nonlinearity.

Material start yielding at the outer fiber of the section when the elastic moment reaches to yield moment value M_y. Material nonlinearity come into affect at this point and after that with application of additional load, yielding will spread over the section from outer fiber to plastic neutral axis. The section will continue yielding until the whole section is yielded to develop full plastic moment M_p. This nonlinearity can be incorporated to the analysis mainly by two approaches. In the first approach plastic hinges are assumed to form at the two ends of a member i.e. all the material nonlinearity is basically lumped at the two ends of a member. This is known as concentrated plasticity (plastic hinge, lumped plasticity) approach. Another approach assumes the plasticity over the whole member known as distributed plasticity (plastic zone) approach (Chan and Chui, 2000).

CONCENTRATED PLASTICITY APPROACH

Concentrated plasticity approach ignores the progressive yielding along the member length. It assumes the material nonlinearity to be lumped in a small region of zero length (Yau and Chan, 1994). It deals with the cross section plastification, which starts at the outer most fiber of the section and ends up with the formation of a hinge at a given point. It assumes that the hinges will form only at the ends and the remaining part of the member will remain elastic. Mashary and Chen (1991) and Yau and Chan (1994) modeled this material nonlinearity by using zero length spring at the member ends. Many other methods are proposed for computer simulation of this hinge property. This approach is easier to apply and significantly save computation time than the distributed plasticity approach. Commonly used methods for modeling plastic hinges are elastic-plastic hinge method, column tangent modulus method, beam-column stiffness degradation method, beam-column strength degradation method and end spring method.

DISTRIBUTED PLASTICITY APPROACH

This approach assumes yielding will be distributed over the length of the member and the cross section. This method discretized structure into many elements and each section is further divided into small fibers in an attempt to monitor stress and strain for all members. Initial imperfections and residual stresses can be included by assigning stresses to each fiber before loading which can be varied along the side and thickness of the section (Chan, 1990). The distributed plasticity approach is more accurate than the concentrated plasticity approach as fundamental stress-strain relationship is directly applied for the computation of forces. This approach requires considerable amount of computation time and huge memory to store data. Thus this method is suitable to analyze simple structures. Commonly used methods for this approach are traditional plastic zone method and simplified plastic zone method.

2.6 Dynamic Analysis of frame

Structural dynamics deal with the behavior of structure under dynamic loading. A static load is one which does not vary with time. A dynamic is any load which changes its magnitude, direction or position with time. If it changes very slowly, the structures response may be determined using static analysis but if the loading varies with time quickly (corresponding to the structures time period), the structures response must be determined using dynamic analysis. Here in this study dynamic term will use for seismic loads.

A structural dynamic analysis differs from the static analysis in two ways. Firstly in a dynamic problem both the applied force and the resulting response in the structure are time variant, i.e. function of time. It does not have a single solution like the static problem. For complete evaluation of structural response one has to investigate the solution over a specific interval of time. And the other one which is the most important feature in dynamic analysis is the act of inertia force. If a load is applied in a structure dynamically, there will be time variant deflection in the structure which will cause acceleration and thus inertia force will be induced. Magnitude of the inertia force depends on the acceleration and mass characteristics of the structure. Unlike static analysis, dynamic problems significantly depend on mass and damping. Three components, mass and damping together with the stiffness characteristics are required to write the equations of motion. Mass will be calculated from all the loads that the structure carries and members self-weight. This mass can be lumped at the joints or distributed over the member. Stiffness is basically provided by the structural components of a system. And the third component Damping is the energy dissipation properties of a material or system. It is a process by which a free vibration could steadily diminishes in amplitude and finally come to rest. In a vibrating system the energy could be dissipated by various mechanisms and often more than one mechanism can be present at the same time.

The equivalent lateral load approach discussed before transforms dynamic force into static forces. But, it cannot reflect the true dynamic response, as characteristic of resonance cannot be explained in a static approach. To include all the dynamic effects in the analysis, mode superposition and modal analysis is a widely accepted method for linear systems. Different types of direct integration methods are used to solve both linear and nonlinear dynamic problem numerically. Different methods are briefly discussed in the following sections.

2.7 Modal Analysis

Modal analysis in structural dynamics is used to determine the natural mode shapes and frequencies of a structure. It is a convenient method for calculating the dynamic response of a linear structural system. The response of a MDF system under externally applied dynamic load can be described by N differential equations in the following form,

$[m]\{\ddot{u}\} + [c]\{\mathring{u}\} + [k]\{u\} = \{p(t)\}$, where

$[m]$ is the mass matrix,

$[c]$ is the damping matrix,

$[k]$ is the stiffness matrix of the system,

$\{p(t)\}$ is the externally applied dynamic force matrix, and

$\{u\}$, $\{\mathring{u}\}$, $\{\ddot{u}\}$ denotes displacement, velocity and acceleration matrix.

The main approach of this method for dynamic analysis is to change N set of coupled equations of motion into N uncoupled equation for a multiple-degree-of-freedom system. Based on the number of DOF, a MDF system has multiple characteristic deflected shapes. Each characteristic deflected shape is called a natural mode of vibration of the MDF system denoted by $ø_n$. The displacement $\{u(t)\}$ of the system can be determined by the superposition of modal contributions. i.e. $\{u(t)\} = \sum_{n=1}^{N} q_n(t)ø_n$, where $q_n(t)$ = modal coordinates. Deflected shape $ø_n$ does not vary with time. The equation, $[k]ø_n = \omega_n^2[m]ø_n$, is the matrix eigen value problem where ω_n is the natural frequency and ø$_n$ is the natural modes of vibration of the system (Chopra, A.K. 1995). This equation has a non trivial solution if,

$$\left| [k] - \omega_n^2 [m] \right| = 0 \ ,$$

This is known as the frequency equation, because after expanding the determinant it creates a polynomial of order N in ω_n^2. This equation has N number of real and positive roots for ω_n^2 i.e. N number of natural vibration frequencies, started with ω_1 be the smallest and ω_n be the largest. If applied force {p(t)} can be written as [s]p(t) with spatial distribution is defined by [s], then the spatial distribution is expanded to its modal components {**s**$_n$}. where, {s$_n$} = Γ_n [m]ø$_n$. Then the equation could be transformed to uncoupled equations in modal coordinates and the solution for the modal coordinate is, $q_n(t) = \Gamma_n D_n(t)$, where D_n is governed by the equation of motion for nth-mode SDF system of the nth mode of the MDF system. The contribution from this mode to modal displacement is, {$u_n(t)$} = ø$_n q_n(t)$ = Γ_nø$_n D_n(t)$. And the equivalent static force associated with the nth mode response is, {$f_n(t)$}={**s**$_n$}{$A_n(t)$}, where $A_n(t) = \omega_n^2 D_n(t)$, is the pseudo acceleration. The nth mode contribution to any response is determined by the static analysis for force {f_n}. By combining all the response contributions from all the modes gives the total dynamic response (Chopra, A.K. 2007).

2.8 Step-by-Step Integration

Analytical solution of a dynamic problem is not possible in cases where the physical properties like geometry and elasticity of material do not remain constant. The stiffness coefficient can be changed with yielding of materials or by significant change in axial force which will cause the change in geometric stiffness coefficient. The applicable method for the analysis of nonlinear system is the numerical step-by-step integration, which is also applicable to linear systems. The main approach of this method is to divide the response history into short time increments and then the response is calculated during each increment assuming it as a linear system with the properties determined at the start of each increment. The properties are updated at the end of each interval based on the deformation and stress, and thus the nonlinear system is idealized as a collection of changing linear systems. In 1959, Newmark N.M. developed a method of computation for dynamic problems in structure. Later modifications are made to this method based on the stability, accuracy etc. Some popular methods are briefly discussed in the following sections.

2.8.1 Newmark’s Method

In this method it is assumed that at time i the values of displacement, velocity and acceleration is known and by numerical integration it can be estimated for time i+1, if the time increment, Δt is very small. Newmark introduce two parameters γ and β to indicate the proportion of acceleration that will enter into the equations for displacement and velocity (Newmark N.M. 1959). The adopted equations are,

$$u_{i+1} = u_i + (\Delta t)\,\mathring{u}_i + [\,(0.5 - \beta)(\Delta t)^2]\,\ddot{u}_i + [\,\beta(\Delta t)^2\,]\,\ddot{u}_{i+1} \qquad (2.1)$$

$$\mathring{u}_{i+1} = \mathring{u}_i + [\,(1 - \gamma)\,\Delta t\,]\,\ddot{u}_i + (\gamma\,\Delta t)\,\ddot{u}_{i+1} \qquad (2.2)$$

The two parameters γ and β in the above two equations are responsible for the stability and accuracy of the system. If γ is taken as zero, a negative damping will result, which will produce a auto vibration from the numerical method. Again if γ is greater than $\frac{1}{2}$, a positive damping addition to the real damping will be introduced to reduce the magnitude of the response. So, generally γ is taken as equal to $\frac{1}{2}$. And better results are obtained with values of β range between $\frac{1}{6}$ to $\frac{1}{4}$ (Newmark, N.M. 1959). Two popular special cases for Newmark's method are as follows -

2.8.1.1 Average Acceleration Method

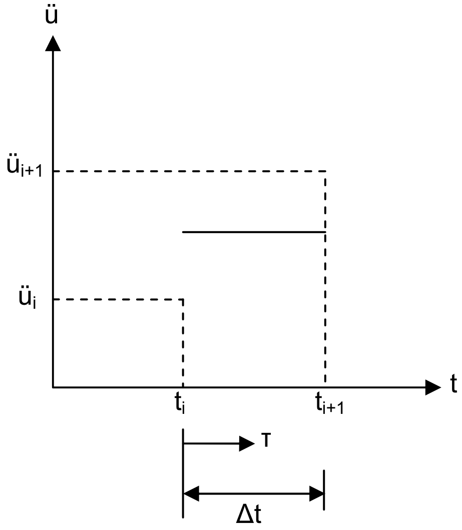

Figure 2.3 Average acceleration

If there is no variation of acceleration over a time step and the value is constant, equal to the value of average acceleration, then,

$\ddot{u}(\tau) = \frac{1}{2}(\ddot{u}_{i+1} + \ddot{u}_i)$. If $(\tau) = \Delta t$, this will yield

$\mathring{u}_{i+1} = \mathring{u}_i + \frac{1}{2}\Delta t\,(\ddot{u}_i + \ddot{u}_{i+1})$, and $u_{i+1} = u_i + (\Delta t)\,\mathring{u}_i + \frac{1}{4}(\Delta t)^2(\ddot{u}_i + \ddot{u}_{i+1})$.

These two equations are same as equation 2.1 and 2.2, if $\gamma = \frac{1}{2}$ and $\beta = \frac{1}{4}$. For this method, maximum velocity response is correct whether value of β other than $\frac{1}{4}$ will cause some error (Newmark N.M. 1959). From stability point of view Newmark's method is stable if,

$$\frac{\Delta t}{T_n} \leq \frac{1}{\pi\sqrt{2}} \frac{1}{\sqrt{\gamma - 2\beta}} \tag{2.3}$$

Where, T_n is the natural time period of the system.

For, $\gamma = \frac{1}{2}$ and $\beta = \frac{1}{4}$, $\frac{\Delta t}{T_n} \leq \infty$ ie average acceleration method is unconditionally stable.

2.8.1.2 Linear Acceleration Method

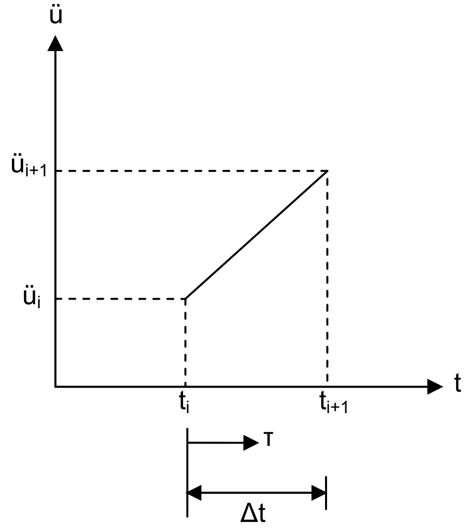

Figure 2.4 Linear acceleration

If the variation of acceleration is linear over a time step, then,

$\ddot{u}(\tau) = \ddot{u}_i + \frac{\tau}{\Delta t}(\ddot{u}_{i+1} - \ddot{u}_i)$. If $(\tau) = \Delta t$, this will yield

$\mathring{u}_{i+1} = \mathring{u}_i + \frac{1}{2}\ \Delta t\ (\ddot{u}_i + \ddot{u}_{i+1})$, and

$u_{i+1} = u_i + (\Delta t)\ \mathring{u}_i + (\Delta t)^2\ (\frac{1}{3}\ddot{u}_i + \frac{1}{6}\ \ddot{u}_{i+1})$.

These two equations are same from equation 2.1 and 2.2, if $\gamma = \frac{1}{2}$ and $\beta = \frac{1}{6}$. Equation 2.3 shows that the linear acceleration method will be stable, if $\frac{\Delta t}{T_n} \leq 0.551$. And so this method is conditionally stable. But stability criteria have not imposed any rule in selecting time step. In general by taking short integration interval, a good accuracy can be achieved from unconditionally stable linear acceleration method.

2.8.2 Wilson θ Method

E.L.Wilson modified the conditionally stable linear acceleration method into unconditionally stable. His proposed method is known as Wilson θ Method. This method assumes that the acceleration will vary linearly over an extended interval, $\delta t = \theta\Delta t$.

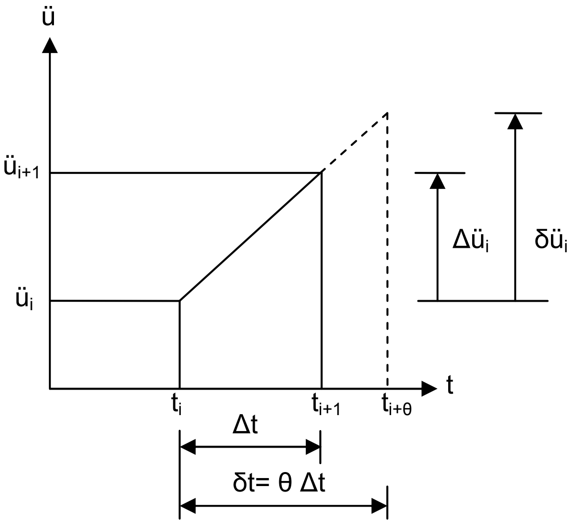

Figure 2.5 Linear variation of acceleration over extended time steps

The parameter θ in this method determines the accuracy and the stability characteristics of the numerical analysis. For θ = 1, this method will turn into Newmark's standard linear-acceleration method. For θ ≥ 1.37, Wilson's method becomes unconditionally stable.

2.8.3 Hilber-Hughes-Taylor Method

In order to introduce numerical damping into Newmark's method without affecting the accuracy Hilber, Hughes and Taylor introduce the parameter α. Where,

$$\gamma = \frac{(1-2\alpha)}{2} \quad \text{and} \quad \beta = \frac{(1-\alpha)^2}{4}$$

The range of this parameter is from $-\frac{1}{3}$ to 0. If α = 0, then this method turns into Newmark's average acceleration method. This would give the higher accuracy but it may produce excess vibrations in the higher modes. Decreasing value of α will increase the amount of numerical damping which will mainly damp the higher frequency modes. Sometimes it is required for a nonlinear solution to converge with using negative α. value (SAP2000).

CHAPTER 3

EFFECT OF FRAME SHAPE AND GEOMETRY ON SEISMIC PERFORMANCE

3.1 Introduction

The SAC joint venture between the Structural Engineers Association of California (SEAOC), the Applied Technology Council (ATC), and the California Universities for Research in Earthquake Engineering(CUREe), proposed 3-story, 9-story and 20-story frames. Several steel frames with these SAC dimensions are used for this study. These frames represent from low-rise to high-rise buildings. Besides these, a 12-story frame is also modeled. Initially all buildings are modeled as Rectangular Moment Frame with all connections being rigid. Later, a Rhombus shape has been proposed to see the effect of shape on the global behavior of the frame. The Rhombus shape has been constructed by placing the Rhombus building inside the Rectangular frame. This Rhombus shape frame has the same height and width ratios as the Rectangular shape. All the member sizes, joint loads and uniformly distributed loading were kept the same for both the shapes.

All the frames are analyzed under five different earthquake excitation data. These earthquakes reflect a wide variation in frequency content. For each height, results are compared between Rectangular and Rhombus shapes. Results include lateral sway, drift, top displacement and member forces. Effect of height-to-width ratios on the fundamental properties of the structure is also observed.

Total eight rigid frames are developed. To describe the results a general building designation is adopted for convenience,

_S – H_W_H/W- OP(_,/ _) - EQ , where

S = story

H = the height of the frame

W = the width of the frame

H/W = the height-to-width ratio of the frame

OP = out put, which can be member forces or displacement

AF = axial force

SF = shear force

BM = bending moment

TDUx = top node displacement along X-direction

MDUx = maximum displacement along X-direction

LDr = Lateral inter story drift

RMR = Rigid Rhombus frame

RCR = Rigid Rectangular frame

EQ = earthquake

ELC = El Centro earthquake

NRG = Northridge earthquake

PKF = Parkfield earthquake

KCL1 = Afyon Bay record for Kocaeli earthquake

KCL2 = Aydin record for Kocaeli earthquake

The building designation follows: 20S – 289_100_2.89 – TDUx (RMR, RCR) – ELC, which will describe a 20 story frame with height-to-width ratio of 2.89 where the height and the width are 289 ft and 200 ft, respectively. The out put describes top displacement along X- direction for both the Rhombus shape and Rectangular shape with all the connections being rigid, and the results are for El Centro earthquake. Thus, BM(RMR/RCR) will describe bending moment as out put. And the result will be the ratio of bending moment for the Rhombus shape and the Rectangular shape.

3.2 Three Story Frame

The analysis starts with the modeling of a three story frame. This three story 4-bay frame is used to observe the effect of earthquake excitation on low rise structures. The rectangular frame is 120ft wide with 30ft bay dimension and the total height of the building is 39 ft. These dimensions are taken from SAC 3-Story building. All the member sizes are W14 X 283. All the connections are considered to be rigid. Total dead load and 25 percentage of live load are considered for calculating member mass. Load calculations are described in Appendix G. The 3-story rectangular frame with corresponding rhombus shape is shown in Figure 3.1. These frames are analyzed under five different earthquake excitation records. The results are plotted in the Appendices A through F of this report as an attempt to show the comparison between the two shapes.

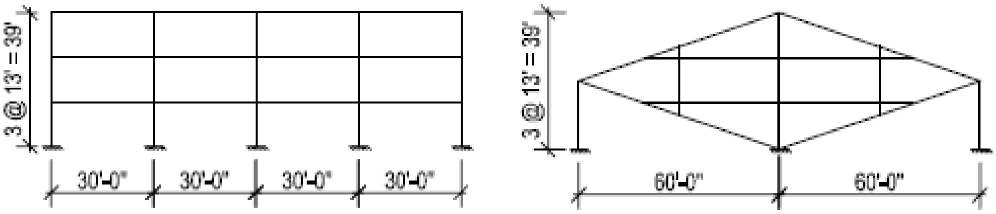

Figure 3.1 Three-Story Rectangular and Rhombus frame

Both of these models are analyzed under modal analysis and the corresponding first couples of mode shapes are given below.

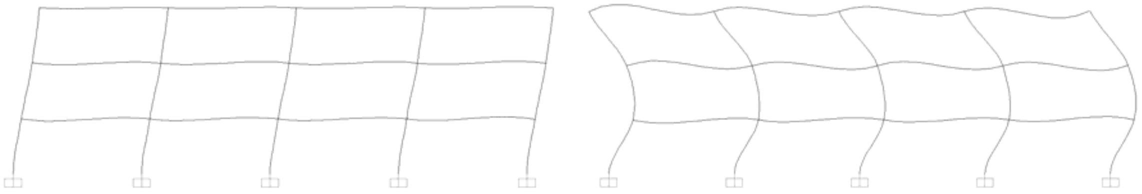

(a) (b)

Figure 3.2 First two Mode Shapes for 3-Story Rectangular Frame
(a) Mode 1, (b) Mode 2

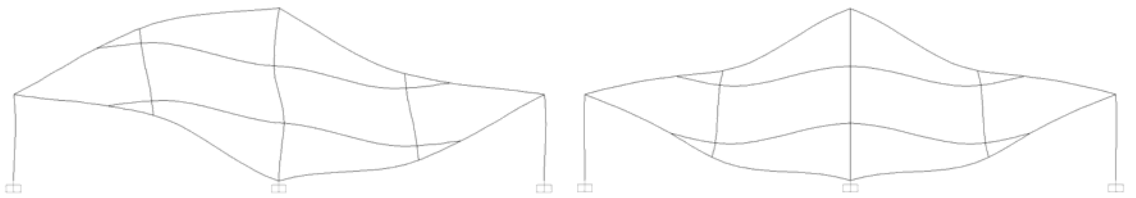

(a) (b)

Figure 3.3 First two Mode Shapes for 3-Story Rhombus Frame
(a) Mode 1, (b) Mode 2

These mode shapes are obtained from the SAP2000 software. Corresponding natural time period and frequencies for first ten modes are tabulated in the following table.

Table 3.1 Modal period and frequencies for 3-Story Frames (SAP 2000)

Mode	3S – 39_120_0.325 – (RCR)		3S – 39_120_0.325 – (RMR)	
	Period (sec)	Frequency (Hz)	Period (sec)	Frequency (Hz)
1	0.56324	1.7754	0.28961	3.4529
2	0.17082	5.8543	0.17561	5.6943
3	0.0964	10.374	0.11076	9.0288
4	0.05435	18.4	0.06529	15.317
5	0.05406	18.499	0.0555	18.019
6	0.05368	18.63	0.05294	18.888
7	0.0479	20.877	0.04959	20.167
8	0.04613	21.679	0.03818	26.191
9	0.04231	23.637	0.03408	29.344
10	0.03836	26.068	0.02795	35.777

3.3 Nine Story Frame

The nine story frame has been modeled with the SAC 9-Story building dimensions. This nine story 5-bay frame is used to observe the effect of earthquake on medium high-rise buildings. The rectangular frame is 150ft wide with 30ft bay dimension, and the total height of the building is 134 ft with a 12ft basement. All the member sizes are W14 X 283. All the connections are considered to be rigid. Total dead load and 25 percentage of live load are considered for calculating member mass. Load calculations are described on Appendix G. The 9-story rectangular frame with equivalent rhombus shape is shown in Figure 3.4. These frames are analyzed under five different earthquake excitation records. The results include top displacements, lateral sway, inter story drifts and member forces. All the results are plotted in the Appendices A through F of this report to compare the performance of individual shape under earthquake excitations.

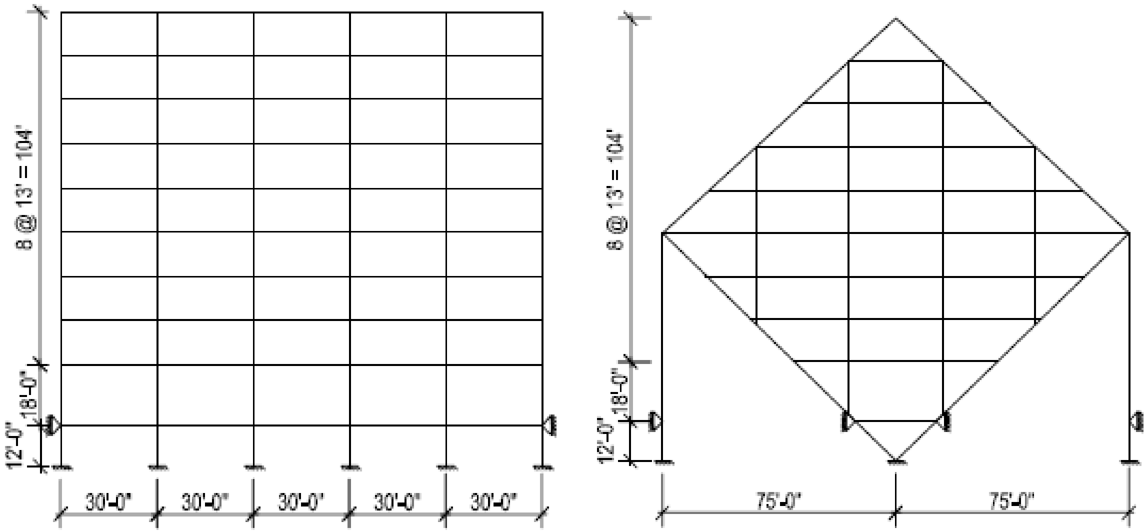

Figure 3.4 Nine-Story Rectangular and Rhombus frame

These models are analyzed under modal analysis and the first couples of mode shapes are given in the following Figures.

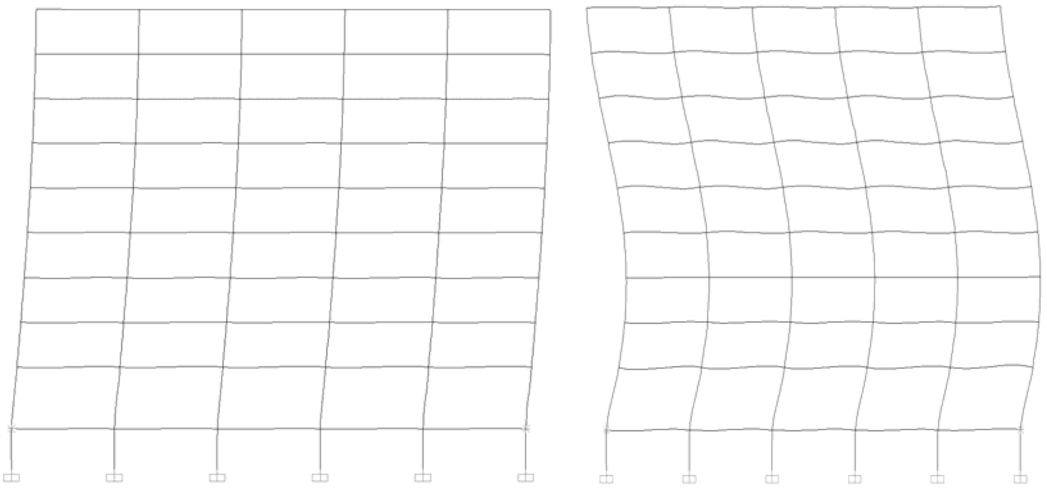

(a) (b)

Figure 3.5 First two Mode Shapes for 9-Story Rectangular Frame
(a) Mode 1, (b) Mode 2

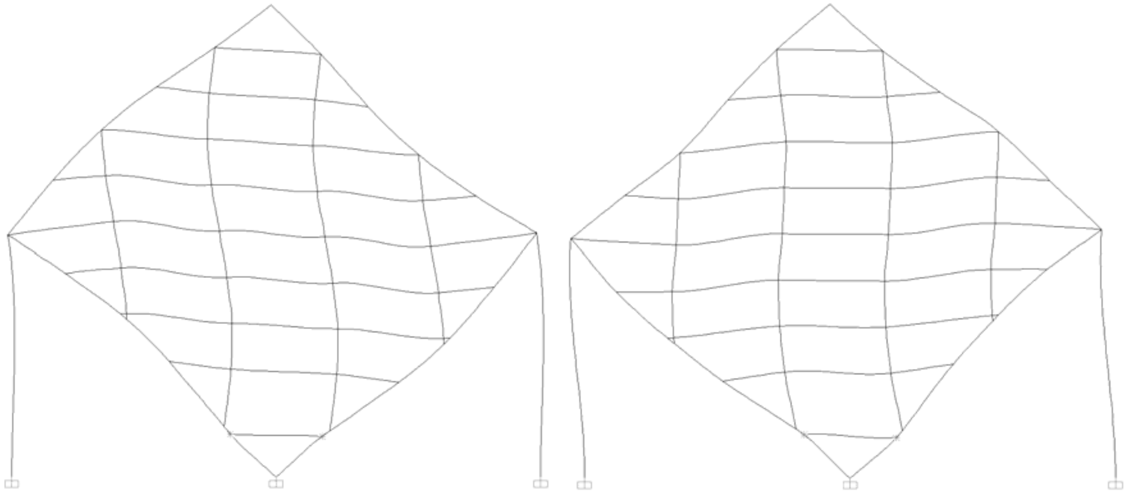

(a) (b)

Figure 3.6 First two Mode Shapes for 9-Story Rhombus Frame
(a) Mode 1, (b) Mode 2

The modal analysis is performed in the SAP2000 platform. Corresponding time period and frequencies for first ten modes are tabulated in the following Table

Table 3.2 Modal period and frequencies for 9-Story Frames (SAP 2000)

Mode	9S – 134_150_0.893 – (RCR)		9S – 134_150_0.893 – (RMR)	
	Period (sec)	Frequency (Hz)	Period (sec)	Frequency (Hz)
1	1.92246	0.52017	0.4332	2.3084
2	0.6213	1.6095	0.37677	2.6542
3	0.3527	2.8353	0.18268	5.474
4	0.23647	4.2289	0.17649	5.6662
5	0.17226	5.8051	0.13888	7.2004
6	0.16484	6.0667	0.12993	7.6968
7	0.16	6.25	0.12041	8.3047
8	0.15317	6.5286	0.1063	9.4078
9	0.1468	6.8121	0.08393	11.915
10	0.13315	7.5105	0.07483	13.364

3.4 Twelve Story Frame

The twelve story 5-bay frame is used to observe the geometric effect of frame under earthquake excitation. The rectangular frame is 150ft wide with 30ft bay dimension, and the total height of the building is 173 ft with a 12ft basement. All the member sizes are W14 X 283. All the connections are considered to be rigid. Total dead load and 25 percentage of live load are considered for calculating member mass. The 12-story rectangular frame with corresponding rhombus shape is shown in Figure 3.7. These frames are analyzed under five different earthquake excitation records. The out put results include top displacement, lateral sway, inter story drift and member forces. All the results are plotted in the Appendices A through F of this report as an attempt to show the comparison between the two shapes.

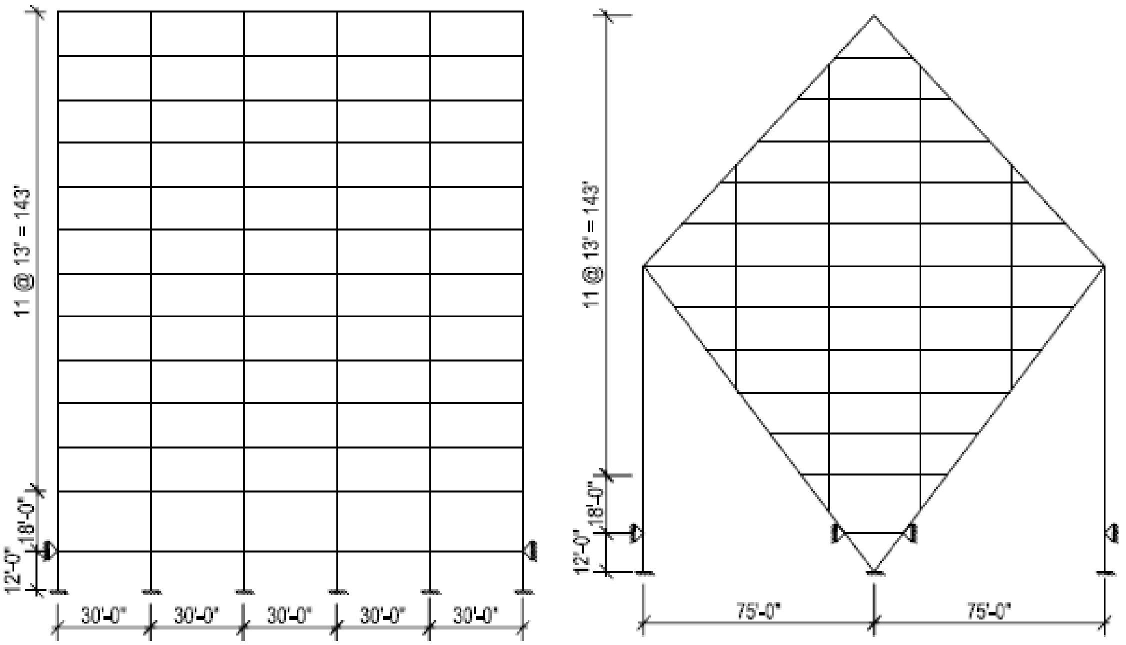

Figure 3.7 Twelve-Story Rectangular and Rhombus frame

Both of these frames are analyzed under modal analysis. In the following Figures, first couples of mode shapes are provided. These shapes are obtained from the SAP2000 software.

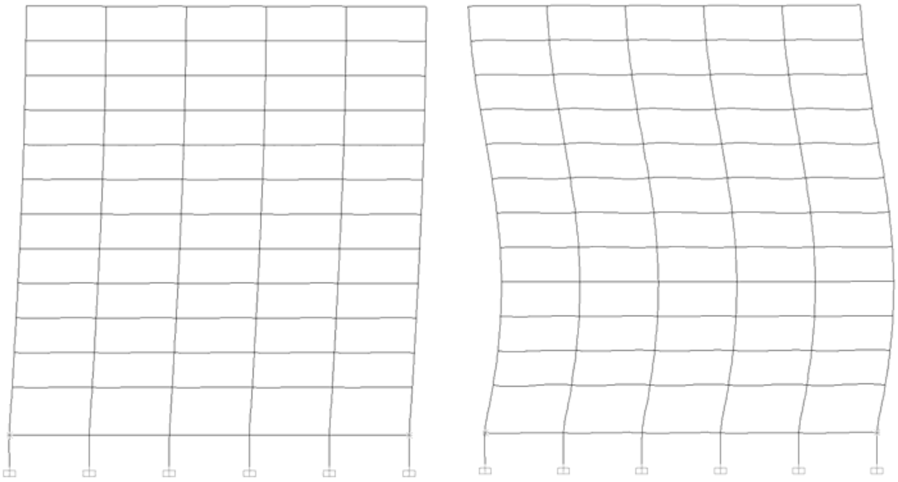

(a) (b)

Figure 3.8 First two Mode Shapes for 12-Story Rectangular Frame
(a) Mode 1, (b) Mode 2

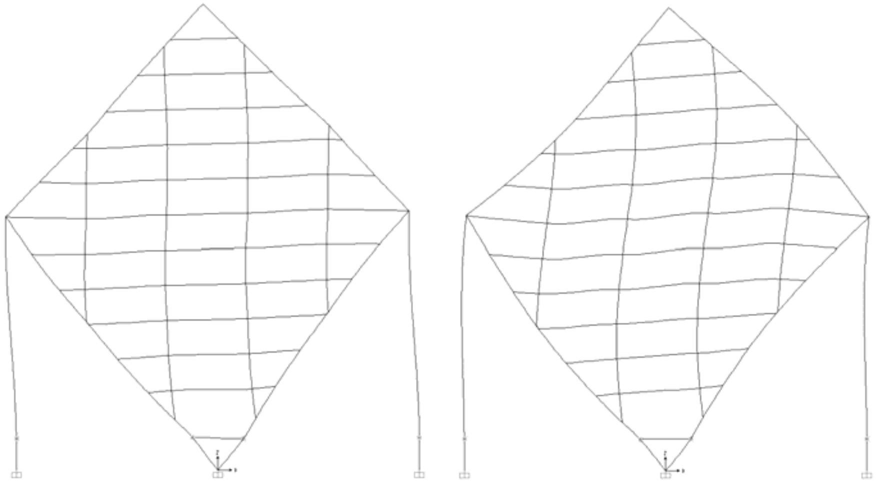

(a) (b)

Figure 3.9 First two Mode Shapes for 12-Story Rhombus Frame
(a) Mode 1, (b) Mode 2

Corresponding time period and frequencies for the first ten modes are tabulated below.

Table 3.3 Modal period and frequencies for 12-Story Frames (SAP 2000)

Mode	12S – 173_150_1.153 – (RCR)		12S – 173_150_1.153 – (RMR)	
	Period	Frequency	Period	Frequency
	(sec)	(Hz)	(sec)	(Hz)
1	2.51114	0.39823	0.5671	1.7634
2	0.82114	1.2178	0.53406	1.8725
3	0.47433	2.1082	0.25183	3.9709
4	0.32474	3.0794	0.22645	4.4159
5	0.24064	4.1556	0.19174	5.2154
6	0.20952	4.7728	0.16486	6.0658
7	0.20019	4.9952	0.1559	6.4144
8	0.18754	5.3323	0.1157	8.643
9	0.18752	5.3327	0.10739	9.3116
10	0.176	5.6818	0.09298	10.755

3.5 Twenty Story Frame

A 20story rectangular frame has been modeled with SAC 20-Story building dimensions. This 20-Story 5 bay frame is used to observe the effect of earthquake on high-rise buildings. The rectangular frame is 100ft wide with 20ft bay width and the total height of the building is 289ft with two basement floor 12ft each. All the member sizes are W24 X 131. All the connections are considered to be rigid. Total dead load and 25 percentage of live load are considered for effective seismic load. 20-story rectangular frames with corresponding rhombus shapes are shown in Figure 3.10. Both of the frames are analyzed with Modal analysis on the SAP2000 platform. First couples of modal shapes obtained from modal analysis are given in Figure 3.11 and 3.12. Corresponding time period and frequencies for first ten modes are given in Table 3.4. These frames are analyzed under five different earthquake excitation records. The results include top displacements, lateral sway, inter story drift and member forces. All the results are plotted in the Appendices A through F of this report to compare the performance of individual shape under earthquake excitation.

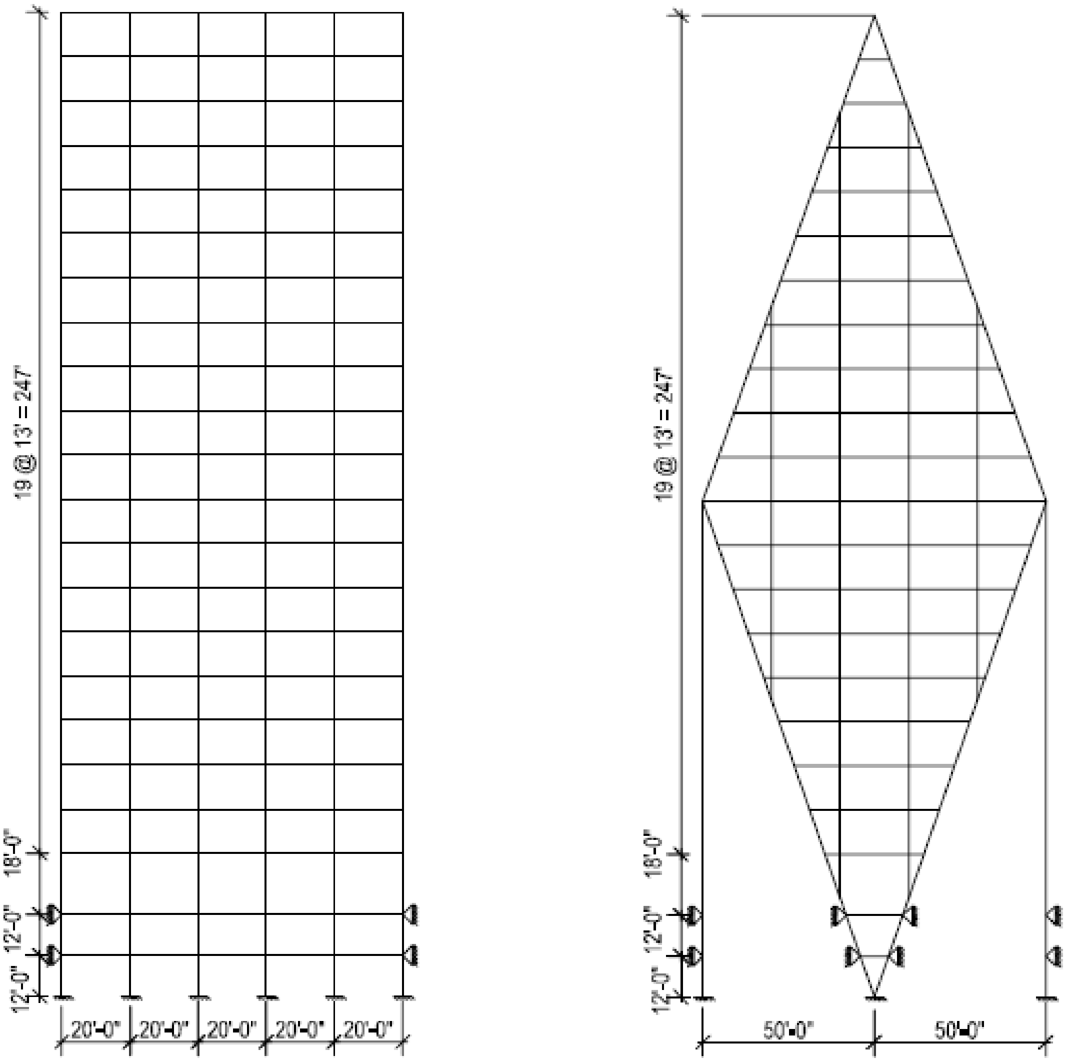

Figure 3.10 Twenty-Story Rectangular and Rhombus frames

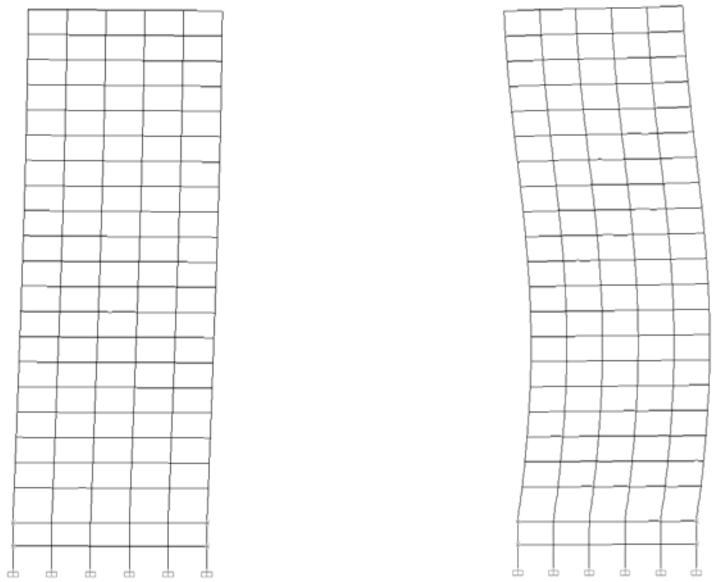

(a) (b)

Figure 3.11 First two Mode Shapes for 20-Story Rectangular Frame
(a) Mode 1, (b) Mode 2

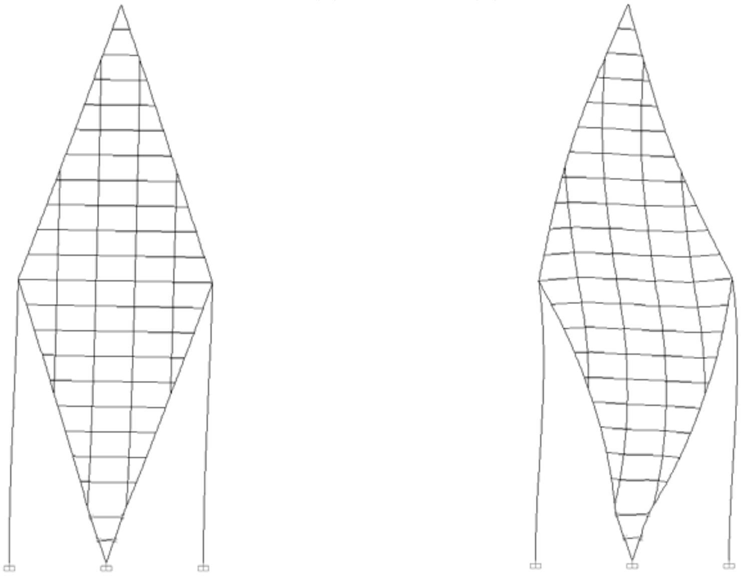

(a) (b)

Figure 3.12 First two Mode Shapes for 20-Story Rhombus Frame
(a) Mode 1, (b) Mode 2

Table 3.4 Modal period and frequencies for 20-Story Frames (SAP 2000)

Mode	20S–289_100_2.89–(RCR)		20S–289_100_2.89-(RMR)	
	Period (sec)	Frequency (Hz)	Period (sec)	Frequency (Hz)
1	2.72965	0.36635	1.58828	0.62961
2	0.87486	1.143	0.48492	2.0622
3	0.49	2.0408	0.279	3.5842
4	0.34352	2.9111	0.25668	3.8959
5	0.31924	3.1324	0.22956	4.3562
6	0.2623	3.8125	0.18013	5.5514
7	0.24444	4.0909	0.15376	6.5037
8	0.20718	4.8266	0.13834	7.2287
9	0.17824	5.6103	0.11651	8.5827
10	0.17207	5.8116	0.10433	9.5849

3.6 Eathquake in consideration

Ground acceleration values in an earthquake vary with time in an irregular manner. As a result, an earthquake is generally composed of infinite number of frequency content. The non periodic acceleration time function can be represented by the Fourier integral –

$$\ddot{u}_g(t) = \frac{1}{2\pi}\int_{-\infty}^{\infty} F(\omega)e^{-i\omega t}\,d\omega$$

A Fourier spectrum constitutes the representation of a time history into the frequency domain. If $\ddot{u}_g(t)$ denotes ground acceleration in the time domain, the Fourier spectrum of $\ddot{u}_g(t)$ is defined as

$$F(\omega) = \int_{-\infty}^{\infty} \ddot{u}_g(t)e^{-i\omega t}\,dt$$

F(ω) represents ground acceleration in frequency domain. The amplitude of the Fourier spectrum is used to identify the harmonic components of the earthquake that has the largest amplitudes. These harmonic components are identified in terms of their frequencies. The amplitude Fourier spectrum of an earthquake may be interpreted as a measure of the total energy contained to that ground motion.

For this study four different earthquakes are used with a wide variety of frequency range. El Centro and Northridge earthquakes represent the high-frequency range, Parkfield earthquake is a medium-frequency earthquake. And two site records are provided for low frequency Kocaeli earthquake.

3.6.1 Generated Earthquake

To observe the resonance effect on 20 story frames, a Sine wave, composed of three different time period is generated; ie it consists of total three frequencies. Another reason for constructing this imaginary earthquake is to verify the SeismoSignal software about it's capability to determine dominant frequencies, as the original frequency contents for this generated data are known. Total time for the generated earthquake is 79.17 sec. It is constructed in a manner, so that in the first part, it will create resonance with the 20 story rhombus frame, and the last part will create resonance with the 20 story rectangular frame. From 0 ~ 10.92 sec, time period, T = 1.365 sec; frequency, f =0.733Hz, with total 8 cycle. In this time range amplitude is almost three times higher than the rest of the vibration. From 10.92 ~ 54.6 sec, time period, T = 5.46 sec; frequency, f = 0.183Hz, with total 8 cycle. And from 54.6 ~ 79.17 sec, time period, T =

2.73 sec; frequency f = 0.366Hz, with total 9 cycle. The generated data is plotted in Figure 3.13.

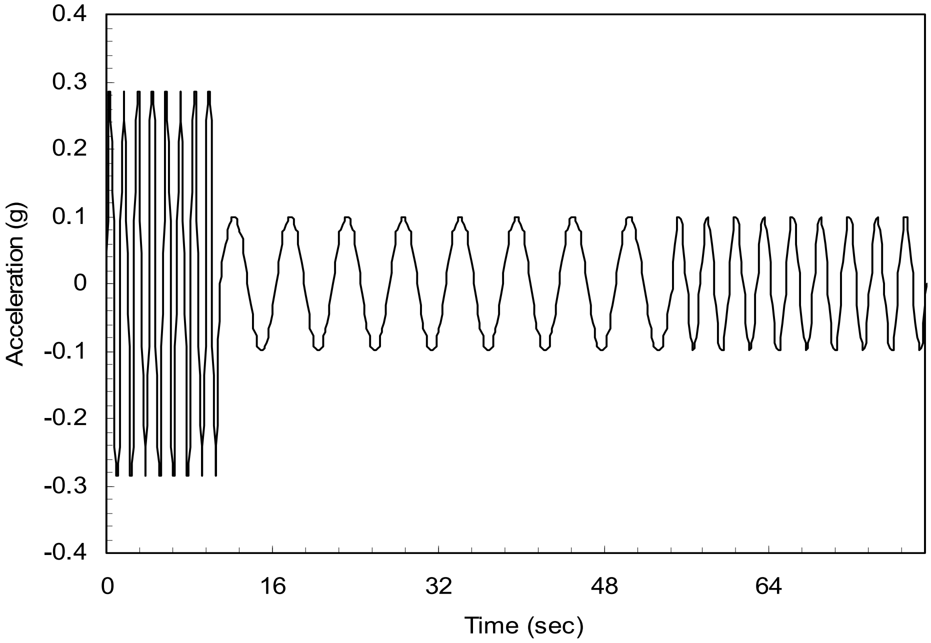

Figure 3.13 Acceleration Time History of Generated Earthquake

Now, if this data is used in SeismoSignal software, it will give three dominant frequencies as in Figure 3.14.

1st dominant, f = 0.183Hz,

2nd dominant, f = 0.733Hz, and

3rd dominant, f = 0.366Hz.

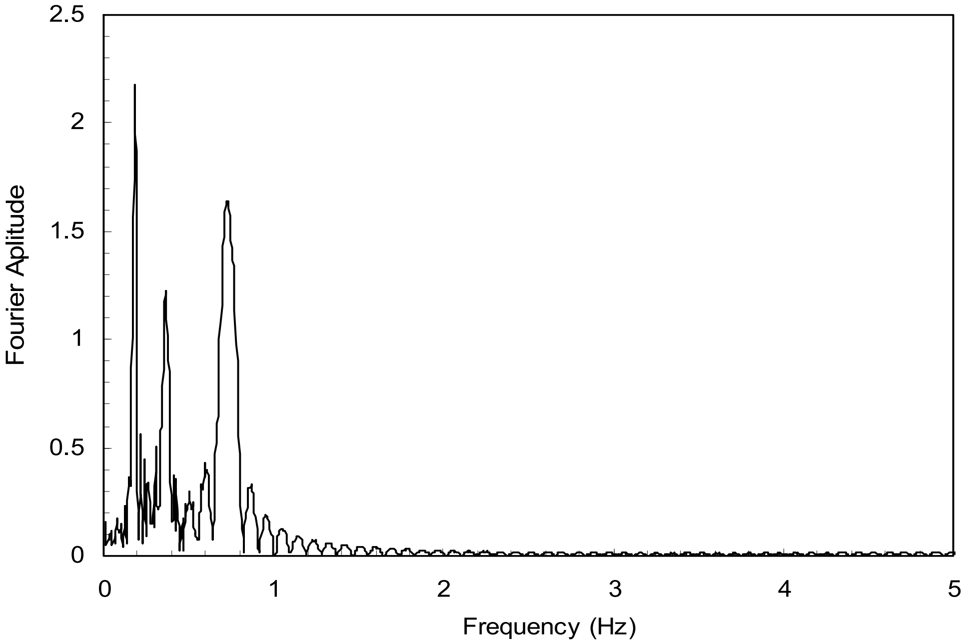

Figure 3.14 Fourier Spectrum of Generated Earthquake

In Figure 3.14, 0.183Hz is the 1st dominant frequency, because it covers most of the time range in Figure 3.13. But the software does not consider only the time range. That is why 0.733Hz is the second dominant instead of 0.366Hz (which is the second large in terms of time range). 0.733Hz is the 2nd dominant, as the amplitude of acceleration of that part is almost three times higher than the other.

To observe the resonance effect, 20S–289_100_2.89–(RMR) and 20S–289_100_2.89–(RCR) frames are analyzed with this data. The resulted top displacements of the two frames are shown in Figure 3.15. Figure shows, rhombus frame gives top displacement in the first part of the total time range, as vibration frequency of that time range is close to the natural frequency of the rhombus frame. And the rectangular frame gives maximum top displacement at the last part of the total time, where vibration frequency is close to the natural frequency of the rectangular frame.

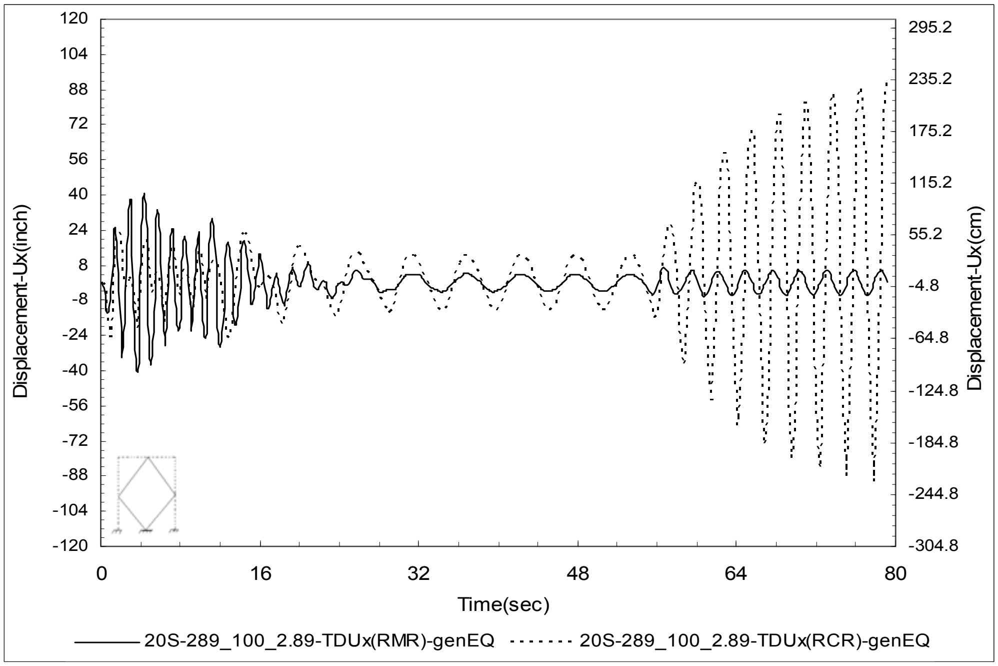

Figure 3.15 20S-289_100_2.89-TDux(RMR,RCR)-generated data

None of the frames experience higher top node displacement at the middle part of the generated data, which one is the dominant frequency range for the total time. Again, the rectangular frame which has resonance effect with the third dominant frequency, gives a maximum top displacement value, which is more than double, than the top displacement for the rhombus frame. So, in the following study, frequencies of the earthquakes are defined as a range instead of giving emphasis on a single dominant frequency.

3.6.2 ElCentro

The epicenter of the El Centro earthquake was in El Centro (Imperial Valley), California. It occurred on May 18, 1940. The exact site, from where data was collected is Imperial Valley, which is located 6 miles away from the epicenter. Nine people were killed by the earthquake. At Imperial, 80 percent of the buildings were damaged to some degree. In the business district of Brawley, all structures were damaged, and about 50 percent had to be condemned. The shock caused 40 miles of surface faulting on the Imperial Fault, part of the San Andreas system in southern California. Total damage has been estimated at about $6 million. The instrument that recorded the accelerogram was attached to the El Centro Terminal Substation Building's concrete floor. The record may have under-represented the high frequency motions of the ground because of soil-structure interaction of the massive foundation with the surrounding soft soil. The earthquake magnitude was 7.1. The total duration was 53.5 seconds. The North-South component of the El Centro earthquake was recorded with 0.02 second interval. First 30 seconds of the earthquake are used for time history analysis. Elcentro represents a high frequency ground shaking. Its major frequency range is between 1.0 Hz to 2.25 Hz based on the Fourier spectrum obtained from the SeismoSignal software. Figure 3.16 represents the acceleration time history of El Centro earthquake in terms of the gravitational acceleration, g. Figure 3.17 represents the Fourier transformation of the earthquake.

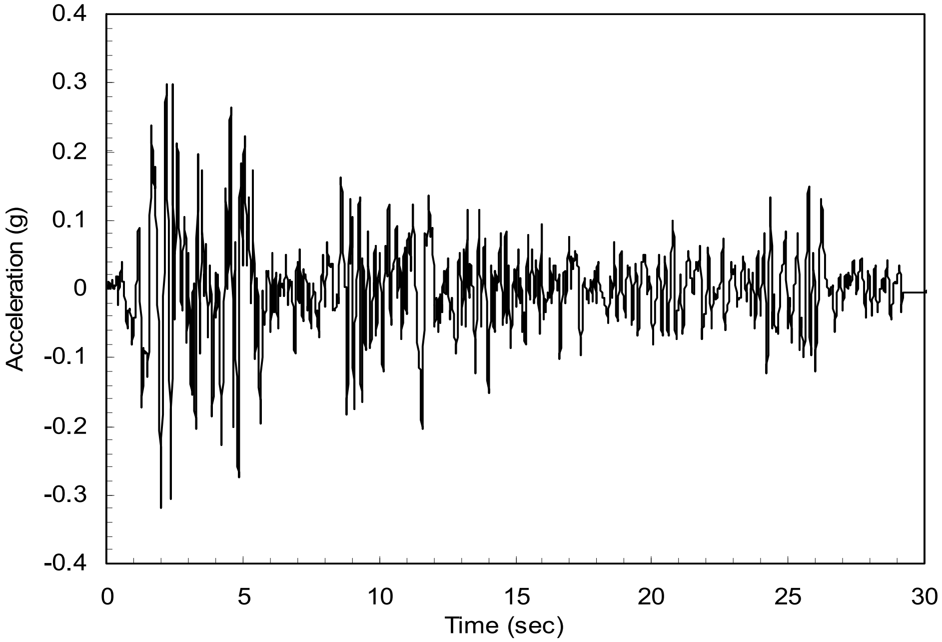

Figure 3.16 Acceleration Time History of El Centro Earthquake

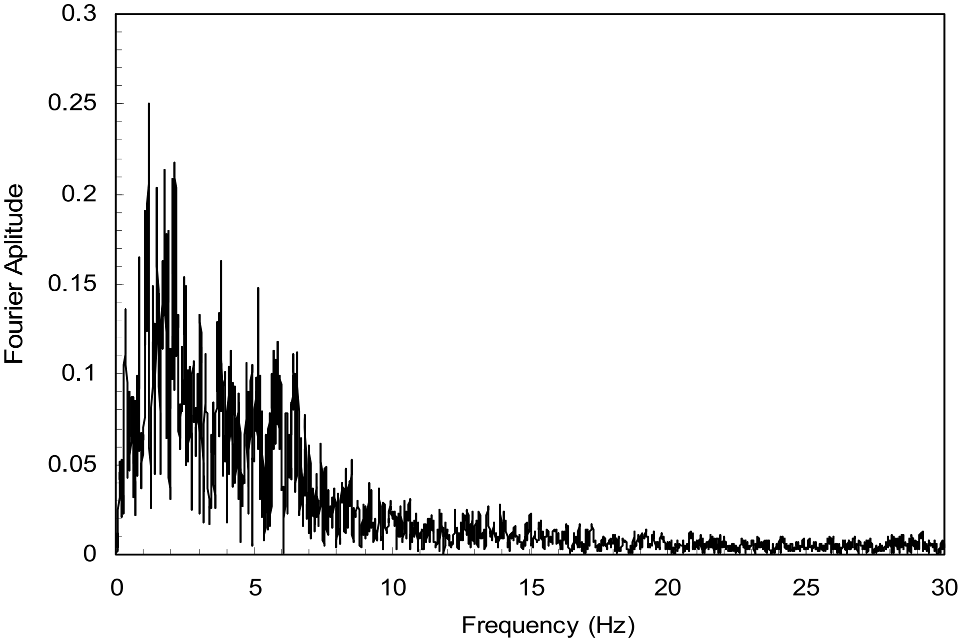

Figure 3.17 Fourier Spectrum of El Centro Earthquake

Table 3.5 Frequency Content for El Centro Earthquake

Earthquake : **Elcentro**			
Major frequency range	1.0Hz ~ 2.25Hz		
Dominant Frequency order	**Frequency (Hz)**	**Power Amplitude**	**Fourier Amplitude**
1st	1.172	0.171	0.25
2nd	2.148	0.127	0.216
3rd	1.782	0.124	0.213
4th	2.075	0.119	0.209

3.6.3 Northridge

The epicenter of Northridge earthquake was in Northridge, California. The Northridge earthquake was occurred at 4:30 a.m. local time on January 17, 1994. This earthquake is significant, as the damage created by this earthquake put a question mark on the design philosophies followed by the engineers at that time. The earthquake occurred along a "blind" thrust fault, close to the San Andreas Fault. The data was collected from Sylmar, Olive View. The earthquake magnitude is 6.7 on the Richter scale. The number of fatalities in the Northridge earthquake was 57. About 9000 people were injured. The total duration was 59.9 seconds, recorded with 0.02 second interval. Northridge is a high frequency earthquake with its major frequency between 0.4 Hz to 3.5 Hz, based on the Fourier spectrum obtained from the SeismoSignal software. Figure 3.18 represents the acceleration time history of Northridge earthquake in terms of the gravitational acceleration, g. Figure 3.19 represents the Fourier transformation of the earthquake. The first 50 second of the record has been used for time history analysis.

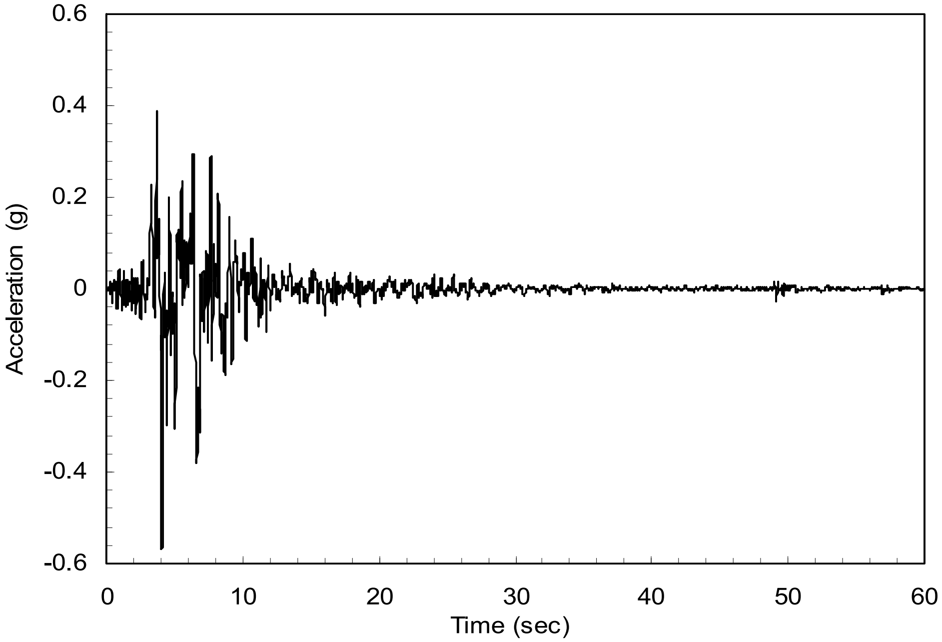

Figure 3.18 Acceleration Time History of Northridge Earthquake

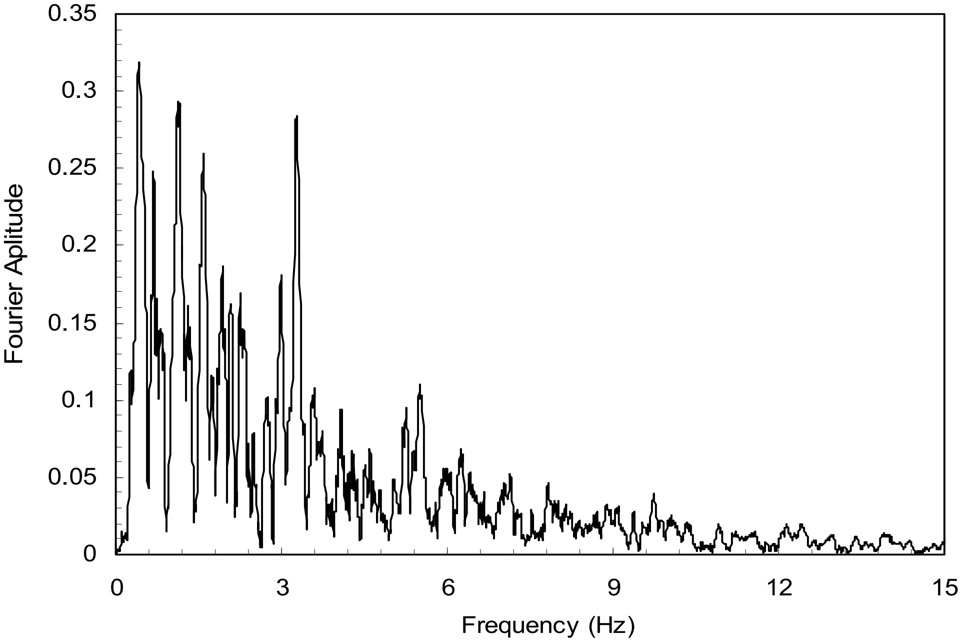

Figure 3.19 Fourier Spectrum of Northridge Earthquake

Table 3.6 Frequency Content for Northridge Earthquake

Earthquake : **Northridge**			
Major frequency range	0.4Hz ~ 3.5Hz		
Dominant Frequency order	**Frequency (Hz)**	**Power Amplitude**	**Fourier Amplitude**
1st	0.415	0.207	0.318
2nd	1.123,1.16	0.175	0.293
3rd	3.271	0.164	0.284
4th	1.587	0.138	0.26

3.6.4 Parkfield

The epicenter of Parkfield earthquake was in Parkfield, California. It occurred on 28th of June, 1966. The data was collected in station Cholame #2, 065 (CDMG STATION 1013). The earthquake magnitude was 6.1 on the Richter scale, and the total duration of the record was 43.7 seconds. The ground acceleration data was taken with 0.01 sec interval. Parkfield represents the medium-frequency earthquake. Its major frequency range is between 0.5 Hz to 1.75 Hz based on the Fourier spectrum obtained from the SeismoSignal software. Figure 3.20 represents the acceleration time history of Parkfield earthquake in terms of the gravitational acceleration, g. Figure 3.21 represents the Fourier transformation of the earthquake. The first 40 seconds of the record are used for time history analysis.

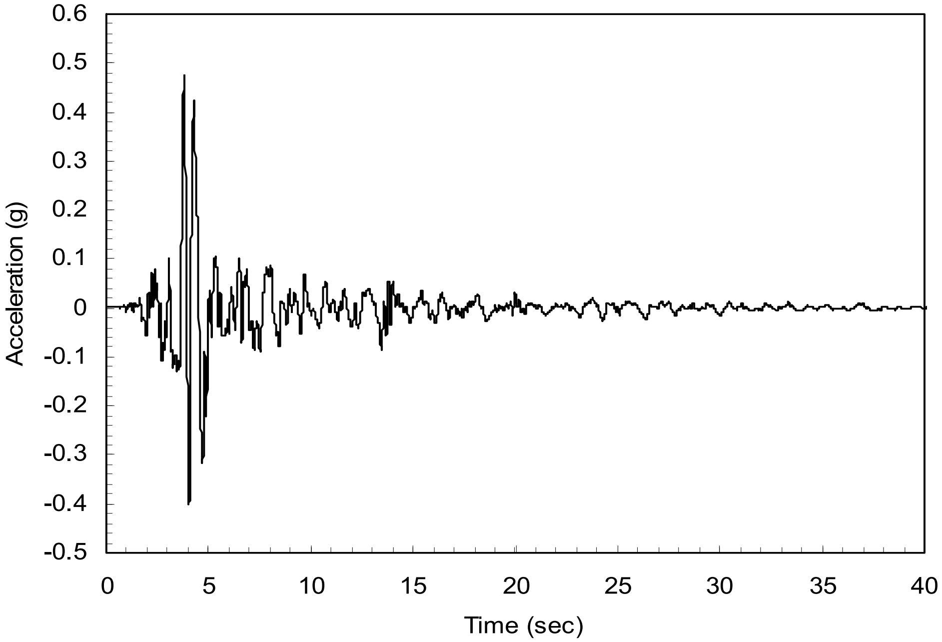

Figure 3.20 Acceleration Time History of Parkfield Earthquake

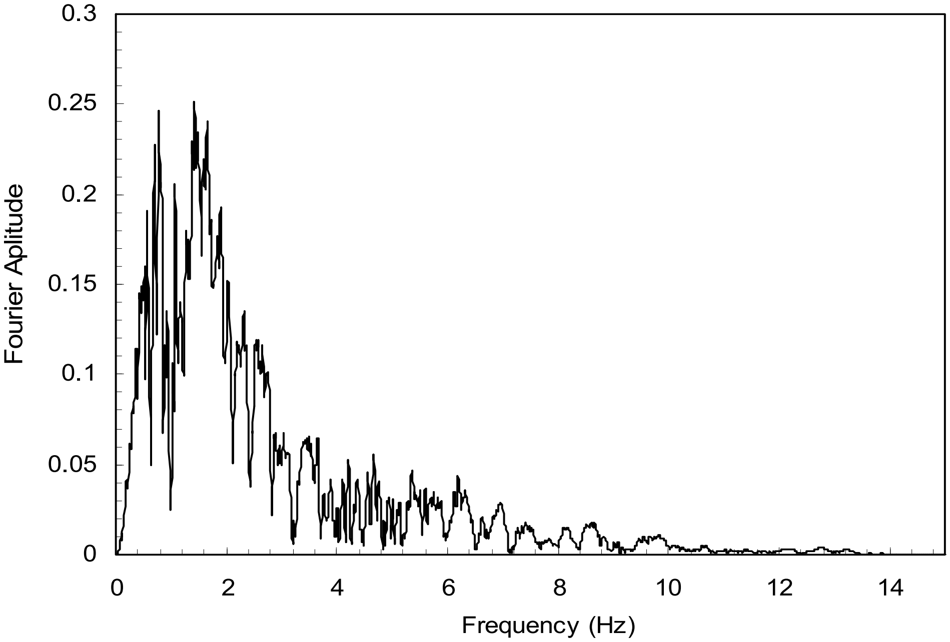

Figure 3.21 Fourier Spectrum of Parkfield Earthquake

Table 3.7 Frequency Content for Parkfield Earthquake

Earthquake : **Parkfield**			
Major frequency range	0.5Hz ~ 1.75Hz		
Dominant Frequency order	**Frequency (Hz)**	**Power Amplitude**	**Fourier Amplitude**
1st	1.428	0.174	0.251
2nd	0.781	0.166	0.246
3rd	1.648	0.158	0.24
4th	0.708	0.142	0.227

3.6.5 Kocaeli

Kocaeli earthquake occurred on August 17, 1999 in the North Anatolian Fault Zone with a macro seismic epicenter near the town of Gölcük, a sub-province of Kocaeli in the western part of Turkey. Two earthquake data from two site locations are used for this earthquake; one is Afyon Bay,N (ERD), Turkey and the other is Aydin,S (ERD), Turkey. The earthquake magnitude was 7.4 on the Richter scale. The total duration of the record for each site was 180.6 and 220.2 seconds respectively. For Afyon Bay N(ERD), data were recorded with 0.0078125 second interval, and for Aydin S(ERD), data were recorded with 0.01 second interval. Kocaeli can be represented as a low frequency earthquake. Its major frequencies for Afyon Bay, N(ERD) record range between 0.80 Hz to 1.2 Hz, and for Aydin, S(ERD) record, this range is between 0.25 Hz to 0.75 Hz. These ranges are based on the Fourier spectrum obtained from the SeismoSignal software. Figure 3.22 and 3.24 presents the acceleration time history of Kocaeli earthquake in terms of the gravitational acceleration, g for two different records. Figure 3.23 and 3.25 represents the Fourier transformation of the corresponding earthquake records.

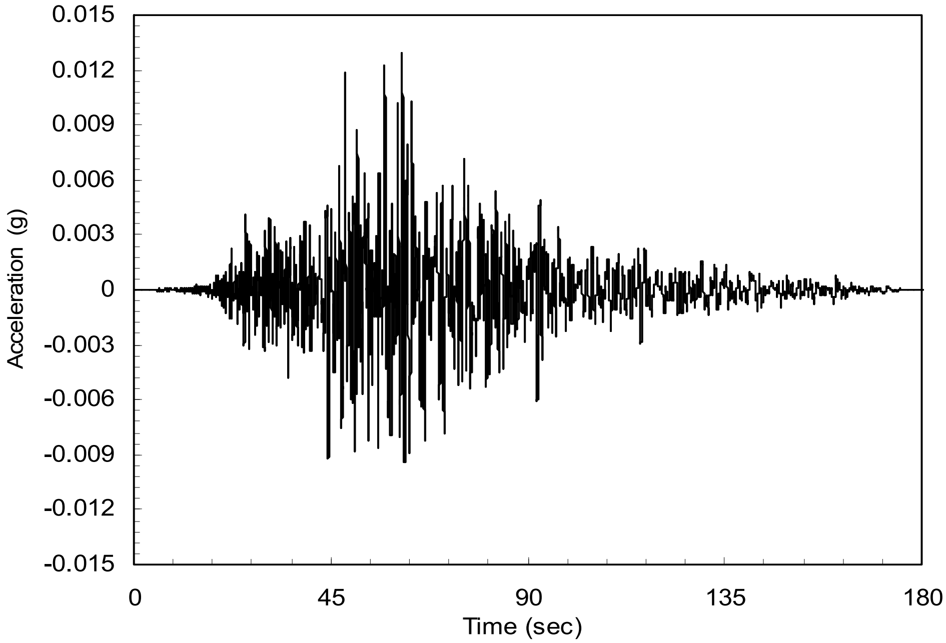

Figure 3.22 Acceleration Time History of Kocaeli[Afyon Bay,N(ERD)] Earthquake

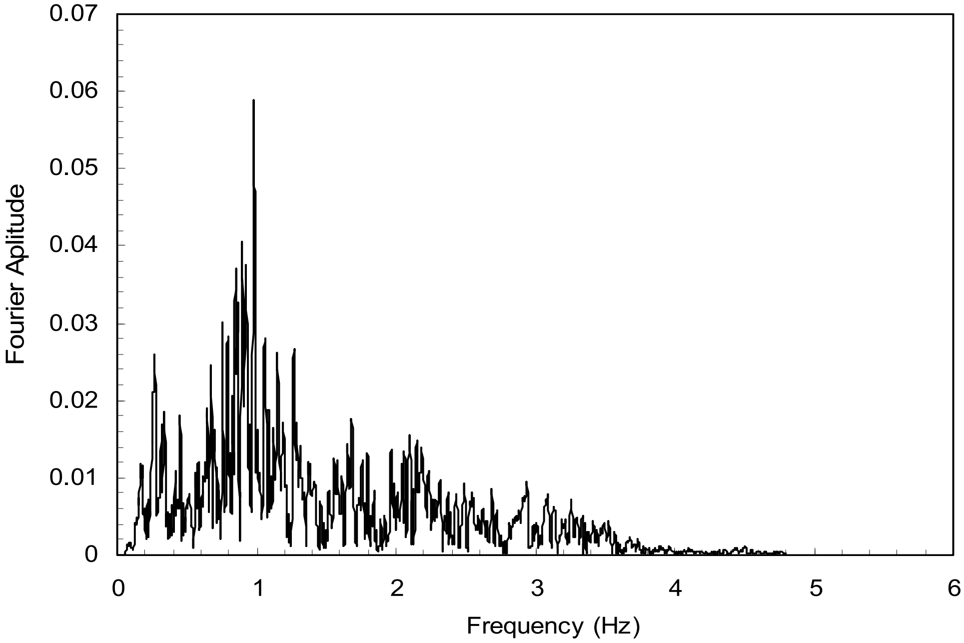

Figure 3.23 Fourier Spectrum of Kocaeli[Afyon Bay,N(ERD)] Earthquake

Table 3.8 Frequency Content for Kocaeli[Afyon Bay,N(ERD)] Earthquake

Earthquake : **Kocaeli[Afyon Bay,N(ERD)]**			
Major frequency range	0.80Hz ~ 1.2Hz		
Dominant Frequency order	**Frequency (Hz)**	**Power Amplitude**	**Fourier Amplitude**
1st	0.98	1.496	0.059
2nd	0.898	0.705	0.04
3rd	0.922	0.611	0.038
4th	0.848	0.584	0.037

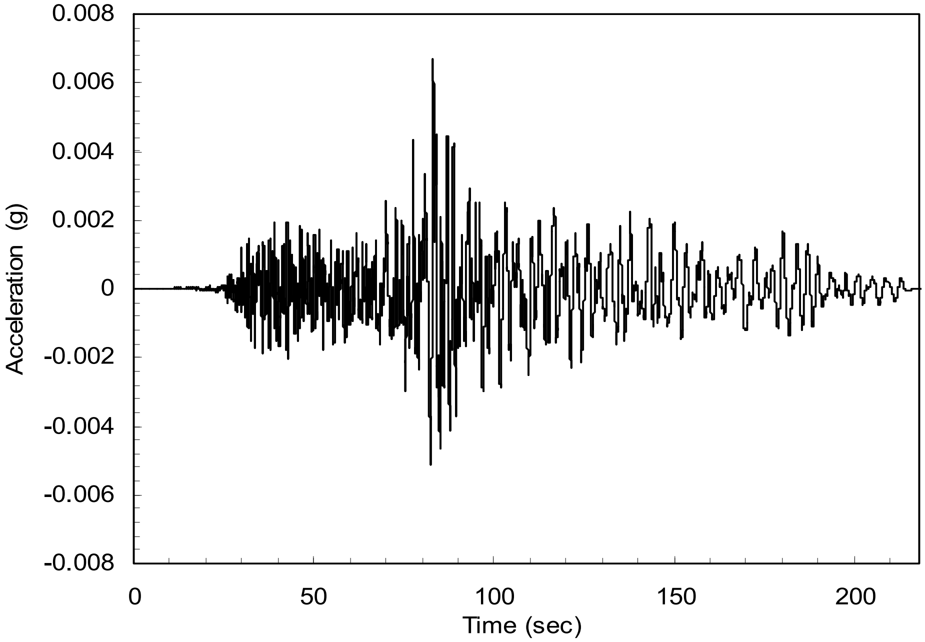

Figure 3.24 Acceleration Time History of Kocaeli[Aydin,S(ERD)] Earthquake

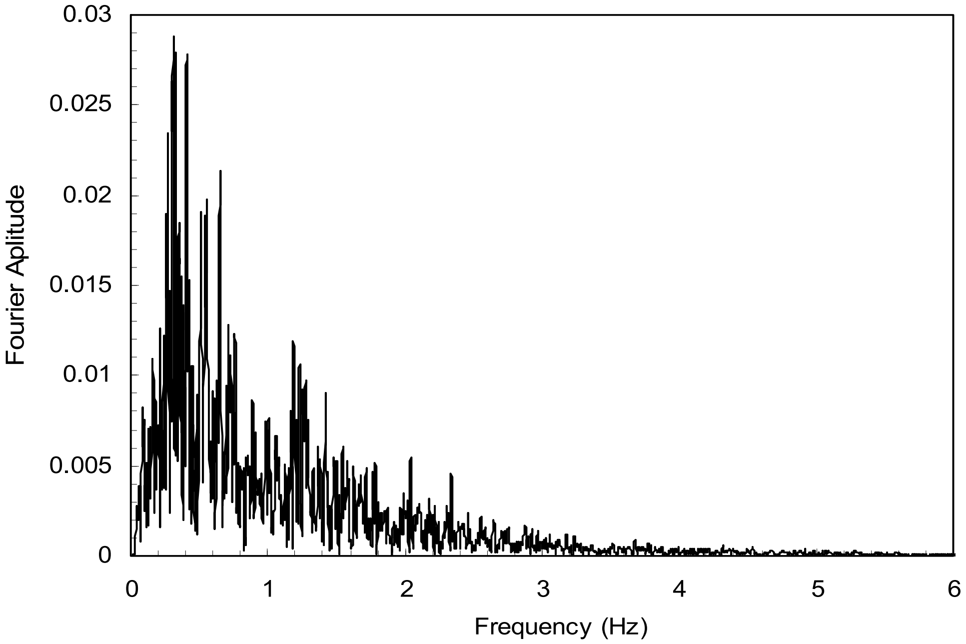

Figure 3.25 Fourier Spectrum of Kocaeli[Aydin,S(ERD)] Earthquake

Table 3.9 Frequency Content for Kocaeli[Aydin,S(ERD)] Earthquake

<table>
<tr><td colspan="4">Earthquake : Kocaeli[Aydin,S(ERD)]</td></tr>
<tr><td>Major frequency range</td><td colspan="3">0.25Hz ~ 0.75Hz</td></tr>
<tr><th>Dominant Frequency order</th><th>Frequency (Hz)</th><th>Power Amplitude</th><th>Fourier Amplitude</th></tr>
<tr><td>1st</td><td>0.308</td><td>1.258</td><td>0.029</td></tr>
<tr><td>2nd</td><td>0.33</td><td>1.184</td><td>0.028</td></tr>
<tr><td>3rd</td><td>0.406</td><td>1.164</td><td>0.028</td></tr>
<tr><td>4th</td><td>0.299</td><td>1.044</td><td>0.026</td></tr>
</table>

Dominant frequency content for all the earthquakes considered are given below :

Table 3.10 Dominant frequency order for the considered earthquake

Dominant Frequency Order	Major Earthquake Frequency Range (Hz)				
	Elcentro	Northridge	Parkfield	Kocaeli Afyon Bay	Kocaeli Aydin
1st	1.172	0.415	1.428	0.98	0.308
2nd	2.148	1.123,1.16	0.781	0.898	0.330
3rd	1.782	3.271	1.648	0.922	0.406
4th	2.075	1.587	0.708	0.848	0.299

3.7 Discussion of the Results

This study starts with the analysis of low rise to high rise steel frames, under different earthquake excitations. Low rise structures are expected to be more vulnerable in high frequency earthquakes than the high rise structures. On the other hand, high rise buildings are more vulnerable in low frequency earthquakes comparing to the low rise buildings. Rhombus shape frames are stiffer than the rectangular shape frames, thus the natural frequency of rhombus frames are higher than the rectangular frames with same aspect ratio. This is described in the previous sections from Table 3.1 to Table 3.4.

In the 3-story, 9-story, 12-story and 20-story frames, rhombus shapes experienced less displacement than the rectangular frames in earthquake analysis. This effect is discussed in terms of top node displacement, lateral sway profile of the frame, and inter story lateral drift. The comparisons between rhombus and rectangular shapes in this chapter are based on the assumption of all the connections being rigid.

Top displacement profiles for the whole time range for an earthquake are shown in Figure A.1 through A.20. For all the frames with different earthquakes, rhombus shape improves building performance than the rectangular shape. In most of the cases, top displacement for rectangular frame is higher than the top displacement for the rhombus frame. Only, for 20S-289_100_2.89 buildings, rhombus shape has comparable top node displacement with the rectangular frame for Parkfield and Afyon Bay record of Kocaeli earthquakes. This is due to the reason that, 20S-289_100_2.89 rhombus frame has natural frequency close to the 4th dominant frequency for Parkfield and Afyon bay records.

Maximum lateral displacement of each floor is plotted from Figure E.1 through E.20. These sway profiles show the maximum lateral displacement of each floor for the total time range of an earthquake. Maximum lateral displacement may occur at different time for different floor level. All the rhombus frames improve building performance than the rectangular frame. But, for 20S-289_100_2.89 rhombus shape, some lower levels of the frame experience a little bit higher displacement than the rectangular frames for Parkfield and Afyon Bay records of Kocaeli earthquakes.

Lateral drift ratio for all the rigid frames are plotted in Figure F.1 through F.20. These inter story drift ratios are calculated with the relative displacement of each floor from the floor below, divided by the corresponding floor height. This parameter is very significant in performance based engineering and should be in acceptable limit as per the requirement of different performance levels. Most of the rhombus shape has less inter story drift ratios compared with the rectangular shape. Only, in the case of 20S-289_100_2.89 rhombus frame, few stories experience a little more drift than the rectangular shape frame for Parkfield and Afyon Bay records for Kocaeli earthquakes.

Performance of the individual rigid frame shapes are closely observed also in terms of internal forces. Axial force, shear force and bending moments are compared. For comparison purpose, maximum internal force values from each floor for rhombus shape is compared with the maximum value from each floor for rectangular shape. Both beams and columns are compared. Diagonal elements for rhombus shapes are considered as columns.

Most of the bending moment ratios between rhombus and rectangular frames in Figure D.1 through D.20 are less than 1. For 3-story frames, bending moment for beams and columns from rhombus frames are much lower than the rectangular frames. The lowest bending moment demand in a column from rhombus frame is around 42 times lower than the rectangular frame. And in case of beam, bending moment demand is around 32 times lower than the demand for rectangular frame.

In the 9-story frames, all the bending moment ratios are less than one except in one story, where demand increases around 17 percent in a column moment for El Centro earthquake. The largest reduction for rhombus frame demand is 25 times lower in beam moment and 33 times lower in column moment than the rectangular shape demand for Aydin record of Kocaeli earthquake. For 12-story frames, most of the bending moment demands for rhombus shape are less than the demands for rectangular frame. One story requires around 30 percent increase in beam moment and two stories require maximum 24 percent increase in column moment for Parkfield earthquake. Aydin record of Kocaeli earthquake reduces the demand for rhombus shape to maximum 454 times lower in the beam moment and maximum 333 times lower in the column moment than the demand for rectangular shape.

For 20-story rhombus frame, few bottom stories require higher moment than the rectangular frame. The maximum demand for beam moment is 155 percent higher and column moment is 482 percent higher than the rectangular frame for Parkfield earthquake. Other than these few cases, in most of the stories, beam and column moment demands are lower for rhombus frame than the rectangular frame. Rhombus shape produces maximum 40 times reduction in beam moments and 53 times reduction in column moments than the rectangular frame for Northridge earthquake.

Shear force ratios between rhombus and rectangular frame as in Figure C.1 through C.20 follow the same trend as bending moment ratios. All the shear force ratios between 3-story rhombus and rectangular frames are less than 1. All the beam shear forces in a 9-story rhombus frame are less than the rectangular frame. The largest reduction is 25 times lower than the rectangular frame for Aydin record of Kocaeli earthquake. One story demands 41 percent higher column shear force than the demand for rectangular frame in ElCentro earthquake. Most of the elements in 12-story rhombus frames have less shear force demand than the rectangular frame. The largest demand reduction in shear for rhombus frame is 385 times lower for beam and 1310 times lower for column than the rectangular frame when subjected to Aydin records of Kocaeli earthquake. Demands increase in couple of stories for rhombus frame. Largest increase in shear force demand for rhombus shape is around 2 times higher in beam shear and 24 percent higher in column shear force demand than the rectangular frame.

For 20-story frame, most of the shear force ratios are less than one. Only a few bottom stories require higher shear force demand for rhombus frame. The largest shear demand is 210 percent higher for beam and 133 percent higher for column than the rectangular frame for Parkfield earthquake. The largest reduction in shear demand for rhombus frame is 18 times lower for beam shear and 133 times lower for column shear, than the rectangular frame for Northridge earthquake.

The members in a rhombus frame experience higher axial force than the rectangular frames. This is due to the inherent property of the framing system, which uses the axial stiffness to resist lateral loads. In most of the cases, axial force demands for rhombus frames are higher than the demands for rectangular frames. In all the rhombus shapes, beams in the mid levels experience higher axial loads. The largest demand for beam axial force is 199 times higher in a 20-story rhombus frame than the rectangular frame for Afyon Bay record for Kocaeli earthquake. And largest demand for column axial force is 680 percent higher in a 12-story rhombus frame column than that of a rectangular frame.

CHAPTER 4

HYBRID FRAME SYSTEMS

4.1 Introduction

High-rise 20-Story frames are considered in this study to observe the effect of semi-rigid connections in resisting earthquake excitations. Rectangular frame with SAC-20story dimensions and the equivalent rhombus frame have been used. Then, width of the rhombus frame has been increased to see the effect of semi-rigid connections on fat rhombus frame. Bi-linear moment rotation curve has been used for assigning semi-rigid connection properties. Three different semi-rigid connection properties have been used. Semi-rigid connections are used along all the beam ends from level 7 to level 11. Hybrid frames with rigid and semi-rigid connections are subjected to several earthquake data, and the change in global behavior of the frame is closely observed.

To describe the results, a general building designation is adopted for convenience,

_S – H_W_H/W- OP(_,/ _) – EQ – E_(B-L) , where,

S = story

H = the height of the frame

W = the width of the frame

H/W = the height to width ratio of the frame

OP = out put, which can be member forces or displacement

AF = axial force

SF = shear force

BM = bending moment

TDUx = top node displacement along X-direction

MDUx = maximum lateral displacement along X-direction

LDr = lateral inter story drift

RMR = Rigid Rhombus frame

RCR = Rigid Rectangular frame

RMSR = Semi-rigid Rhombus frame

RCSR = Semi-rigid Rectangular frame

EQ = earthquake

ELC = El Centro earthquake

NRG = Northridge earthquake

PKF = Parkfield earthquake

KCL1 = Afyon Bay record for Kocaeli earthquake

KCL2 = Aydin record for Kocaeli earthquake

E = the initial stiffness for the semi-rigid connections. Only the initial stiffness value has been used in the building designations to express the semi-rigid connections properties. Details of the connection properties with designations are given in section 4.2.3.

B = the beginning story of the range in which semi-rigid connections are placed.

L = the last story of the range in which semi-rigid connections are placed.

The building designation follows: 20S – 289_100_2.89 – BM(RMSR/RMR) – NRG – E1m(7-11), which will describe a 20 story frame with height to width ratio of 2.89, where the height and the width are 289 ft and 100 ft respectively. It will express bending moment as out put, and the result will be the ratio of bending moment between Rhombus frame with semi-rigid connections and the Rhombus frame with all rigid connections. The frames are analyzed under Northridge earthquake. And the last part defines, that initial stiffness of the semi-rigid connection is 1 million, which are placed at the beam-to-column joints from story 7 to 11.

4.2 Semi-rigid Connection

Connections in a beam-column frame are used to transfer internal forces from one member to another. Generally, a beam-column connection assumed as either rigid or pinned. In a rigid connection, it is assumed that the stiffness of the connection is large enough to transfer all the moments from the beam to column to provide lateral stiffness, and in this process, the relative rotation between the members will be zero. On the other hand, in a pinned connection, no moment will be transferred between the connecting members. But in the real structures, connections do not behave either of these two ideal conditions. Many connections that are been widely used in the present day, fall between these two conditions. When a moment is applied to a connection, there will be some relative rotation (in case of rigid connection which is assumed to be zero) between the adjoining members. And this type of connection is termed as semi-rigid connections.

4.2.1 Moment-Rotation models

Semi-rigid connection is one of the major sources of nonlinearity in a steel frame. Generally, the axial and shear deformations are assumed to be negligible compared to the flexural deformation. For that reason, only the flexural deformation is considered to have effect on rotational deformation of a connection in this study. Figure 4.1 shows rotational deformation of a connection.

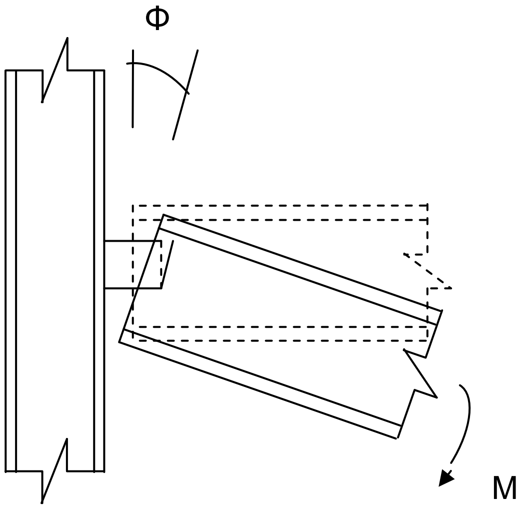

Figure 4.1 Rotational deformation of a connection due to flexure

Thus, a moment versus rotation curve can express the connection behavior in a form of, $M = f(\varphi)$, where M is the connection moment, and φ is the relative rotation between the adjoining members. Many analytical, mathematical and mixed models, which combine analytical and mathematical models, are proposed. In a moment-rotation curve, the basic properties are strength, stiffness and the ductility. These properties are shown in Figure 4.2.

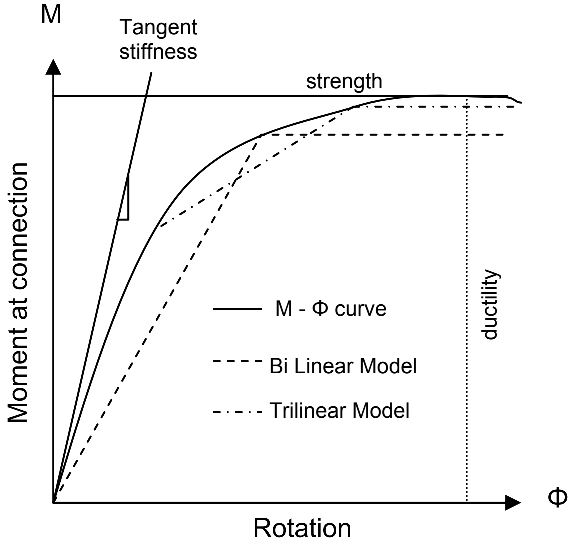

Figure 4.2 Typical moment-rotation curves

To include the effect of a semi-rigid connection, a connection spring can be introduced at the joining point of a beam and column. The two ends of a beam thus connected by the spring with the columns formed a hybrid element, which is shown in Figure 4.3. Rotation of the connection is defined as the relative angle between the two ends of the spring which is assumed to be a zero length element.

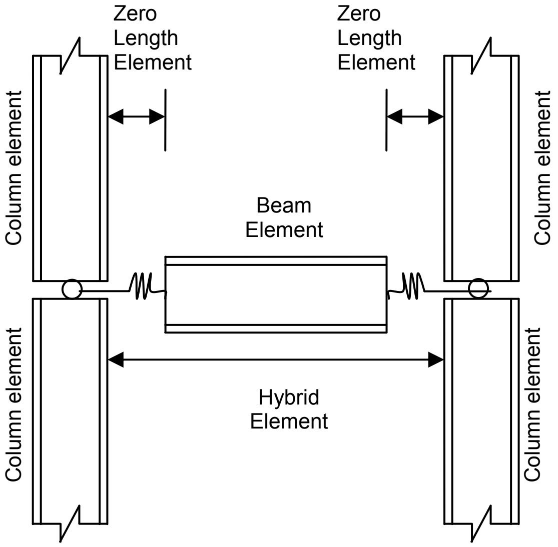

Figure 4.3 Semi-rigid element of a Hybrid frame

4.2.2 Bi-linear semi-rigid Connection Properties

A moment-rotation curve is used as a medium to express the nonlinear behavior of a connection. Many M- φ relations have been proposed. In this study, to simulate semi-rigid behavior of the connection, different bilinear moment-rotation curves have been used for simplicity, with no provision for ultimate capacity. A general bilinear moment rotation curve is shown in Figure 4.4.

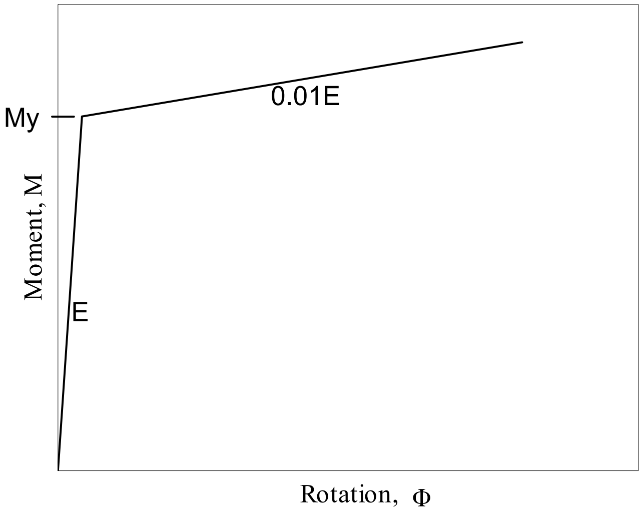

Figure 4.4 Bi-linear moment-rotation curve

Figure 4.4 shows bilinear connection model used in this study, which requires few parameters to describe. These are initial and post yield stiffness and yield moment. In all the cases, ratio of the post yield to initial stiffness is taken as 0.01. The initial stiffness of the connection changes from a low value to higher one in an attempt to describe a wide range of semi-rigid connections. Yield moment value changes with the initial stiffness. The different parameter values are tabulated in Table 4.1.

Table 4.1 Semi-rigid Connection properties

Designation	Initial Stiffness kip-in/rad	Post-Yield Stiffness kip-in/rad	Post yield to initial stiffness ratio	Yield Moment kip-in
E1m	1,000,000	10,000	0.01	1989
E3m	3,000,000	30,000	0.01	2323
E5m	5,000,000	50,000	0.01	3030

4.3 Two-Story Test Frame

For verification of the proposed modeling for semi-rigid connection, a simple structure is required whose response is known. For this purpose a 2-Story one bay frame, which is analyzed before using semi-rigid connection by Bhatti and Hingtgen (1995) and King and Chen (1993) was chosen. The geometry and dimensions of that simple frame modeled by them is shown in Figure 4.5. In this study, this frame is modeled in Opensees software in an attempt to verify it's capability to incorporate semi-rigid connection property in the region of beam-column connections. Four vertically downward 100 kips load is acting at node 3, 4, 5 and 6; and two horizontal 10 kips load is acting at node 3 and 5.

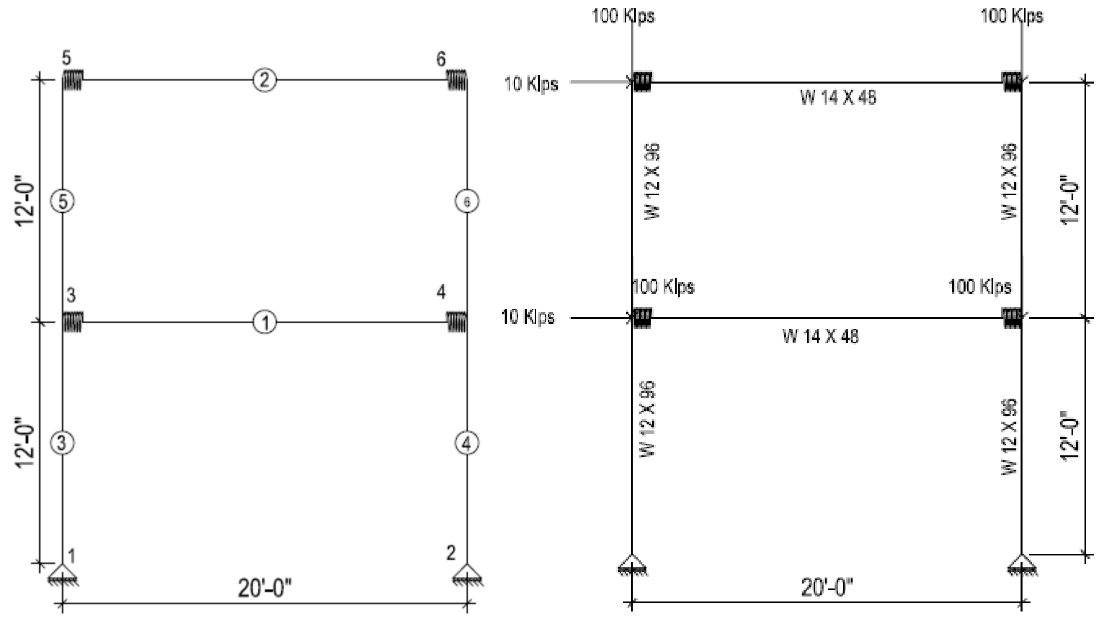

Figure 4.5 Two story one bay test frame

At first, the frame is analyzed assuming all the connections being rigid with no geometric effect and the results are compared with the previous results from the papers. In the next stage, geometric effect is considered in the form of P-Δ effects with the connections being rigid. Finally, both the geometric nonlinearity (P-Δ) and the connection nonlinearity are incorporated. Connection nonlinearity is due to the semi-rigid property of the connections. Semi-rigid connections are being simulated using zero length spring elements at the end of the beam elements. Each 2-noded spring element has two transitional and one rotational degree of freedom at each node. But transitional degrees of freedom are assumed identical and rotational degrees of freedom are different to simulate relative rotation as in semi-rigid connection.

For moment-rotation curve, a bilinear elastic plastic moment-rotation curve has been used. The moment-rotation curves used by King and Chen (1993) and Bhatti and Hingtgen (1995) are shown in Figure 4.6. Present study follows the M-φ relationship used by Bhatti and Hingtgen (1995), where they assumed initial stiffness for elastic region with a value of 786732 kip-in/rad and Yield moment as 1989 kip-in.

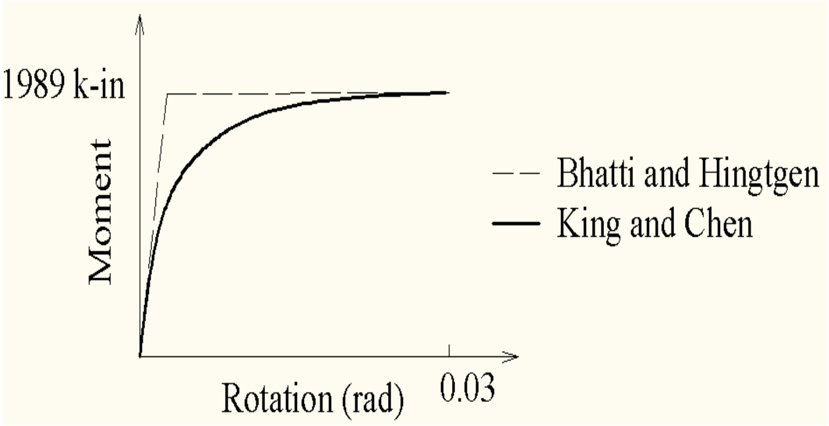

Figure 4.6 Moment-Rotation relation used in previous study (Bhatti and Hingtgen,1995)

Lateral displacements at node 3 and 5, and absolute bending moments of all the elements are tabulated in Table 4.2 and 4.3 for comparison.

Table 4.2 Lateral displacement (inch) for 2-Story test frame

	Rigid without P- Δ		Rigid with P- Δ		Semi-rigid with P- Δ	
	Node #3	Node#5	Node #3	Node #5	Node #3	Node #5
Bhatti & Hingtgen	1.011	1.509	1.168	1.731	1.477	2.292
King & Chen	-	-	1.16	1.82	2.02	3.26
This Study	1.01184	1.51099	1.1623	1.72528	1.47056	2.28543

Table 4.3 Absolute Maximum Bending Moment (kip-inch) for 2-Story test frame

Element #		1	2	3	4	5	6
Rigid without P- Δ	Bhatti & Hingtgen	1450	711	1443	1437	711	711
	King & Chen	-	-	-	-	-	-
	This Study	1449	711	1443	1437	711	711
Rigid with P- Δ	Bhatti & Hingtgen	1654	795	1677	1669	794	795
	King & Chen	1649	794	1670	1664	794	794
	This Study	1653	796	1675	1669	796	796
Semi-rigid with P- Δ	Bhatti & Hingtgen	1634	902	1739	1731	902	902
	King & Chen	1560	1116	1837	1834	1116	1116
	This Study	1633	903	1736	1731	903	903

The data presented in Table 4.2 and 4.3 verifies that the output from Opensees is reliable based on the previous results. The results from the present study are much closer with the results from Bhatti and Hingtgen (1995), as in both the cases moment-rotation relation is similar which is a bilinear elastic plastic curve, while King and Chen (1993) had used a different moment-rotation relation which may cause some difference.

4.4 20-Story Rectangular Hybrid Frame

Initially, a 20story frame has been modeled in Opensees software with SAC 20-Story building dimensions. This 20-Story 5 bay frame is used in this study to observe the effect of earthquake on high-rise buildings. The rectangular frame is 100 ft wide with 20 ft bay dimension, and the total height of the building is 289ft with two basement floor, 12ft each. All the member sizes are W24 X 131. Total dead load and 25 percentages of live loads are considered for calculating effective seismic load. Load calculations are described in Appendix G. At first, all the connections are considered to be rigid. Later, partially restrained connections are incorporated in the structure to see the effect of semi-rigid connections in the hybrid frames. All beam-to-column connections from level-7 to 11 are modeled as partially restrained. This configuration is selected based on the previous study by Dobrinka Radulova (2009). The semi-rigid connections are incorporated in the model by using a zero length spring element at the ends of the beam members as shown in figure 4.3. Then, the semi-rigid connection property is assigned to this spring element. Three different semi-rigid connections as per Table 4.1 have been used. 20-story rectangular hybrid frame is shown in Figure 4.7. One rigid and three 20-story hybrid rectangular frames are analyzed under five different earthquake excitation records. Performance of the hybrid rectangular frame is compared with the rigid rectangular frame and rigid rhombus frame.

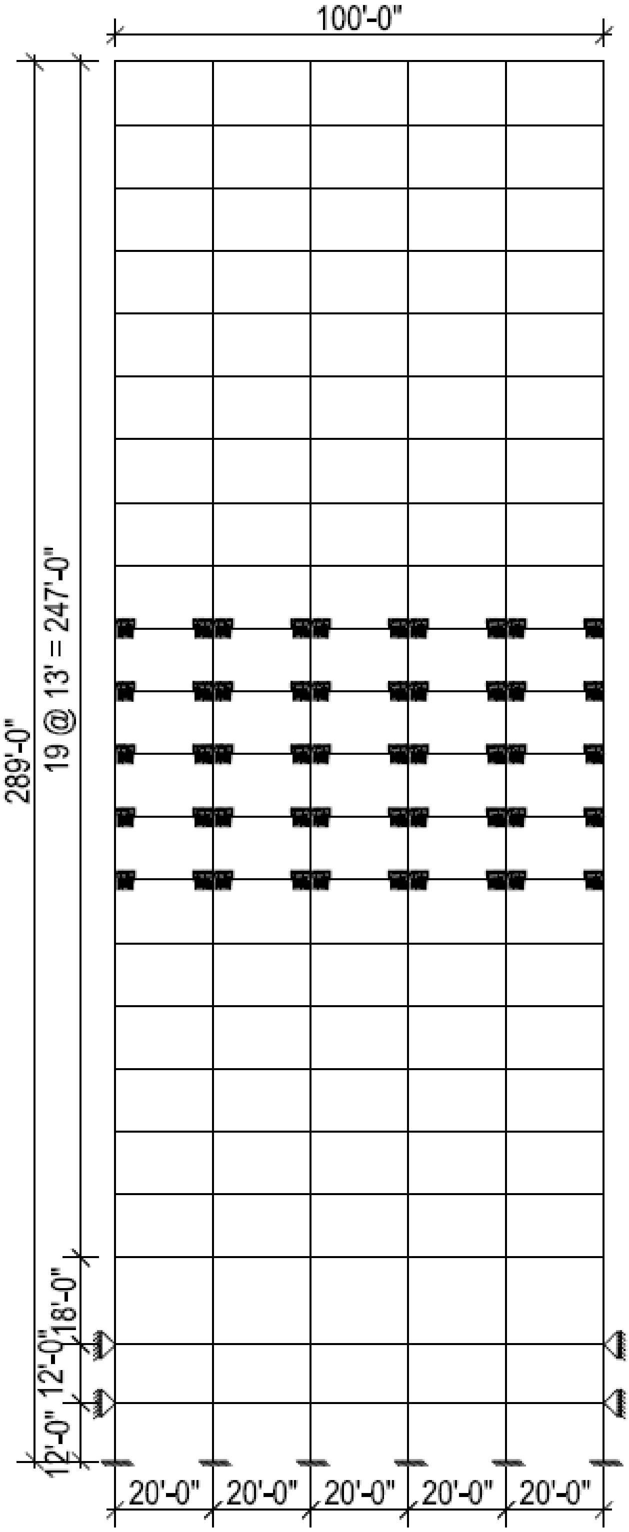

Figure 4.7 Hybrid Rectangular: 20S – 289_100_2.89 – (RCSR) – E(7-11)

4.5 20-Story Rhombus Hybrid Frame

The 20-Story base rhombus frame has been modeled in Opensees software as discussed in section 3.5. This frame is used in this study to observe the effect of semi-rigid connections on rhombus shape buildings. To see the effect of height-to-width ratio on the performance of the high rise structure, total width of this building is increased to 300ft. From 5, bay number increases to 15; Total Height and individual bay width remain same. All the member sizes are W24 X 131. At the beginning all the connections are considered to be rigid. Then, partially restrained connections are used on all the beam ends from levels 7 though 11. The semi-rigid connections are introduced as a zero length spring element following the previous section 4.4. Three different semi-rigid connections as per Table 4.1 have been used. 20-story rhombus hybrid frames are shown in Figure 4.8 and 4.9. Two rigid and six 20-story hybrid rhombus frames are analyzed under five different earthquake excitation records.

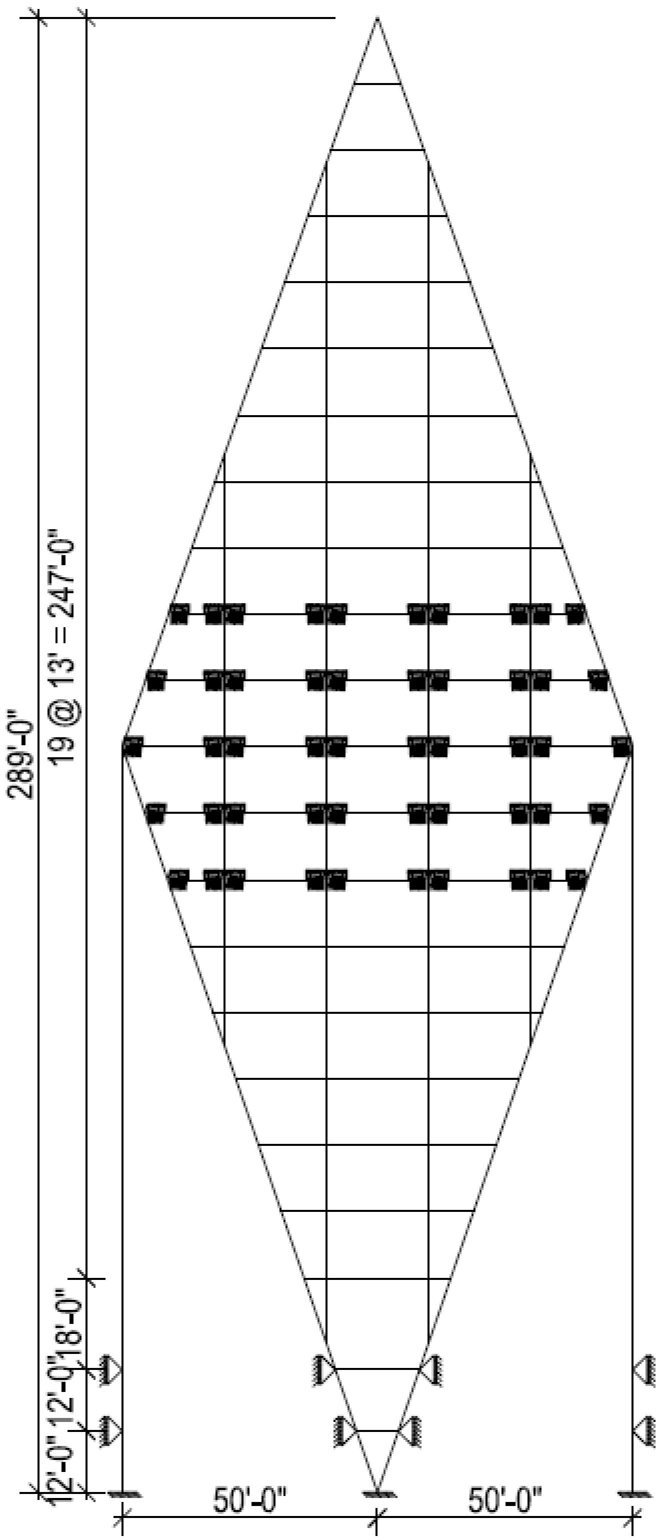

Figure 4.8 Hybrid Rhombus: 20S – 289_100_2.89 – (RMSR) – E(7-11)

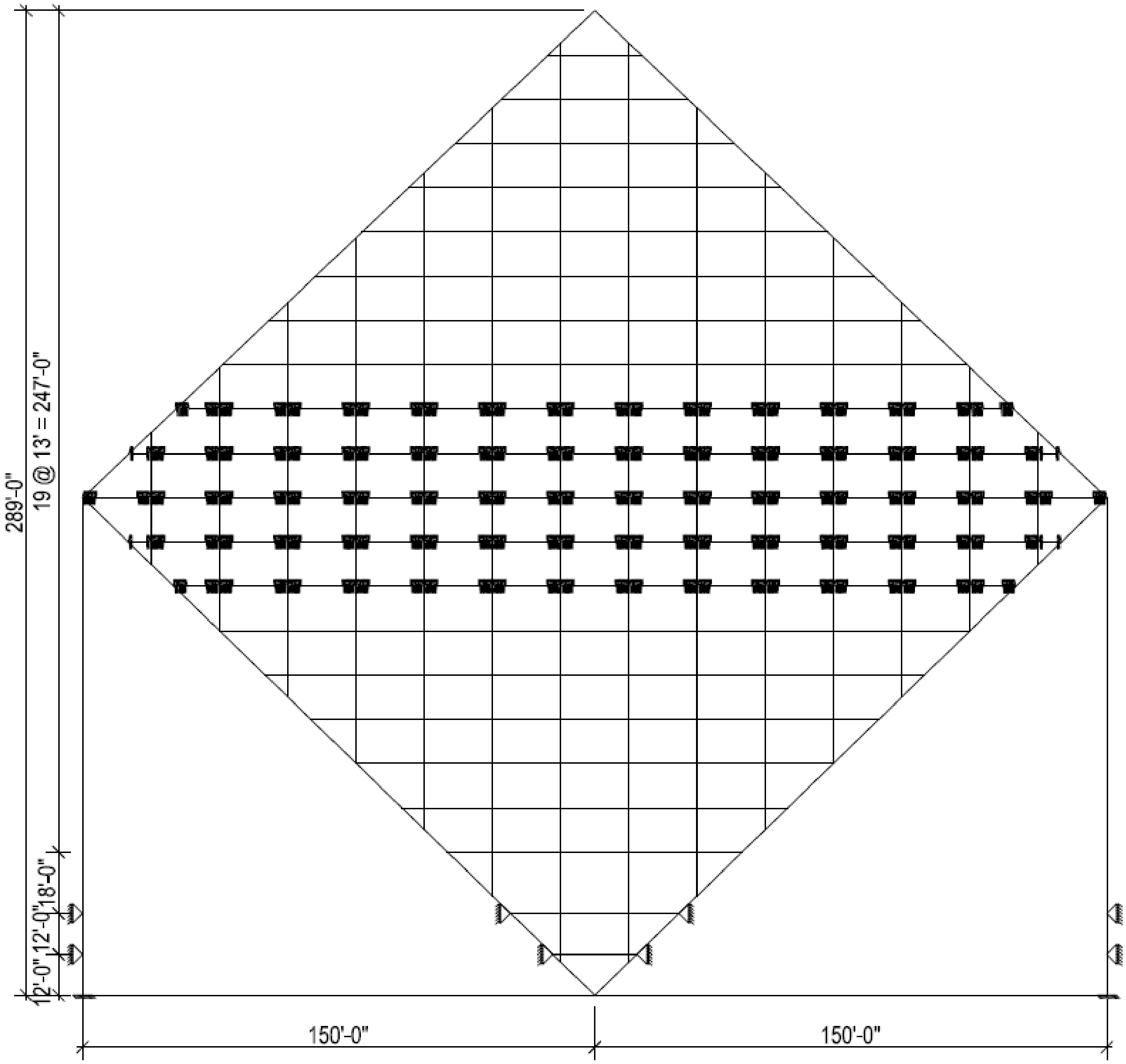

Figure 4.9 Fat Hybrid Rhombus: 20S – 289_300_0.963 – (RMSR) – E(7-11)

4.6 Discussion of the Results

In this chapter, hybrid frames are compared with the corresponding rigid frames. Then, the rectangular hybrid frame is compared with the rigid rhombus frame. Hybrid rectangular frames show improved performance than the rectangular rigid frame in most of the cases. Top node displacements for rectangular rigid and hybrid frames are shown in Figure A.21 through A.25. Maximum displacements for each story are plotted from Figure E.21 through E.25. Figure 4.10 shows the displacement profile for 20S – 289_100_2.89–(RCR, RCSR)–E1m (7-11) frames. It shows, for ElCentro, Northridge and Parkfield earthquakes, maximum lateral sway decreased for hybrid rectangular frame comparing to the rigid rectangular frame. But hybrid frame gives more lateral displacement than rigid frame when subjected to the Kocaeli earthquakes.

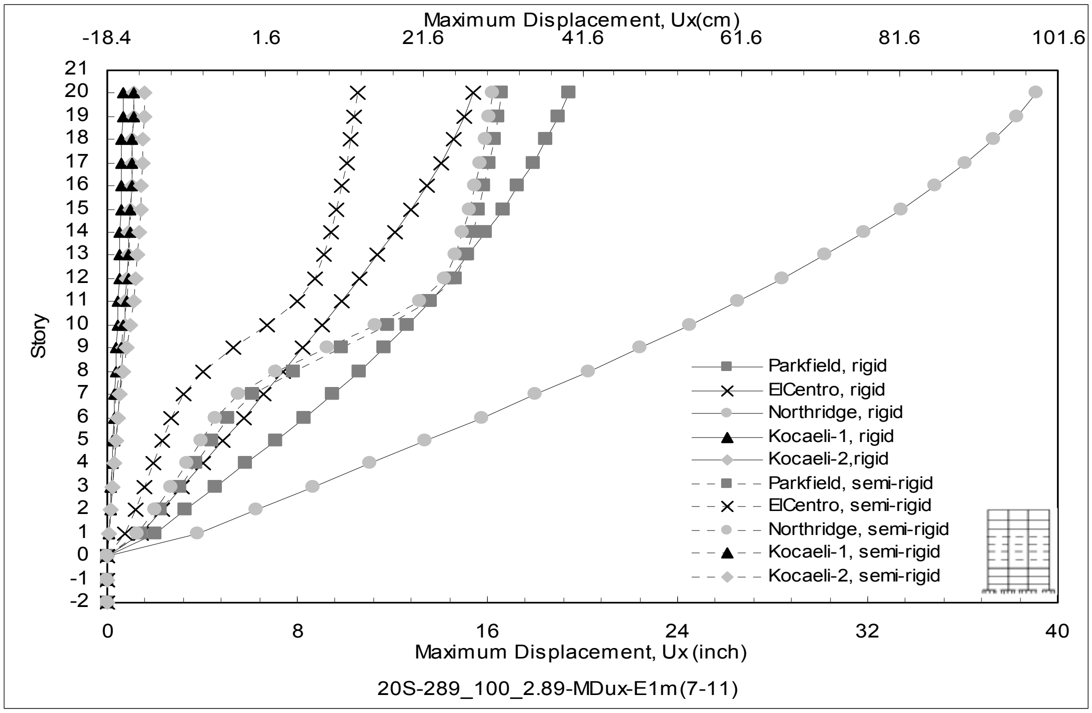

Figure 4.10 Maximum lateral sway 20S-289_100_2.89–MDUx (RCR,RCSR)–E1m(7-11)

This can be explained by comparing the frequency of the frame with the earthquake frequencies. Earthquake frequencies are tabulated in chapter 3 from Table 3.5 through 3.10. Hybrid and rigid frame frequencies obtained from the Opensees software are tabulated in Table 4.4.

Table 4.4 Rectangular rigid and hybrid frame frequencies (Opensees)

Mode	20S –289_100_2.89–RCR	20S-289_100_2.89-RCSR-E1m (7-11)
	(Hz)	(Hz)
1	0.3962	0.34146
2	1.24918	1.18438
3	2.24456	1.89239
4	3.21852	2.85043
5	4.24537	3.92719
6	5.30505	4.73884
7	6.42361	5.98415
8	7.58788	7.08584
9	8.80896	8.24295
10	10.0716	9.56393

First two mode frequencies for the hybrid frame are much closer to the first two dominant frequencies for Afyon Bay and Aydin records for Kocaeli earthquake. This causes resonance effect for hybrid frame when subjected to Kocaeli earthquake. Earlier it was defined that, ElCentro and Northridge are high frequency, and Parkfield is a medium frequency earthquakes. High rise structures have low frequencies, and semi-rigid connections reduce it more. So, high and medium frequency earthquakes do not create resonance effect on hybrid rectangular frames unless the original rigid structure is too stiff.

Inter story lateral drifts for rigid and hybrid rectangular frames are plotted in Figure F.21 through F.25. Figure 4.11 shows the inter story drift profile for hybrid and rigid rectangular frame for one type of semi rigid connections. For Northridge earthquake, hybrid frame experience less drift than the rigid frame. Hybrid frame subjected to ElCentro and Parkfield earthquake gives greater drift values in the mid levels of the structure than the rigid rectangular frame. These increases in the lateral drift in hybrid frame are due to the placing of semi-rigid connections at the mid levels of the structure. Semi-rigid connections make a structure flexible and for that reason, in those levels the structure experience more drifts than the rigid frame. Both records from Kocaeli earthquake gives more drift values in hybrid frame than the rigid rectangular frame due to resonance effect discussed before.

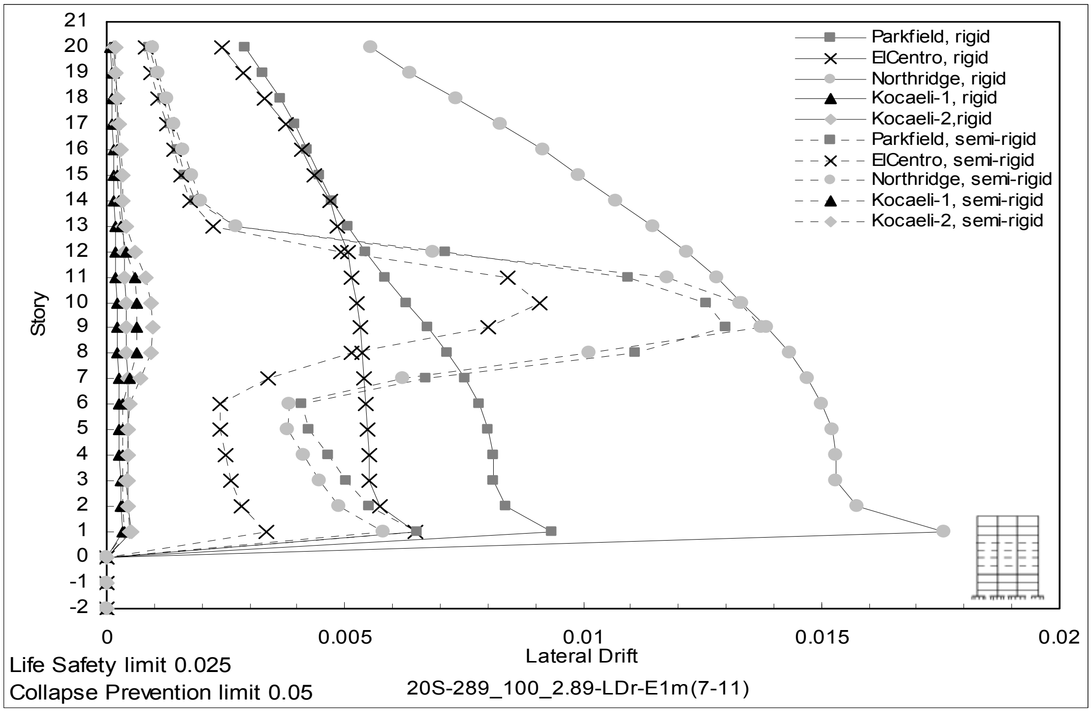

Figure 4.11 20S – 289_100_2.89–LDr (RCR,RCSR) –E1m(7-11)

Internal forces are also compared between hybrid and rigid rectangular frames. In most of the cases, hybrid frames perform better than the rigid frames, when subjected to high and medium frequency earthquakes. But hybrid frames do not perform as expected, under low frequency Kocaeli earthquake. This is due to the resonance effect. Figure 4.12 shows the beam bending moment ratios from hybrid and rigid rectangular frame.

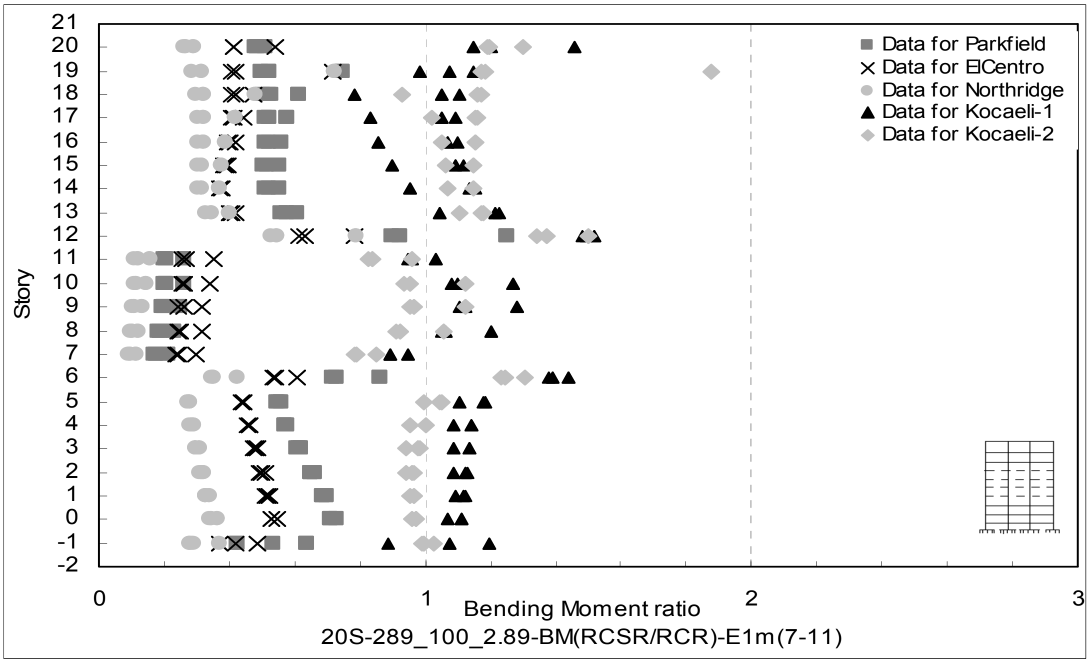

Figure 4.12 20S – 289_100_2.89 – BM (RCSR/RCR) – E1m(7-11) for Beams

Shear force and bending moment ratios in Figure C.21 thorough C.25 and D.21 through D.25 shows the similar pattern. Except low frequency Kocaeli earthquake, in most of the cases hybrid frames demand less forces than the rigid frames. The beam bending moment demand reduces 11 times lower than the demand from rigid rectangular frame. None of the beams in ElCentro and Northridge earthquake demand more beam bending force than the rigid rectangular frame. The maximum increase in beam bending moment demand is 2 times higher than the rigid frame for Aydin record of Kocaeli earthquake. Maximum column moment demand increase in hybrid frames is 2.5 times higher than the rigid rectangular frame.

Axial force ratios between hybrid and rigid rectangular frames are shown through Figure B.21 through B.25. Axial force demand for hybrid frames increase at the mid level due to the placing of semi-rigid connections at these locations. Maximum increase in beam axial force is 108 times higher than the rigid frame when subjected to Aydin record of Kocaeli earthquake. And maximum decrease in demand is 26 times lower than the rigid frame for Northridge earthquake. In most of the cases axial force demand is less for hybrid rectangular frames. Only demand increase when subjected to Kocaeli records. Highest increase is 50 percent than the rigid frame. Maximum decrease in column axial force demand is 7 times lower than the rigid rectangular frame for Northridge earthquake.

Hybrid rhombus frame is also compared with the rigid rhombus frame. But the effect of semi-rigid connections in the rhombus frame is not that much significant as observed in case of rectangular frame. Frequency of rigid and hybrid frames are almost equal. Frequencies obtained for hybrid and rigid rhombus frame modeled in Opensees software is tabulated in table 4.5.

Table 4.5 Rhombus rigid and hybrid frame frequencies (Opensees)

Mode	20S –289_100_2.89–RMR	20S-289_100_2.89-RMSR-E1m (7-11)
	(Hz)	(Hz)
1	0.64306	0.63469
2	2.251356	1.728858
3	3.985531	3.653391
4	4.878337	4.468481
5	6.906455	6.060516
6	7.946315	7.009683
7	9.560905	8.739879
8	10.88132	9.966534
9	12.51924	11.65015
10	14.31197	13.53017

Semi-rigid connections can not provide expected flexibility to the hybrid rhombus frame. As, both of the hybrid and rigid frame bear almost same frequency, Figure A.26 to A.30 and E.26 to E.30 shows top node displacement and sway profile which do not significantly varies for hybrid rhombus frames than the rigid rhombus frames. Figure 4.13 shows the lateral sway for 20S –289_100_2.89–(RMR, RMSR)–E1m (7-11) frames. Figure F.26 through F.30 show, that the frame has more lateral drift in the mid levels for hybrid frames than the rigid rhombus frame, as semi-rigid connections are placed in those places. On the other levels with rigid connections, hybrid rhombus frame demand less lateral drift than the rigid rhombus frame. Figure 4.14 shows inter story drifts for 20S – 289_100_2.89–(RMR, RMSR)–E1m (7-11) frames.

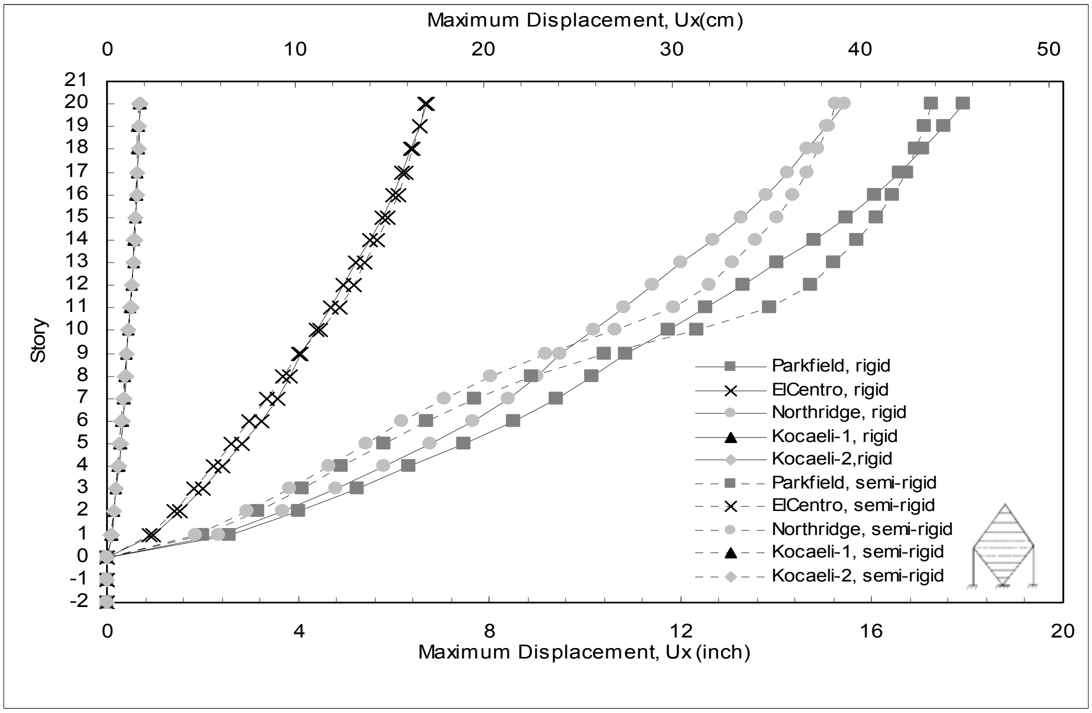

Figure 4.13 Maximum lateral sway 20S-289_100_2.89-MDUx(RMR,RMSR)-E1m(7-11)

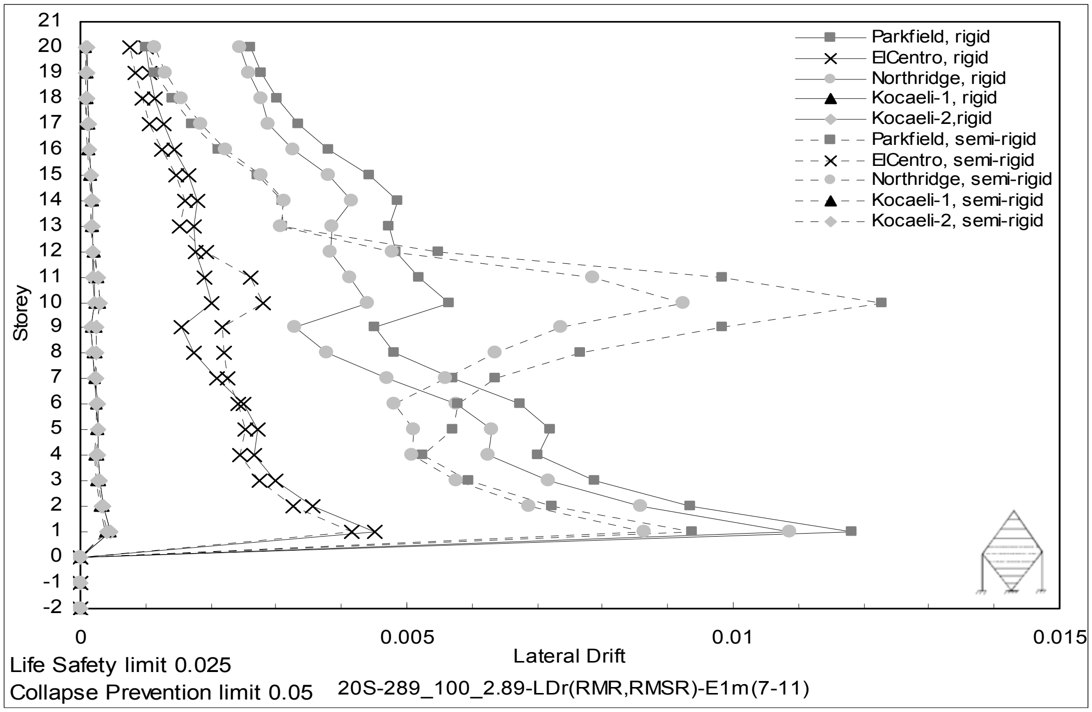

Figure 4.14 20S –289_100_2.89–LDr (RMR,RMSR)–E1m(7-11)

Hybrid rhombus frame does not show better redistribution pattern of internal forces as hybrid rectangular frame has shown previously. Placing of semi-rigid connections at the mid levels scattered points at that level for internal force ratios between hybrid and rigid rhombus frames. Below and upper level of frame does not experience significant change in demand for hybrid rhombus frame than the rigid rhombus frame. Figure 4.15 shows the beam bending moment ratio between hybrid and rigid frames.

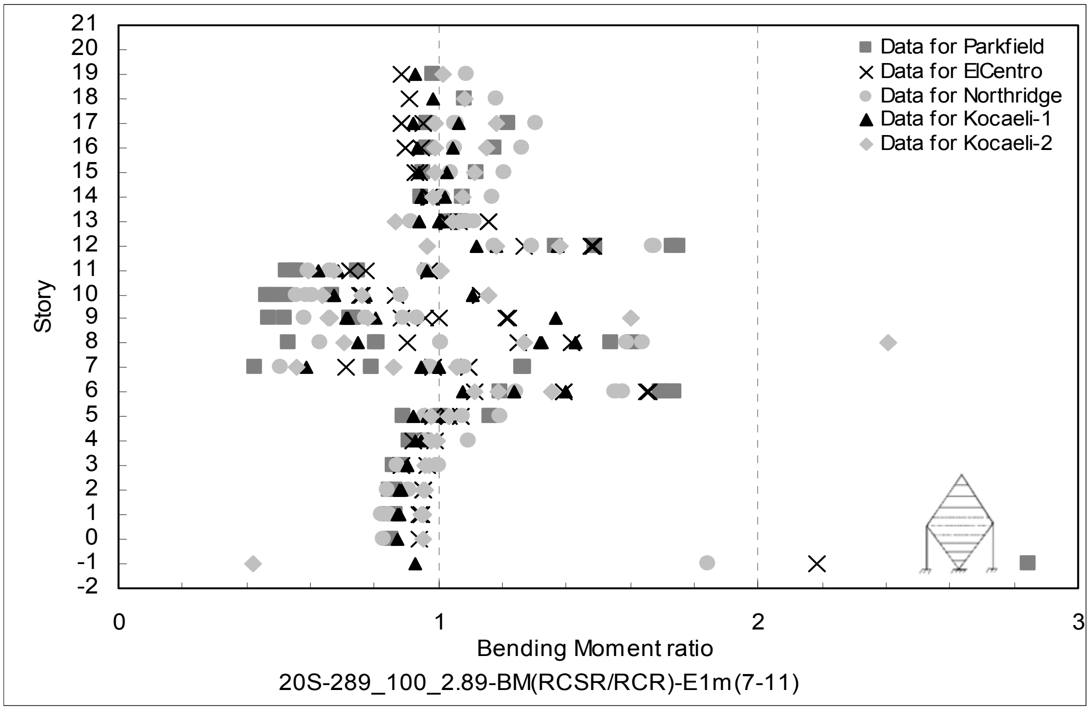

Figure 4.15 20S – 289_100_2.89 – BM (RMSR/RMR) – E1m(7-11) for Beams

With the usage of stiffer semi-rigid connections, the internal force ratios move to near 1. These are shown in figure B.26 to B.30, C.26 to C.30 and D.26 to D.30. Maximum column axial force demand for hybrid rhombus frame is around 7 times higher and minimum is 5 times lower than the rigid rhombus frame demand for Aydin record of

Kocaeli earthquake. Maximum beam shear demand is 192 percent higher and minimum demand is 138 percent lower for hybrid rhombus frame than rigid rhombus frame for Aydin record of Kocaeli earthquake. Hybrid rhombus frame demand maximum 185 percent higher moment than the rigid rhombus frame subjected to Parkfield earthquake, and minimum beam moment demand is 138 percent lower for hybrid rhombus frame than the rigid rhombus frame.

Internal forces for the rigid rhombus frames are compared to the hybrid rectangular frames. Ratios of axial force demand between rigid rhombus frame and hybrid rectangular frame are shown in figure B.31 to B.35. In most of the cases, rigid rhombus frame demands more column axial force, than the hybrid rectangular frame. The maximum demand of column axial force for the rigid rhombus frame is 5.5 times higher than the demand for hybrid rectangular frame, subjected to Parkfield earthquake. The column axial force demands on the top floors for rigid rhombus frame are significantly lower than the hybrid rectangular frame. The minimum demand for column axial force for rigid rhombus frame is 26 times lower than the hybrid rectangular frame for Aydin record of Kocaeli earthquake.

Figure C.31 to C.35 and D.31 to D.35 shows the shear force and bending moment ratios between rigid rhombus frame and hybrid rectangular frame. Rigid rhombus frame improves building performance for low earthquake records. And the minimum bending moment required by rigid rhombus frame is 71 times lower for column, and 24 times lower for beam, than the hybrid rectangular frame, for Aydin record of Kocaeli earthquake. Most of the beams and columns below mid level of the rigid rhombus frame, demand more shear force and bending moment than the hybrid rectangular frame subjected to medium and high frequency earthquakes. The maximum beam bending moment demand for rigid rhombus frame is 3.4 times higher than the hybrid rectangular frame bending demand, for Parkfield earthquake. Top floors above mid levels of rigid rhombus frame demand less shear and bending moment for column and beams. Minimum bending moment demand for rigid rhombus frame is around 12 times lower than the demand for hybrid rectangular frame for ElCentro earthquake.

Figures B.36 to B.40, C.36 to C.40 and D.36 to D.40 show the axial force, shear force and bending moment ratios between fat hybrid rhombus frame with the fat rigid rhombus frame. This frames are designated by 20S –289_300_0.963–(RMR, RMSR)–(7-11). Results from this frames show scattered point in the mid levels where semi rigid connections are placed. On the other levels, these internal force ratios move close to one.

CHAPTER 5

CONCLUSIONS AND RECOMMENDATIONS

5.1 Summary

The primary objective of this study is to present an efficient building geometric shape for earthquake force resisting frame system. A rhombus shape is created from the popular rectangular moment frame for this purpose. In the first stage, several rhombus frames have been constructed to cover from low-rise to high-rise buildings. Then, these frames are analyzed under five earthquake records with wide frequency contents. The results are compared with the rectangular frames with the same geometric aspect ratios. Then, different semi-rigid connection properties are introduced in the high rise rhombus and rectangular frames. Behaviors of hybrid frames with both rigid and semi-rigid connections, when subjected to earthquake excitations, are closely observed, and results are compared with their equivalent rigid frames. The width of the high rise rhombus frame is increased to observe the effect on seismic performance. This fat rhombus frame is also compared with its equivalent hybrid frames. In the last stage, the rigid rhombus frame is compared with the hybrid rectangular frame.

5.2 Conclusions

Comparing four rigid rhombus frames to four rigid rectangular frames under five earthquake records, the rhombus frames performed better than the rectangular frames. Introducing semi-rigid connections in the high-rise structures, the hybrid rectangular frame with rigid and semi-rigid connections showed improved performance over the rigid rectangular frame. Comparing the hybrid rectangular frame to the rigid rhombus frame, the major conclusions drawn from this study are summarized below –

- Rigid rhombus frames are much stiffer than the rigid rectangular frames.
- Top node displacements and lateral sway values from the 3-, 9-, 12- and 20-story rigid rhombus frames are less than that of the equivalent rigid rectangular frames.
- For all the considered earthquakes, 3-, 9- and 12- story rigid rhombus frames experience less inter story drift than the rectangular rigid frames. But, few stories of a 20-story rigid rhombus frame experience a little more drift than the rigid rectangular frame for Parkfield and Afyon Bay records for Kocaeli earthquakes.
- In most of the cases, rigid rhombus frames demand less shear force and bending moment than the rigid rectangular frames.
- In few cases, bottom stories of 20-story rigid rhombus frame demand more shear force and bending moment than the rigid rectangular frame. But, this is negligible comparing to the reduction of demand in other stories.
- Rigid rhombus frames demand more axial force than the rigid rectangular frames. This is true for both the beams and columns. Beams in the middle portion of the rigid rhombus frames demand maximum axial force in most of the cases.

- Semi-rigid connections increase the flexibility of the frames, and thus reduce the frequency of the structure. Semi-rigid connections have significant influence on reducing the frequency of rectangular frames; but they do not have a significant effect on rhombus frames.
- 20-story rectangular hybrid frames with semi-rigid connections in the mid levels exhibited improve building performance over the equivalent rigid rectangular frame, when subjected to medium and high frequency earthquakes. Due to reduction of frame frequency, by use of semi-rigid connection the probability of resonance in high and medium frequency earthquakes is lowered. This results in less internal forces demand. But for low frequency earthquakes, high rise rectangular frames with semi-rigid connections are good candidates to produce resonance.
- Hybrid rectangular frames exhibit more lateral drift in the stories where semi-rigid connections are placed. Sometimes this condition could result in a soft story mechanism. Experienced judgment is required for placing semi-rigid connections in rectangular frames.
- The location pattern used in this study for semi-rigid connections does not have much effect on the rhombus shape hybrid frame. Frame frequency reduces slightly. The frame does show some flexibility on the stories, where semi-rigid connections are placed, but the effect on the global behavior of the frame is insignificant.

- A fat hybrid rhombus frame behaves in the same way as a base hybrid rhombus frame.
- Redistribution of internal forces depends on the semi-rigid connection property. Hybrid frames with relatively stiffer semi-rigid connections, demand internal forces almost same as that for rigid frames.
- High rise rigid rhombus frames perform better than the high rise hybrid rectangular frames in low frequency earthquakes.

5.3 Recommendations

As this study attempts to propose a new earthquake resistance framing system, the following recommendations for future work are made –

- Semi-rigid connections need to be applied at different locations in the rhombus frames to observe the seismic performance. Here in this study, semi-rigid connections are placed only on the mid stories. Different pattern of placing semi-rigid connections may significantly modify the results for rhombus shape.
- Modifications in the frame assembly can be tried to reduce the axial force demand in Rhombus frame.
- Comparisons to be made with other bracing systems such as concentrically braced frame and eccentrically braced frame.

APPENDIX A

TOP LATERAL DISPLACEMENT

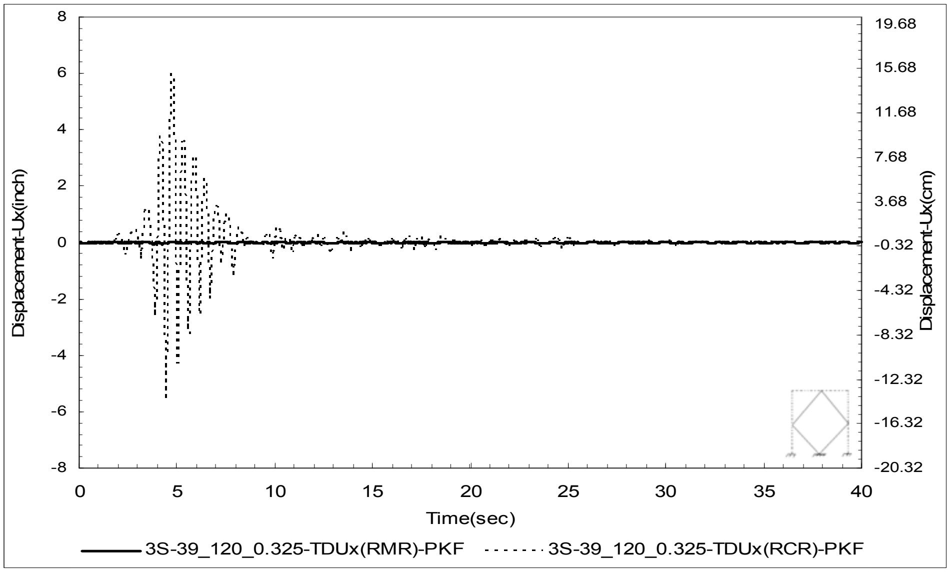

Figure A.1 Top lateral displacement for 3S-39_120_0.325-PKF

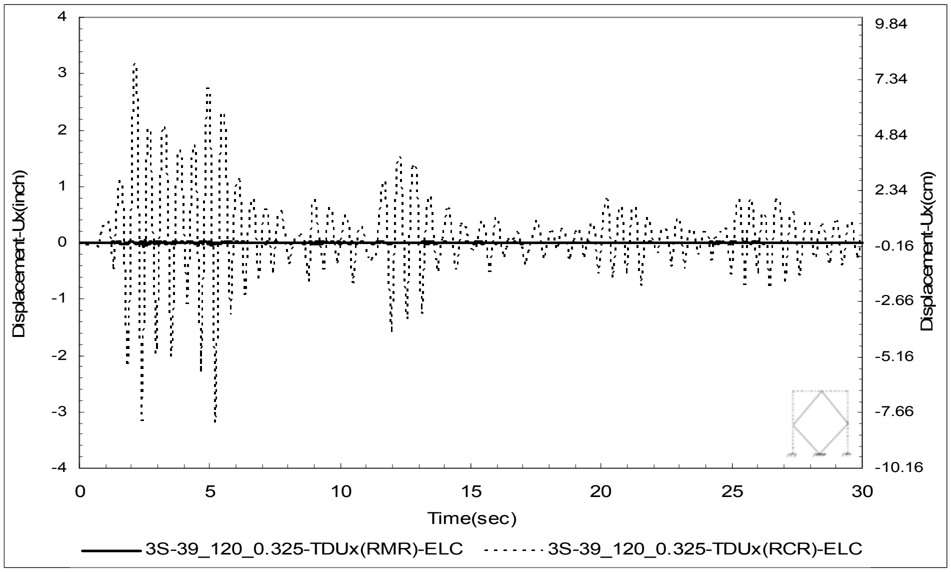

Figure A.2 Top lateral displacement for 3S-39_120_0.325-ELC

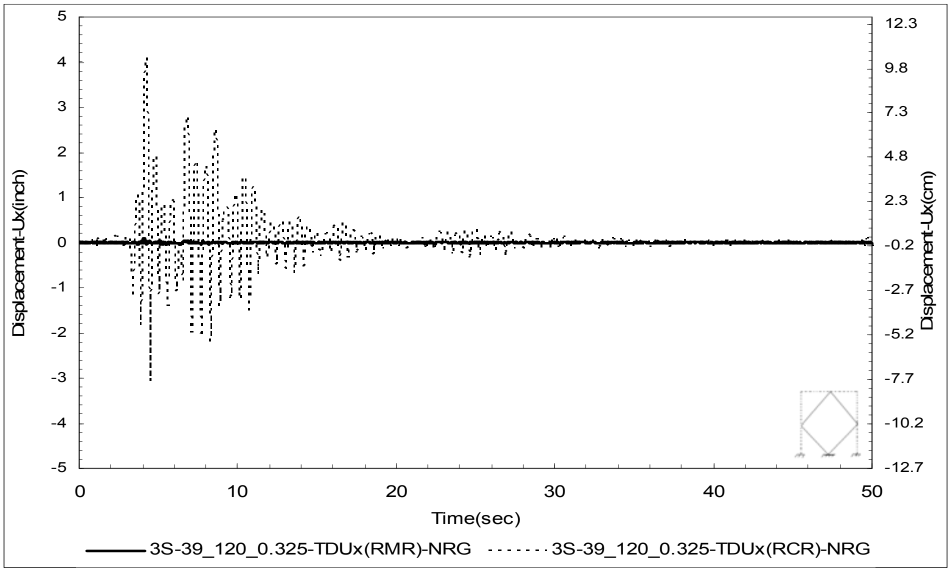

Figure A.3 Top lateral displacement for 3S-39_120_0.325-NRG

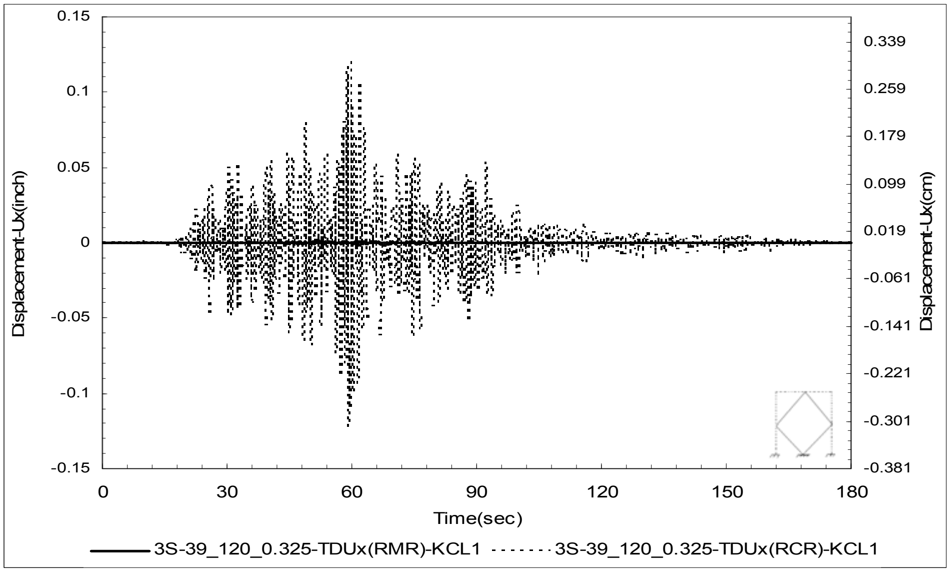

Figure A.4 Top lateral displacement for 3S-39_120_0.325-KCL1

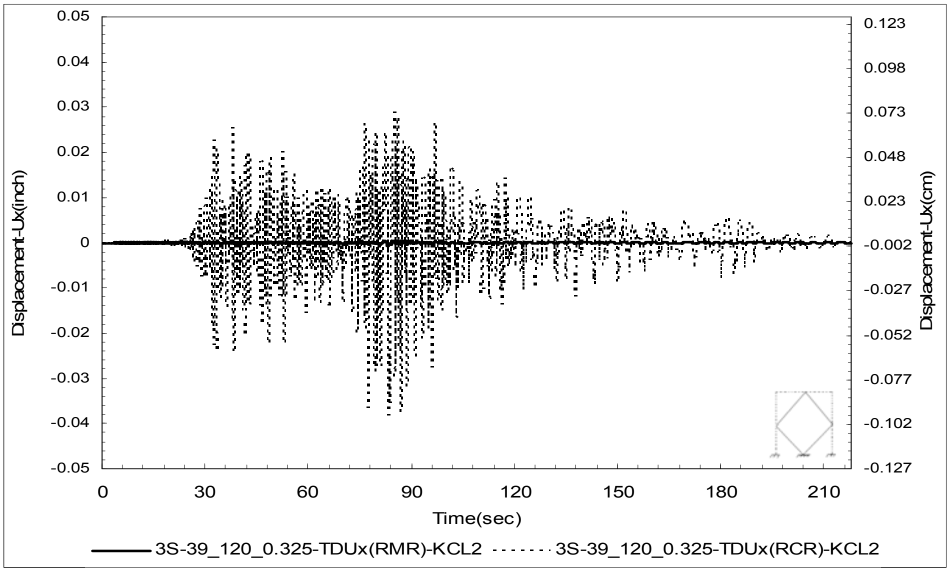

Figure A.5 Top lateral displacement for 3S-39_120_0.325-KCL2

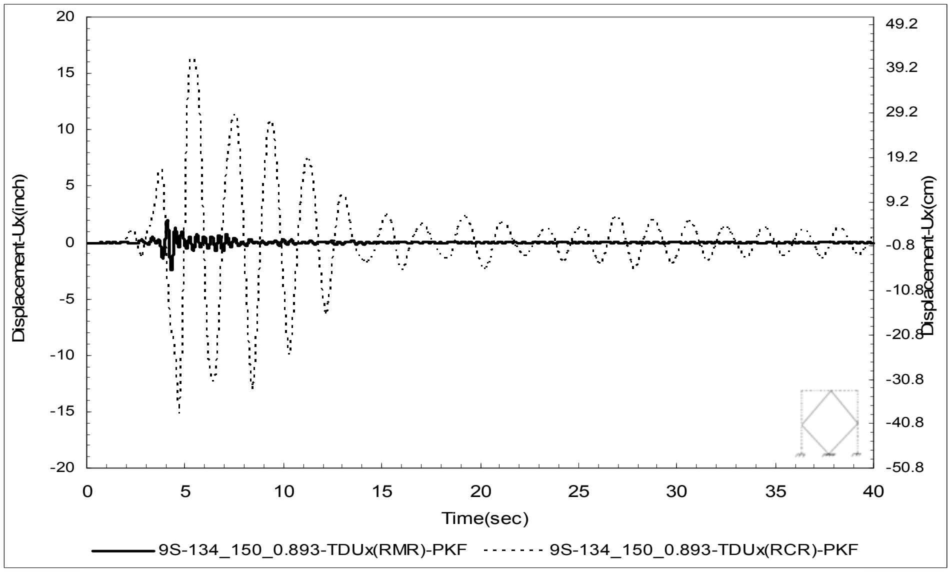

Figure A.6 Top lateral displacement for 9S-134_150_0.893-PKF

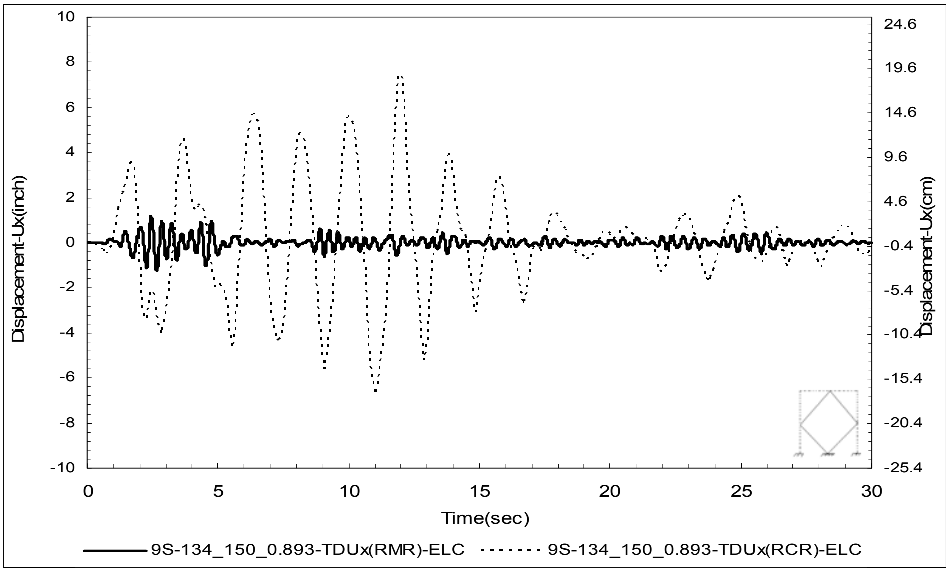

Figure A.7 Top lateral displacement for 9S-134_150_0.893-ELC

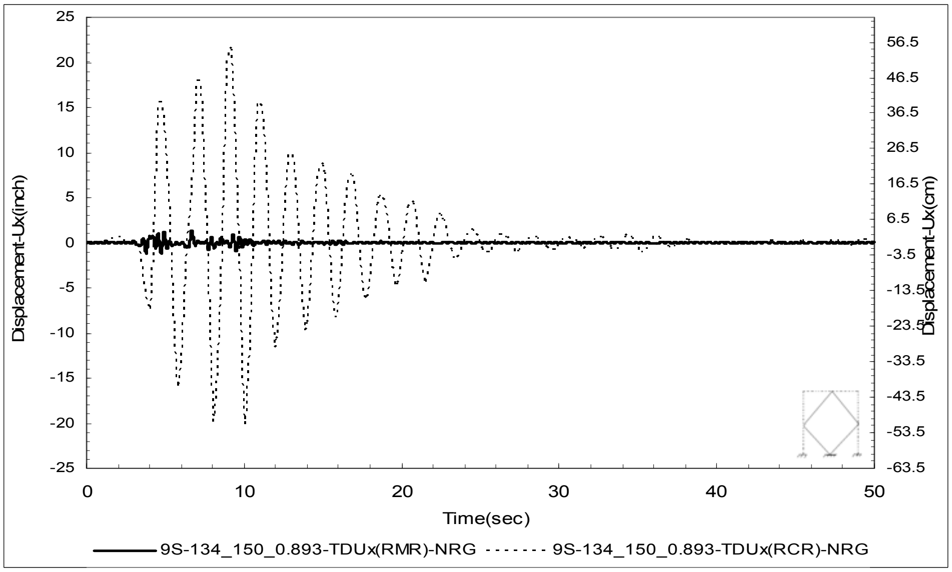

Figure A.8 Top lateral displacement for 9S-134_150_0.893-NRG

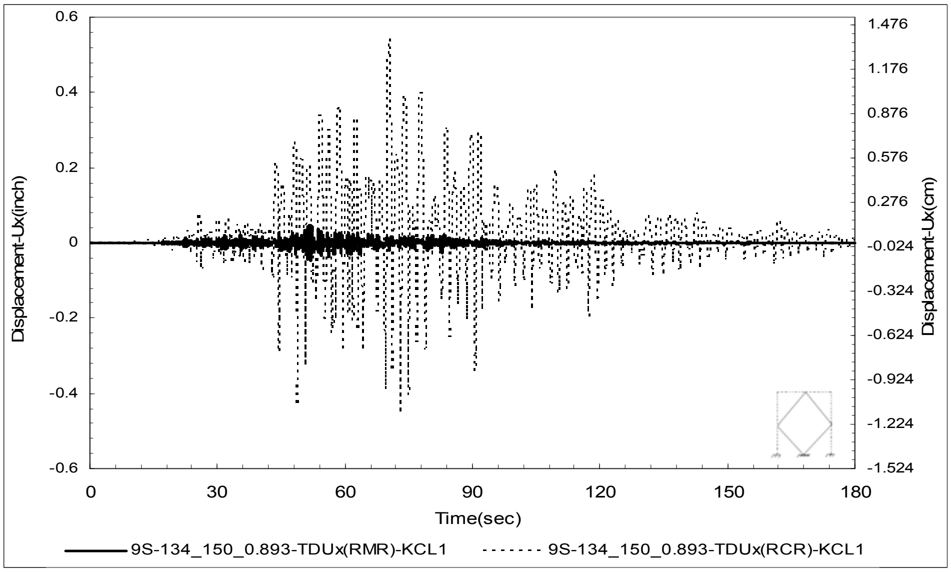

Figure A.9 Top lateral displacement for 9S-134_150_0.893-KCL1

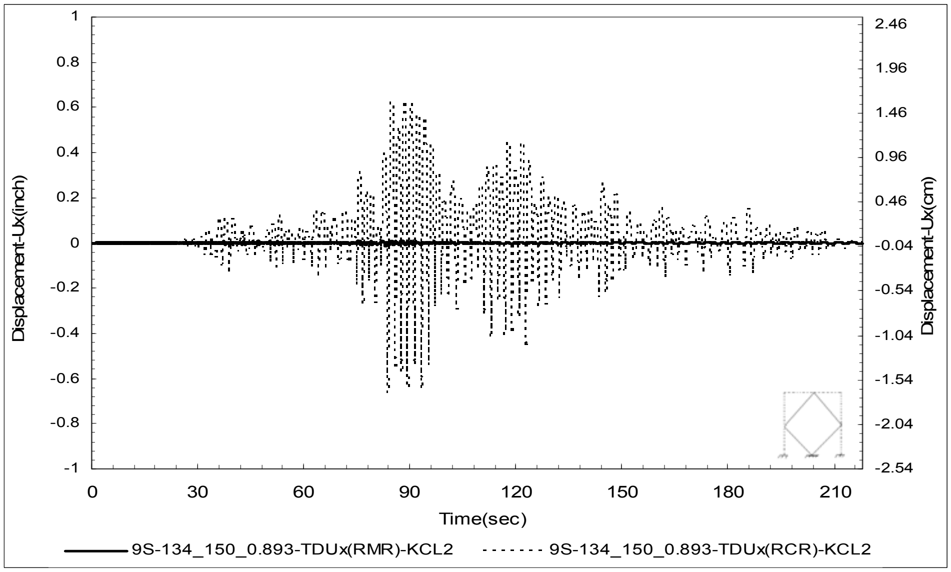

Figure A.10 Top lateral displacement for 9S-134_150_0.893-KCL2

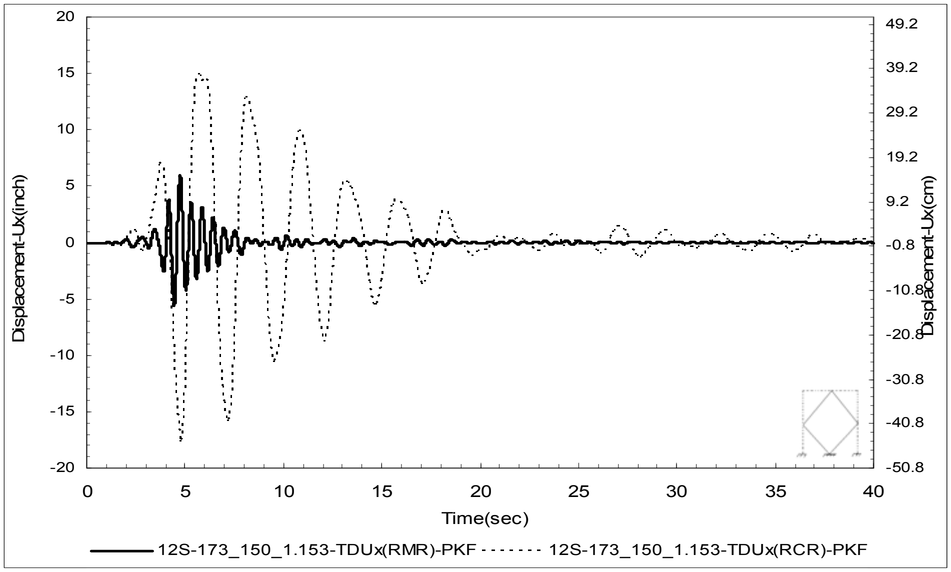

Figure A.11 Top lateral displacement for 12S-173_150_1.153-PKF

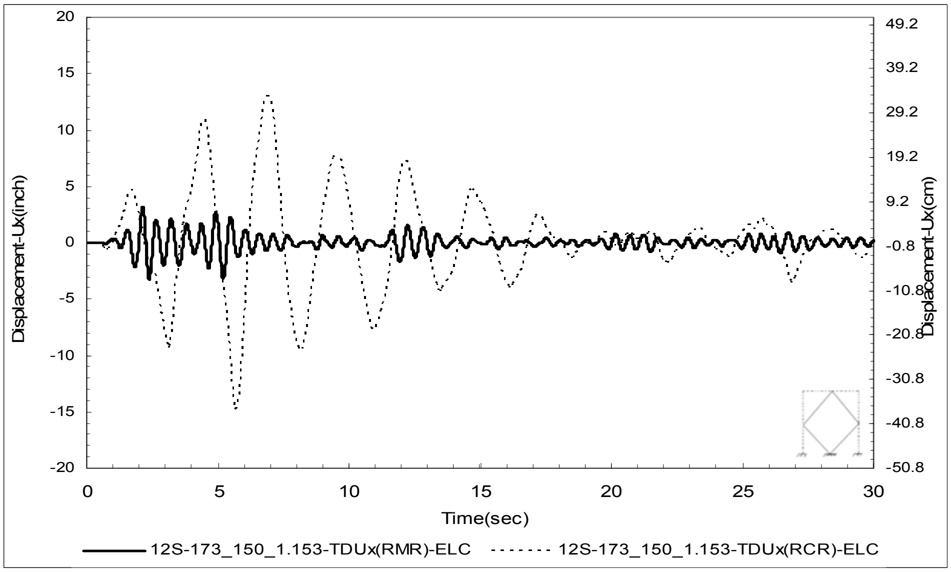

Figure A.12 Top lateral displacement for 12S-173_150_1.153-ELC

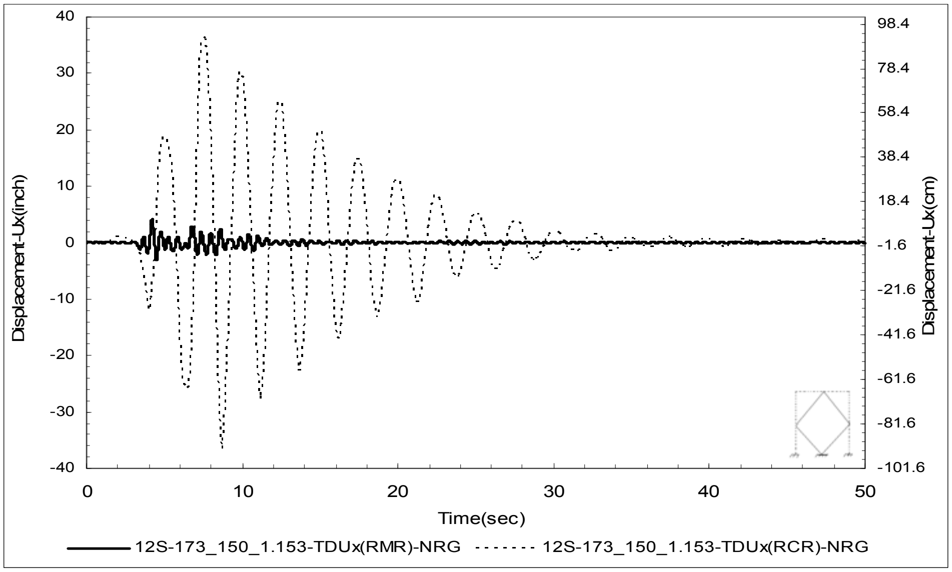

Figure A.13 Top lateral displacement for 12S-173_150_1.153-NRG

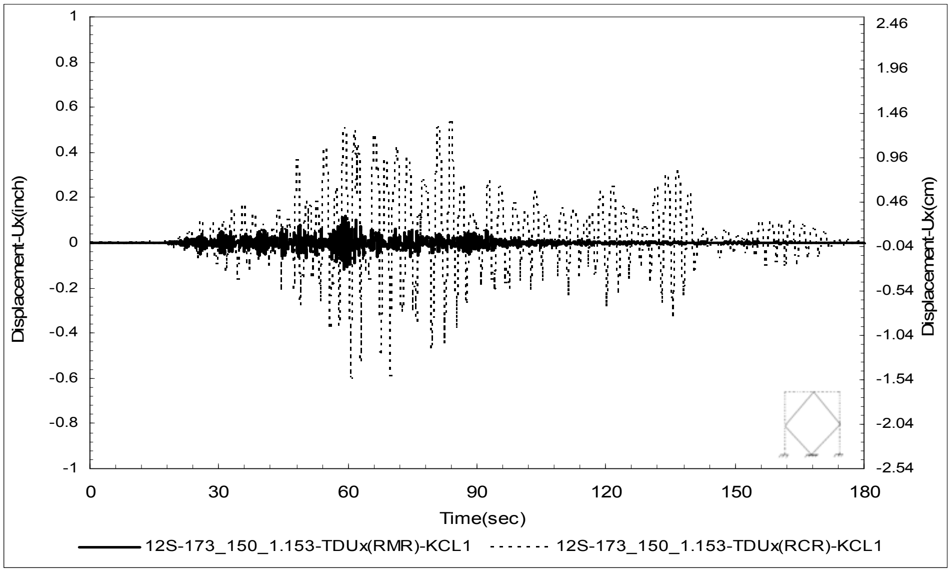

Figure A.14 Top lateral displacement for 12S-173_150_1.153-KCL1

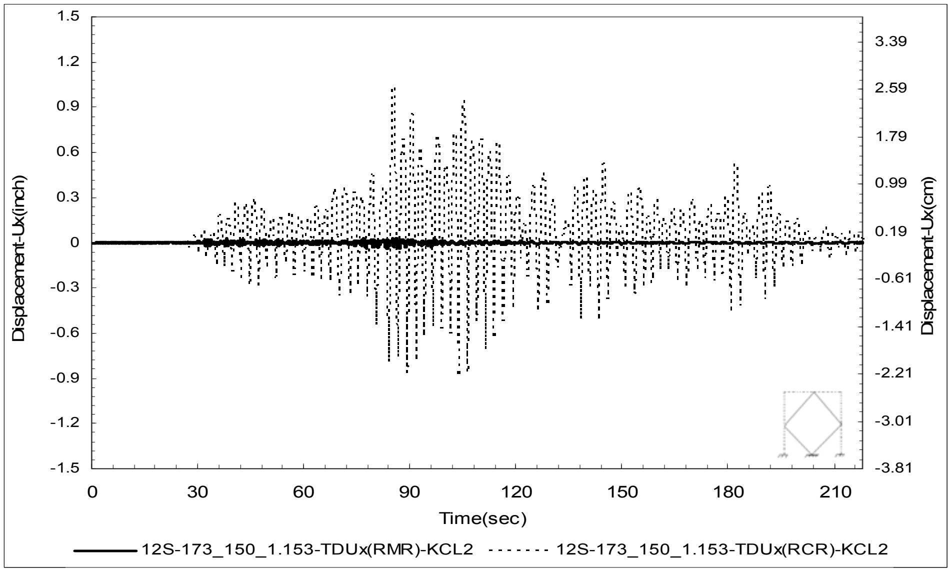

Figure A.15 Top lateral displacement for 12S-173_150_1.153-KCL2

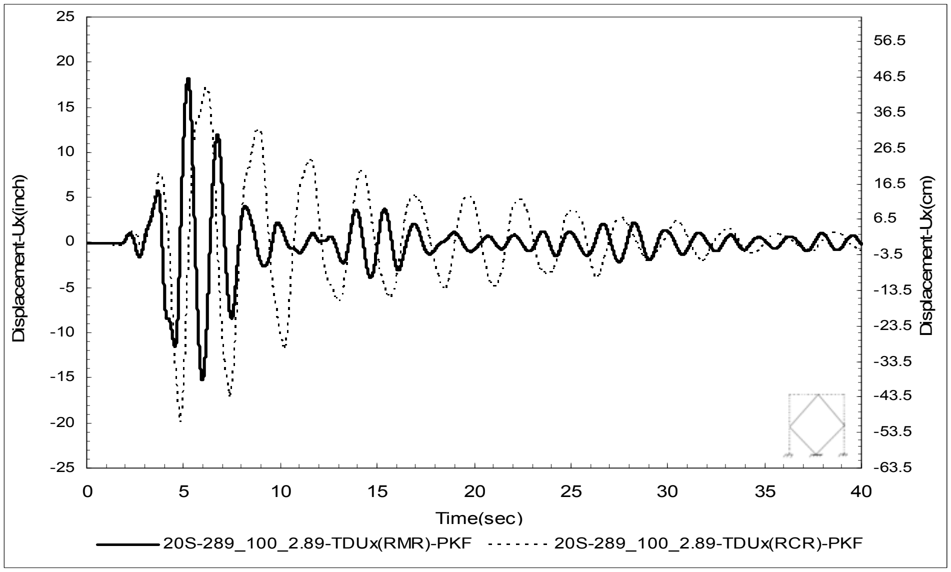

Figure A.16 Top lateral displacement for 20S-289_100_2.89-PKF

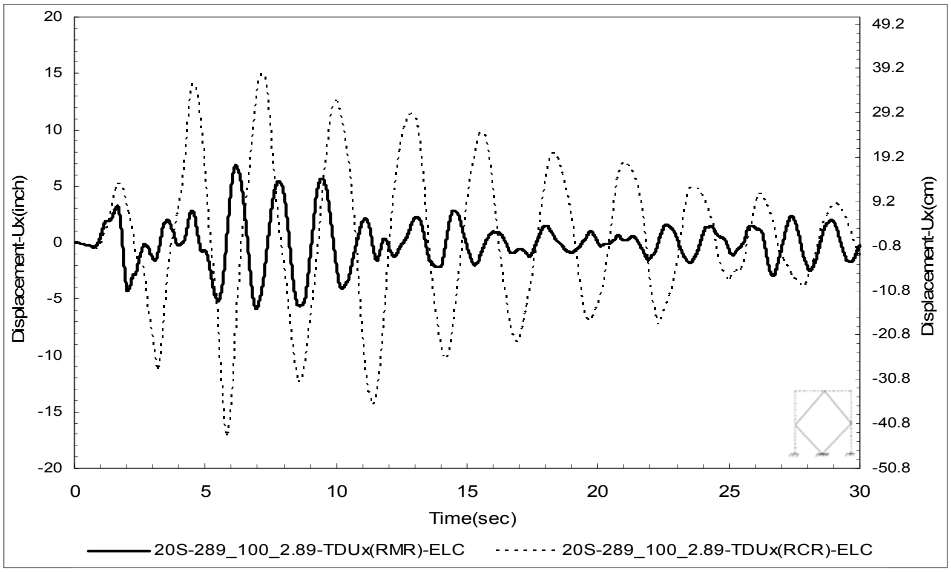

Figure A.17 Top lateral displacement for 20S-289_100_2.89-ELC

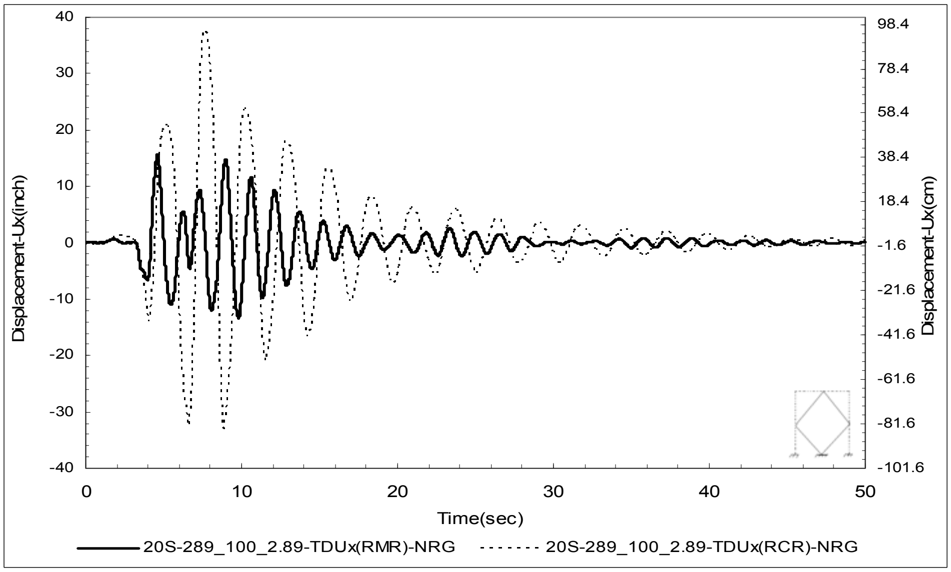

Figure A.18 Top lateral displacement for 20S-289_100_2.89-NRG

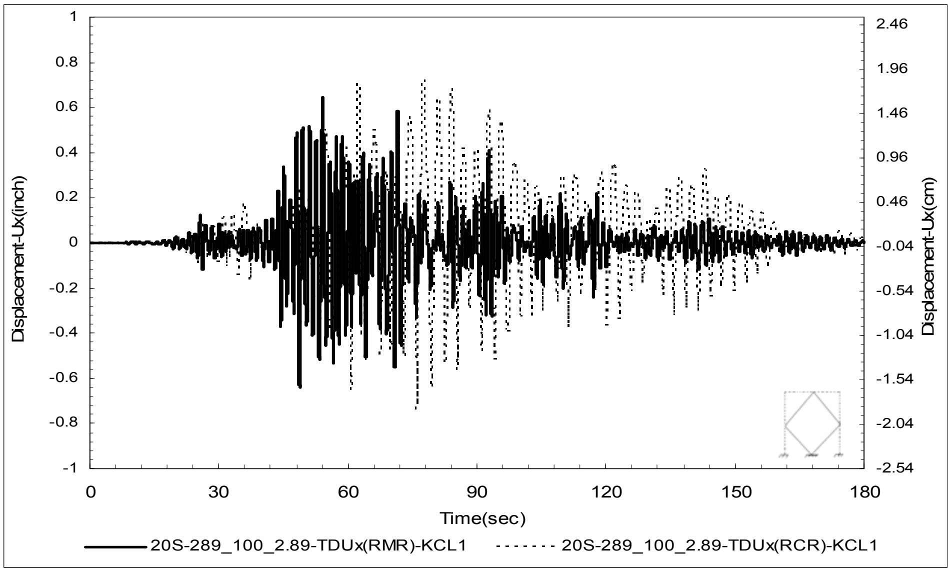

Figure A.19 Top lateral displacement for 20S-289_100_2.89-KCL1

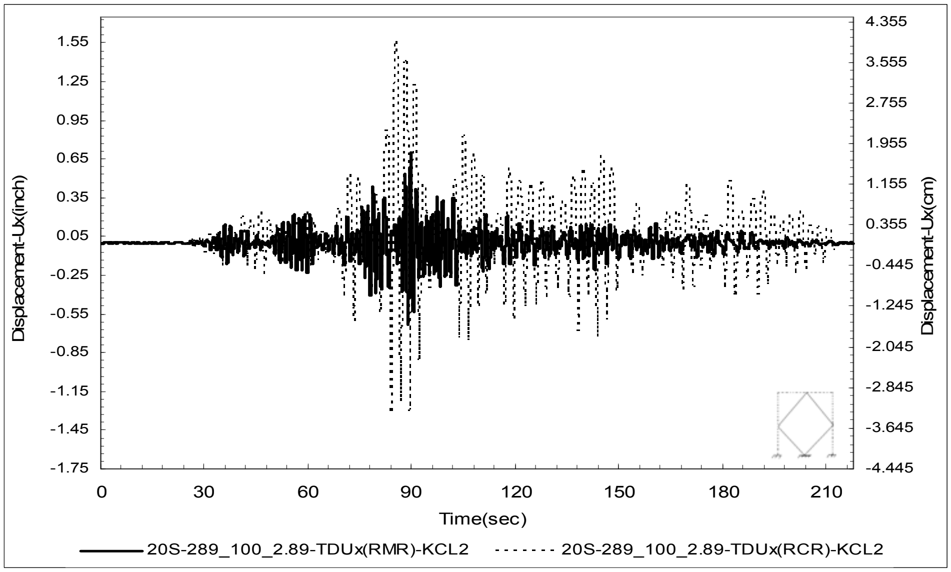

Figure A.20 Top lateral displacement for 20S-289_100_2.89-KCL2

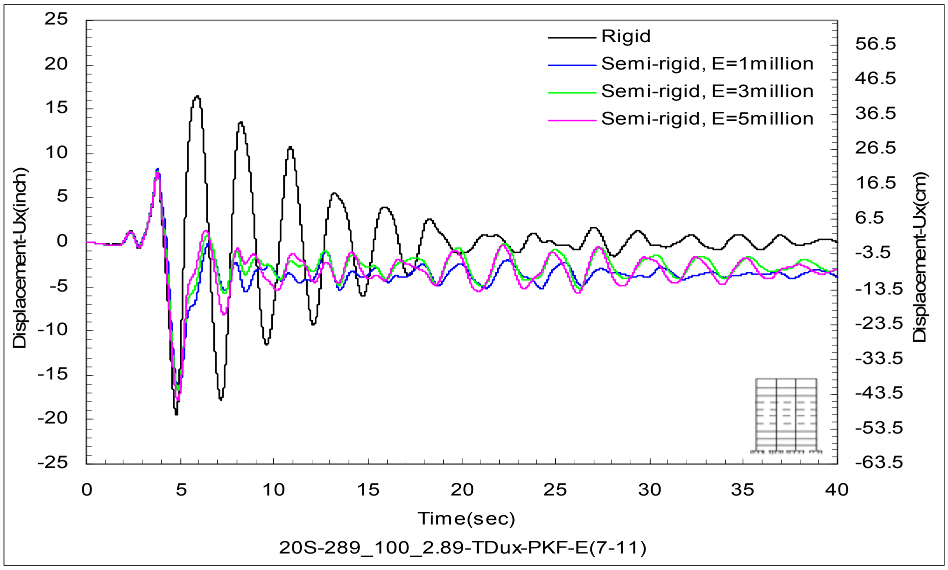

Figure A.21 Top lateral displacement for 20S-289_100_2.89-PKF

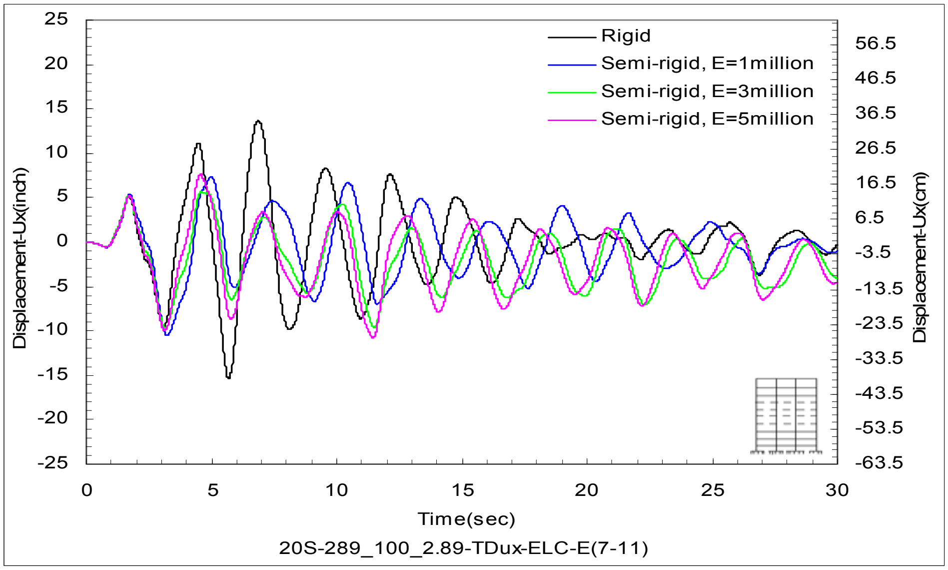

Figure A.22 Top lateral displacement for 20S-289_100_2.89-ELC

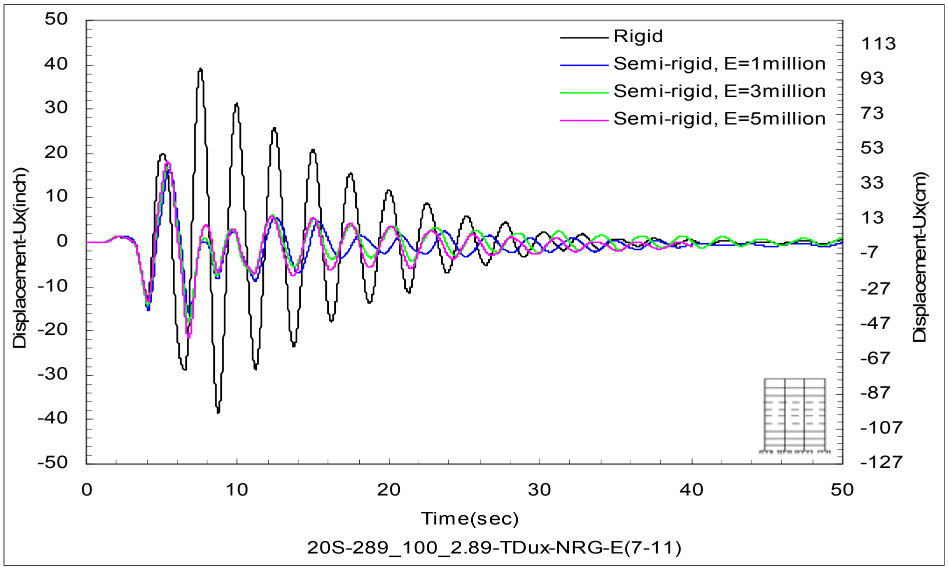

Figure A.23 Top lateral displacement for 20S-289_100_2.89-NRG

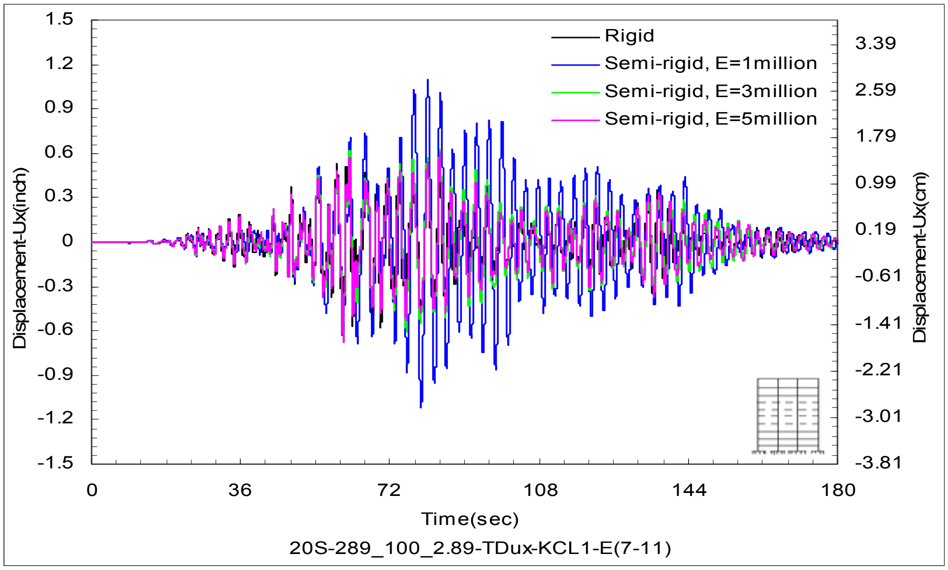

Figure A.24 Top lateral displacement for 20S-289_100_2.89-KCL1

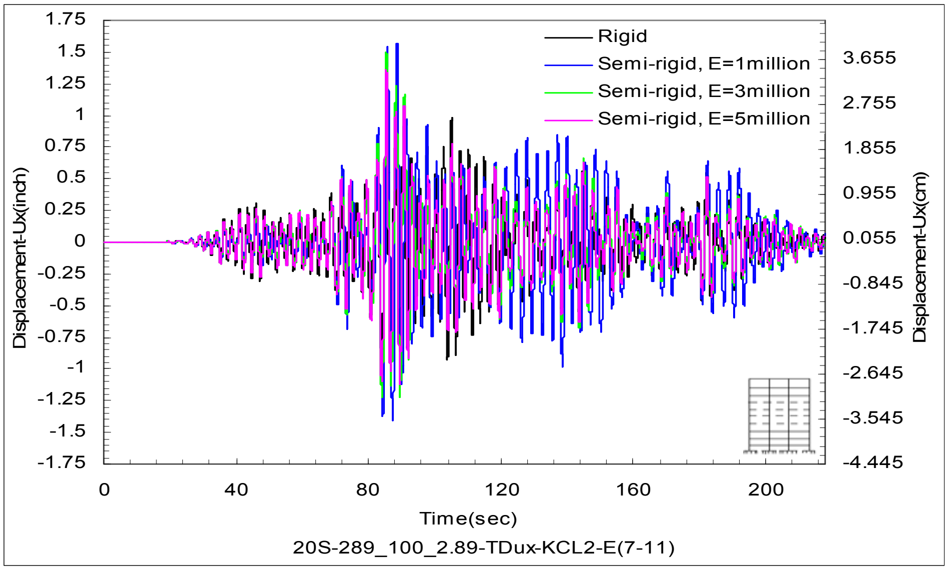

Figure A.25 Top lateral displacement for 20S-289_100_2.89-KCL2

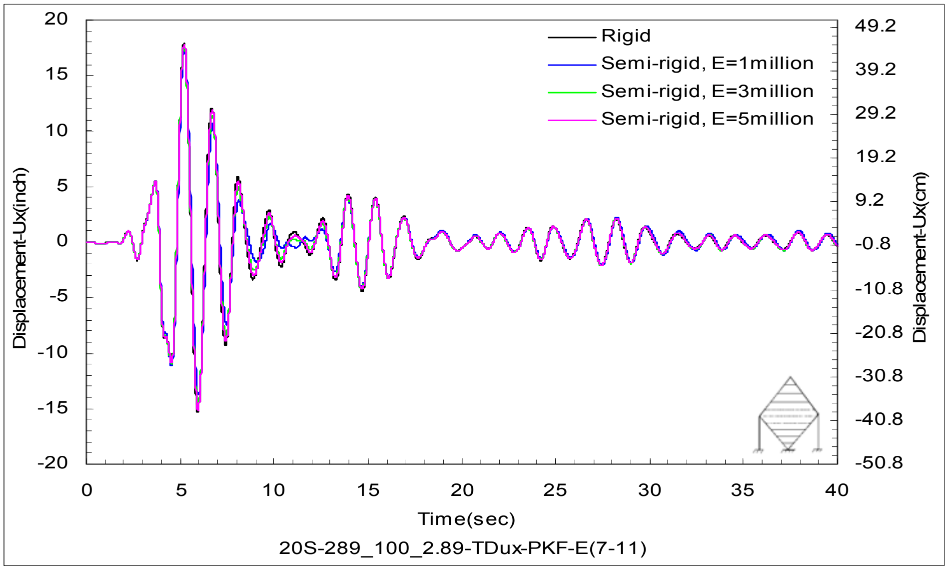

Figure A.26 Top lateral displacement for 20S-289_100_2.89-PKF

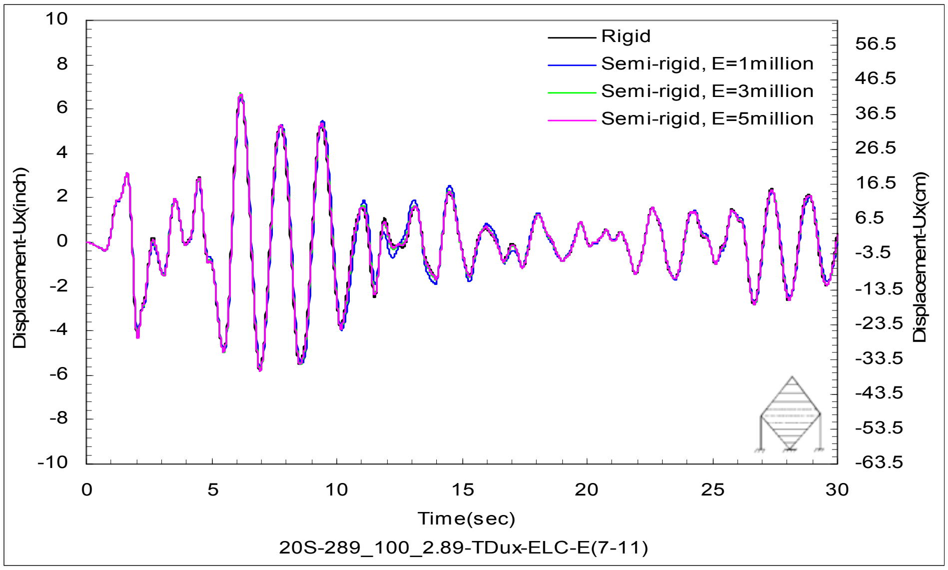

Figure A.27 Top lateral displacement for 20S-289_100_2.89-ELC

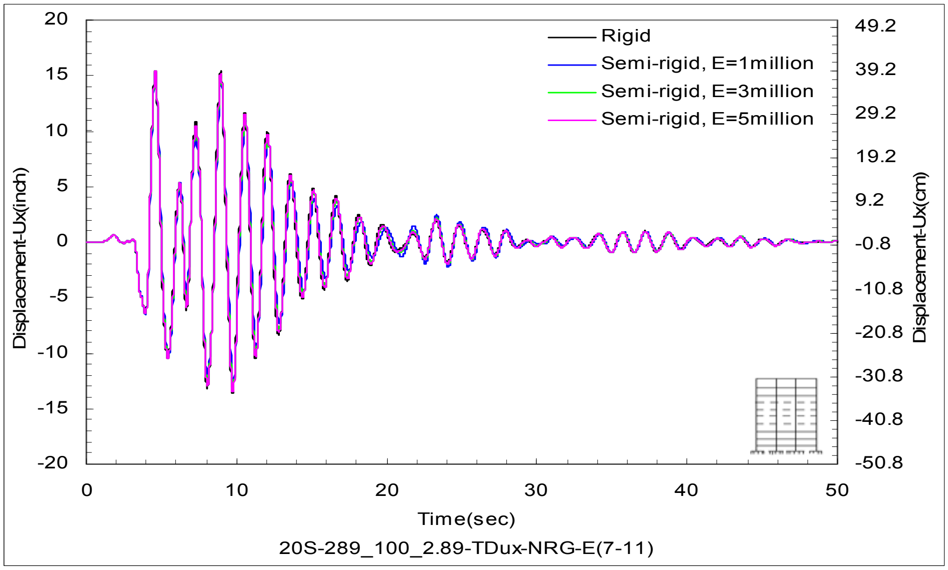

Figure A.28 Top lateral displacement for 20S-289_100_2.89-NRG

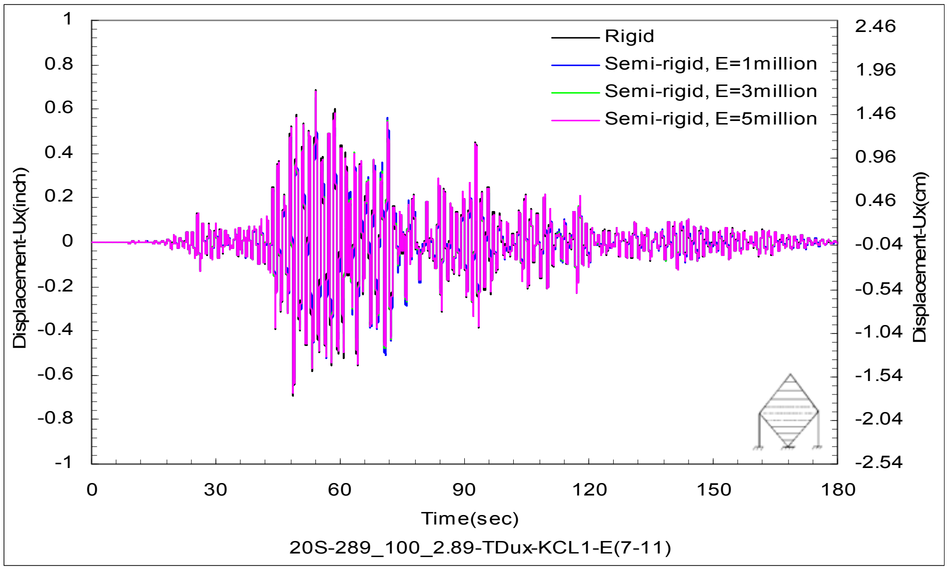

Figure A.29 Top lateral displacement for 20S-289_100_2.89-KCL1

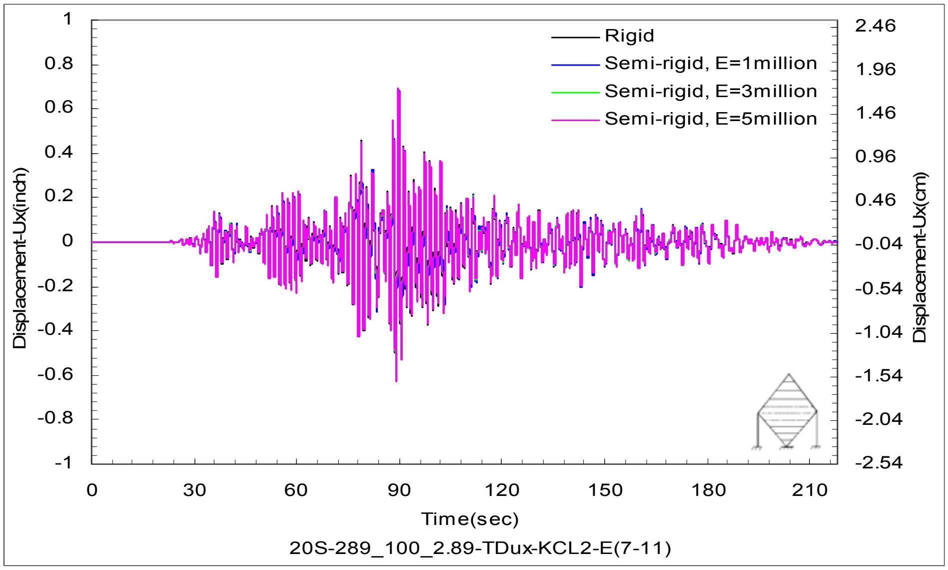

Figure A.30 Top lateral displacement for 20S-289_100_2.89-KCL2

APPENDIX B

AXIAL FORCES IN THE FRAME ELEMENTS

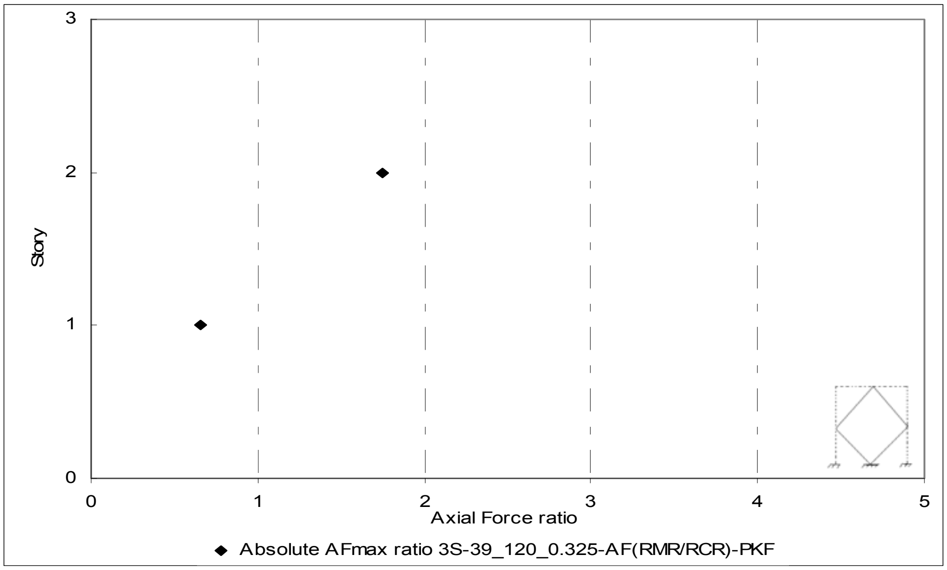

a)

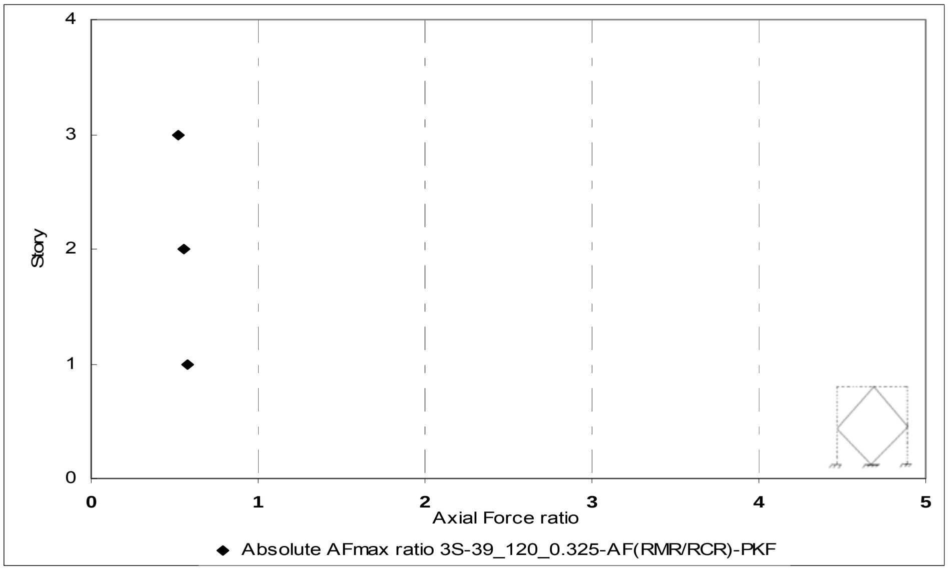

b)

Figure B.1 Axial Force ratio for 3S-39_120_0.325-PKF
a)Beams, b)Columns

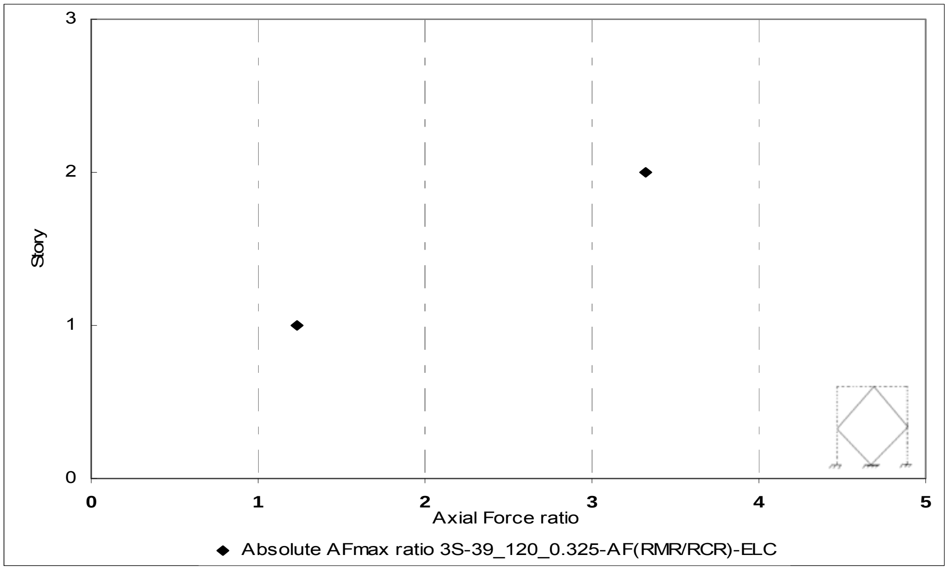

a)

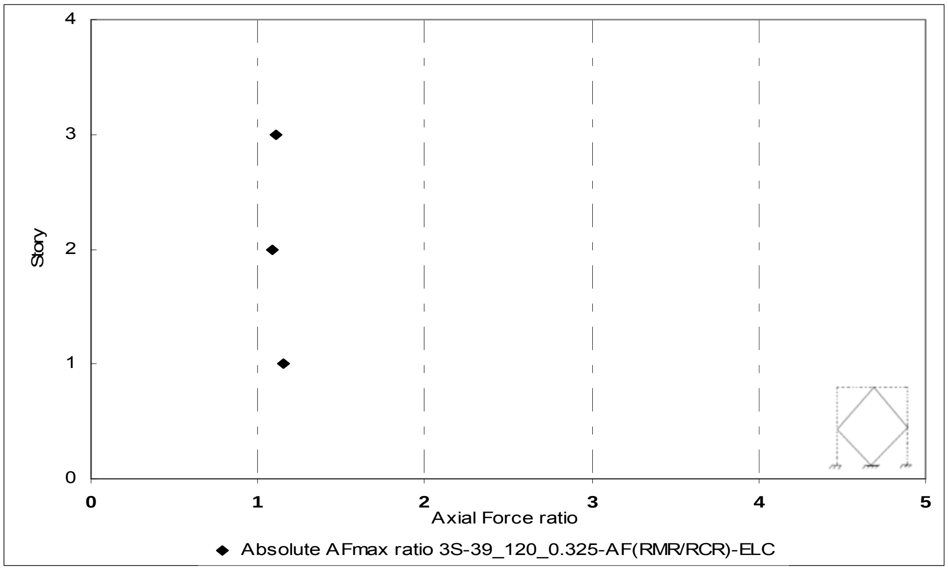

b)

Figure B.2 Axial Force ratio for 3S-39_120_0.325-ELC
a)Beams, b)Columns

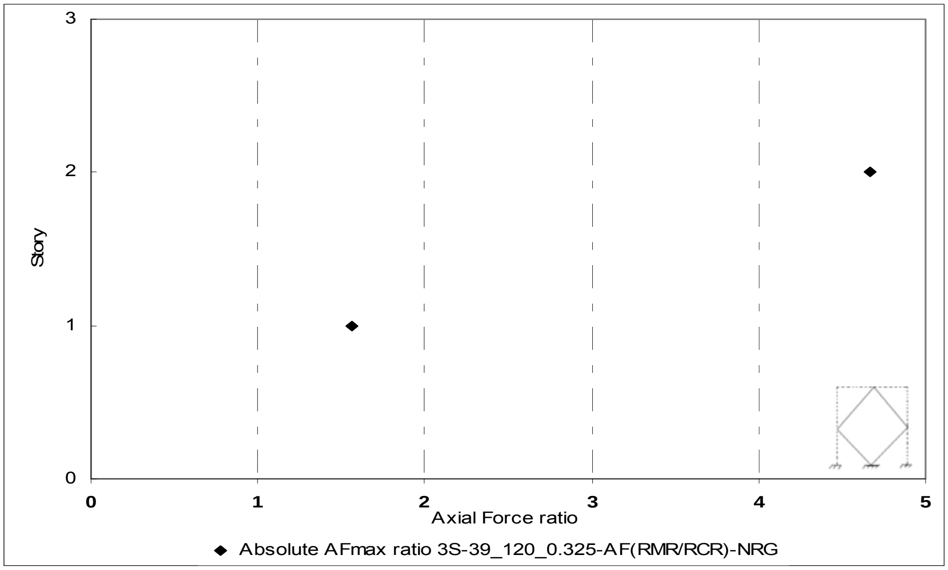

a)

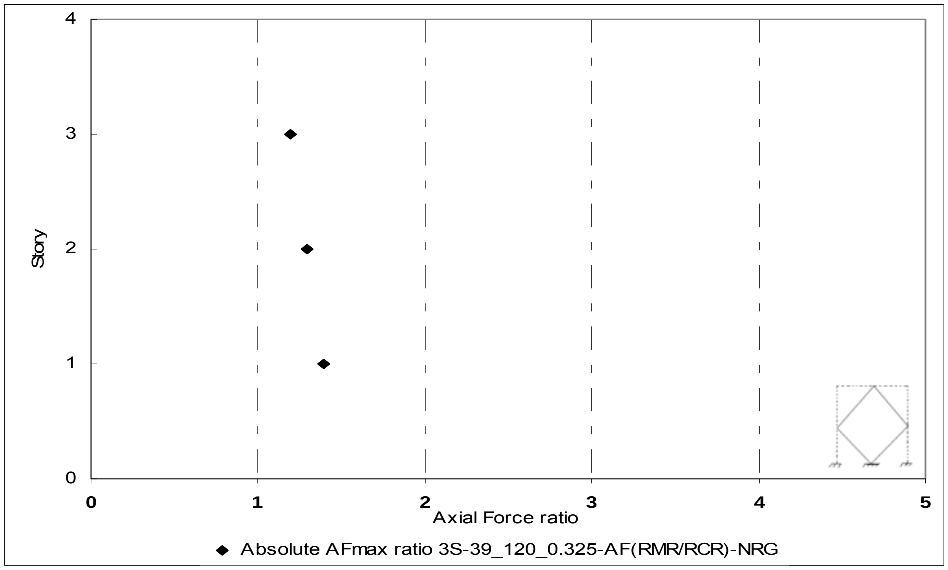

b)

Figure B.3 Axial Force ratio for 3S-39_120_0.325-NRG
a)Beams, b)Columns

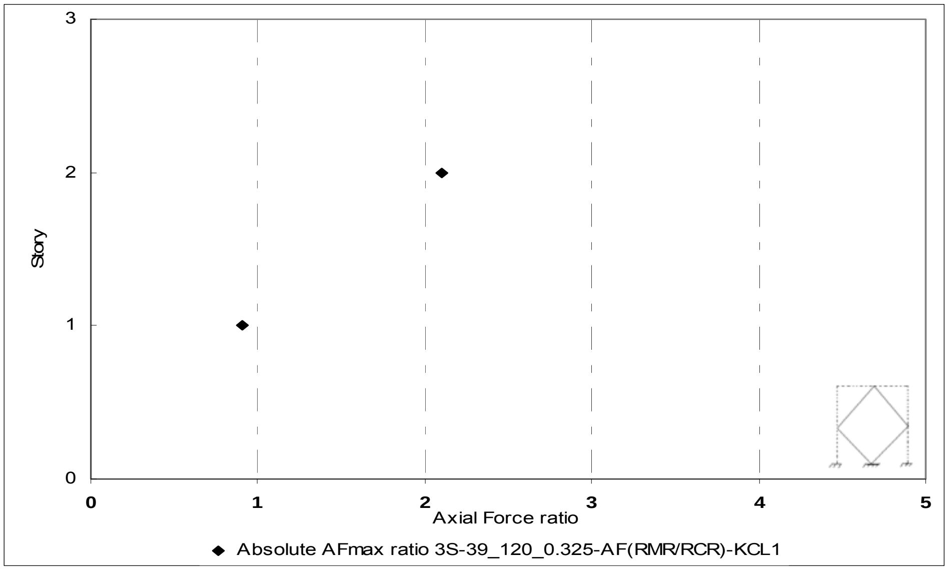

a)

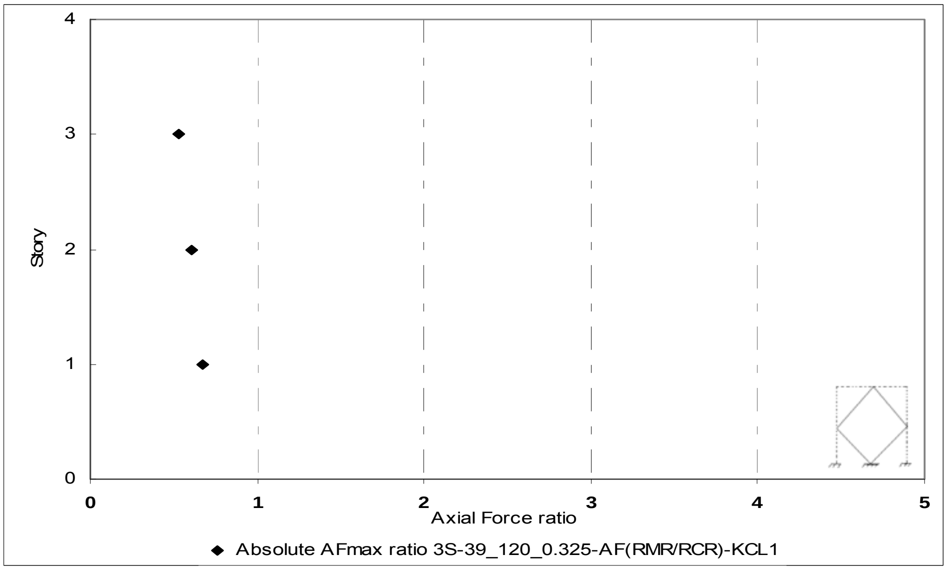

b)

Figure B.4 Axial Force ratio for 3S-39_120_0.325-KCL1
a)Beams, b)Columns

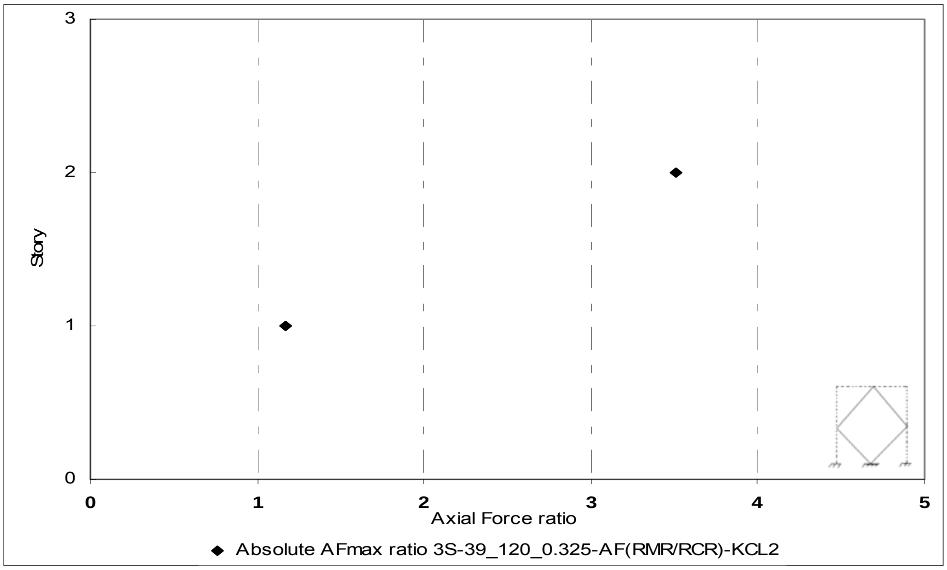

a)

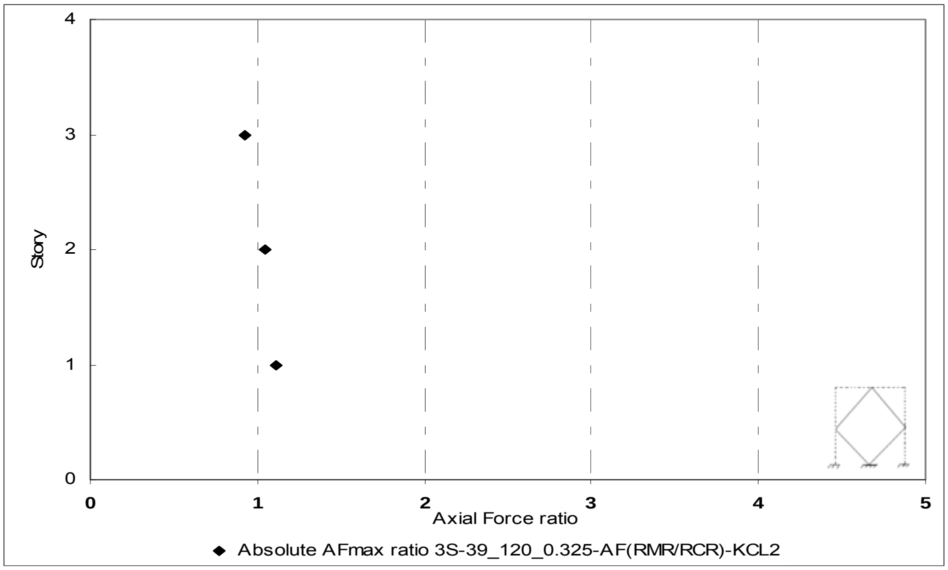

b)

Figure B.5 Axial Force ratio for 3S-39_120_0.325-KCL2
a)Beams, b)Columns

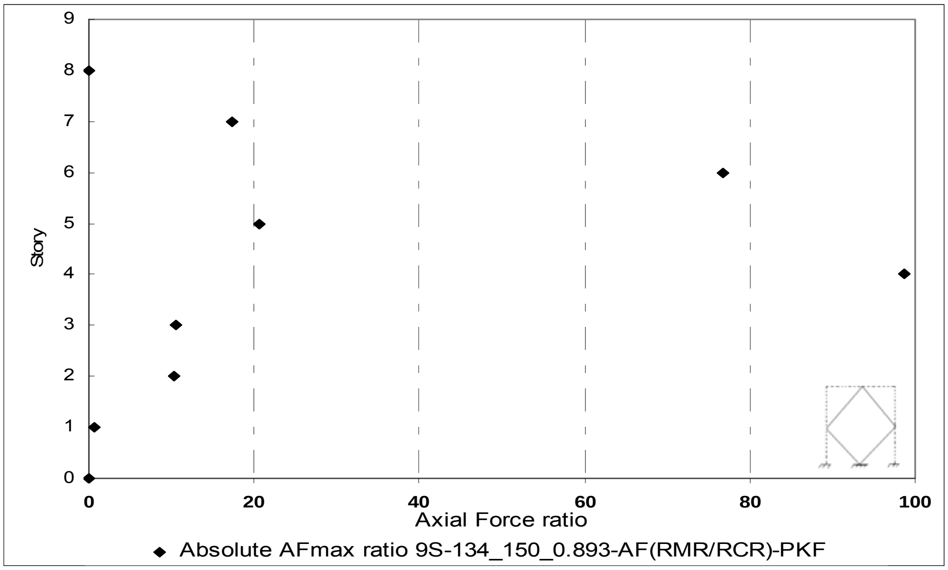

a)

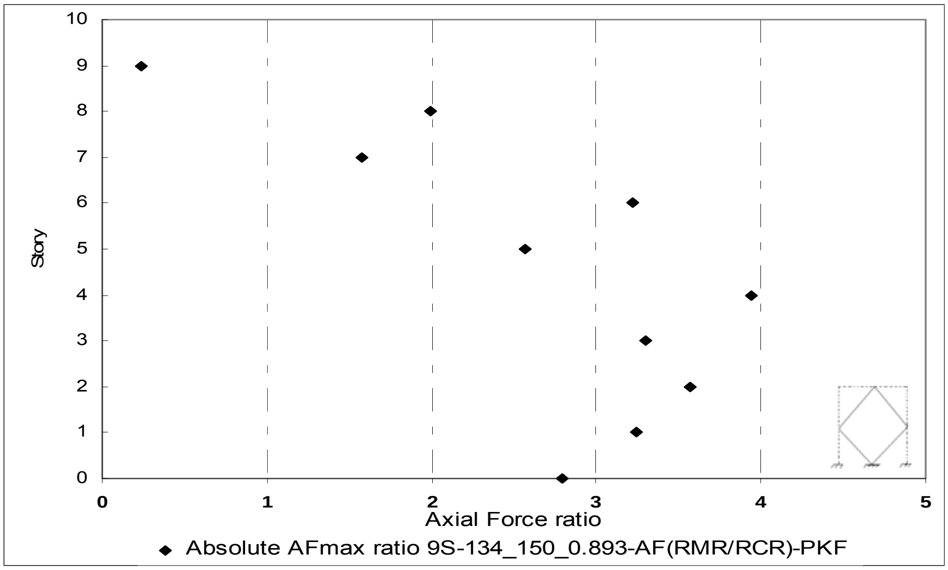

b)

Figure B.6 Axial Force ratio for 9S-134_150_0.893-PKF
a)Beams, b)Columns

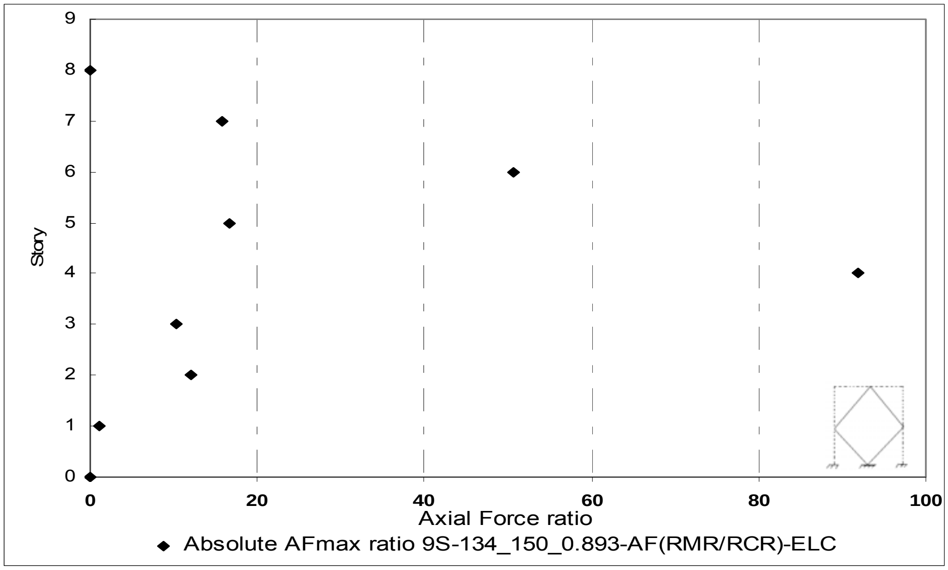

a)

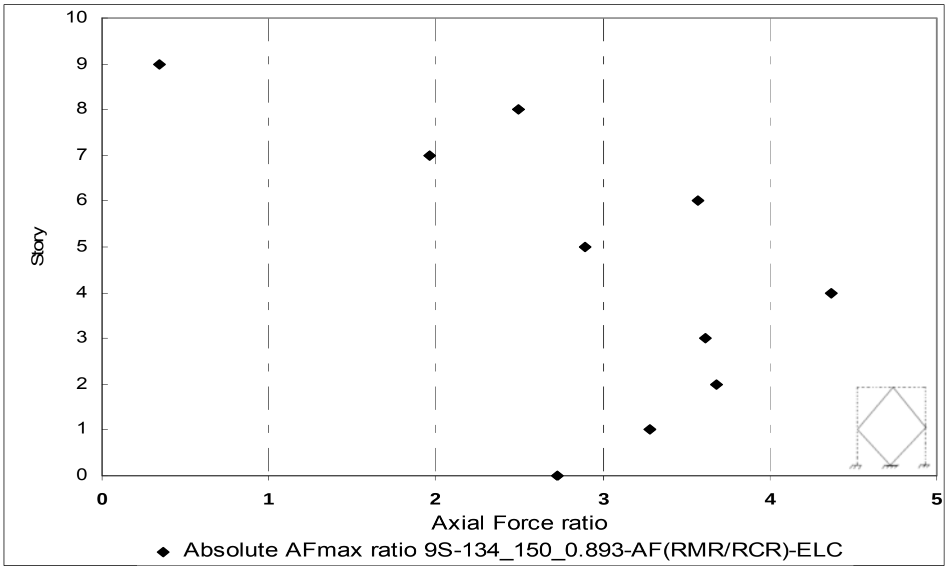

b)

Figure B.7 Axial Force ratio for 9S-134_150_0.893-ELC
a)Beams, b)Columns

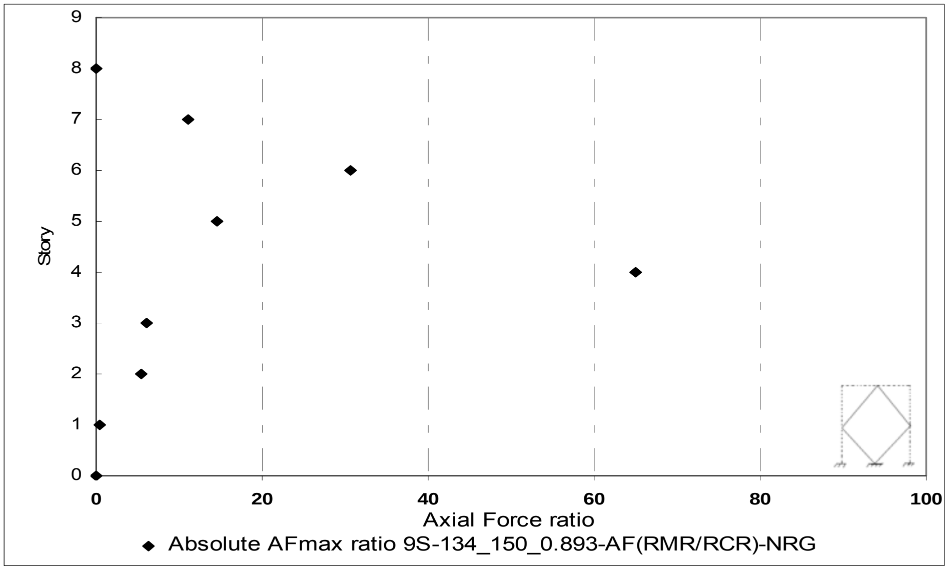

a)

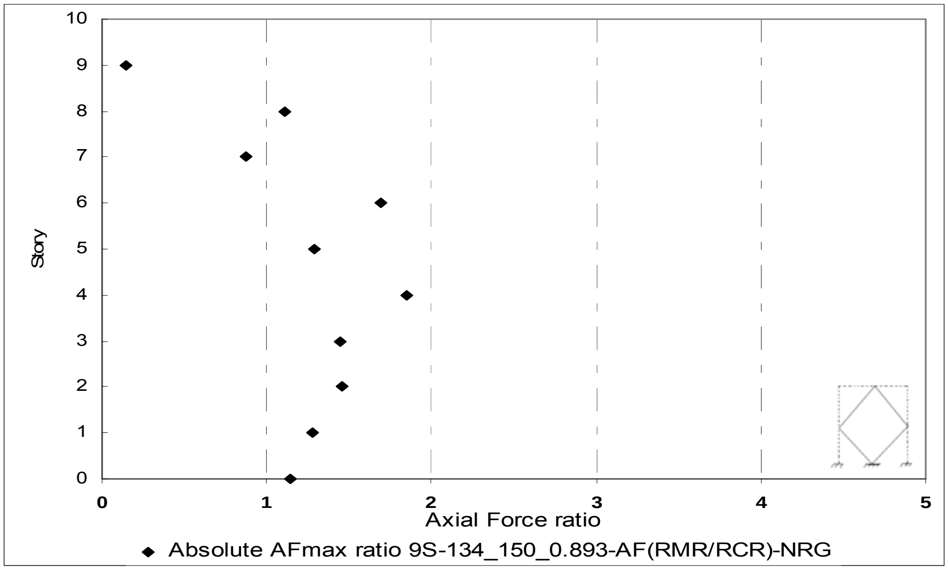

b)

Figure B.8 Axial Force ratio for 9S-134_150_0.893-NRG
a)Beams, b)Columns

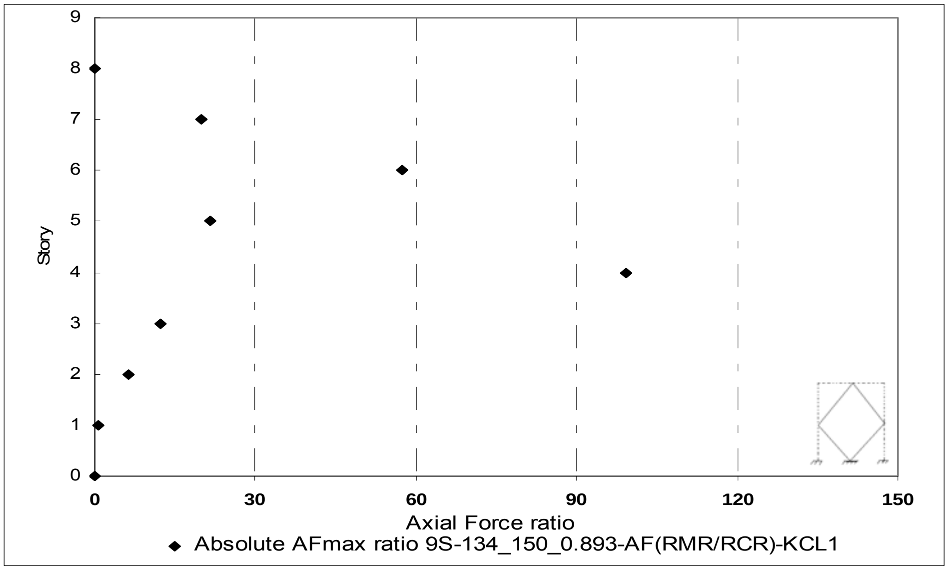

a)

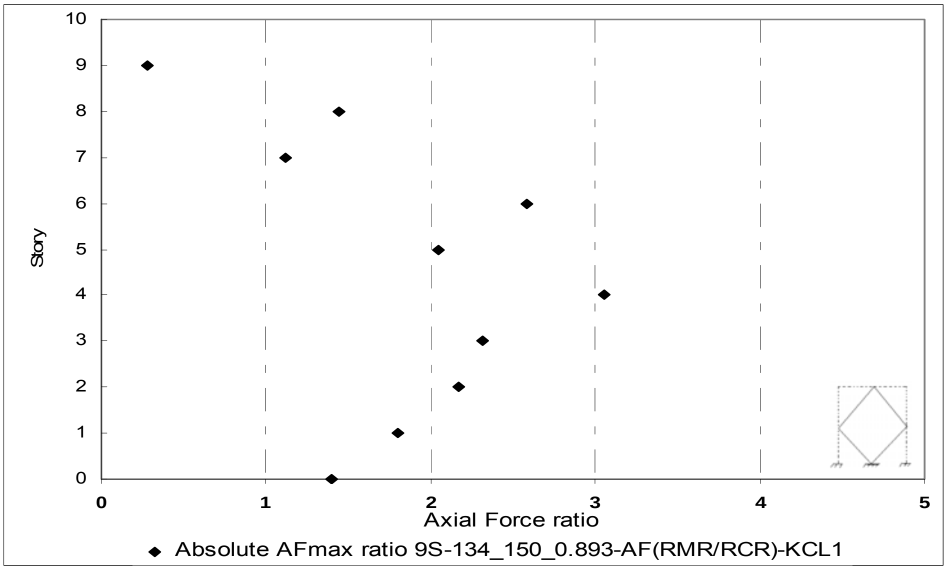

b)

Figure B.9 Axial Force ratio for 9S-134_150_0.893-KCL1
a)Beams, b)Columns

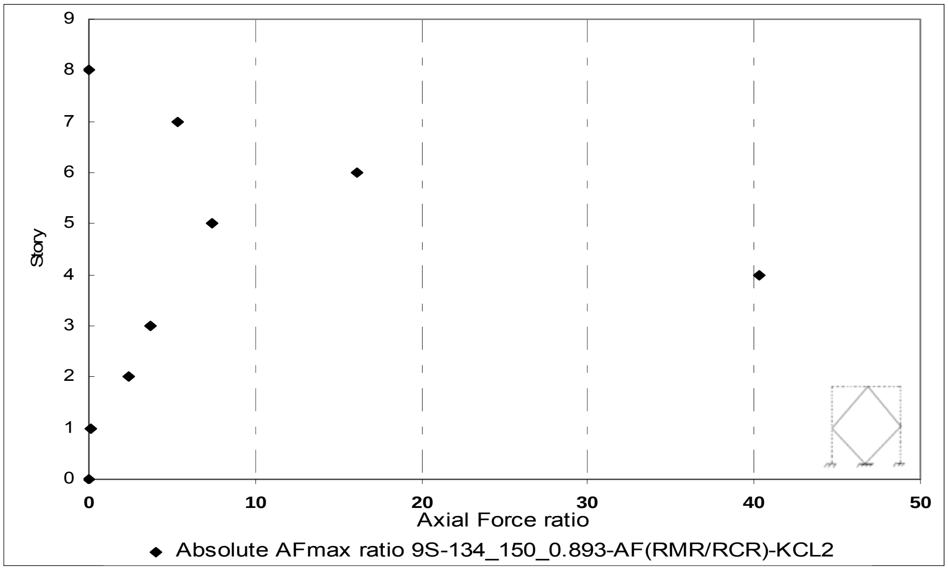

a)

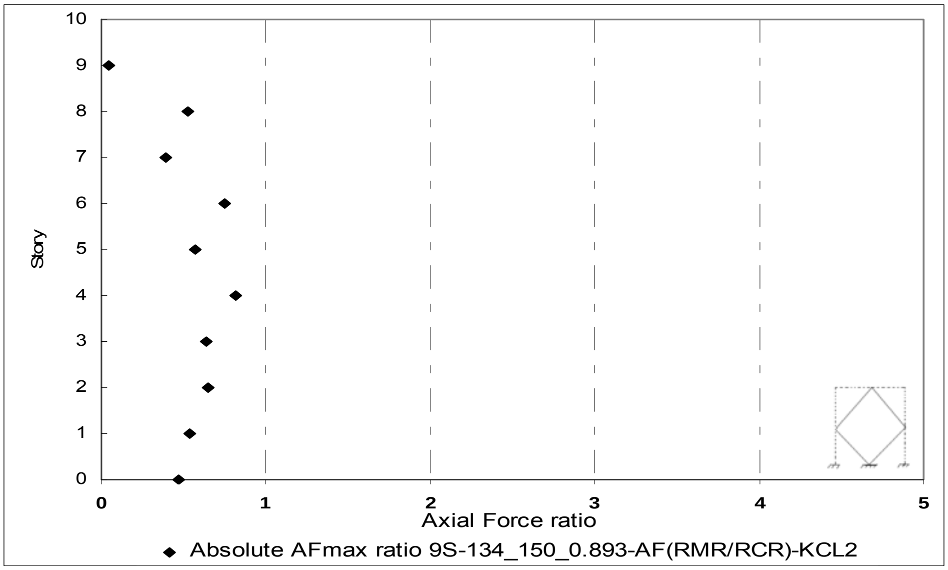

b)

Figure B.10 Axial Force ratio for 9S-134_150_0.893-KCL2
a)Beams, b)Columns

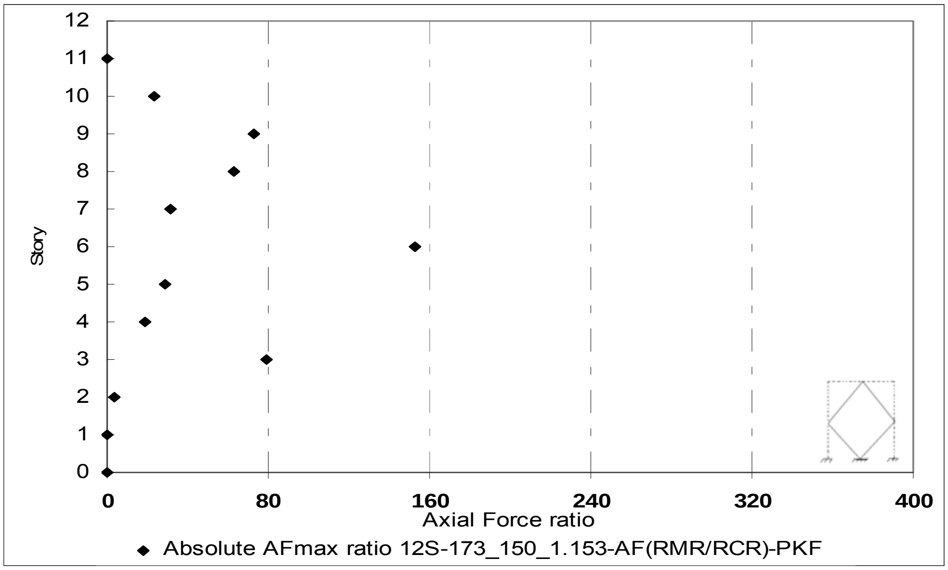

a)

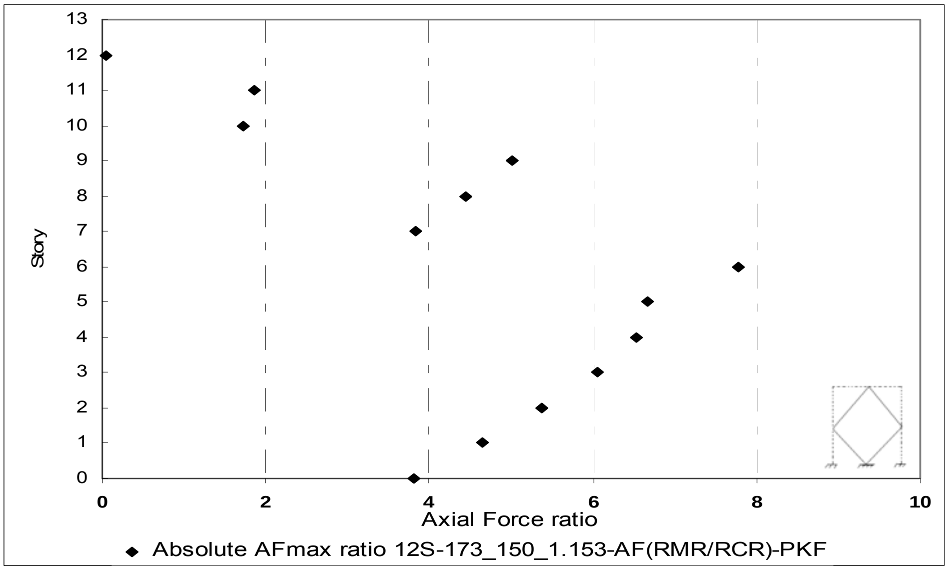

b)

Figure B.11 Axial Force ratio for 12S-173_150_1.153-PKF
a)Beams, b)Columns

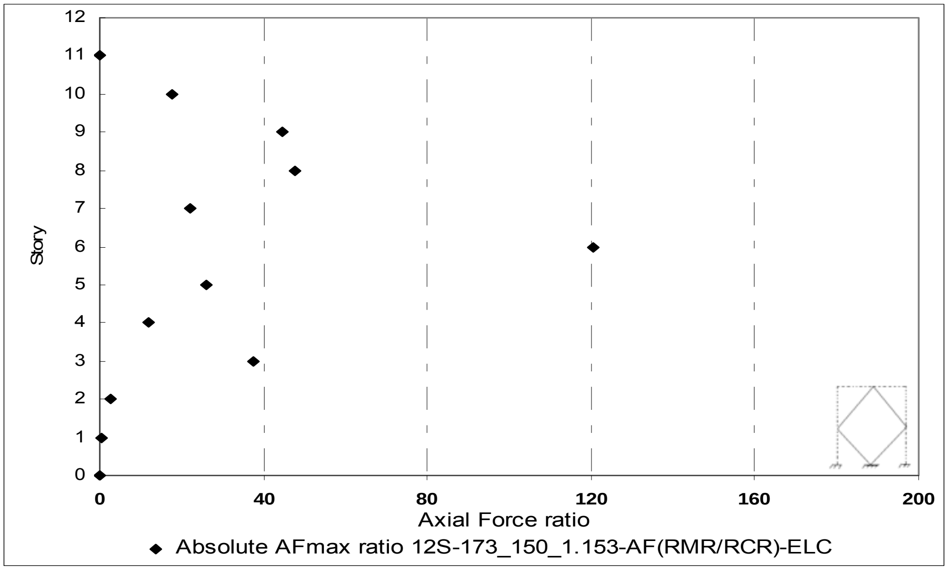

a)

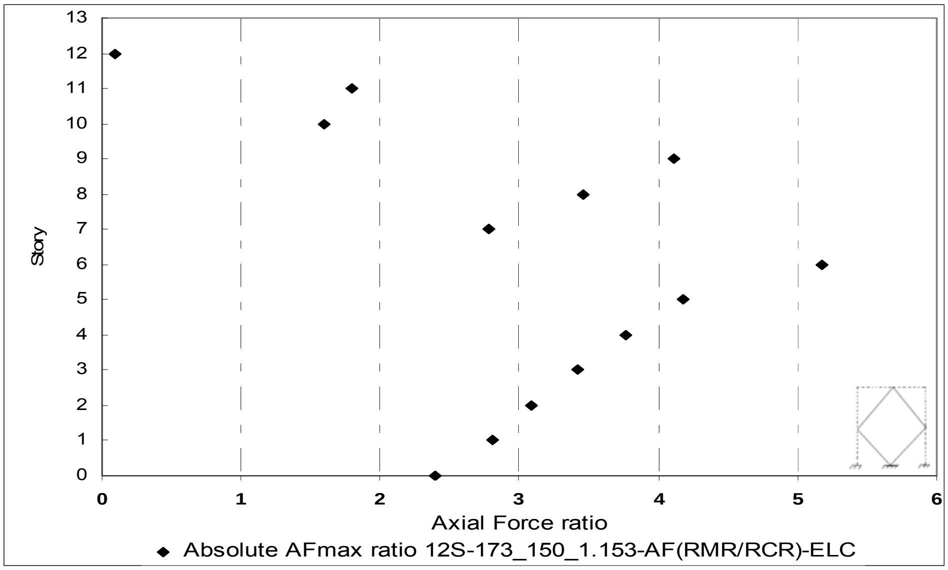

b)

Figure B.12 Axial Force ratio for 12S-173_150_1.153-ELC
a)Beams, b)Columns

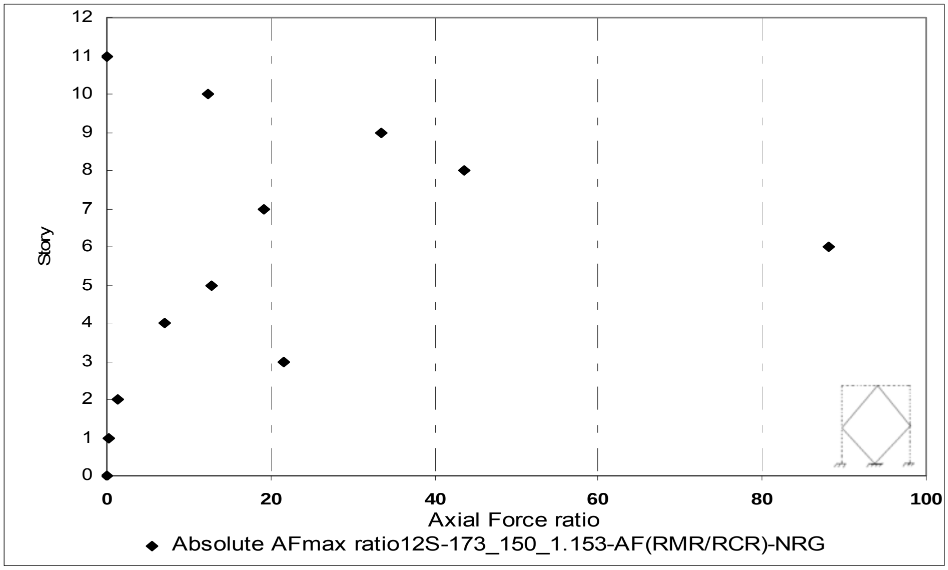

a)

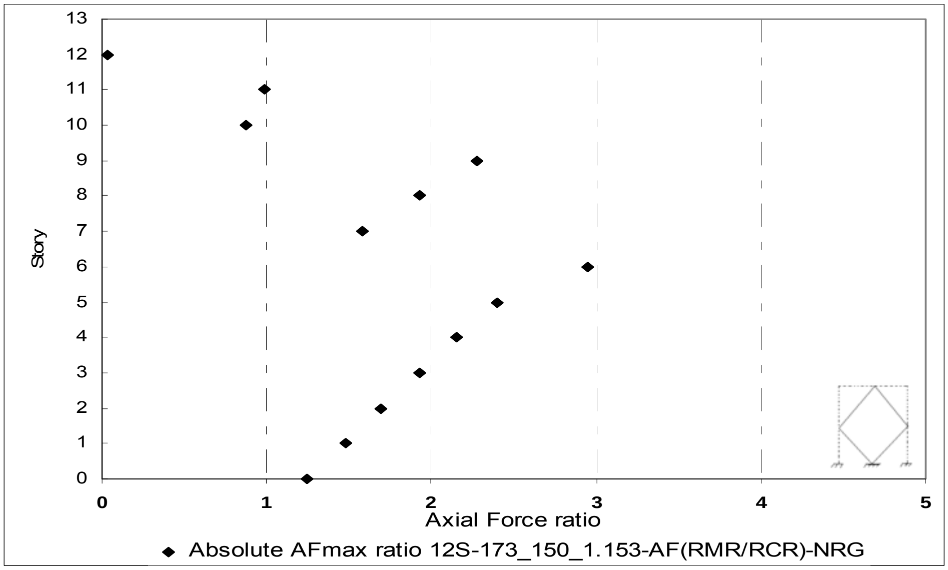

b)

Figure B.13 Axial Force ratio for 12S-173_150_1.153-NRG
a)Beams, b)Columns

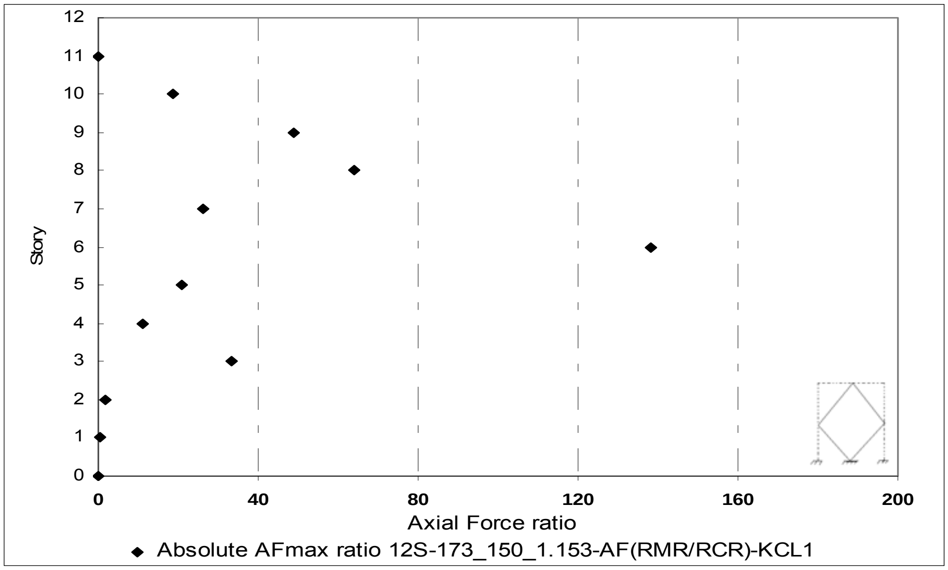

a)

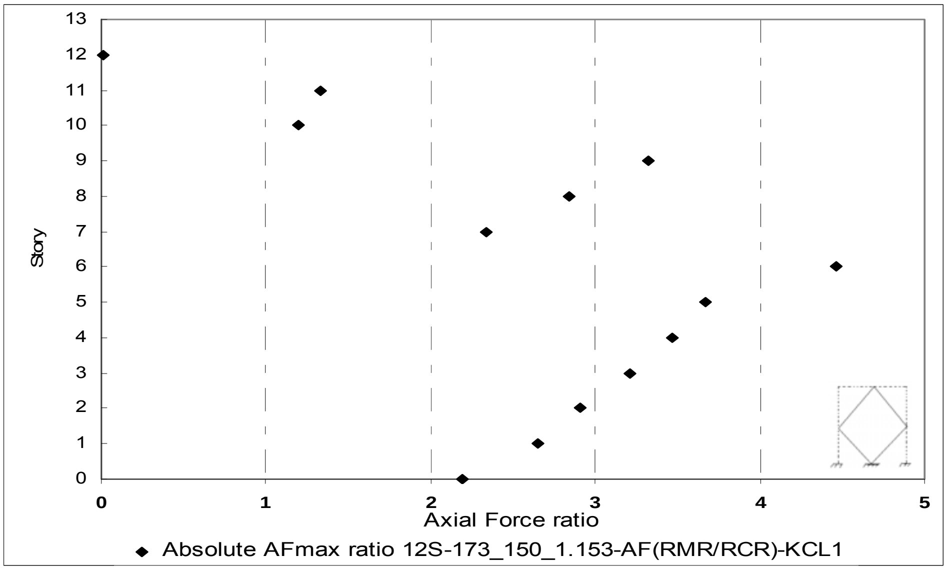

b)

Figure B.14 Axial Force ratio for 12S-173_150_1.153-KCL1
a)Beams, b)Columns

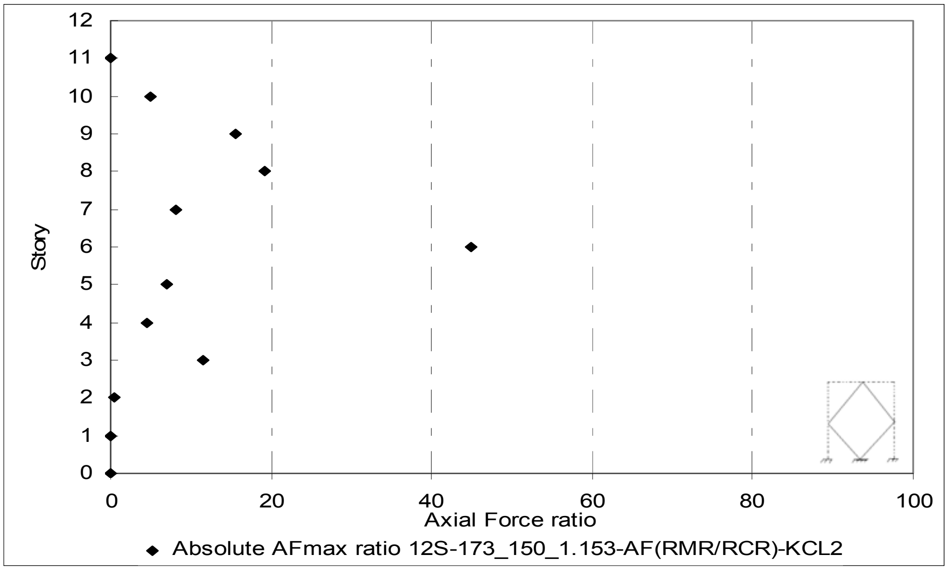

a)

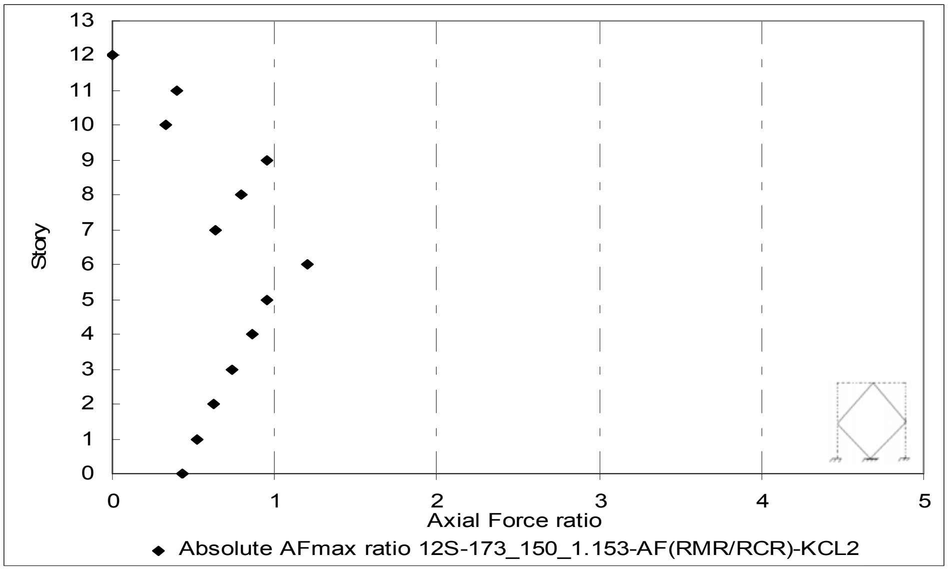

b)

Figure B.15 Axial Force ratio for 12S-173_150_1.153-KCL2
a)Beams, b)Columns

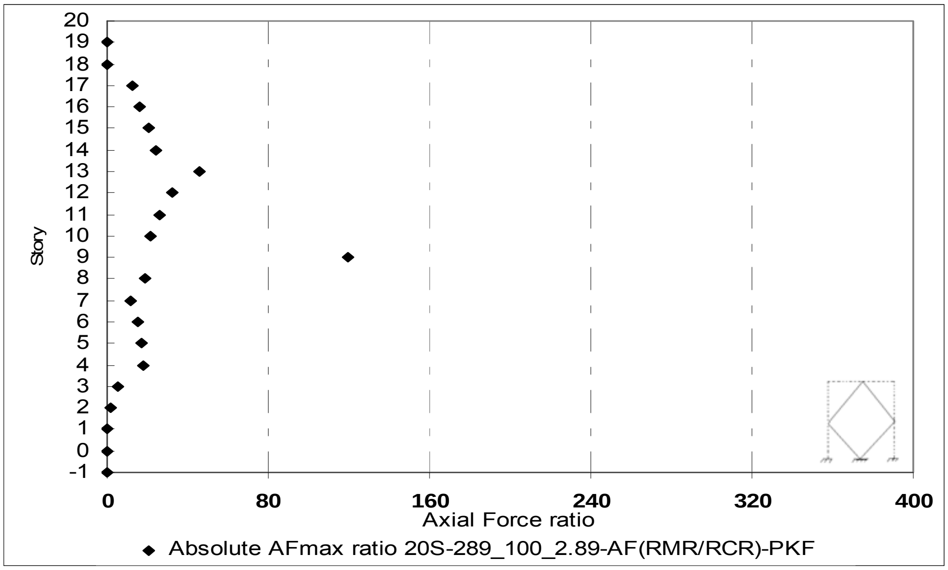

a)

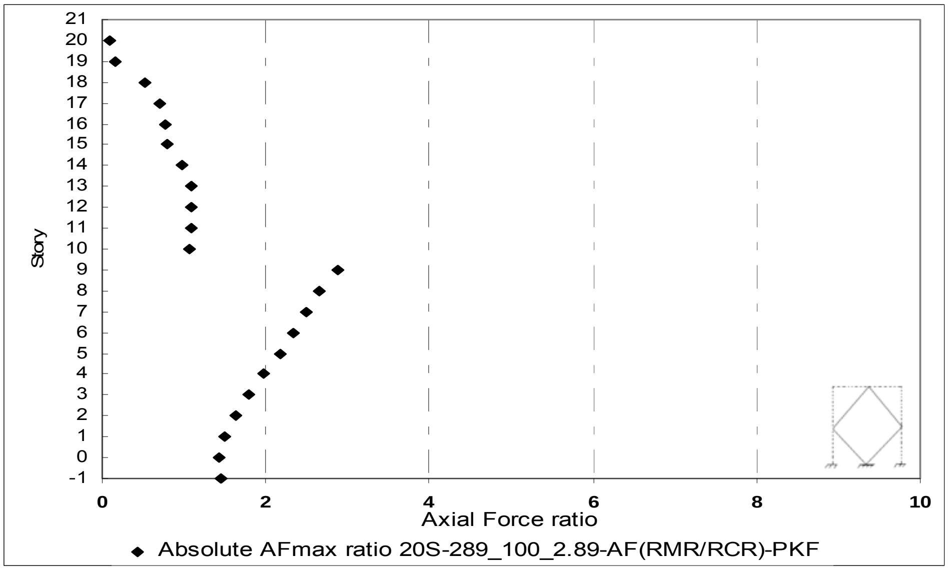

b)

Figure B.16 Axial Force ratio for 20S-289_100_2.89-PKF
a)Beams, b)Columns

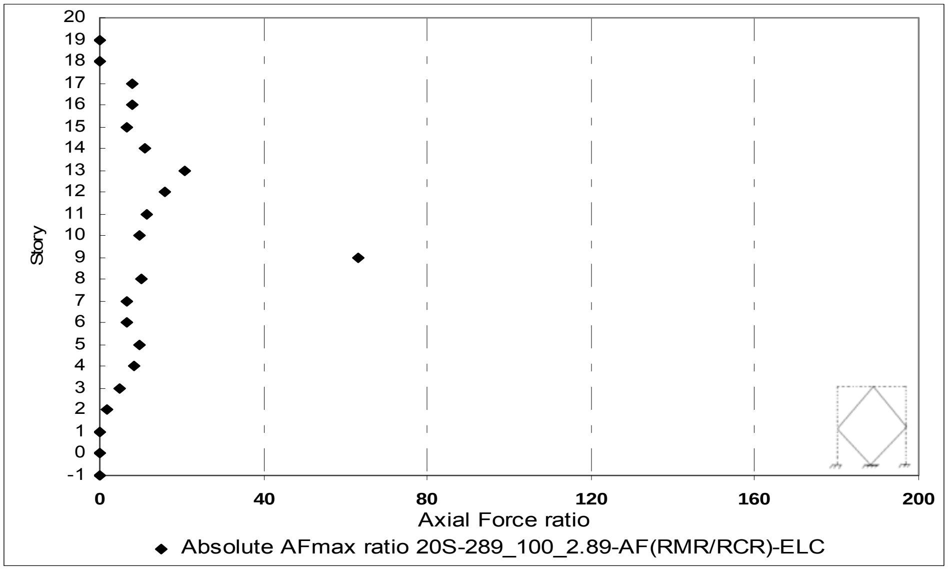

a)

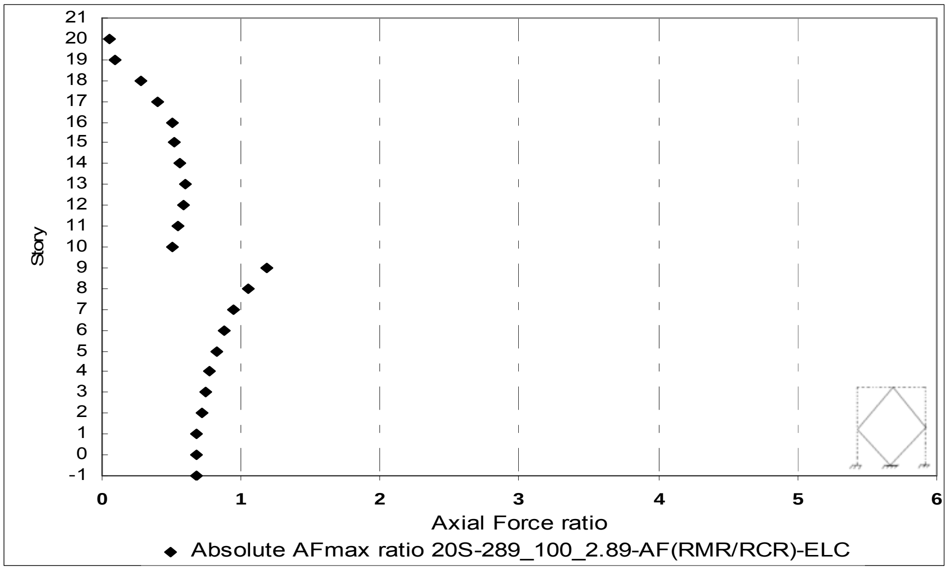

b)

Figure B.17 Axial Force ratio for 20S-289_100_2.89-ELC
a)Beams, b)Columns

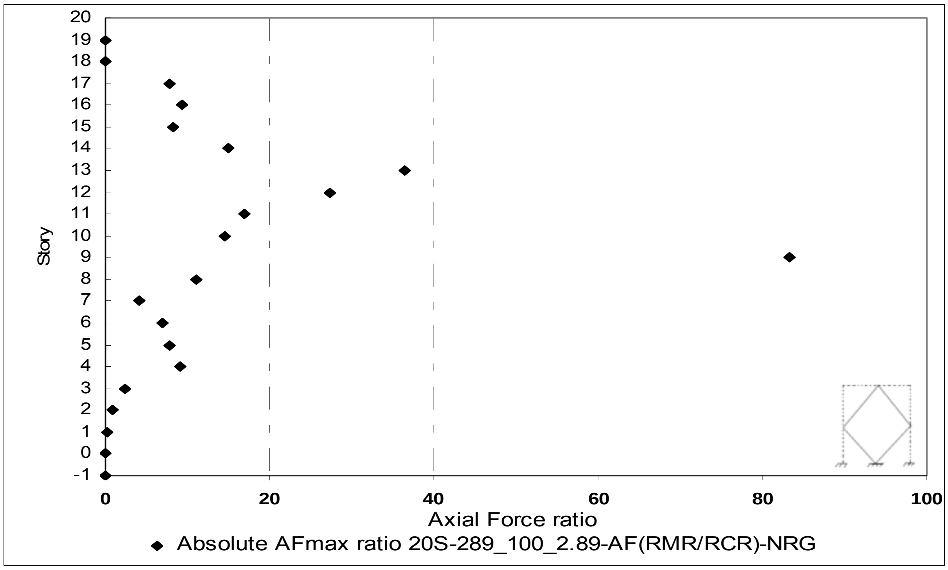

a)

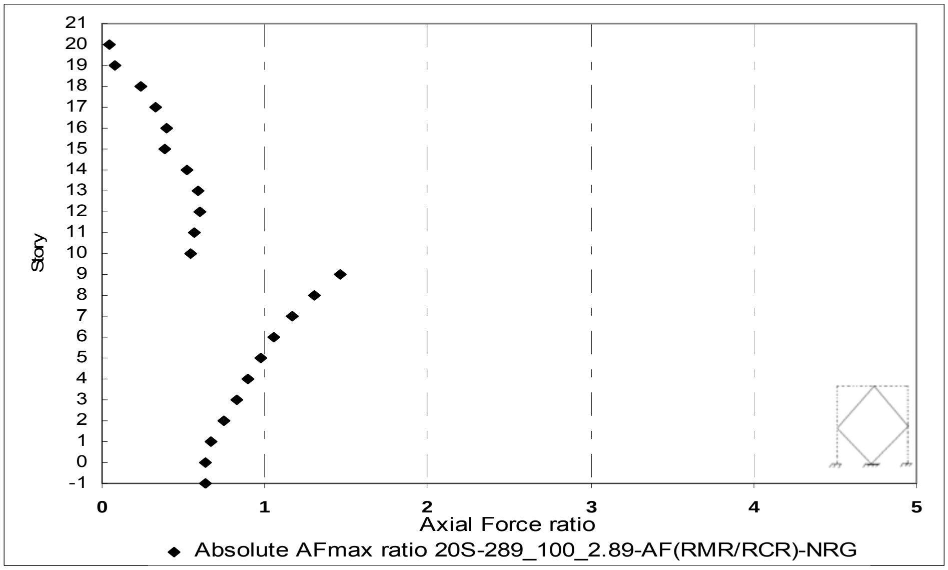

b)

Figure B.18 Axial Force ratio for 20S-289_100_2.89-NRG
a)Beams, b)Columns

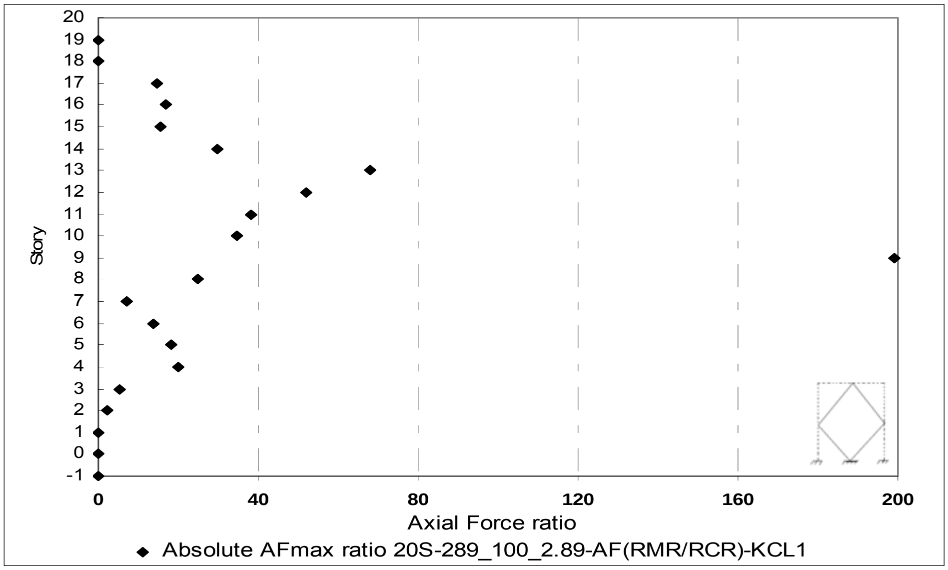

a)

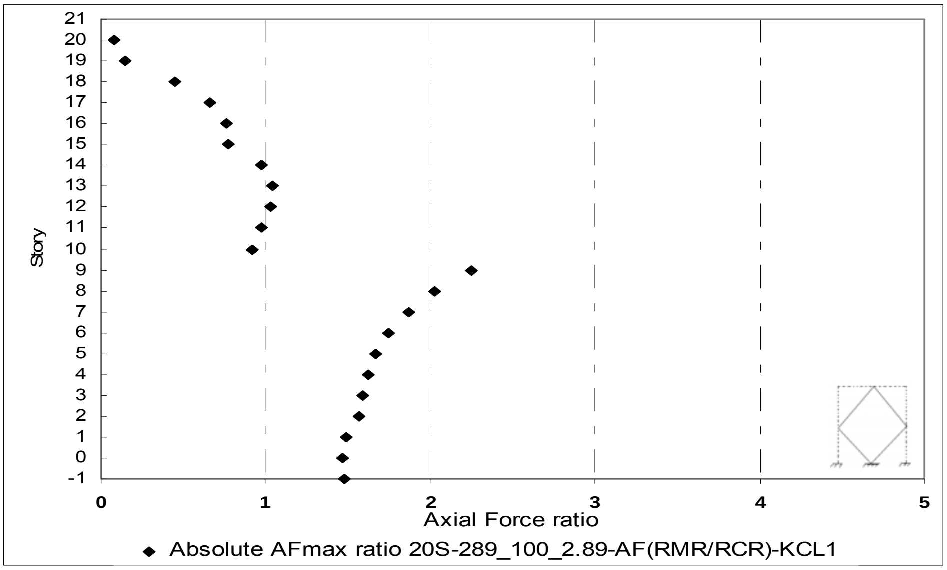

b)

Figure B.19 Axial Force ratio for 20S-289_100_2.89-KCL1
a)Beams, b)Columns

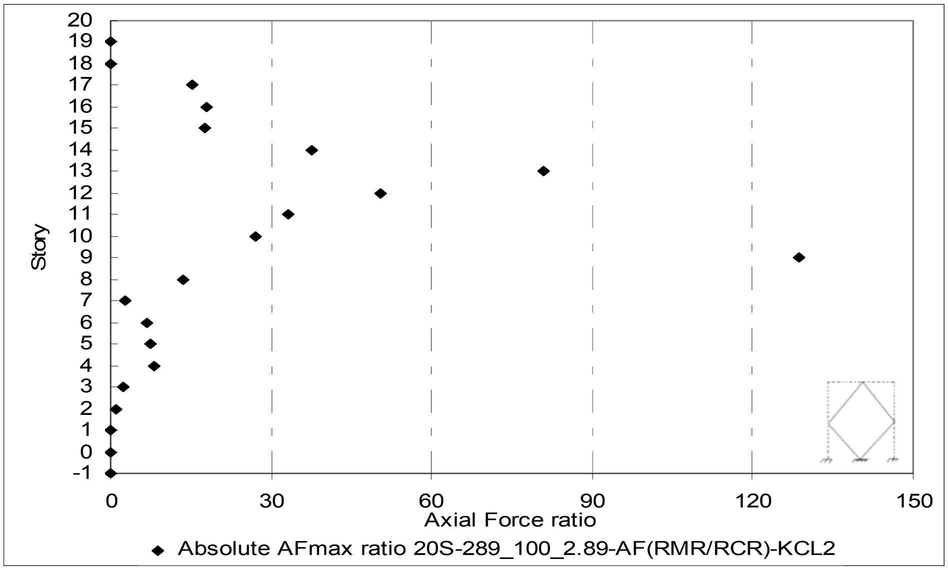

a)

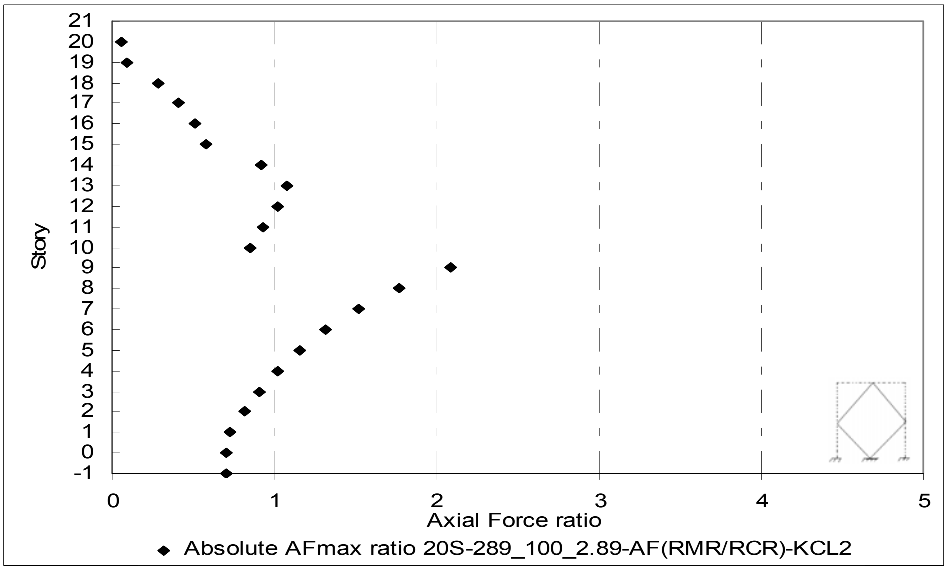

b)

Figure B.20 Axial Force ratio for 20S-289_100_2.89-KCL2
a)Beams, b)Columns

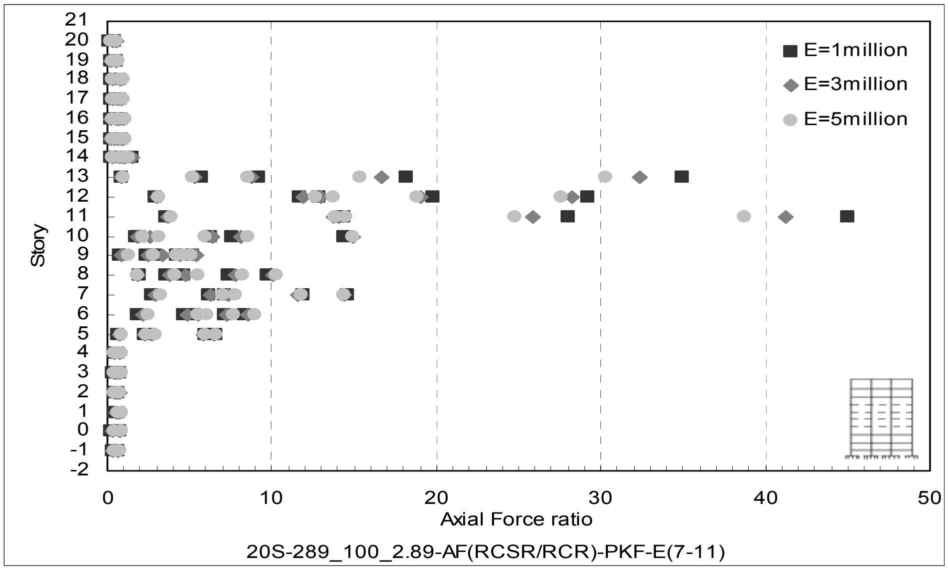

a)

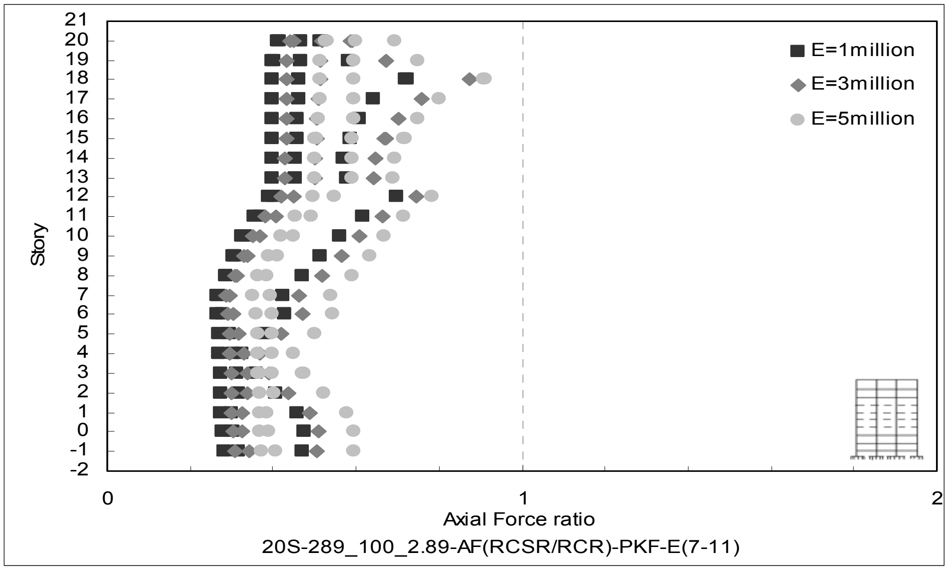

b)

Figure B.21 Axial Force ratio for 20S-289_100_2.89-PKF
a)Beams, b)Columns

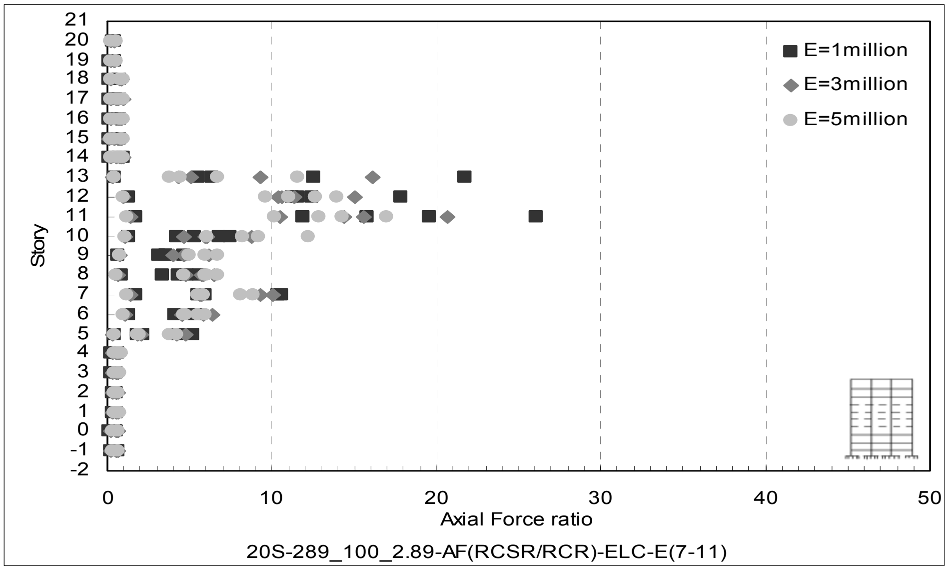

a)

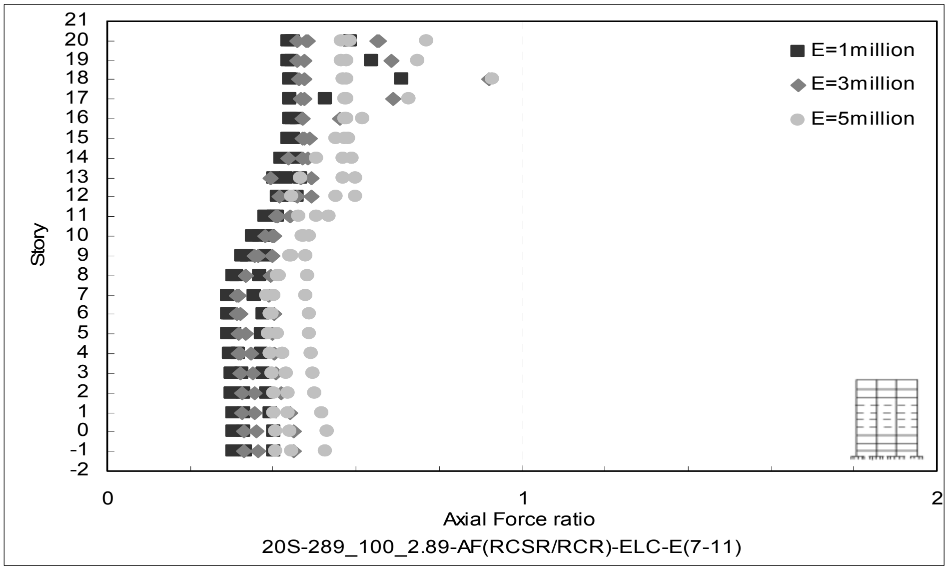

b)

Figure B.22 Axial Force ratio for 20S-289_100_2.89-ELC
a)Beams, b)Columns

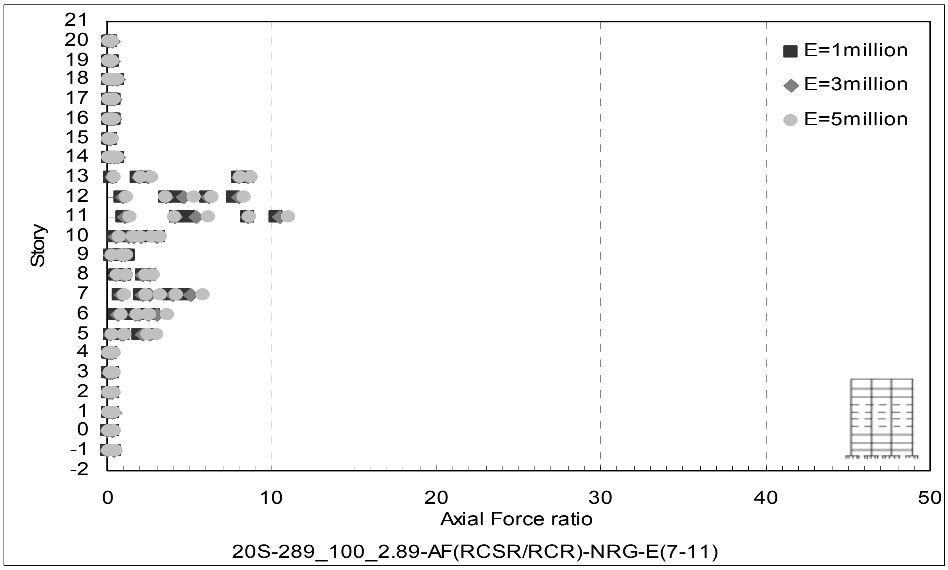

a)

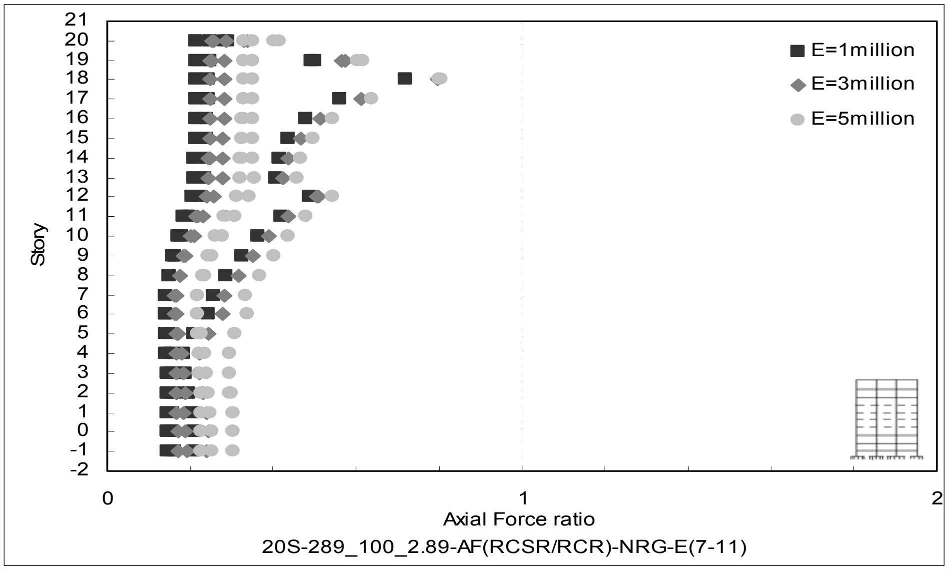

b)

Figure B.23 Axial Force ratio for 20S-289_100_2.89-NRG
a)Beams, b)Columns

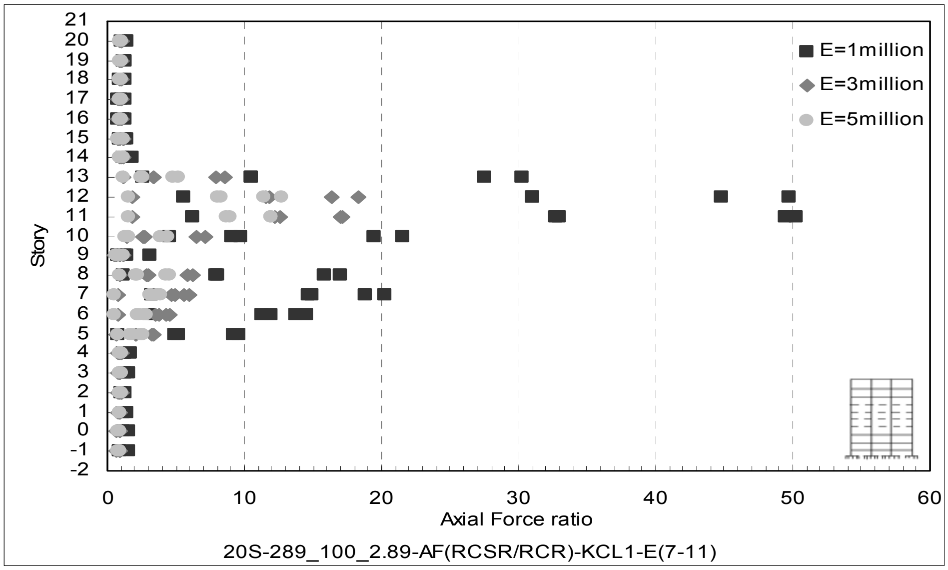

a)

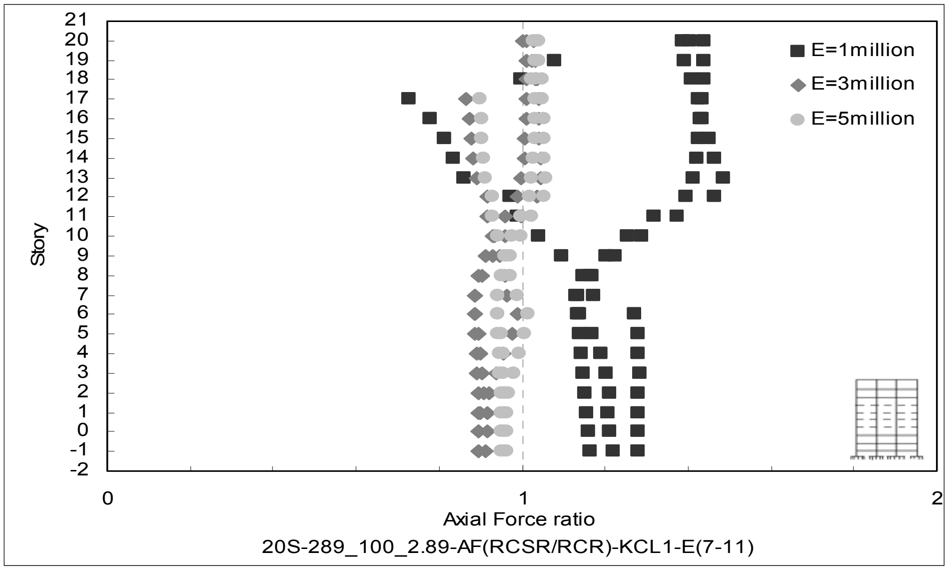

b)

Figure B.24 Axial Force ratio for 20S-289_100_2.89-KCL1
a)Beams, b)Columns

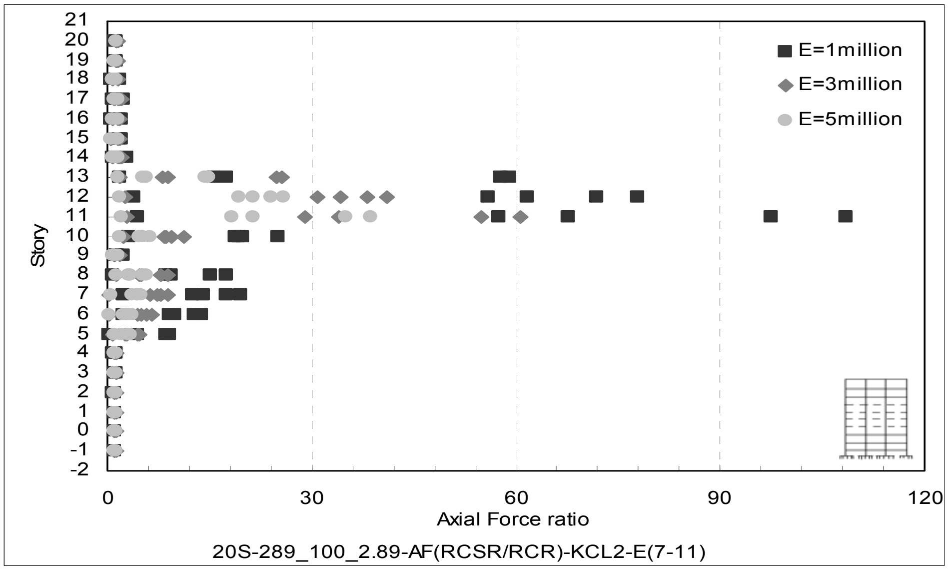

a)

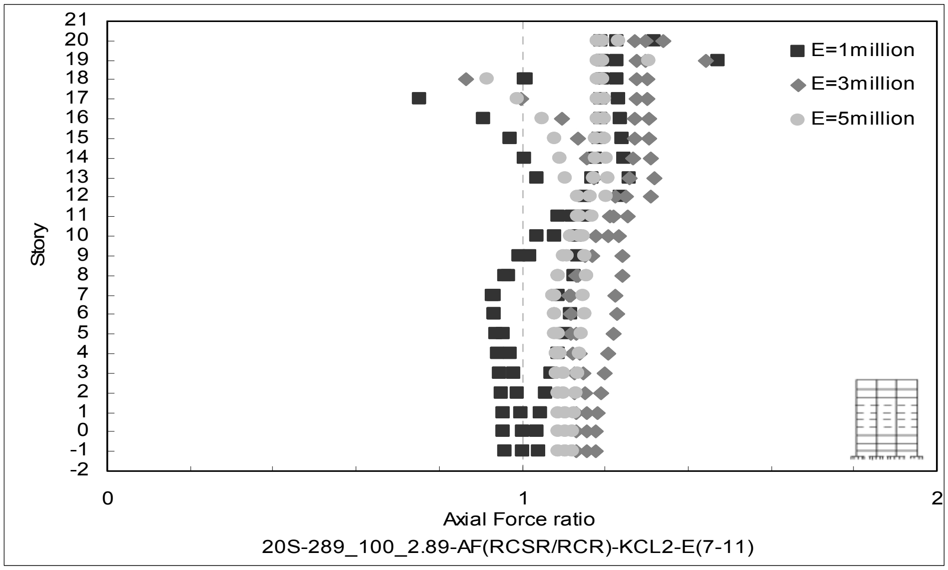

b)

Figure B.25 Axial Force ratio for 20S-289_100_2.89-KCL2
a)Beams, b)Columns

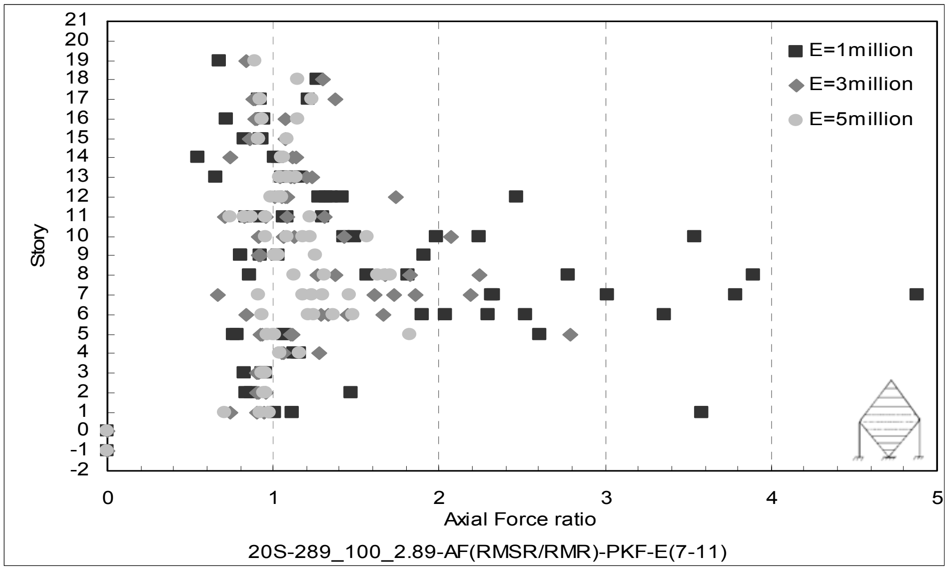

a)

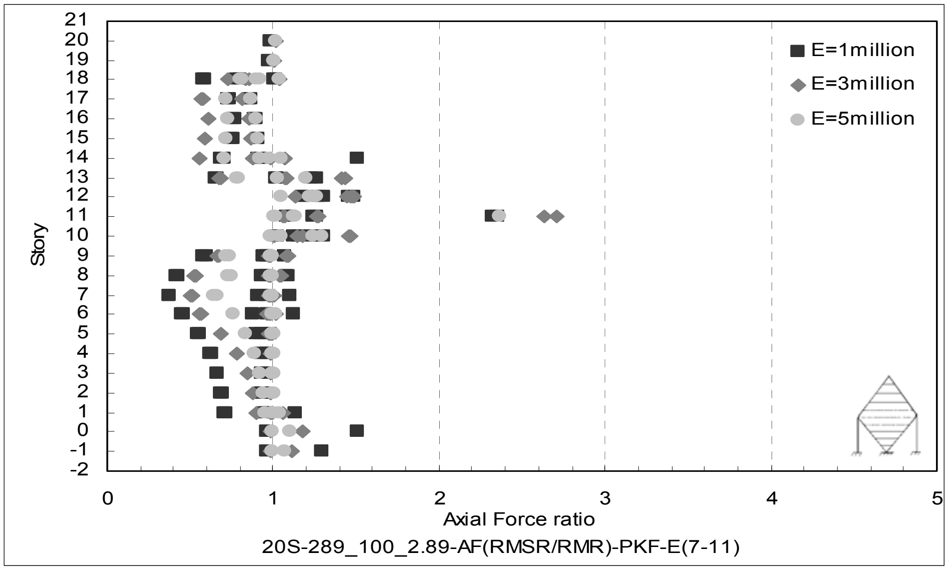

b)

Figure B.26 Axial Force ratio for 20S-289_100_2.89-PKF
a)Beams, b)Columns

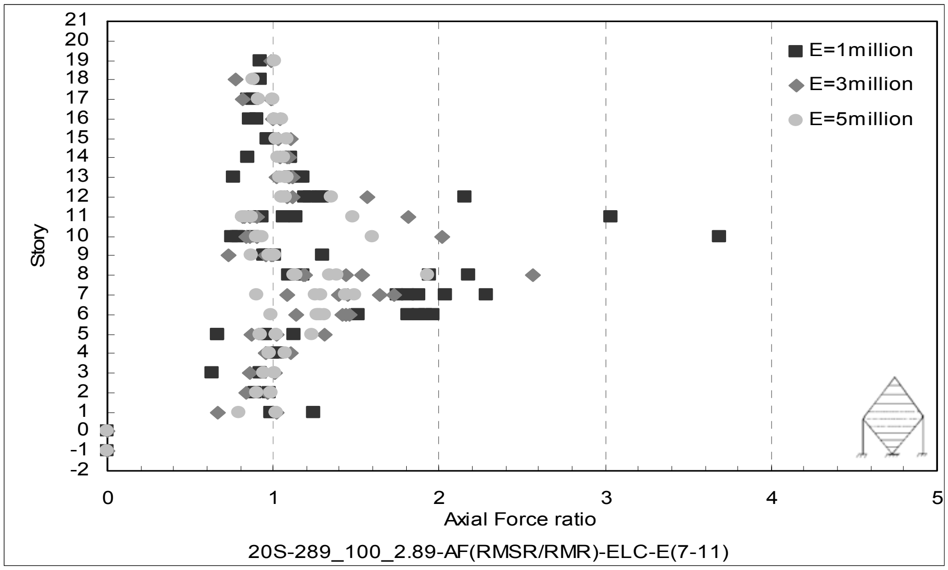

a)

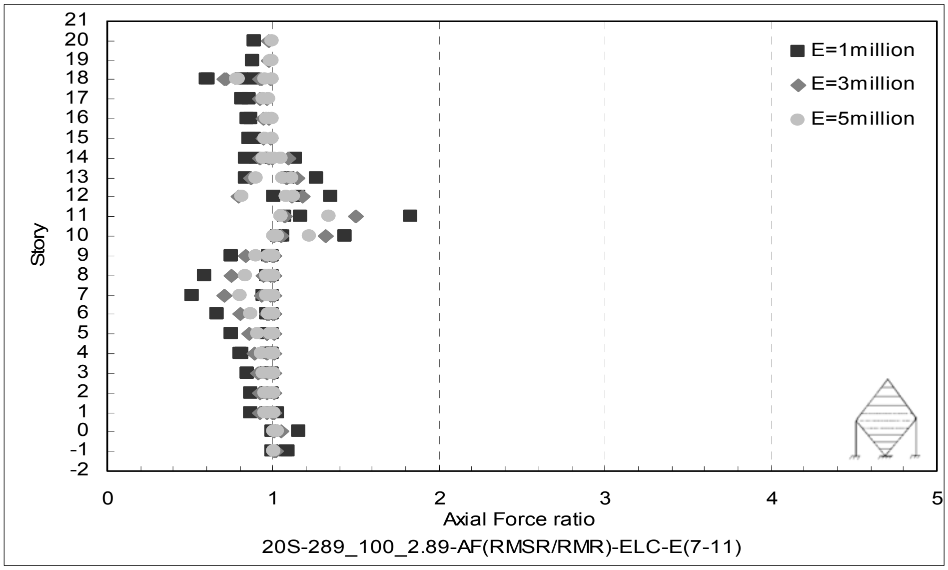

b)

Figure B.27 Axial Force ratio for 20S-289_100_2.89-ELC
a)Beams, b)Columns

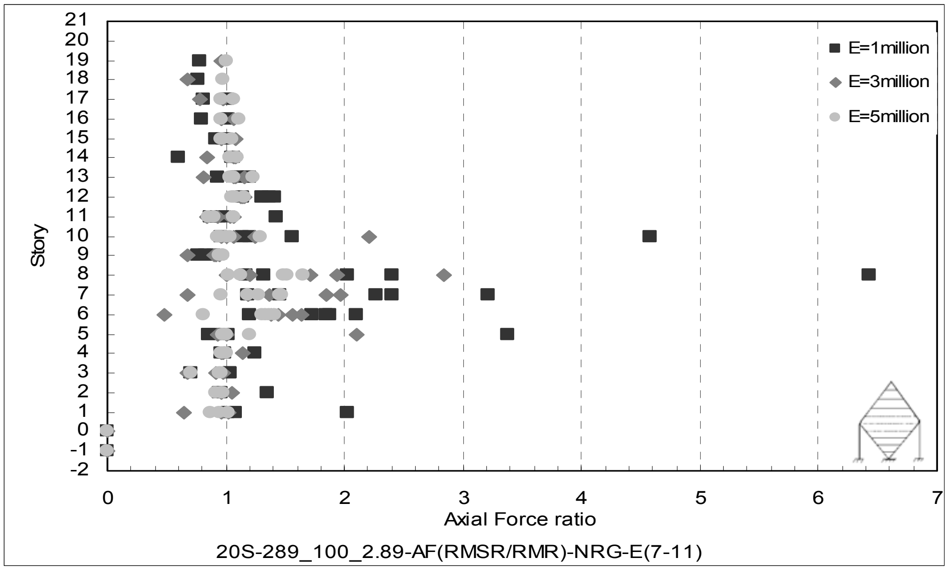

a)

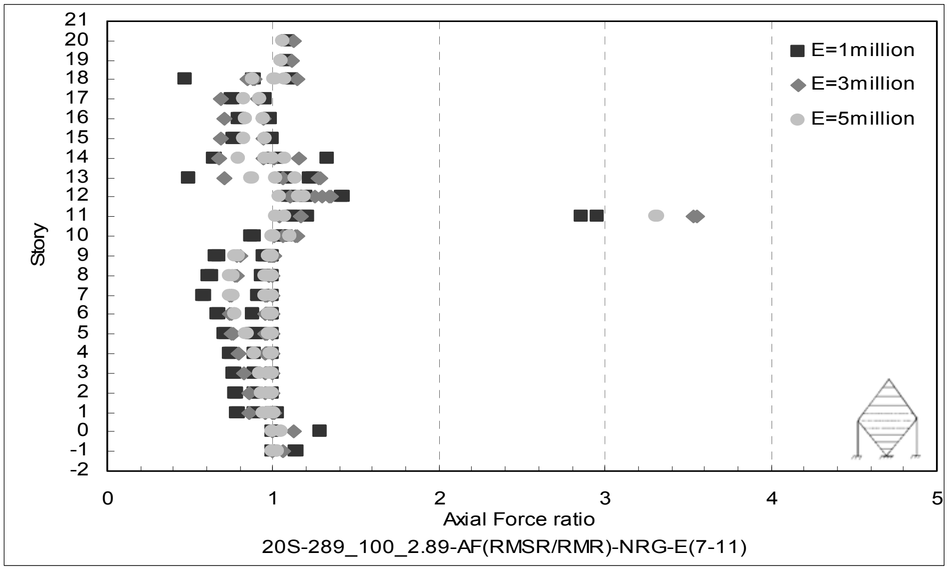

b)

Figure B.28 Axial Force ratio for 20S-289_100_2.89-NRG
a)Beams, b)Columns

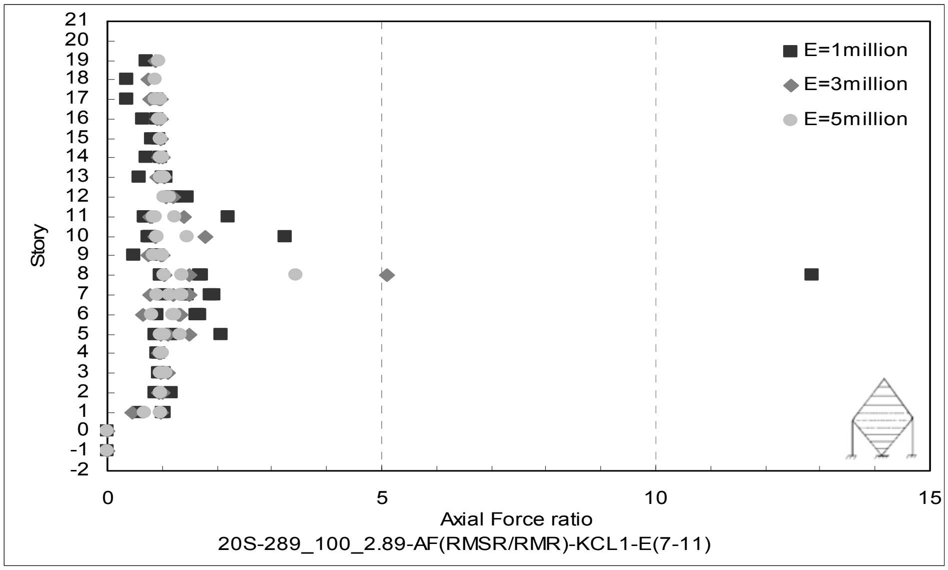

a)

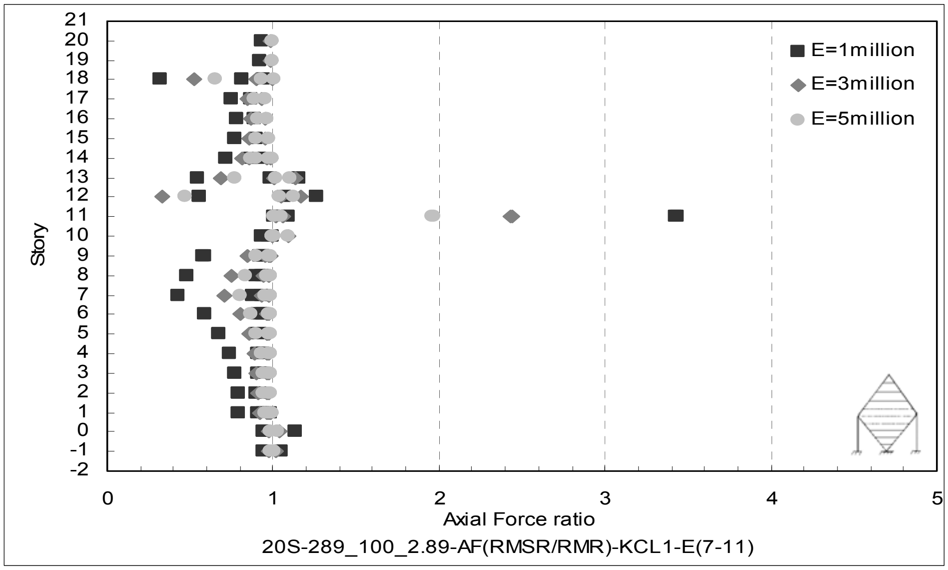

b)

Figure B.29 Axial Force ratio for 20S-289_100_2.89-KCL1
a)Beams, b)Columns

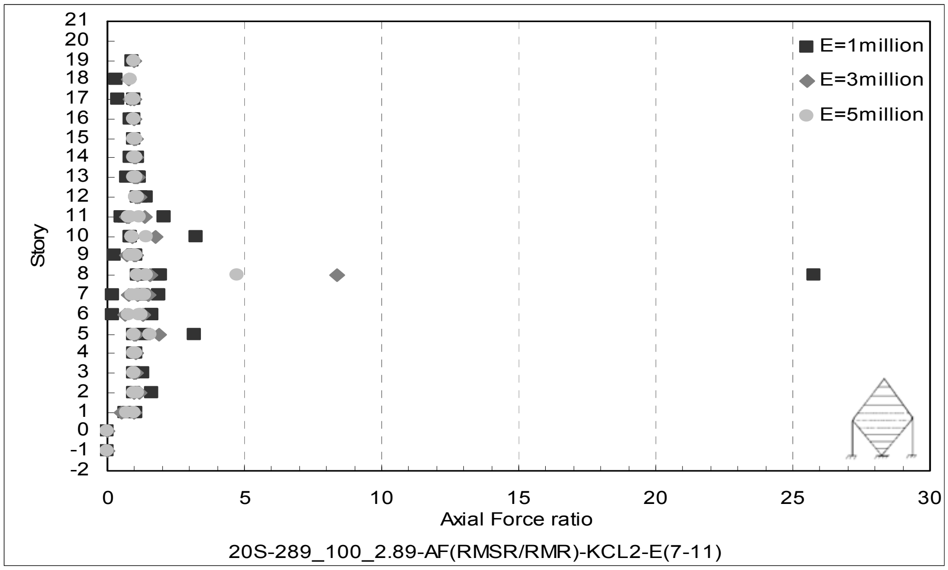

a)

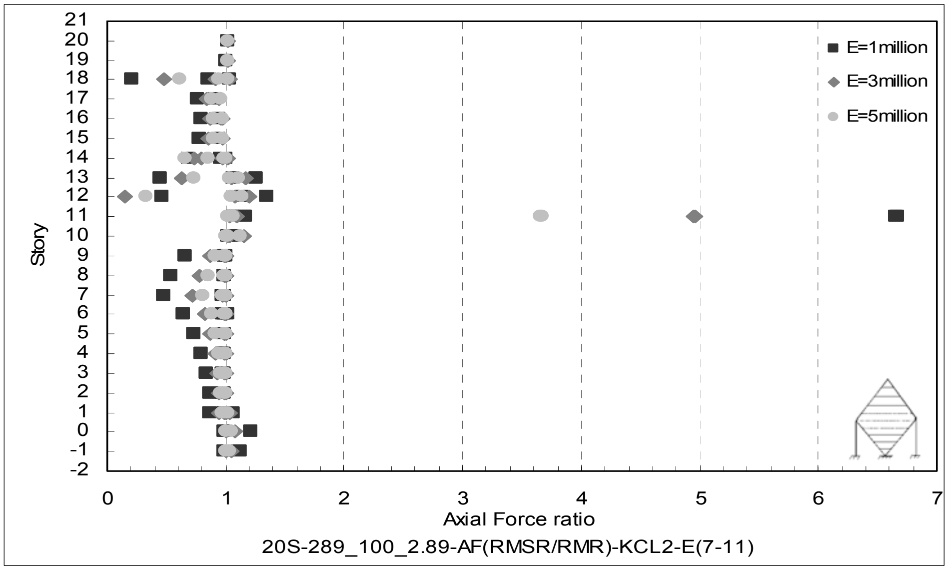

b)

Figure B.30 Axial Force ratio for 20S-289_100_2.89-KCL2
a)Beams, b)Columns

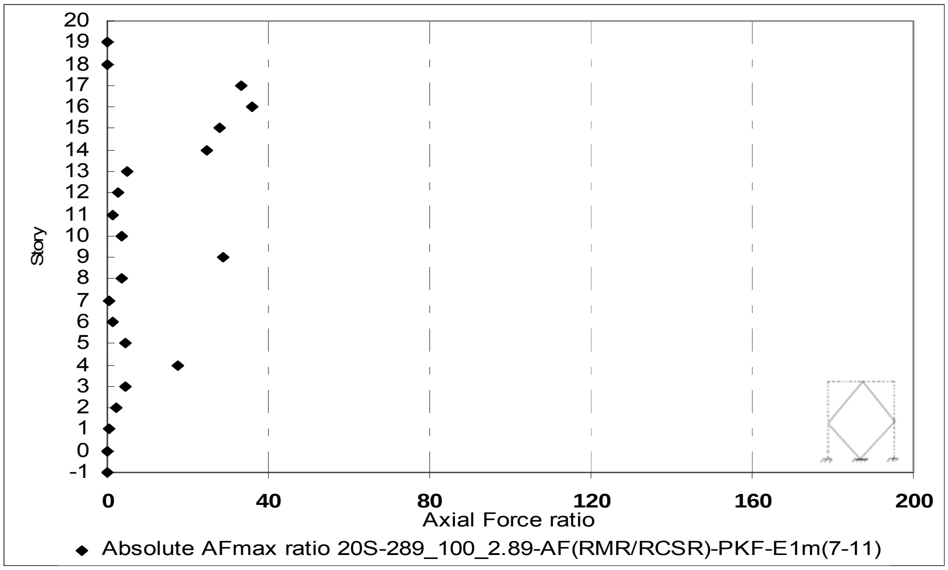

a)

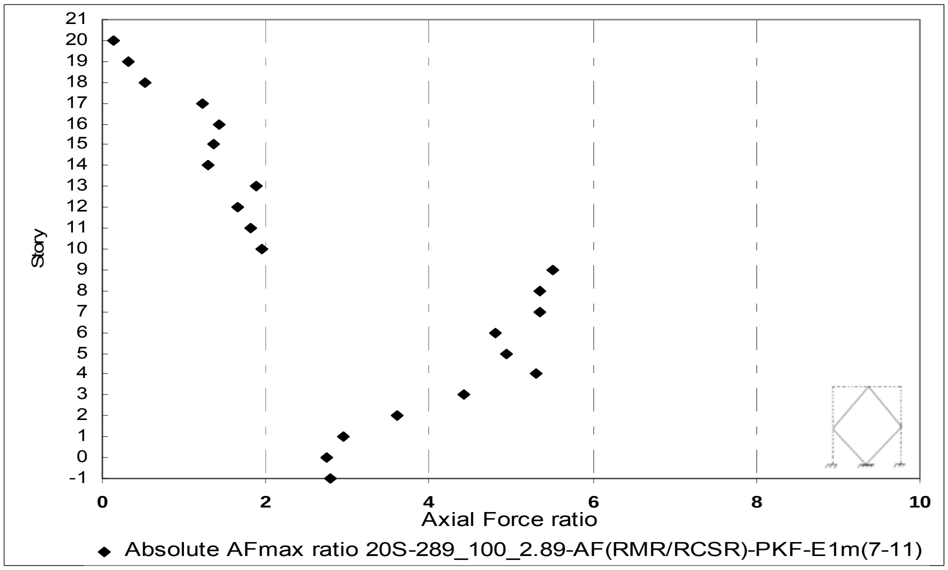

b)

Figure B.31 Axial Force ratio for 20S-289_100_2.89-PKF
a)Beams, b)Columns

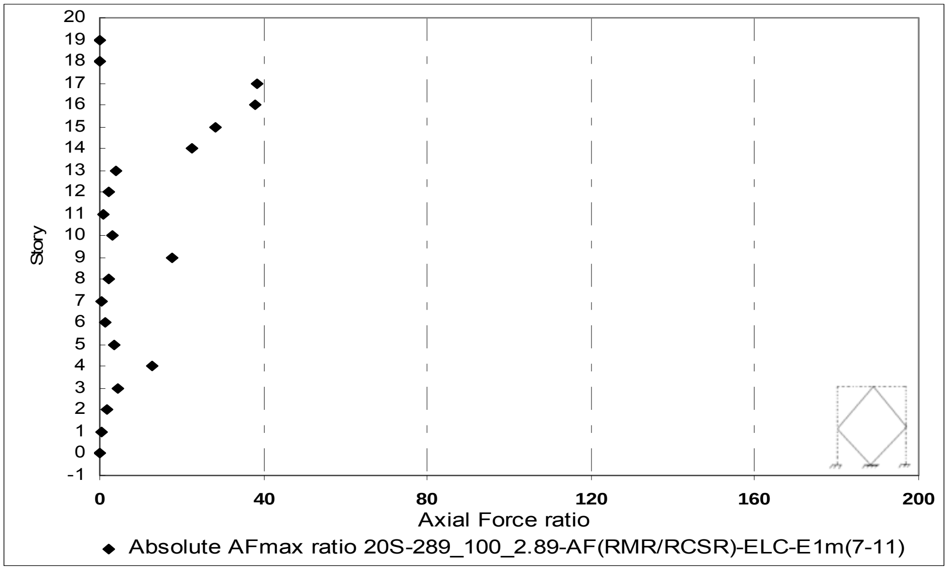

a)

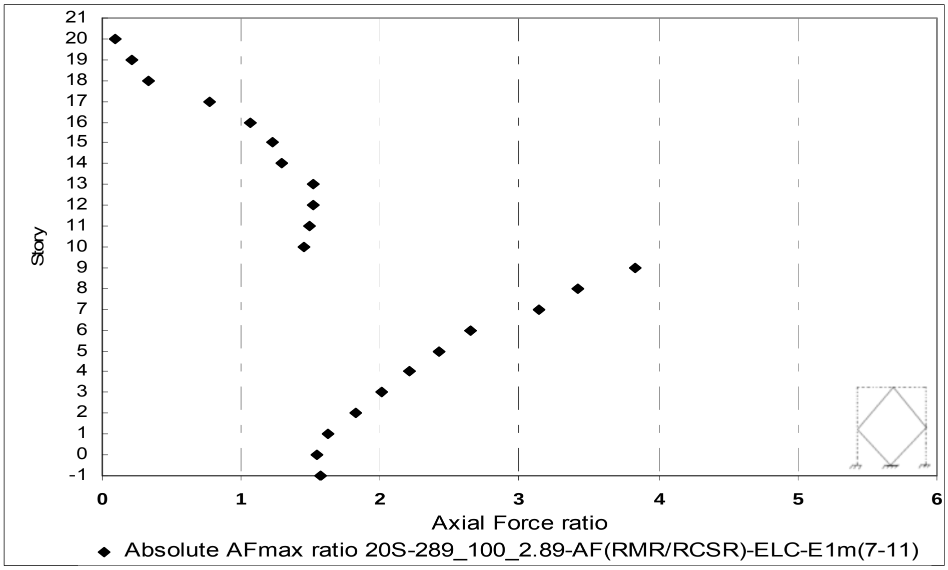

b)

Figure B.32 Axial Force ratio for 20S-289_100_2.89-ELC
a)Beams, b)Columns

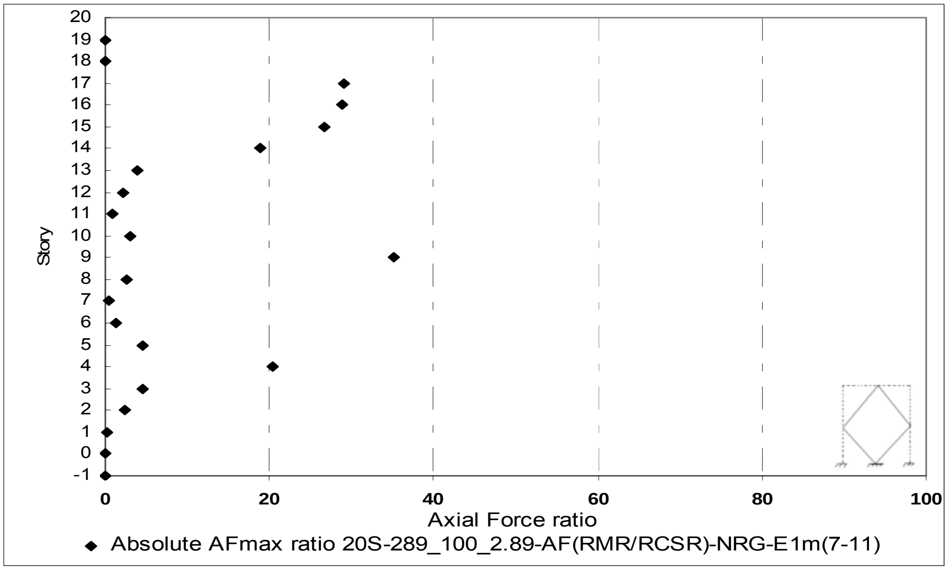

a)

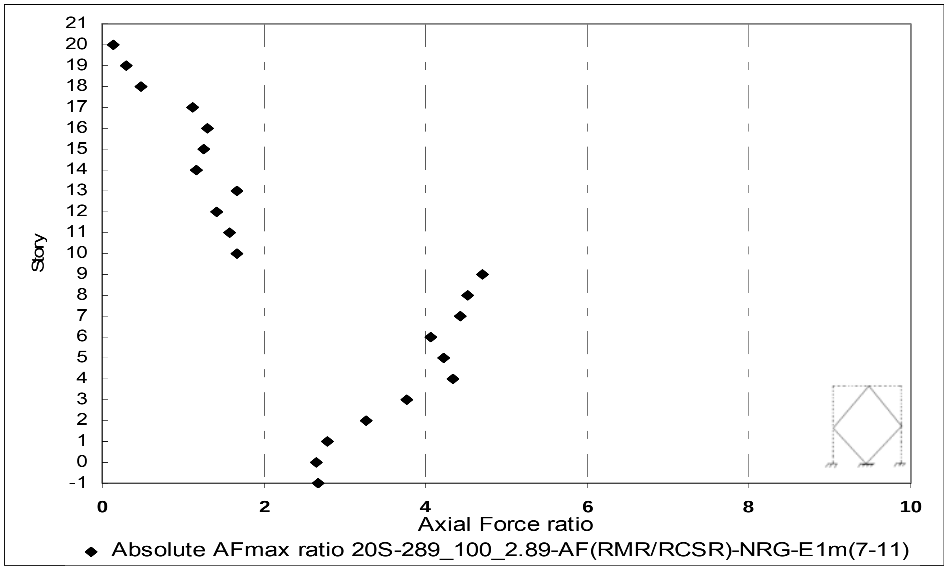

b)

Figure B.33 Axial Force ratio for 20S-289_100_2.89-NRG
a)Beams, b)Columns

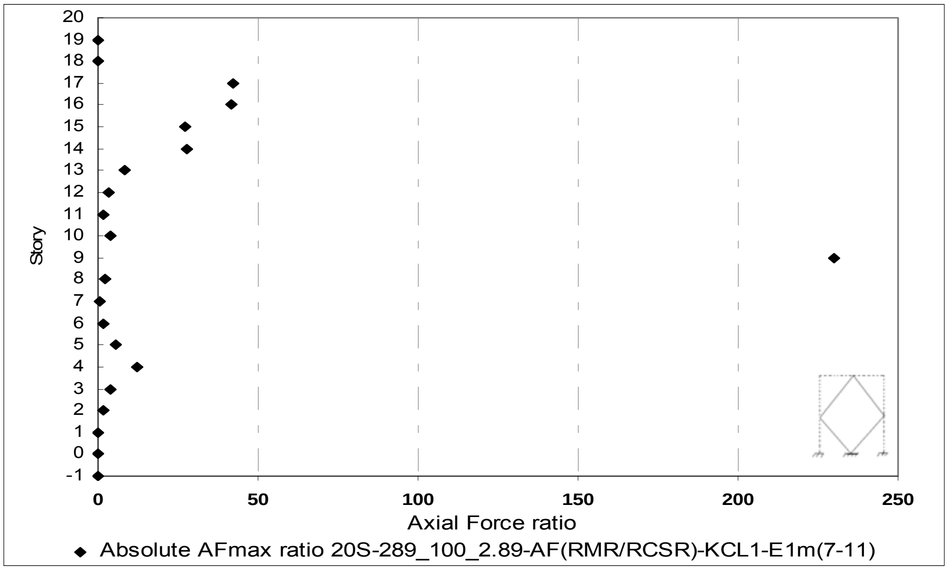

a)

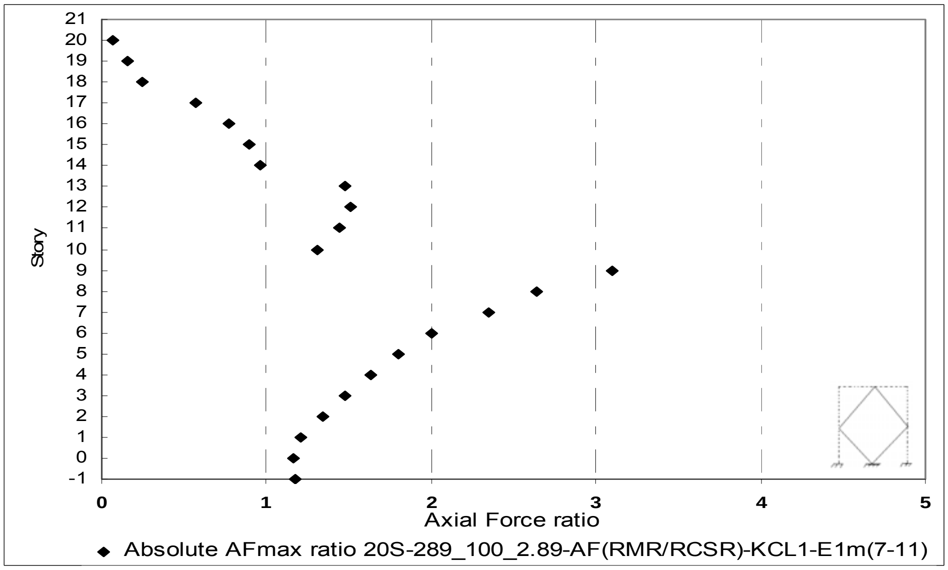

b)

Figure B.34 Axial Force ratio for 20S-289_100_2.89-KCL1
a)Beams, b)Columns

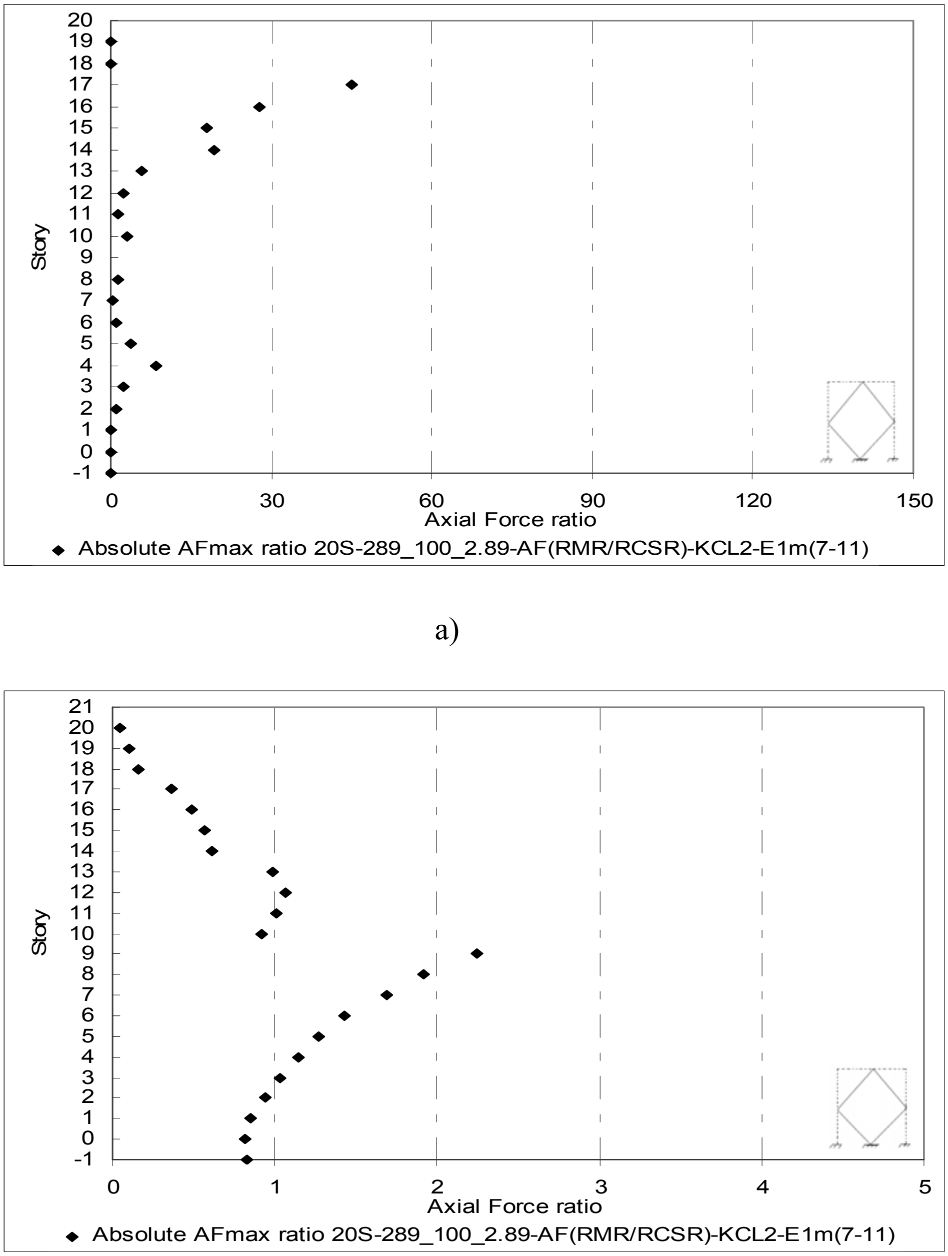

a)

b)

Figure B.35 Axial Force ratio for 20S-289_100_2.89-KCL2
a)Beams, b)Columns

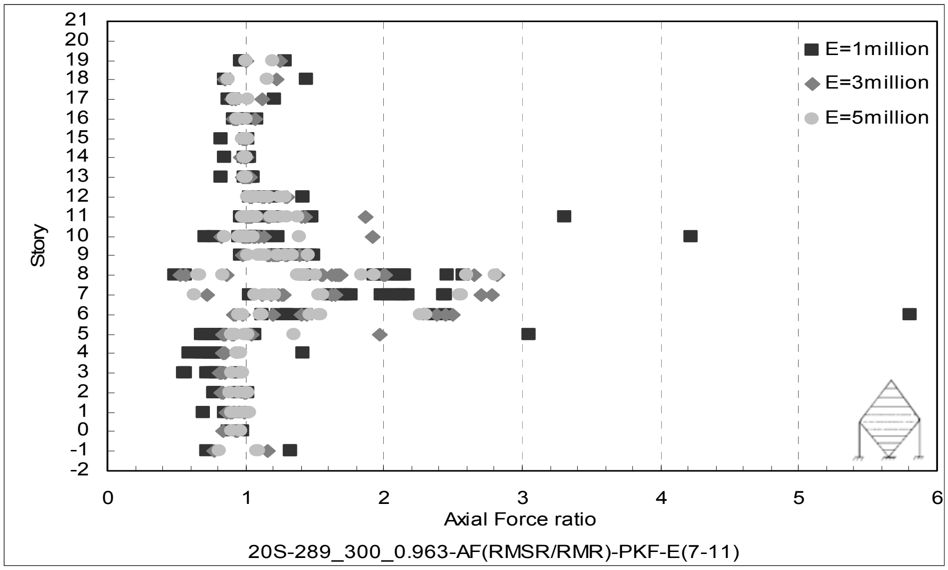

a)

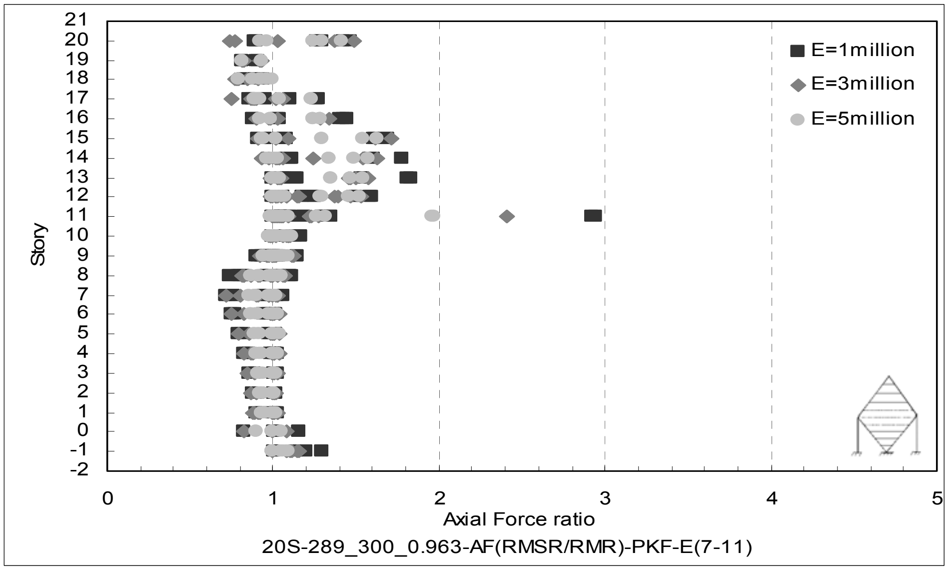

b)

Figure B.36 Axial Force ratio for 20S-289_300_0.963-PKF
a)Beams, b)Columns

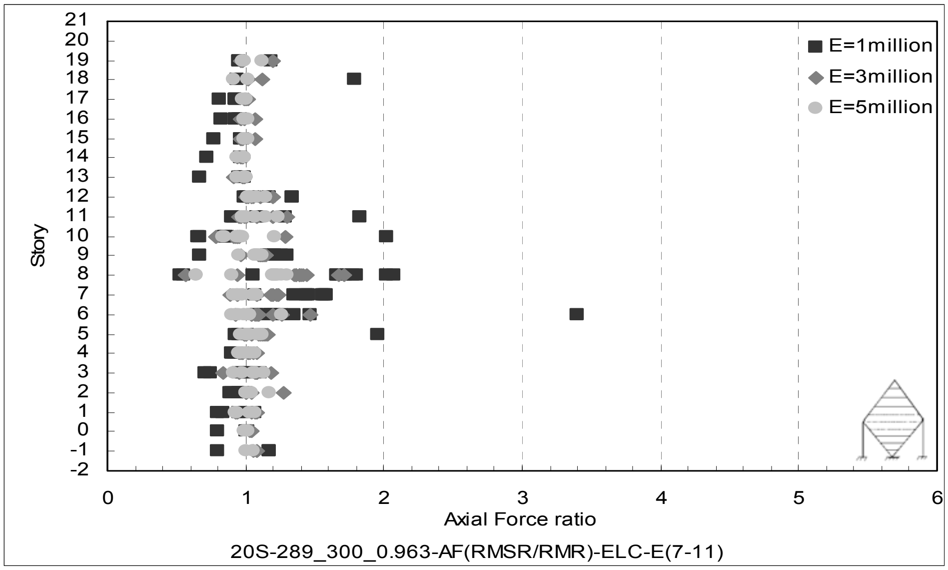

a)

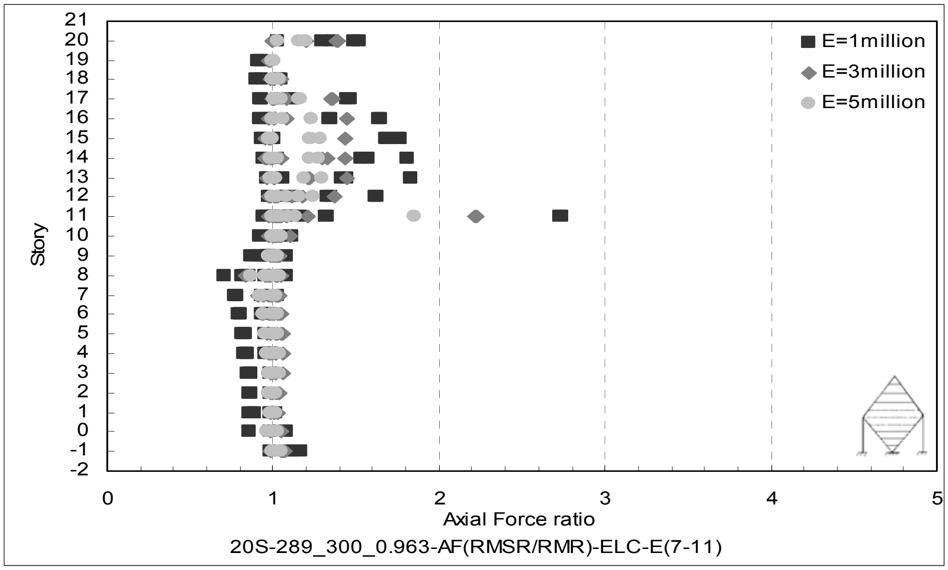

b)

Figure B.37 Axial Force ratio for 20S-289_300_0.963-ELC
a)Beams, b)Columns

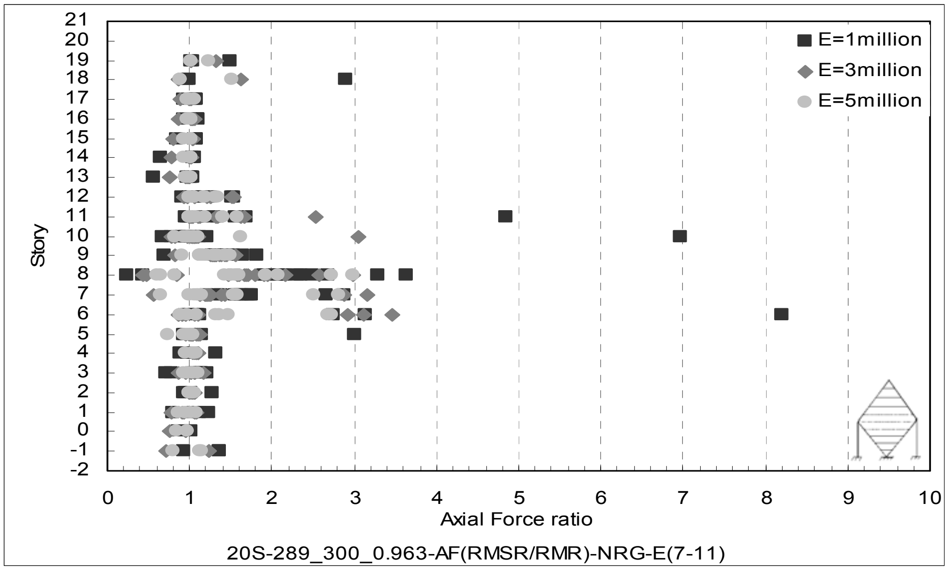

a)

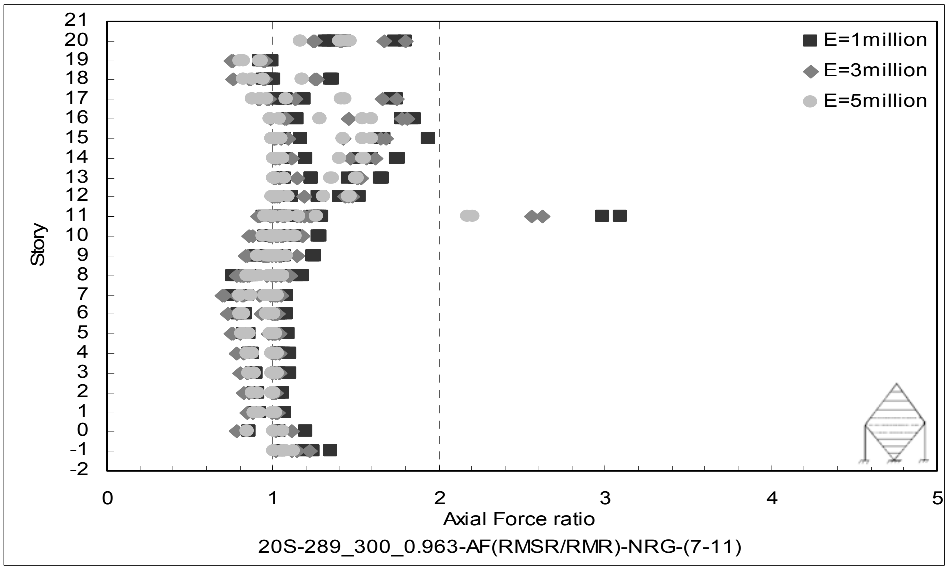

b)

Figure B.38 Axial Force ratio for 20S-289_300_0.963-NRG
a)Beams, b)Columns

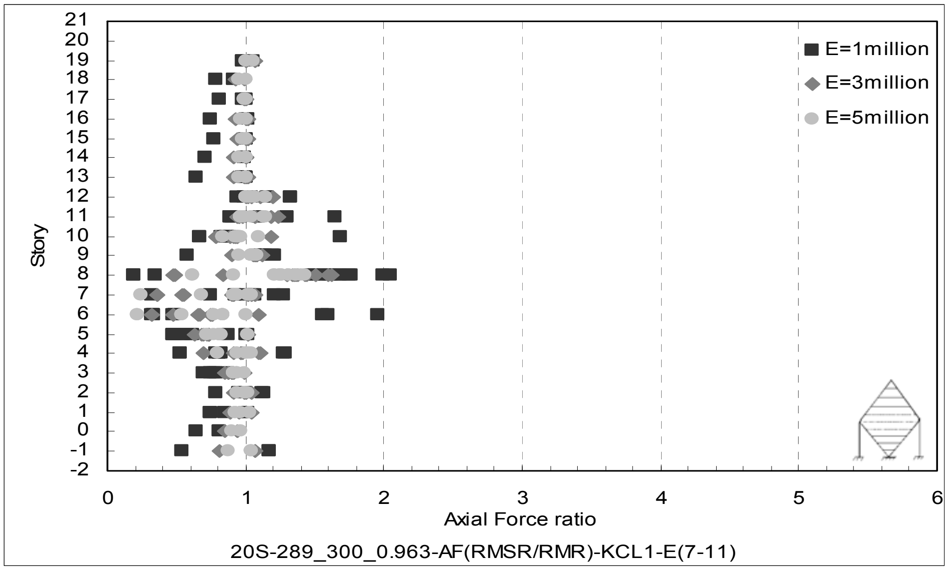

a)

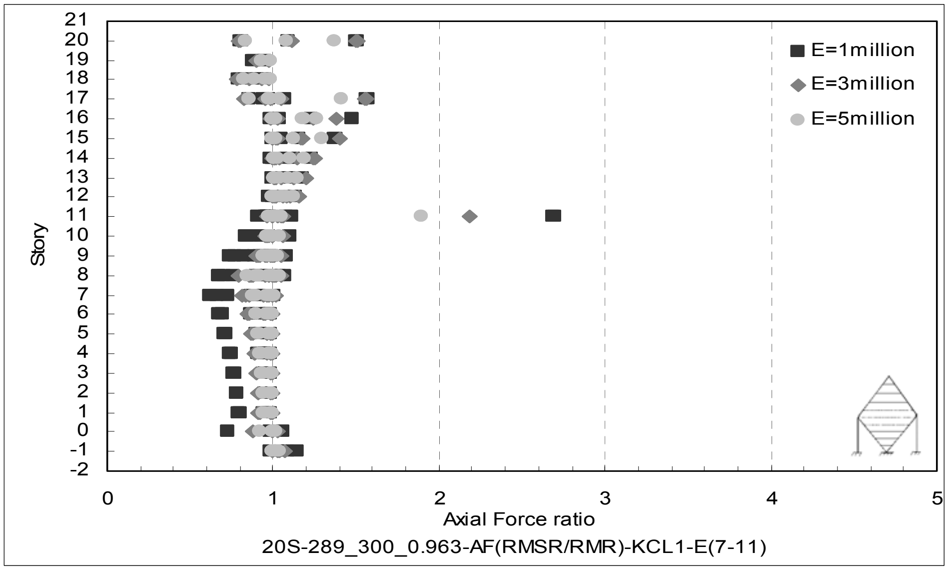

b)

Figure B.39 Axial Force ratio for 20S-289_300_0.963-KCL1
a)Beams, b)Columns

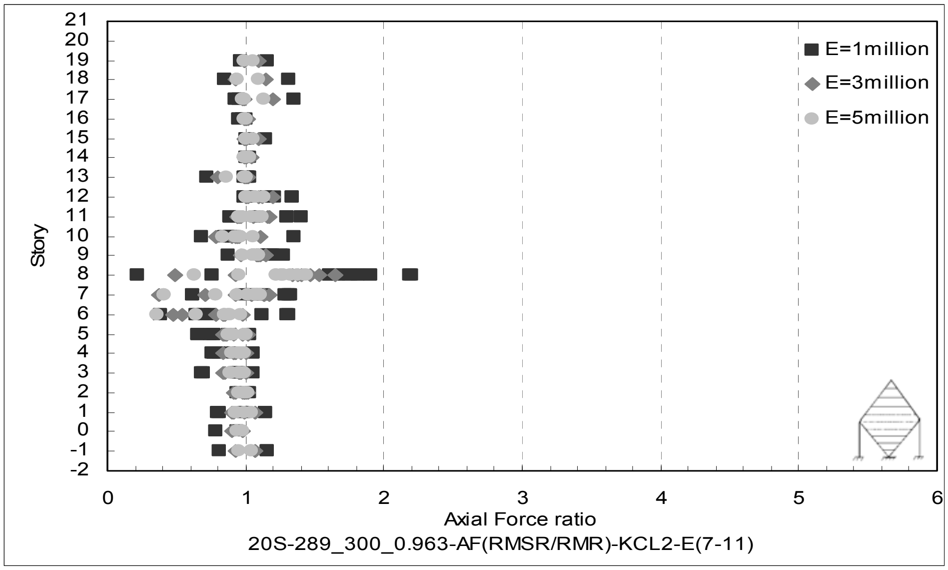

a)

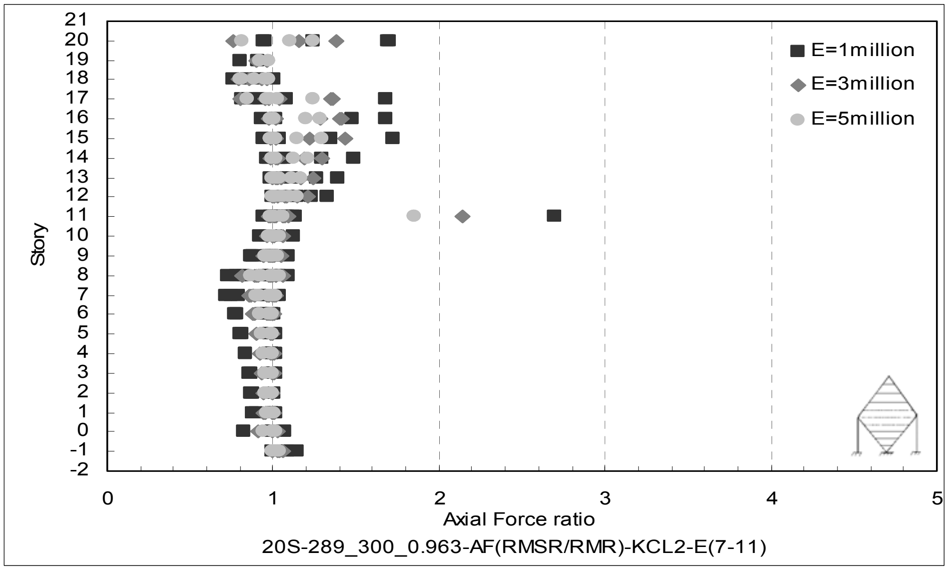

b)

Figure B.40 Axial Force ratio for 20S-289_300_0.963-KCL2
a)Beams, b)Columns

APPENDIX C

SHEAR FORCES IN THE FRAME ELEMENTS

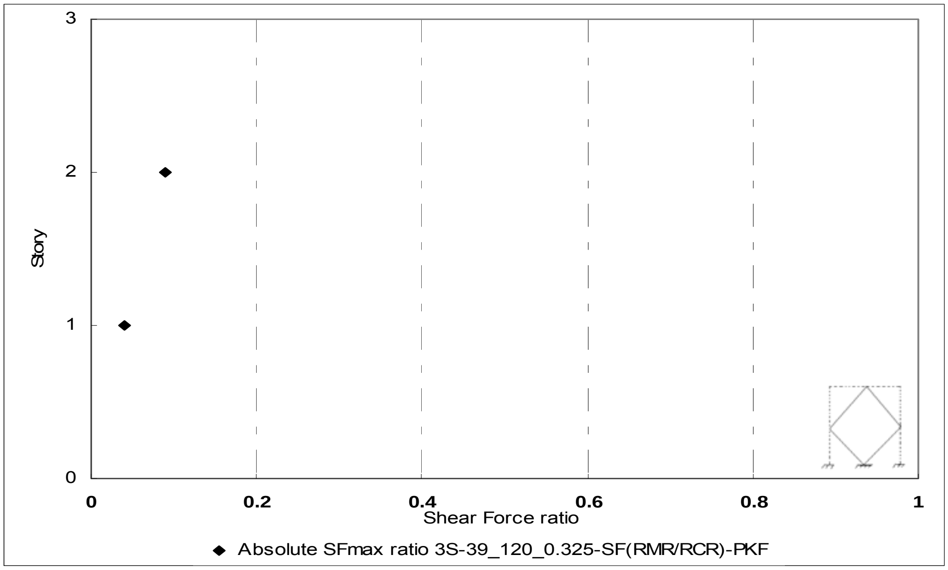

a)

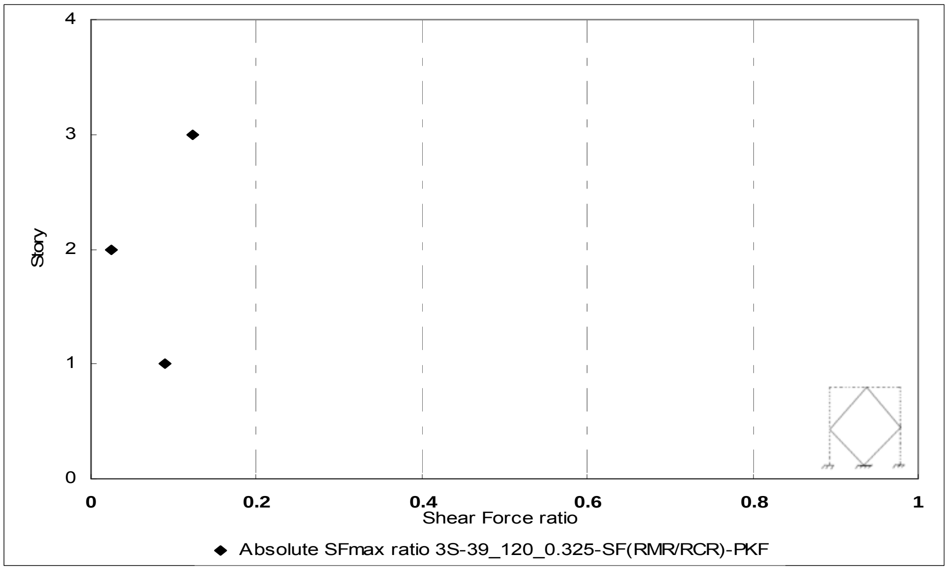

b)

Figure C.1 Shear Force ratio for 3S-39_120_0.325-PKF
a)Beams, b)Columns

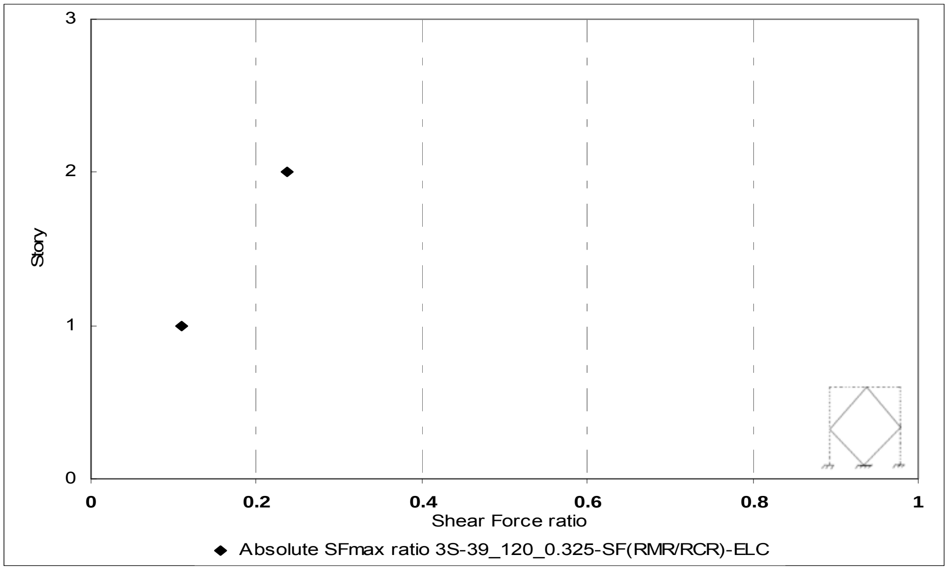

a)

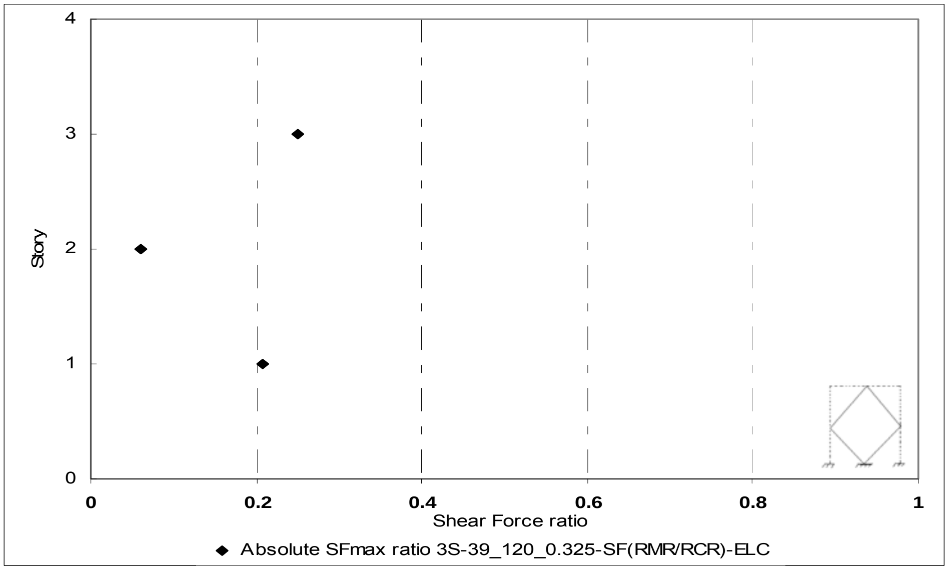

b)

Figure C.2 Shear Force ratio for 3S-39_120_0.325-ELC
a)Beams, b)Columns

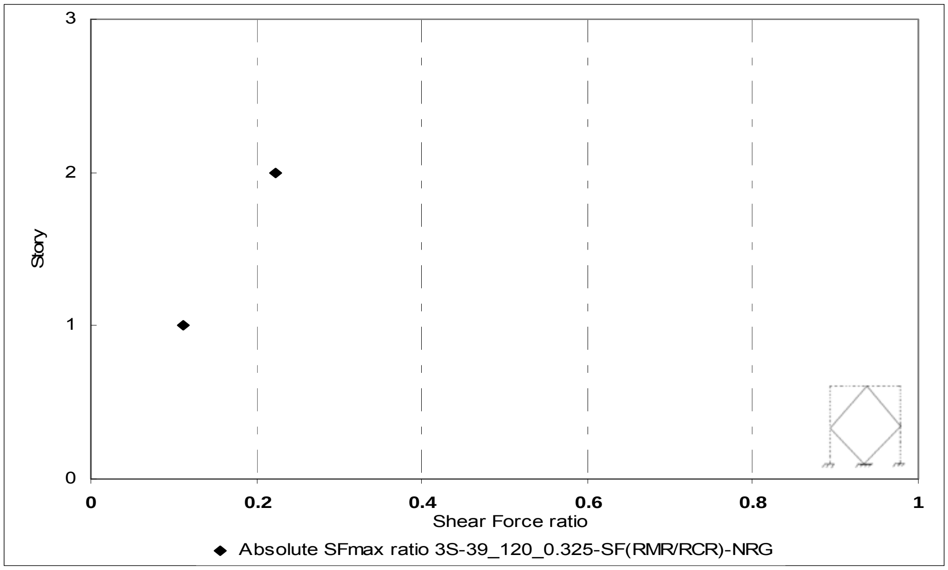

a)

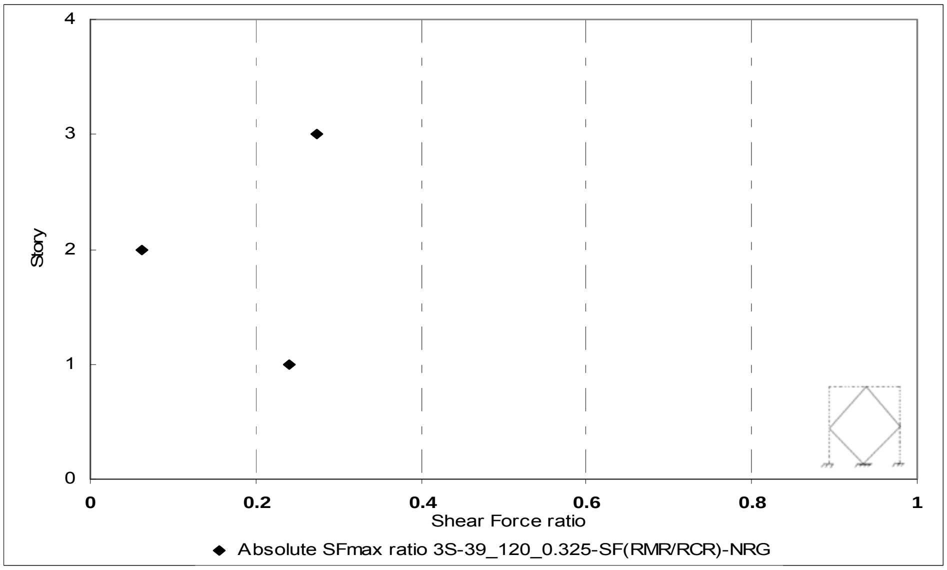

b)

Figure C.3 Shear Force ratio for 3S-39_120_0.325-NRG
a)Beams, b)Columns

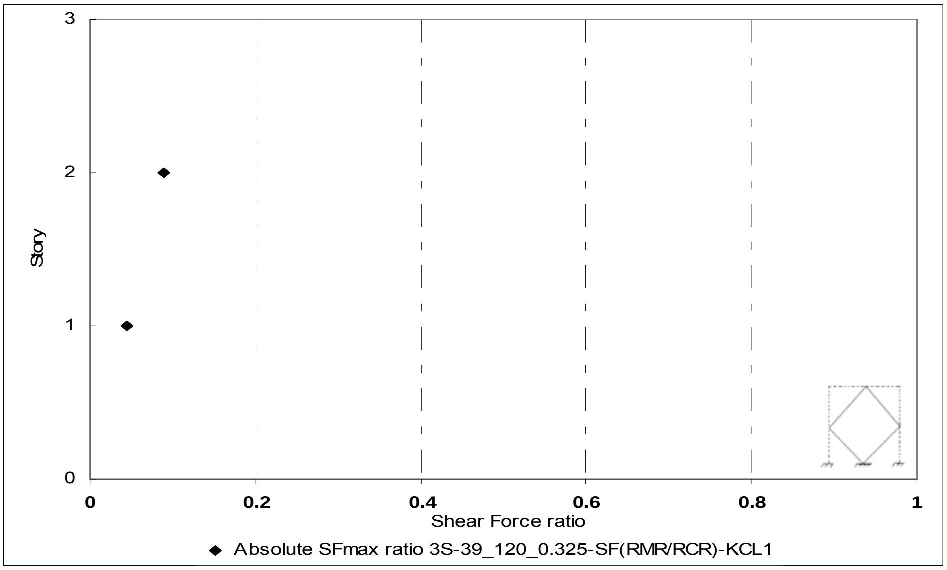

a)

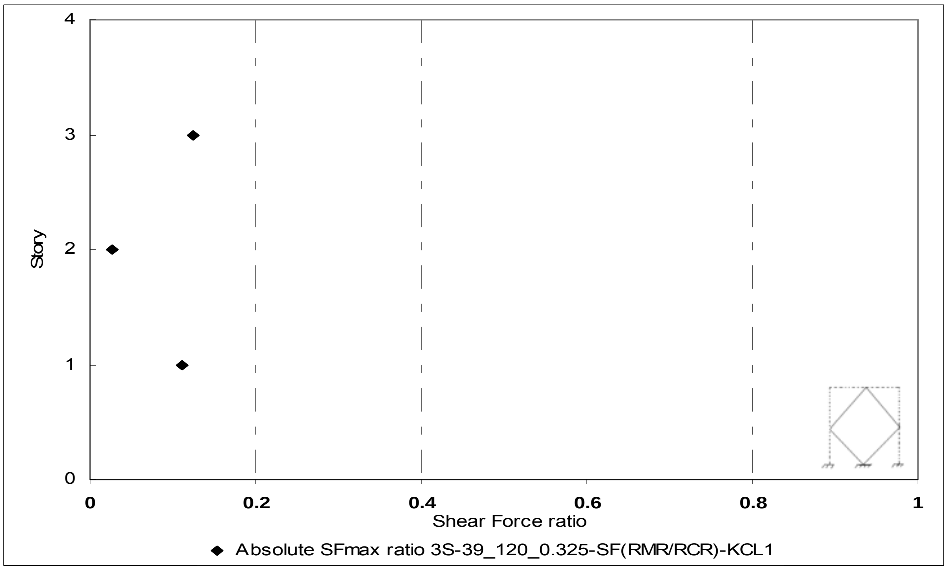

b)

Figure C.4 Shear Force ratio for 3S-39_120_0.325-KCL1
a)Beams, b)Columns

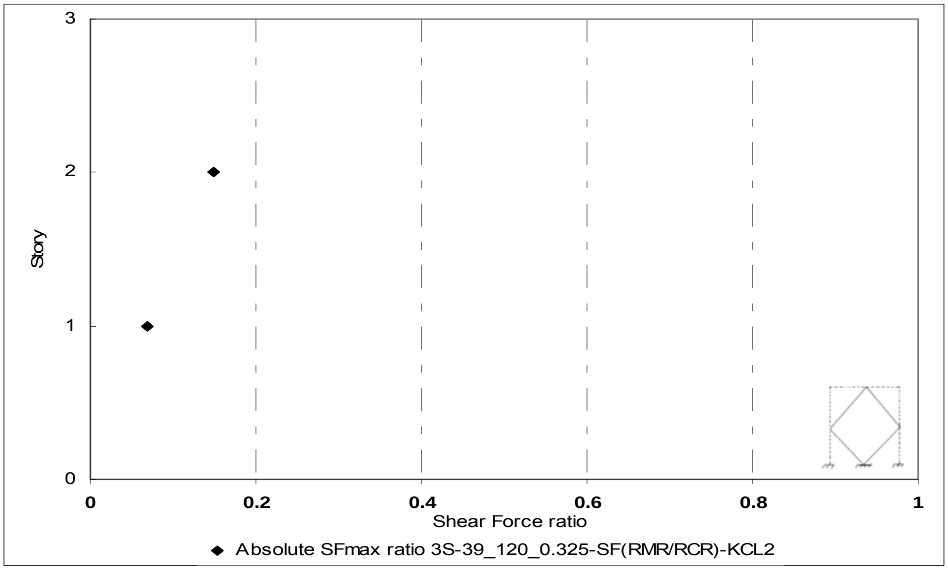

a)

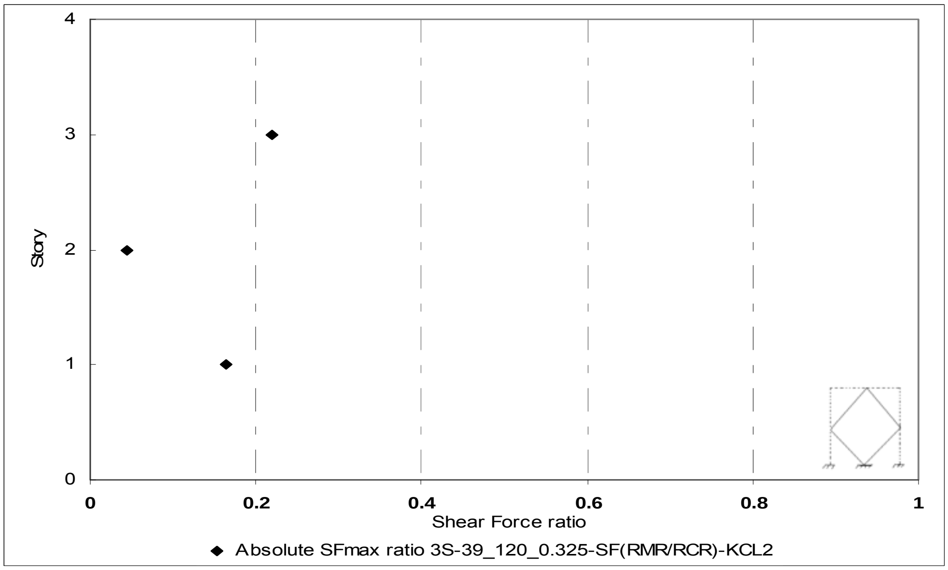

b)

Figure C.5 Shear Force ratio for 3S-39_120_0.325-KCL2
a)Beams, b)Columns

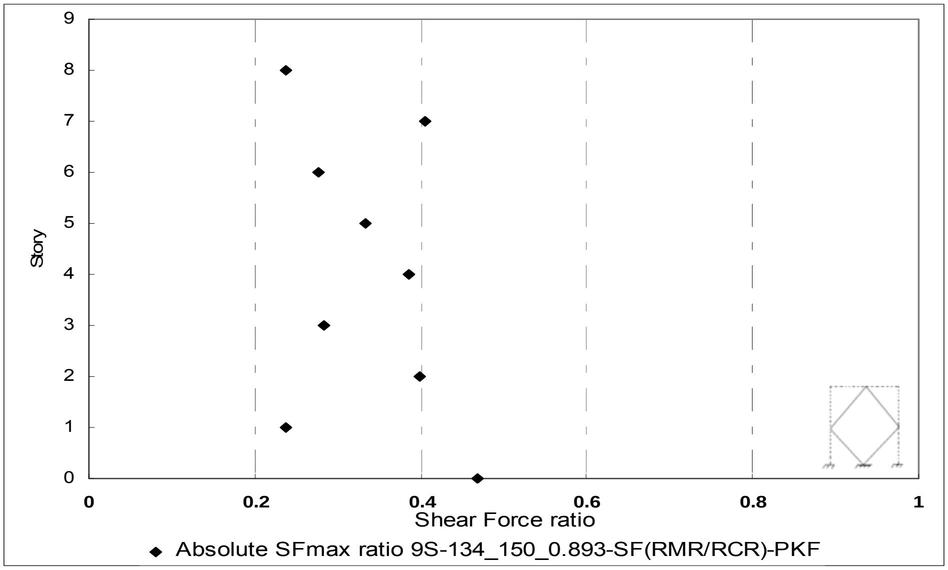

a)

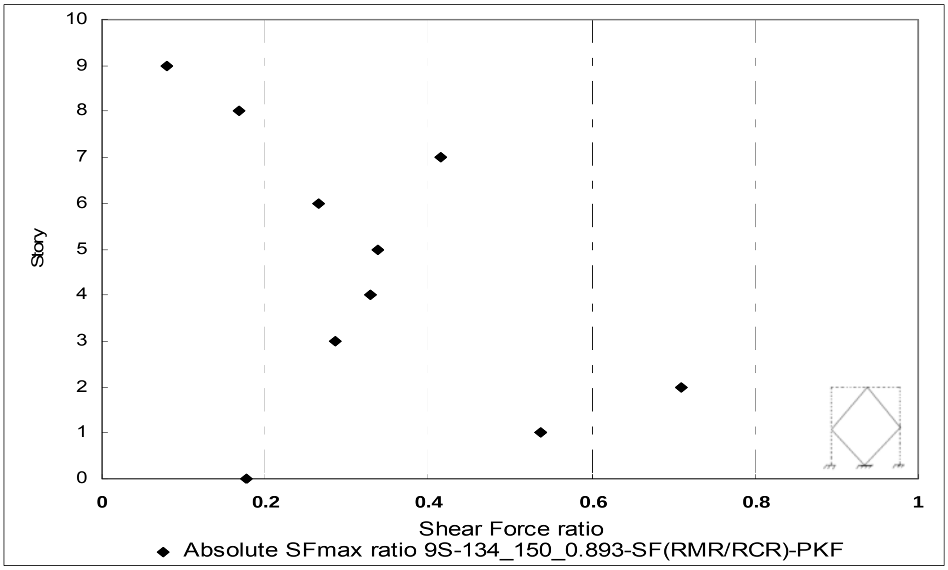

b)

Figure C.6 Shear Force ratio for 9S-134_150_0.893-PKF
a)Beams, b)Columns

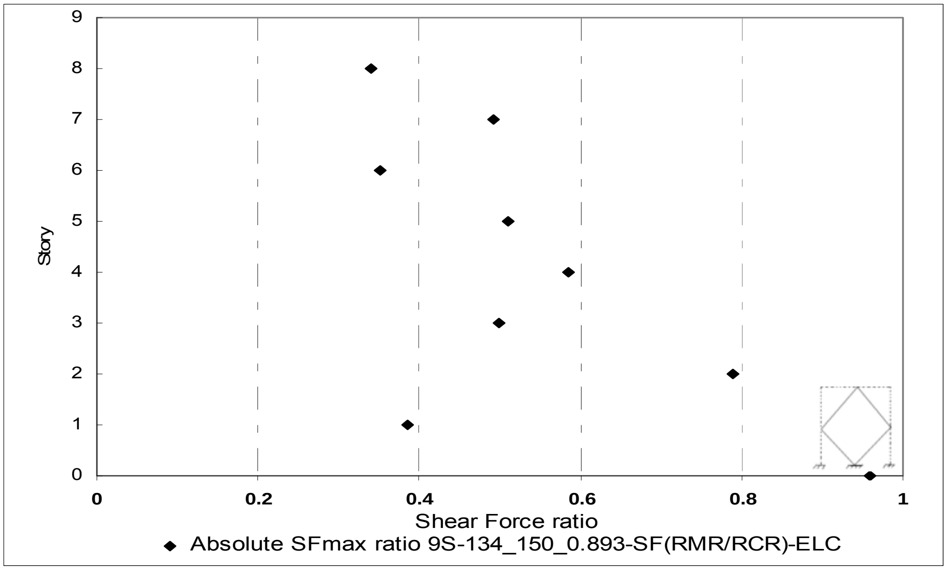

a)

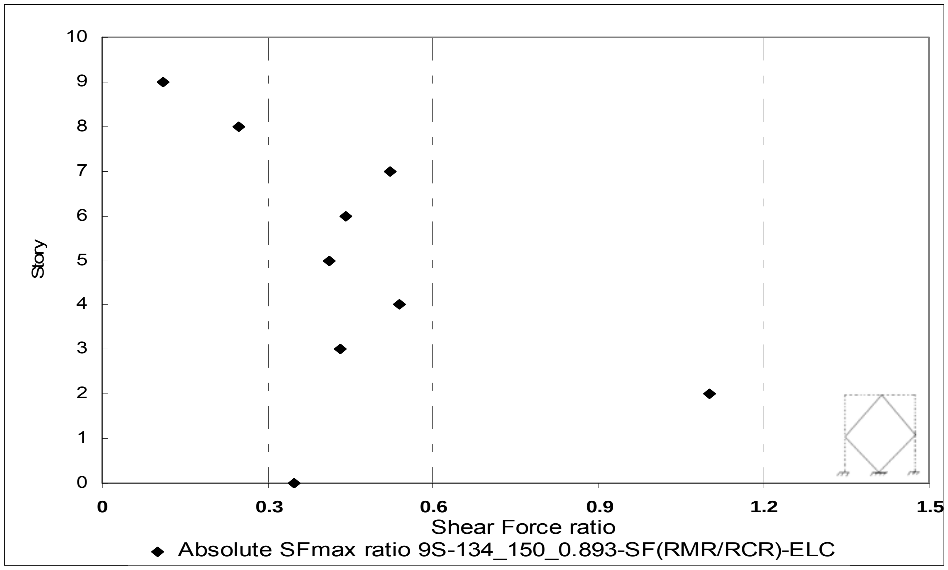

b)

Figure C.7 Shear Force ratio for 9S-134_150_0.893-ELC
a)Beams, b)Columns

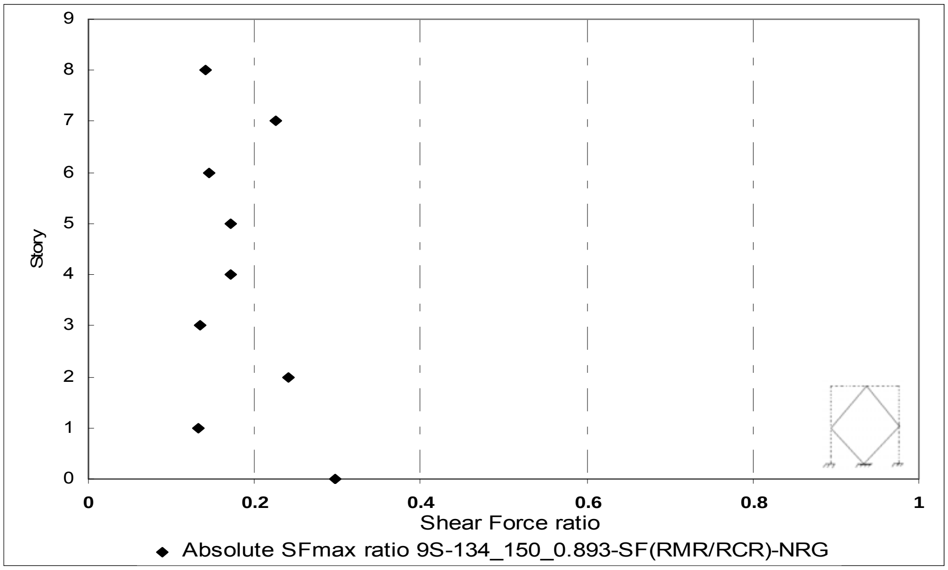

a)

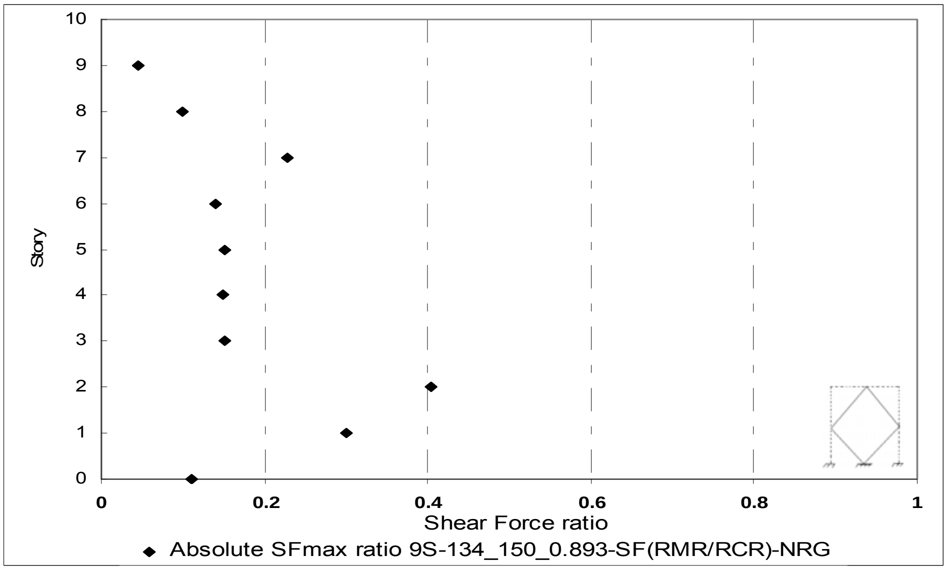

b)

Figure C.8 Shear Force ratio for 9S-134_150_0.893-NRG
a)Beams, b)Columns

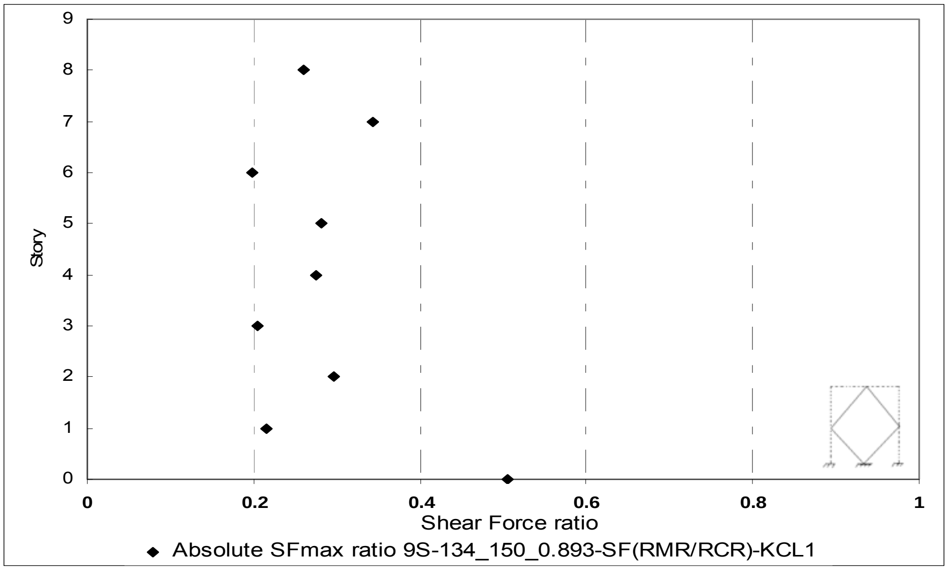

a)

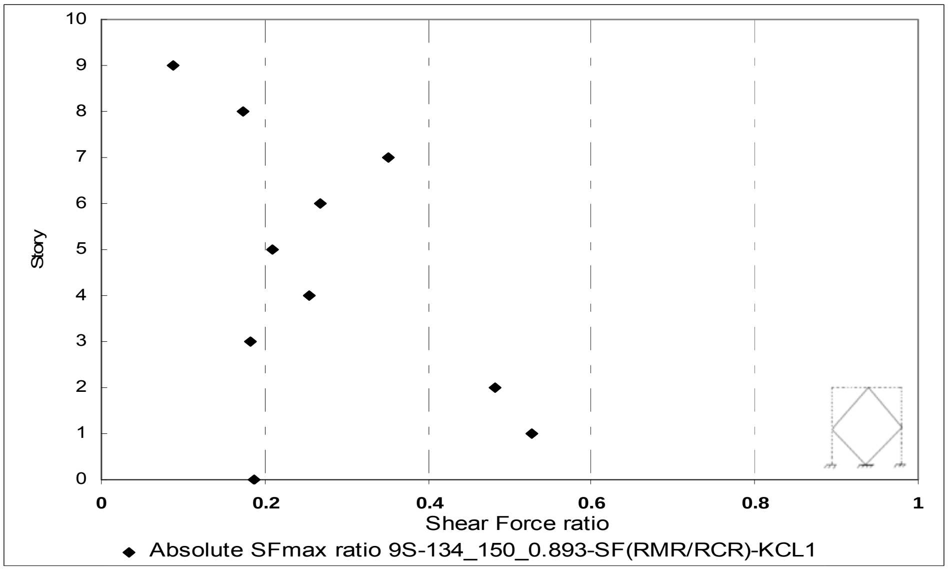

b)

Figure C.9 Shear Force ratio for 9S-134_150_0.893-KCL1
a)Beams, b)Columns

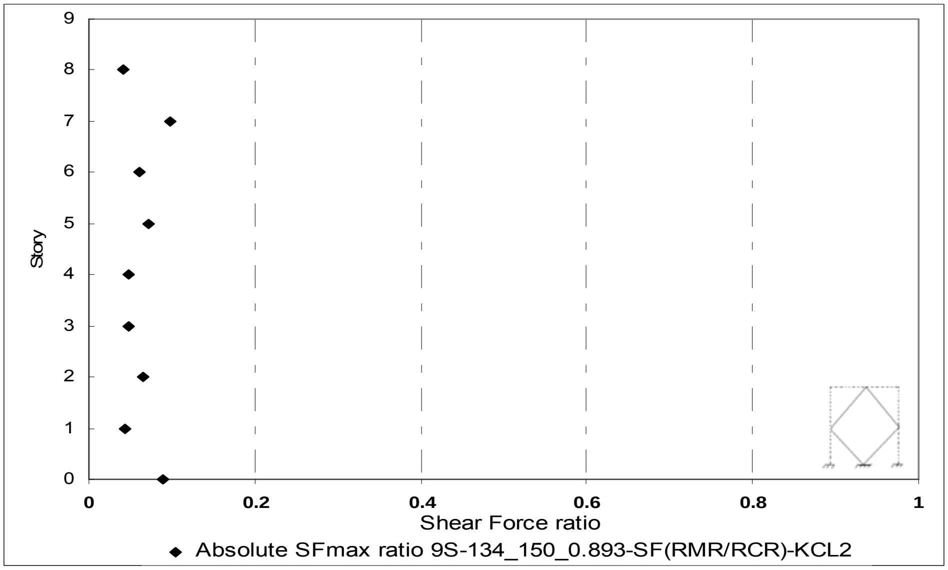

a)

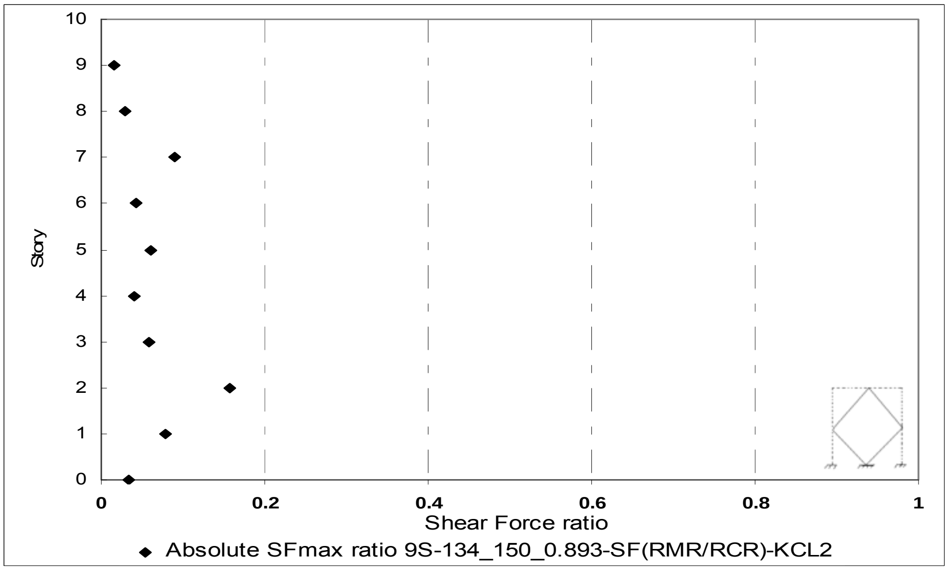

b)

Figure C.10 Shear Force ratio for 9S-134_150_0.893-KCL2
a)Beams, b)Columns

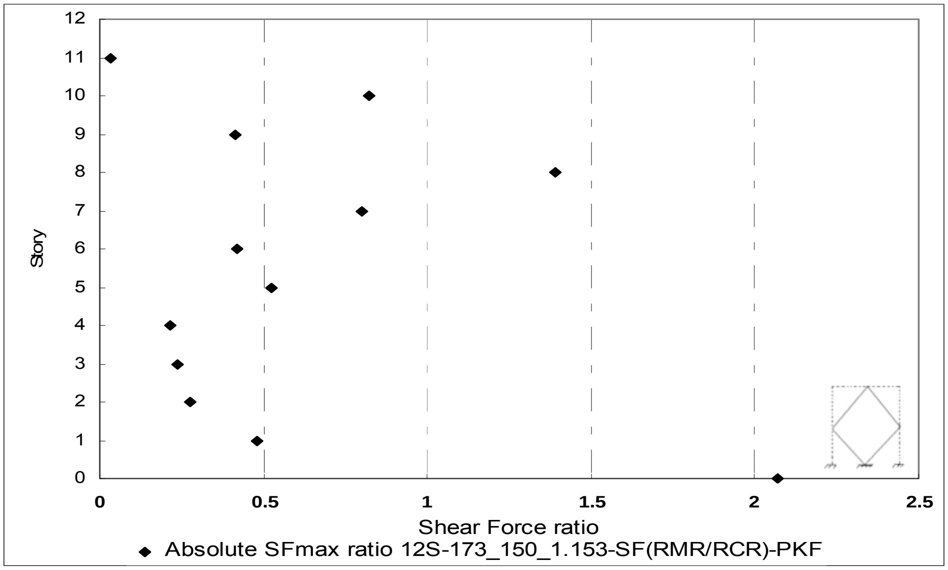

a)

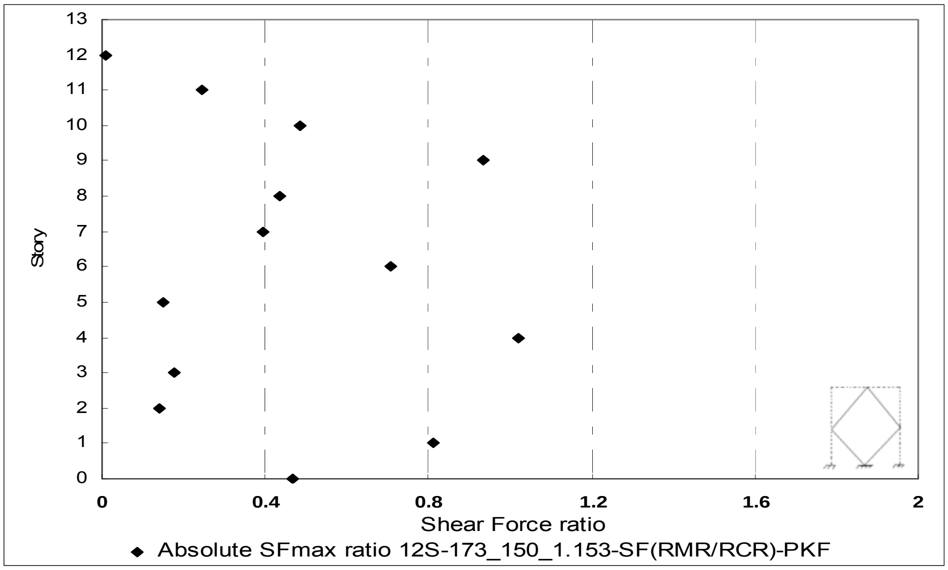

b)

Figure C.11 Shear Force ratio for 12S-173_150_1.153-PKF
a)Beams, b)Columns

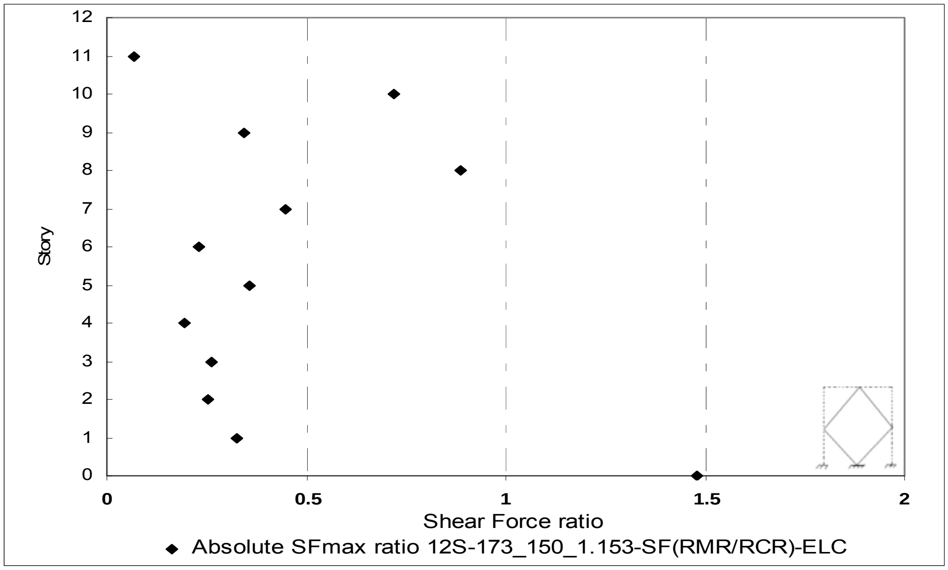

a)

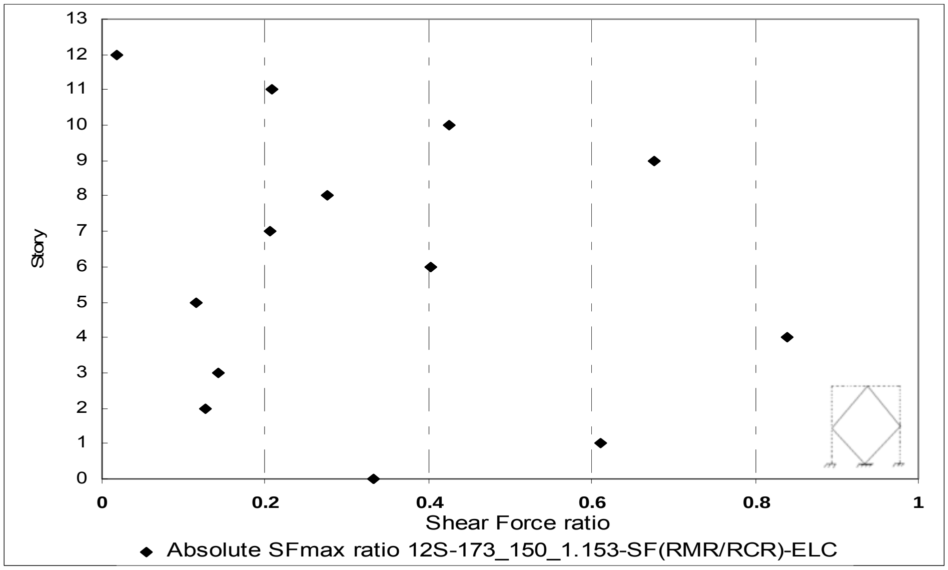

b)

Figure C.12 Shear Force ratio for 12S-173_150_1.153-ELC
a)Beams, b)Columns

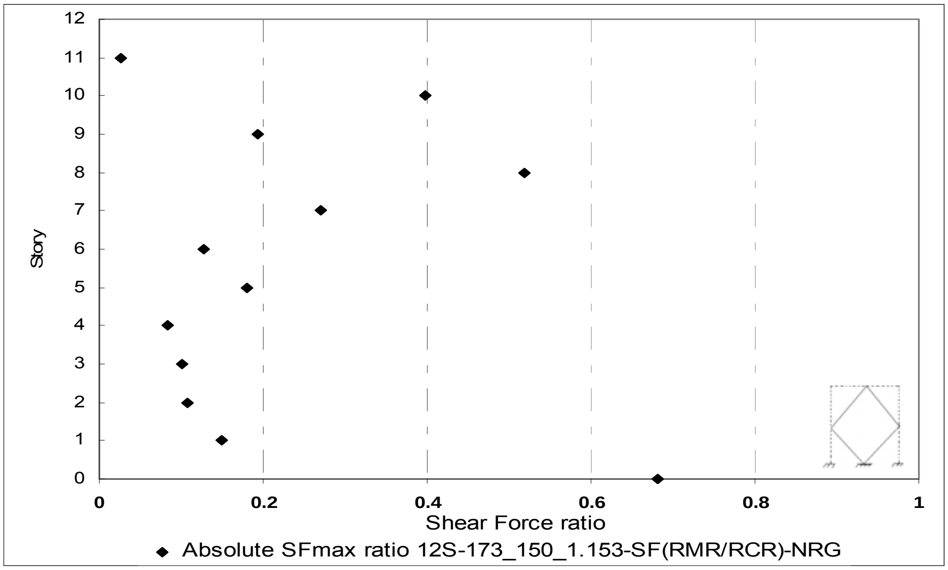

a)

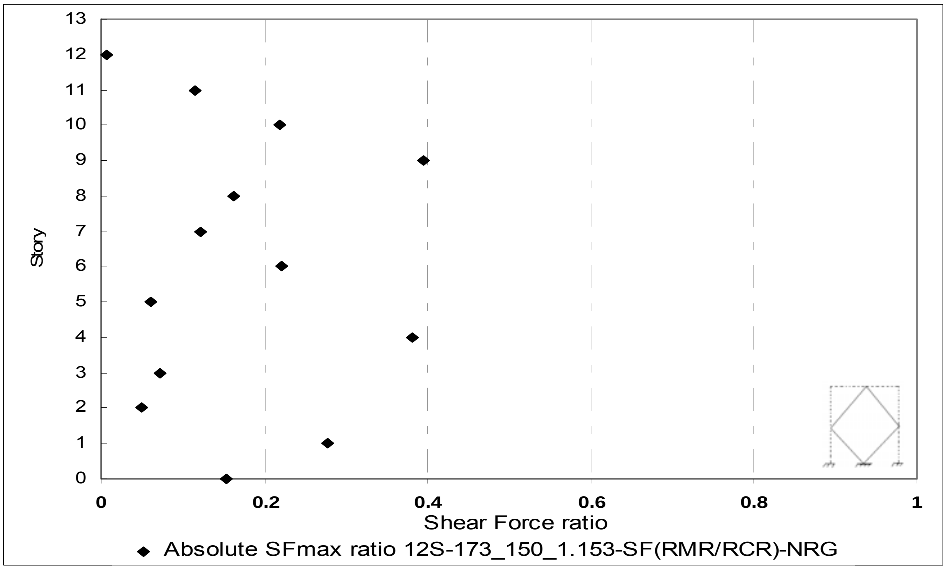

b)

Figure C.13 Shear Force ratio for 12S-173_150_1.153-NRG
a)Beams, b)Columns

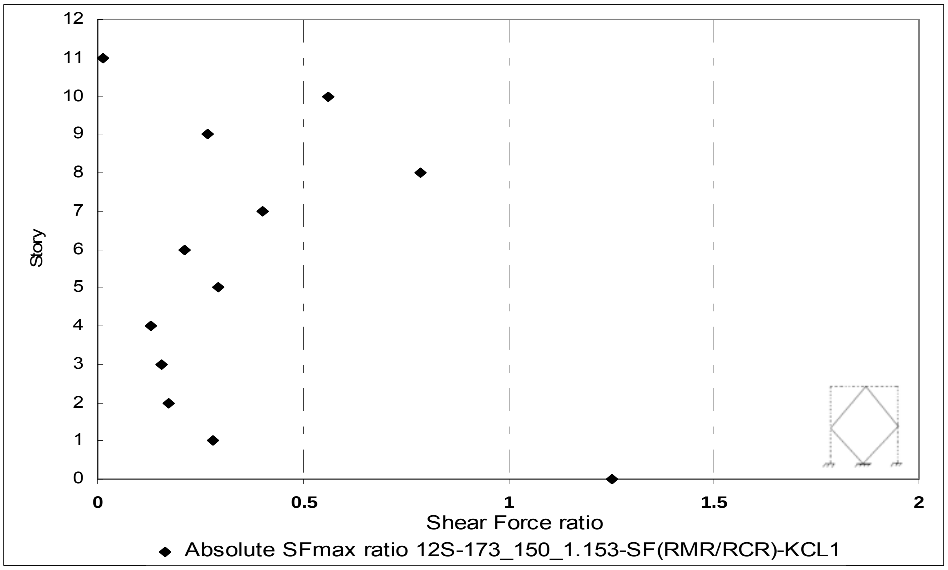

a)

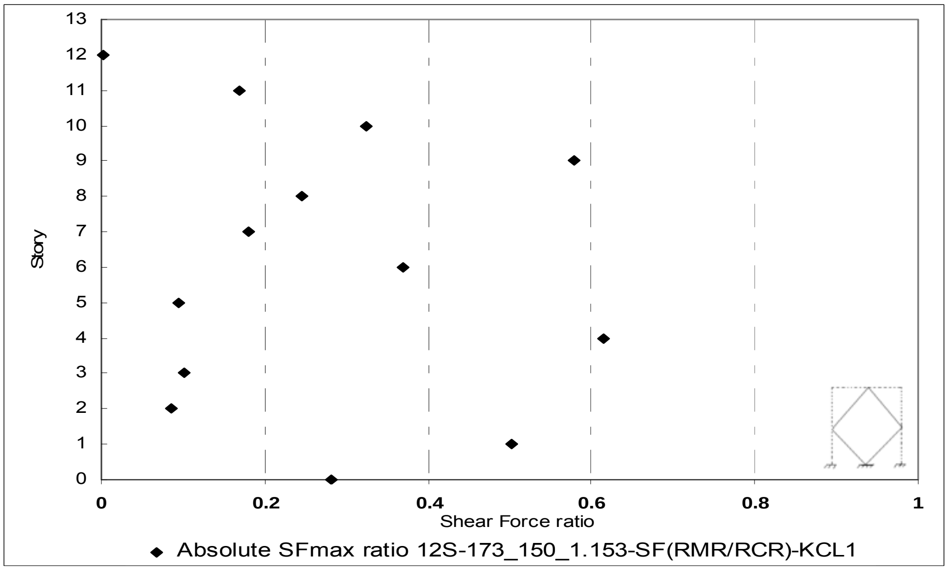

b)

Figure C.14 Shear Force ratio for 12S-173_150_1.153-KCL1
a)Beams, b)Columns

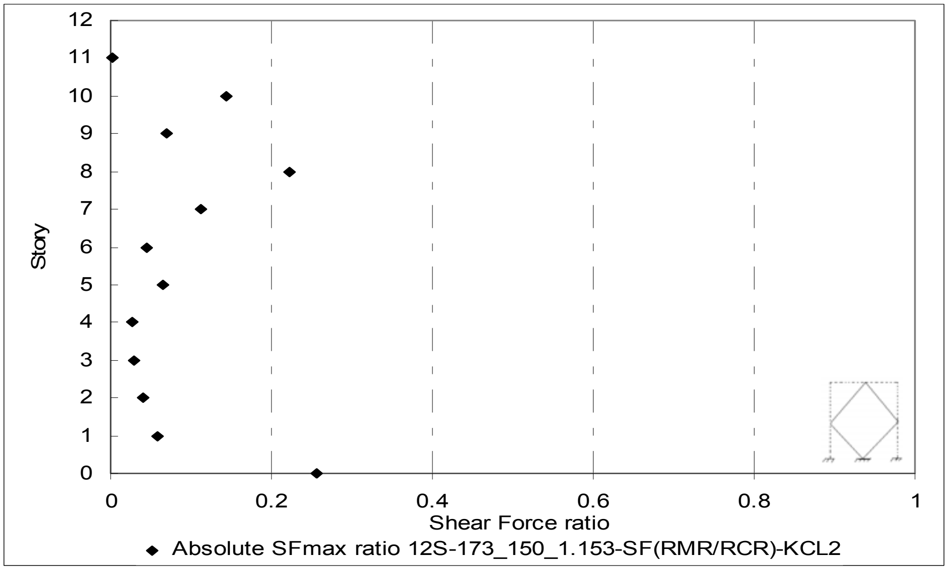

a)

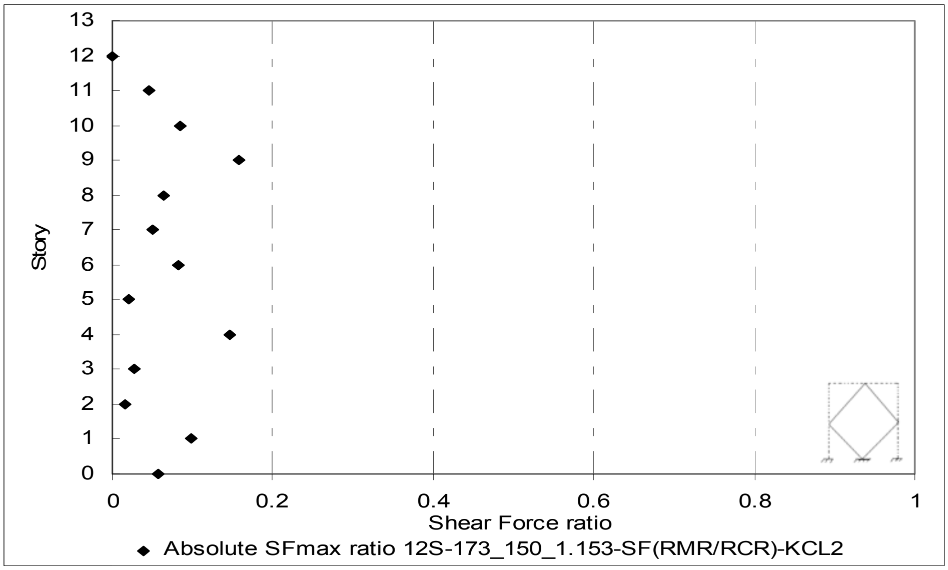

b)

Figure C.15 Shear Force ratio for 12S-173_150_1.153-KCL2
a)Beams, b)Columns

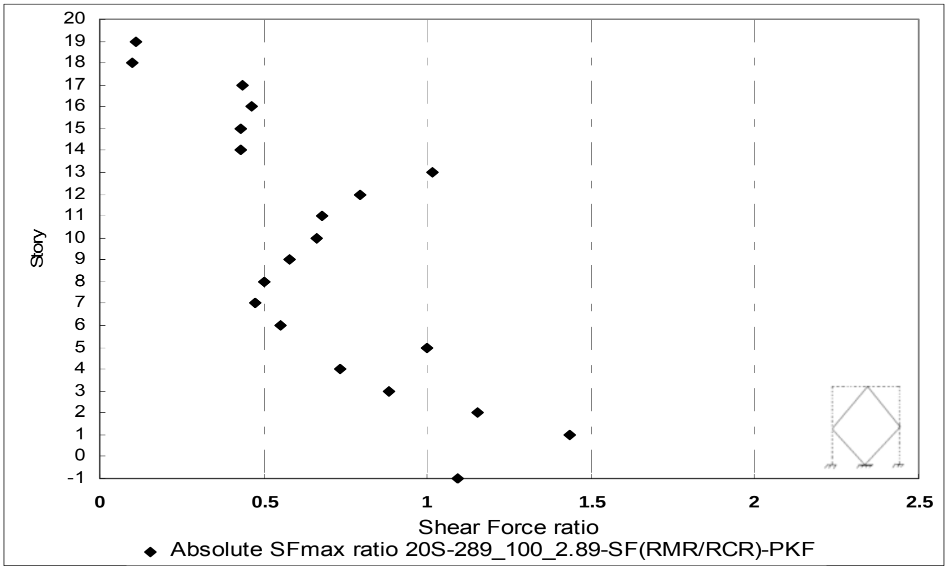

a)

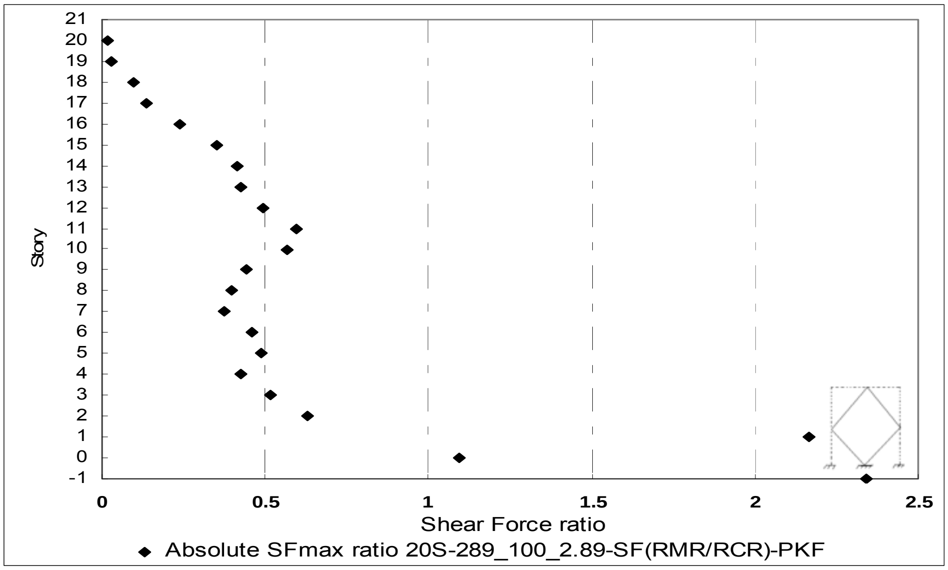

b)

Figure C.16 Shear Force ratio for 20S-289_100_2.89-PKF
a)Beams, b)Columns

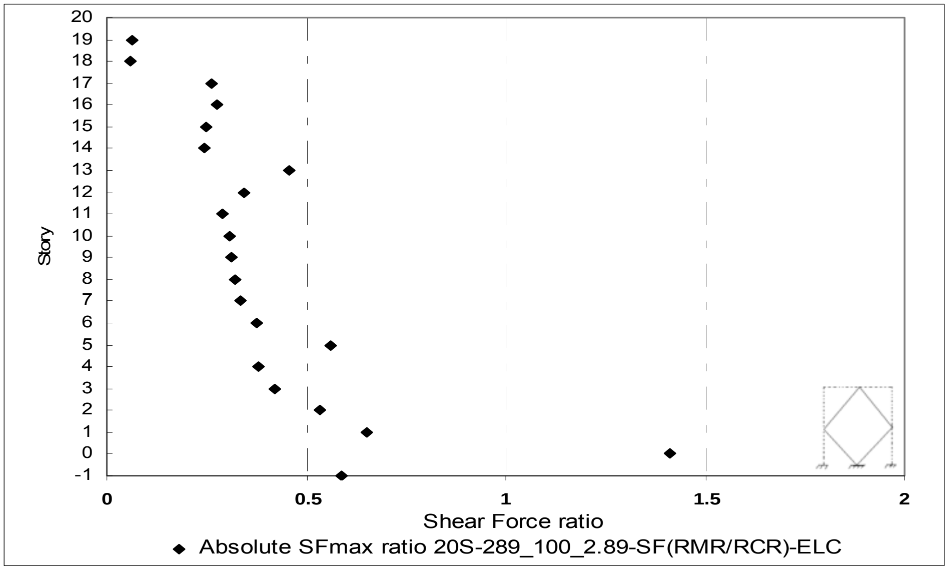

a)

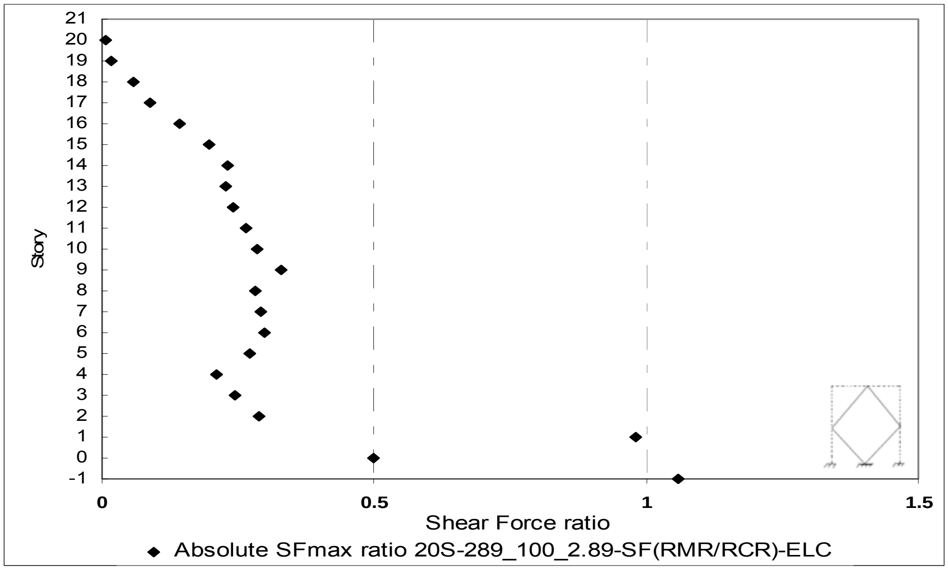

b)

Figure C.17 Shear Force ratio for 20S-289_100_2.89-ELC
a)Beams, b)Columns

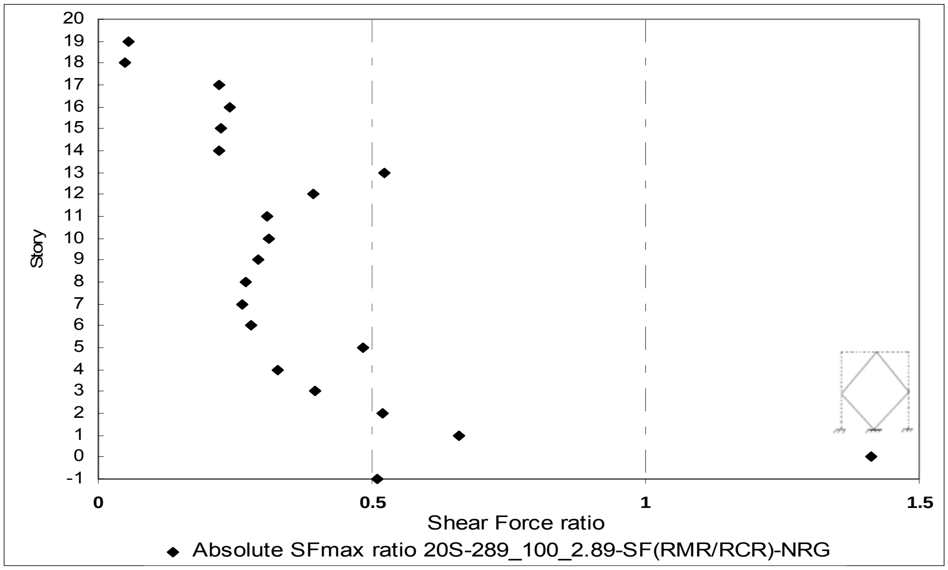

a)

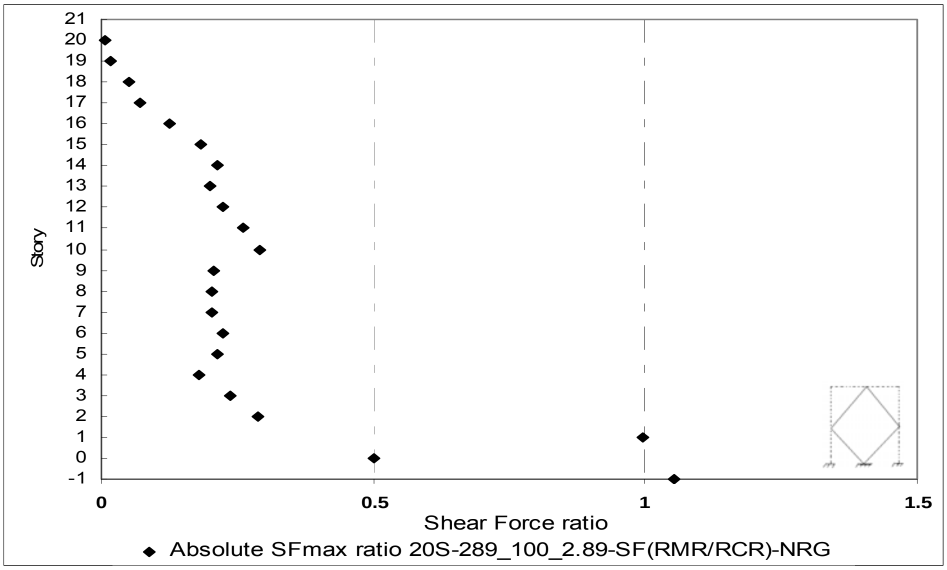

b)

Figure C.18 Shear Force ratio for 20S-289_100_2.89-NRG
a)Beams, b)Columns

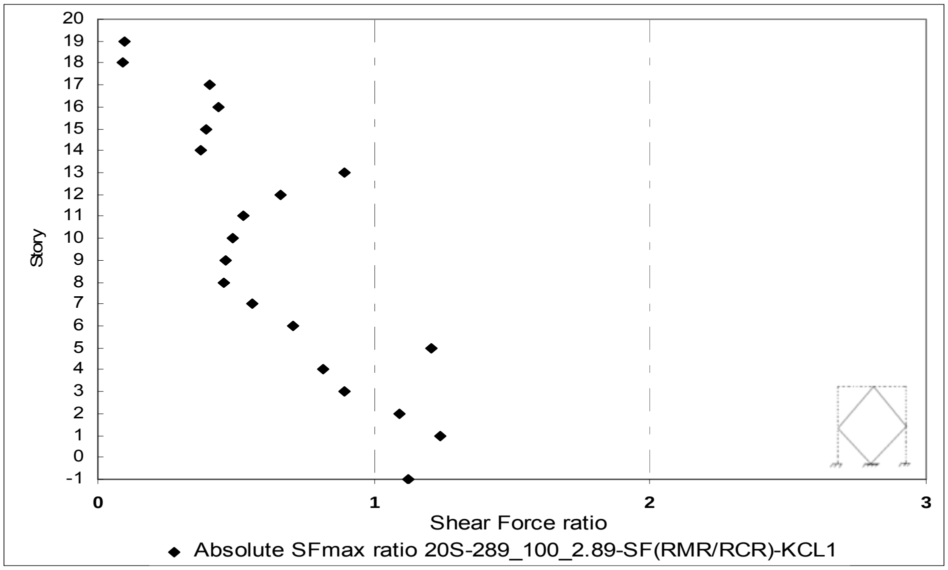

a)

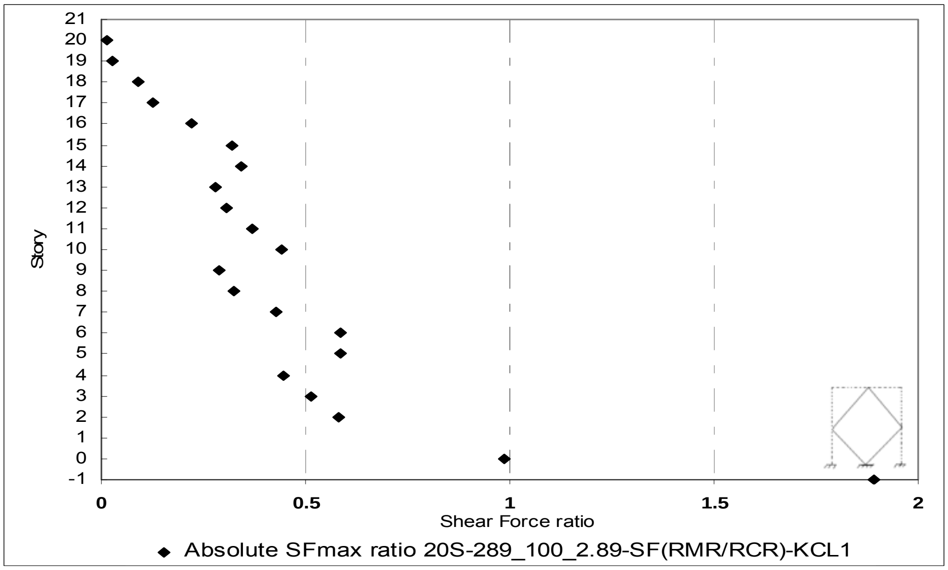

b)

Figure C.19 Shear Force ratio for 20S-289_100_2.89-KCL1
a)Beams, b)Columns

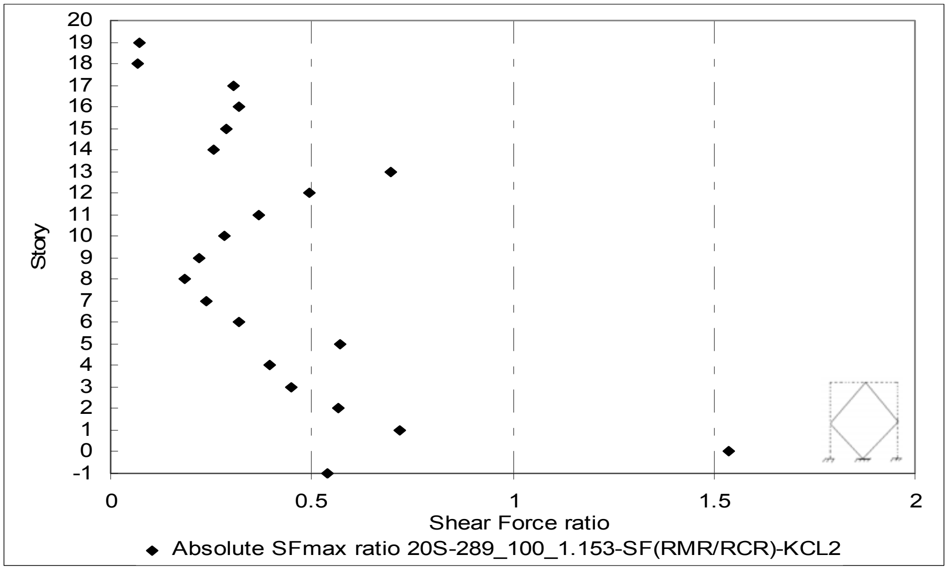

a)

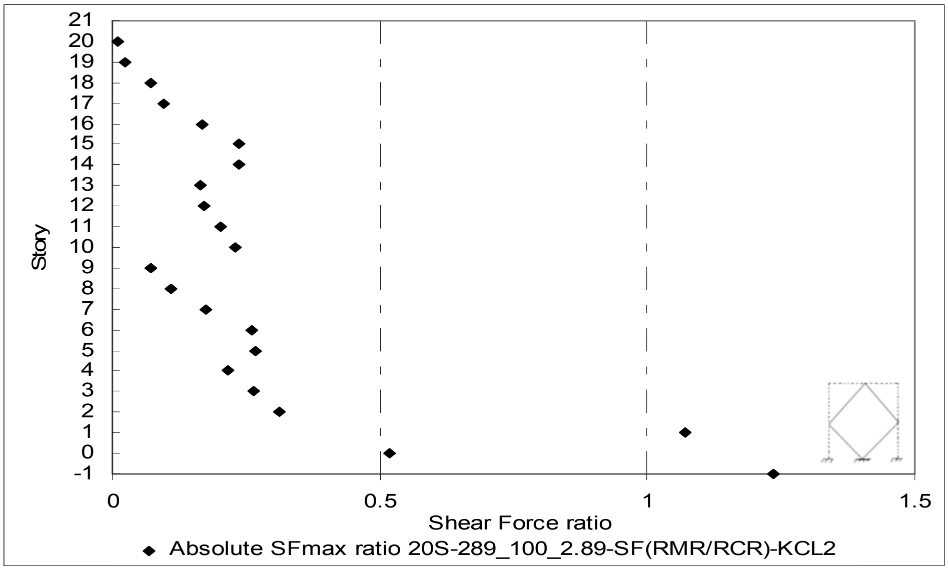

b)

Figure C.20 Shear Force ratio for 20S-289_100_2.89-KCL2
a)Beams, b)Columns

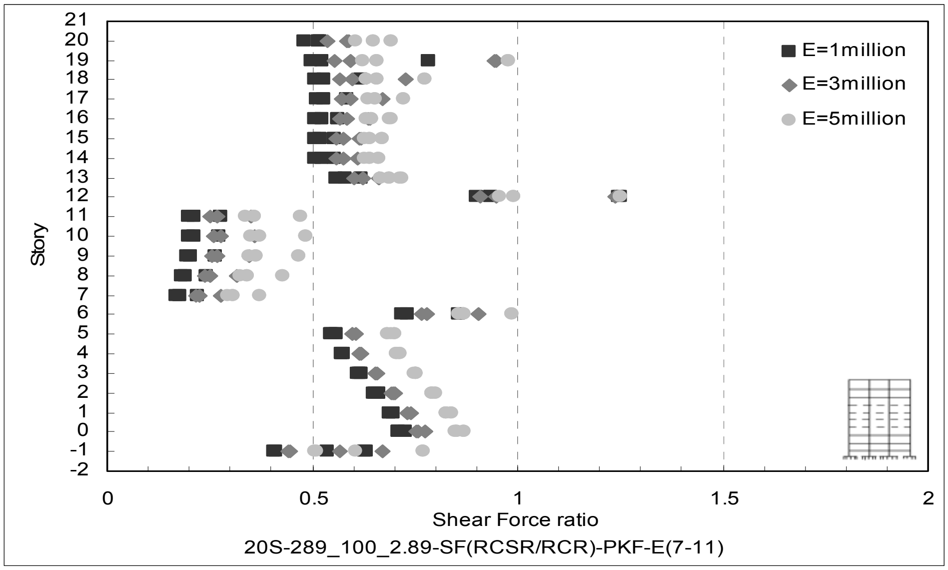

a)

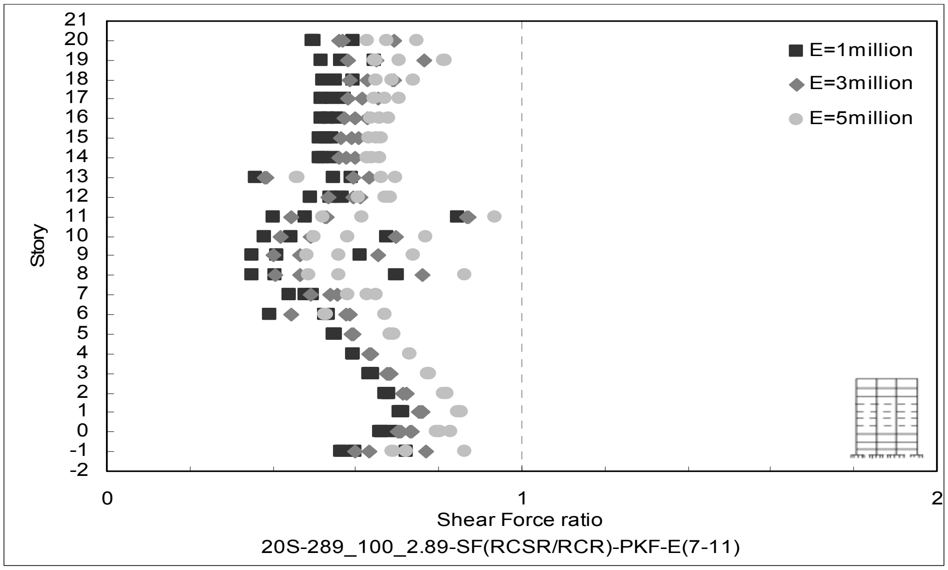

b)

Figure C.21 Shear Force ratio for 20S-289_100_2.89-PKF
a)Beams, b)Columns

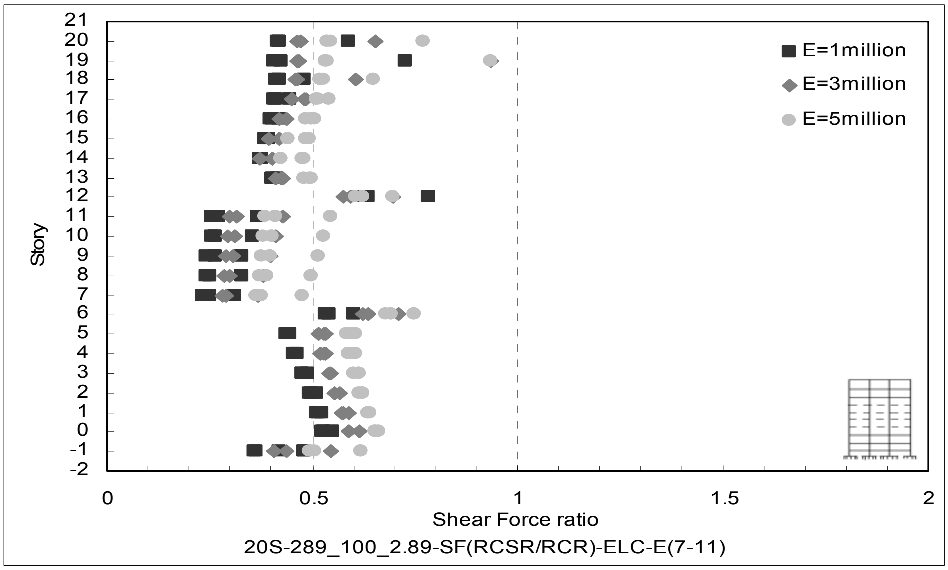

a)

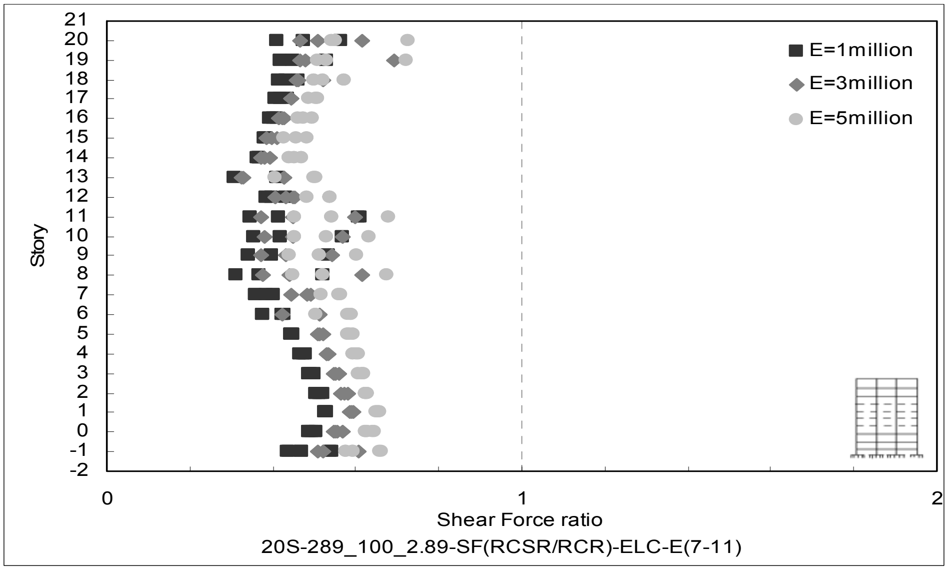

b)

Figure C.22 Shear Force ratio for 20S-289_100_2.89-ELC
a)Beams, b)Columns

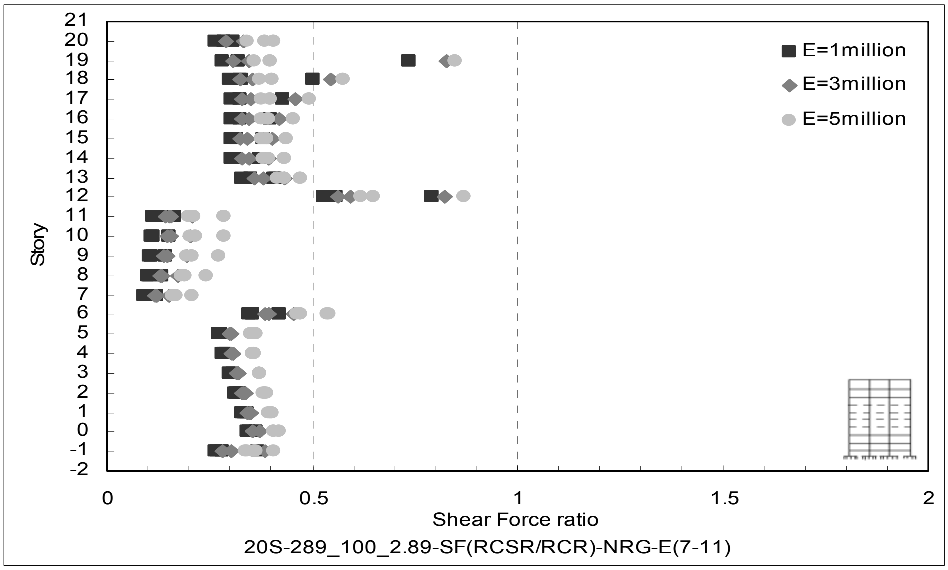

a)

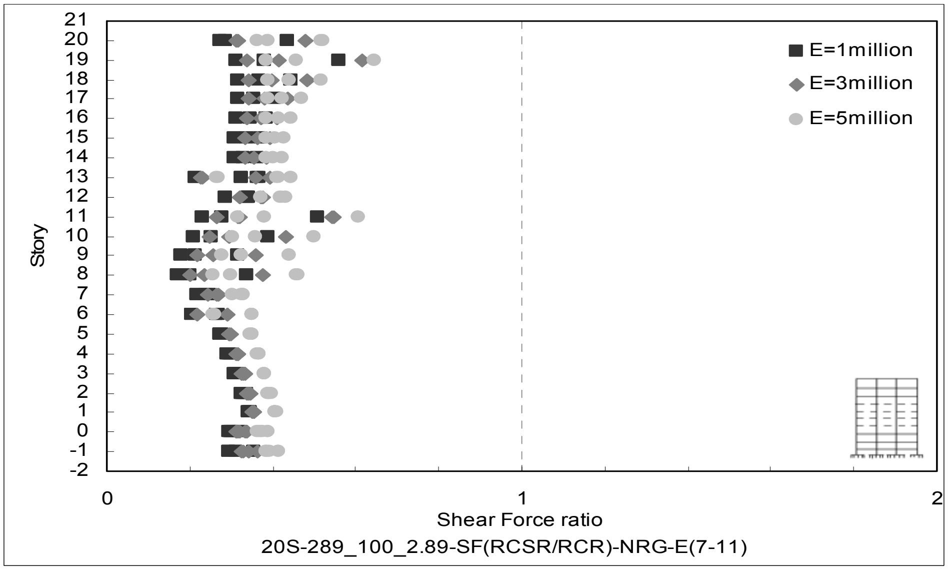

b)

Figure C.23 Shear Force ratio for 20S-289_100_2.89-NRG
a)Beams, b)Columns

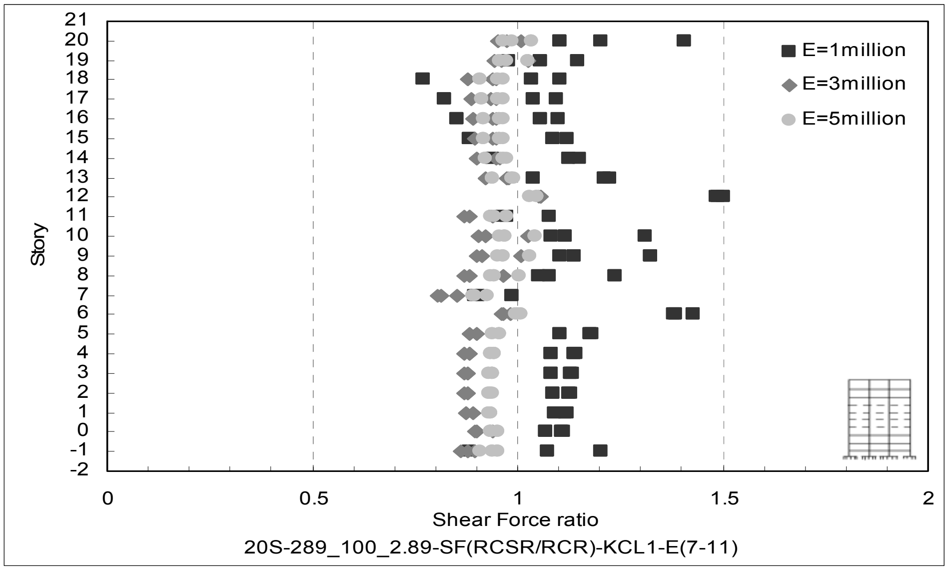

a)

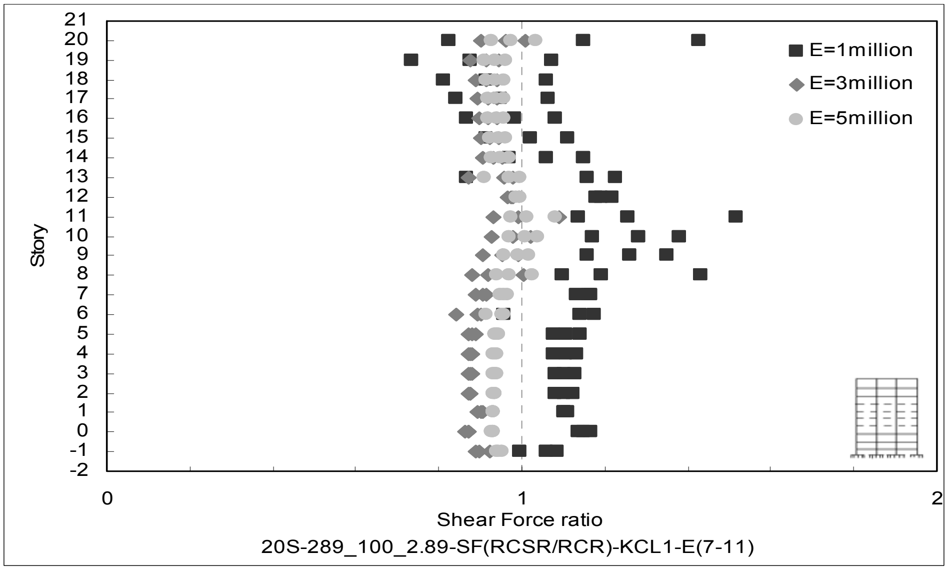

b)

Figure C.24 Shear Force ratio for 20S-289_100_2.89-KCL1
a)Beams, b)Columns

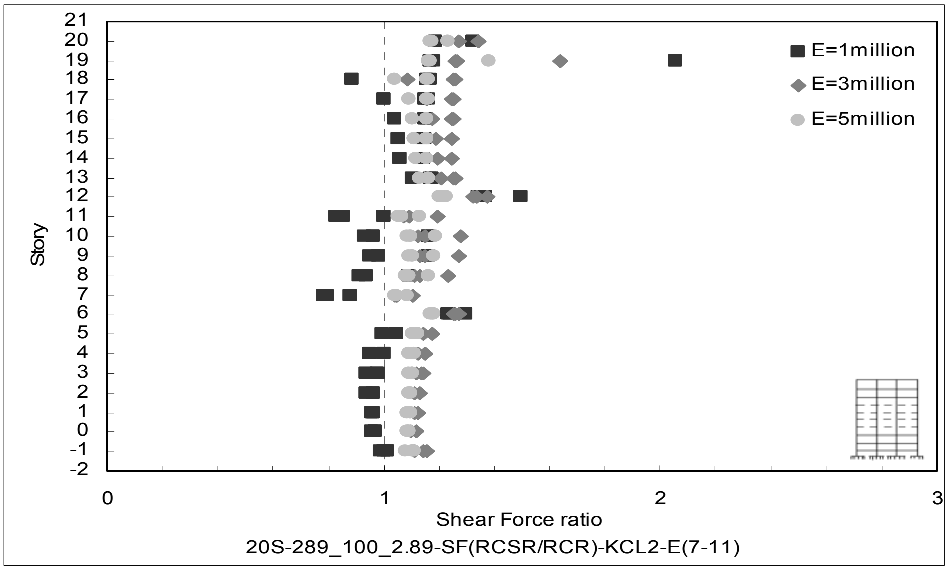

a)

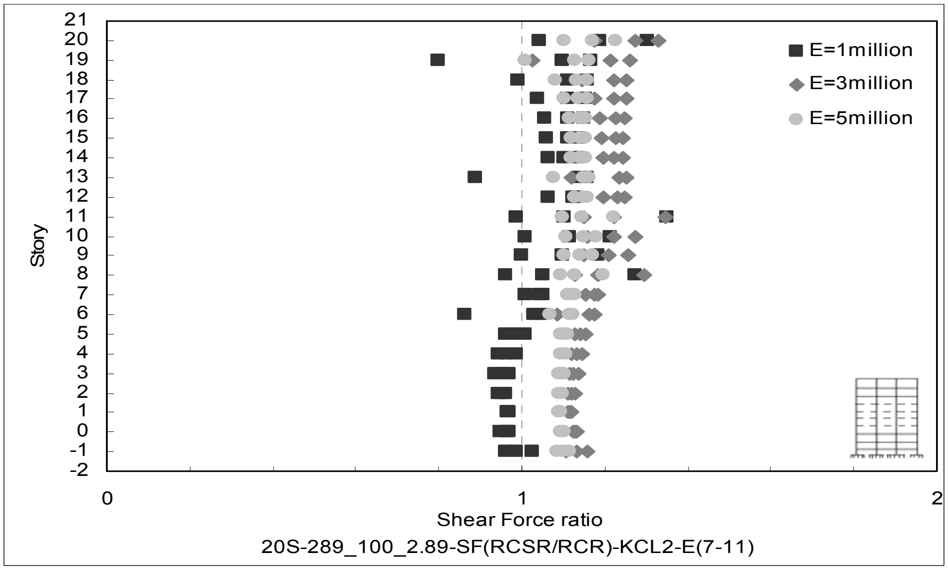

b)

Figure C.25 Shear Force ratio for 20S-289_100_2.89-KCL2
a)Beams, b)Columns

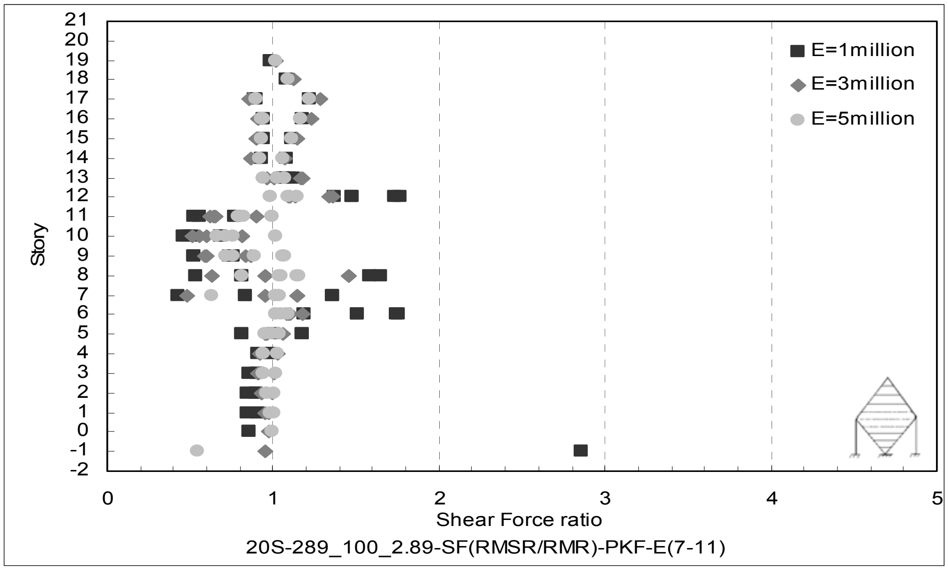

a)

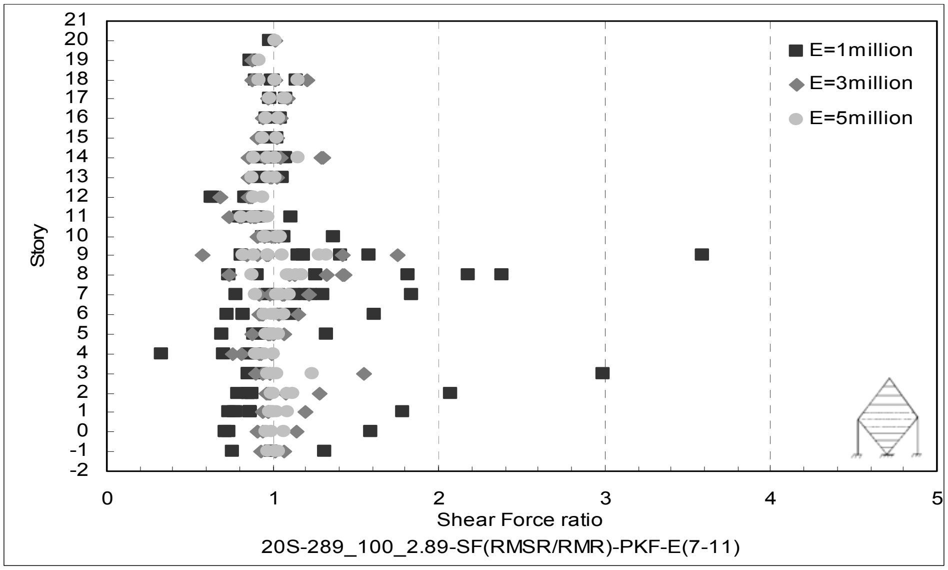

b)

Figure C.26 Shear Force ratio for 20S-289_100_2.89-PKF
a)Beams, b)Columns

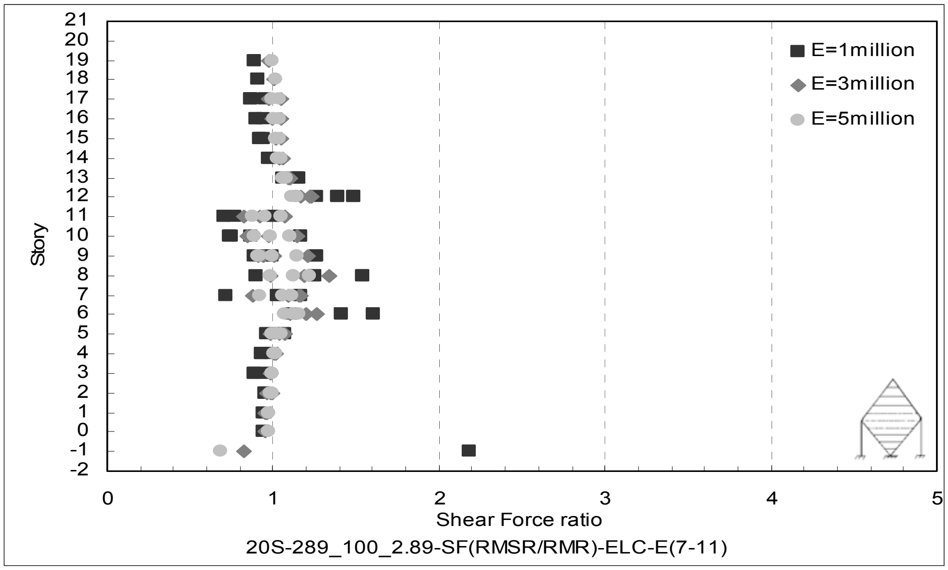

a)

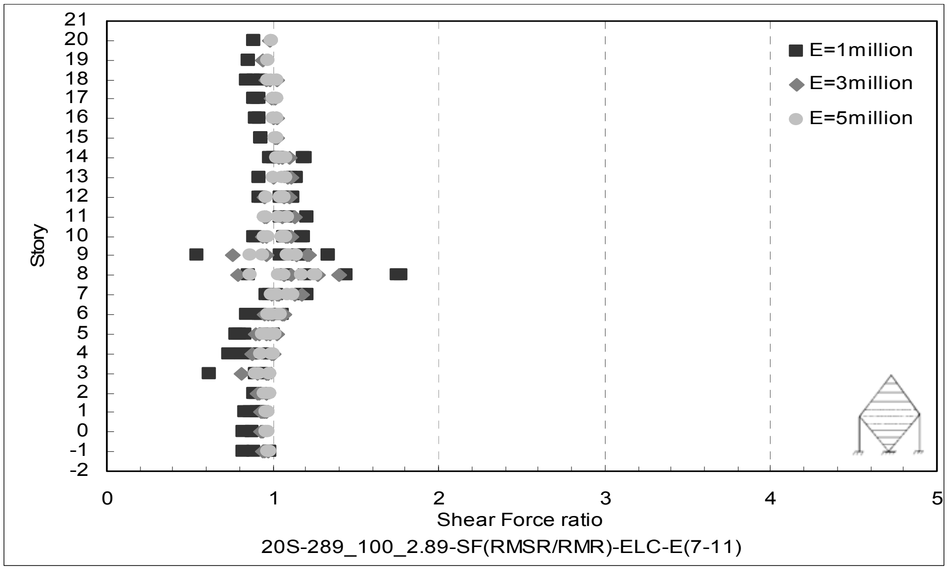

b)

Figure C.27 Shear Force ratio for 20S-289_100_2.89-ELC
a)Beams, b)Columns

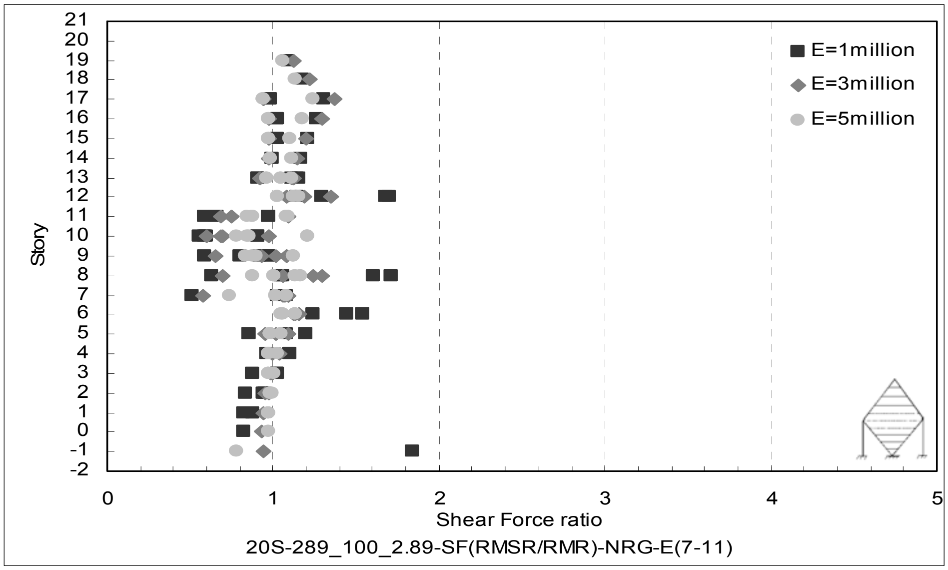

a)

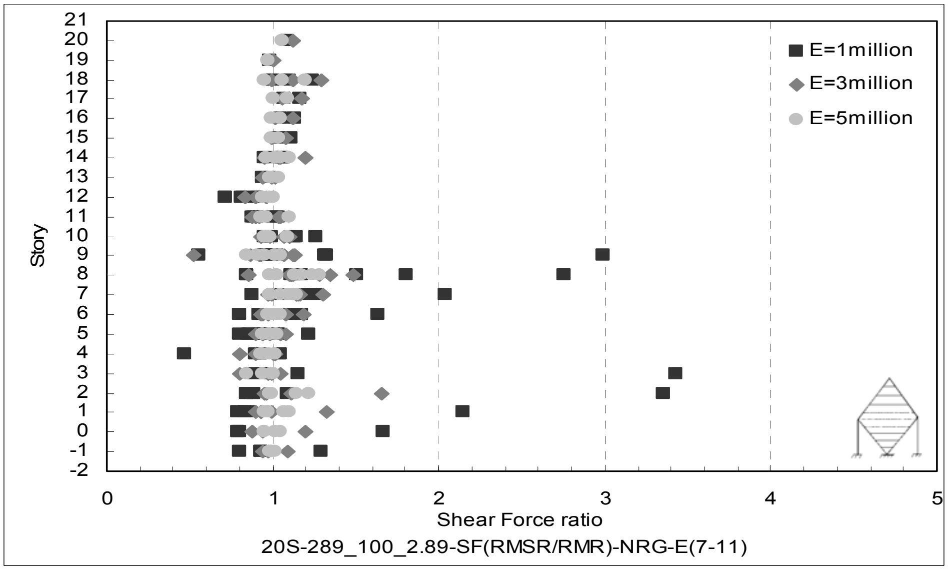

b)

Figure C.28 Shear Force ratio for 20S-289_100_2.89-NRG
a)Beams, b)Columns

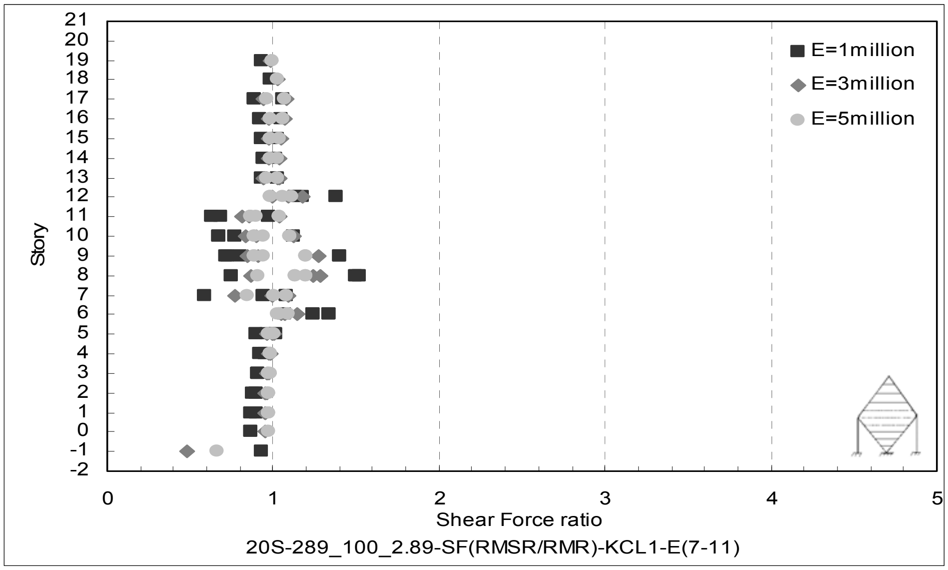

a)

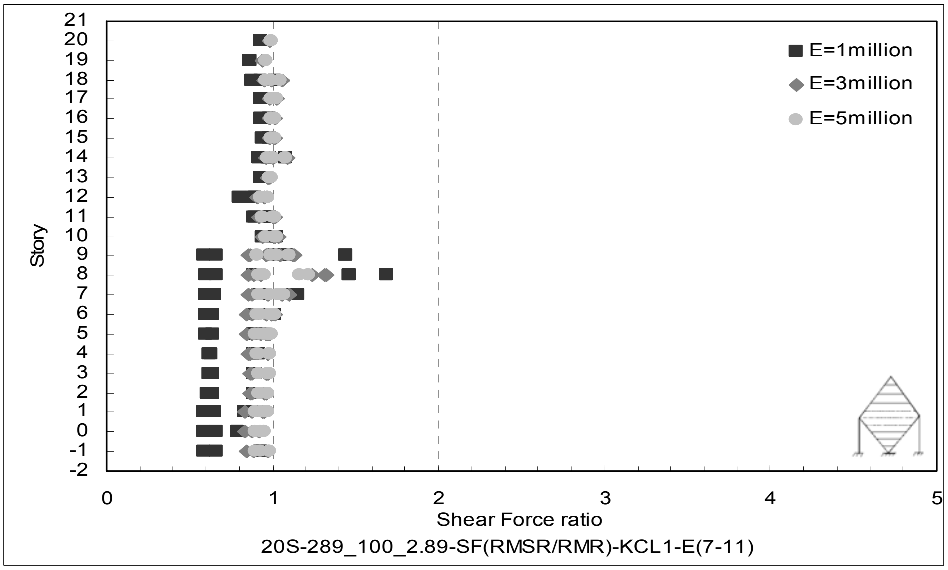

b)

Figure C.29 Shear Force ratio for 20S-289_100_2.89-KCL1
a)Beams, b)Columns

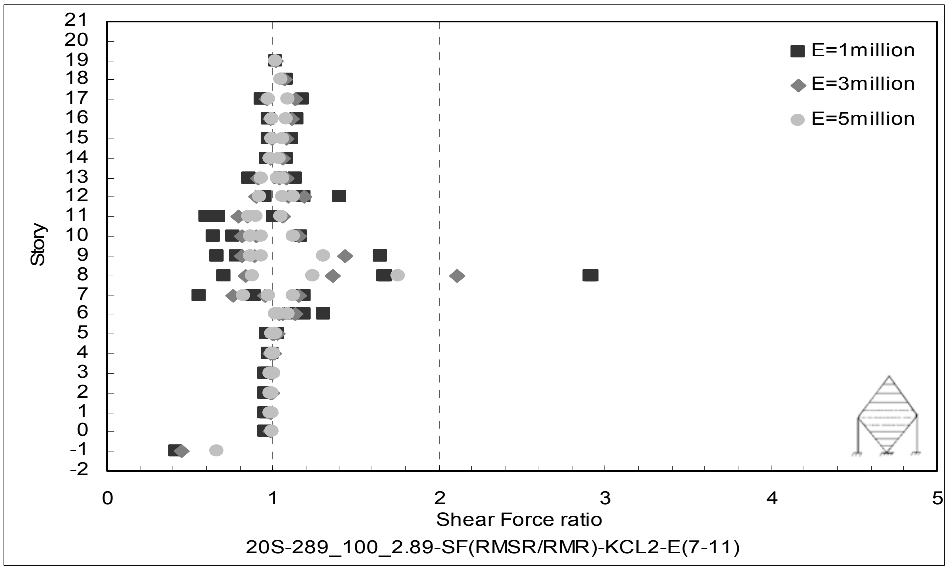

a)

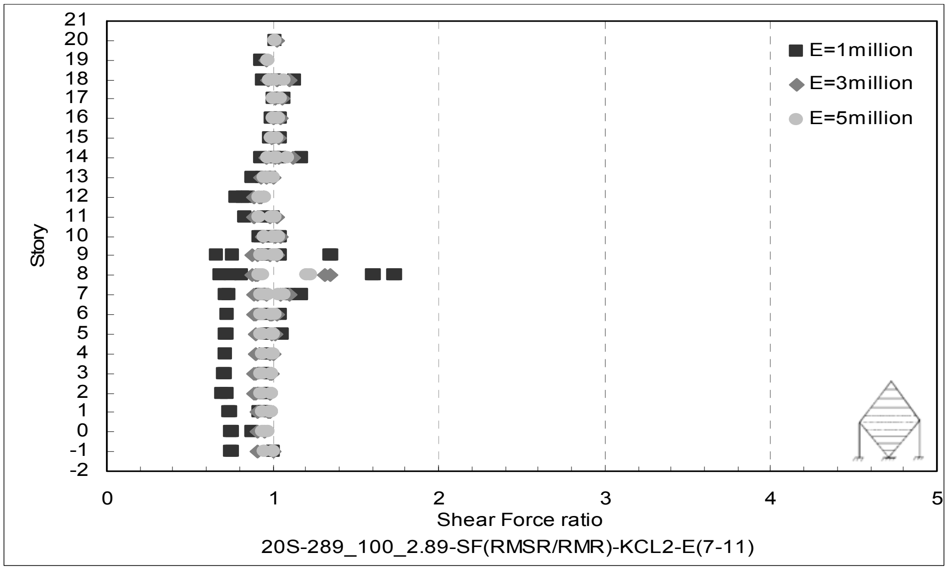

b)

Figure C.30 Shear Force ratio for 20S-289_100_2.89-KCL2
a)Beams, b)Columns

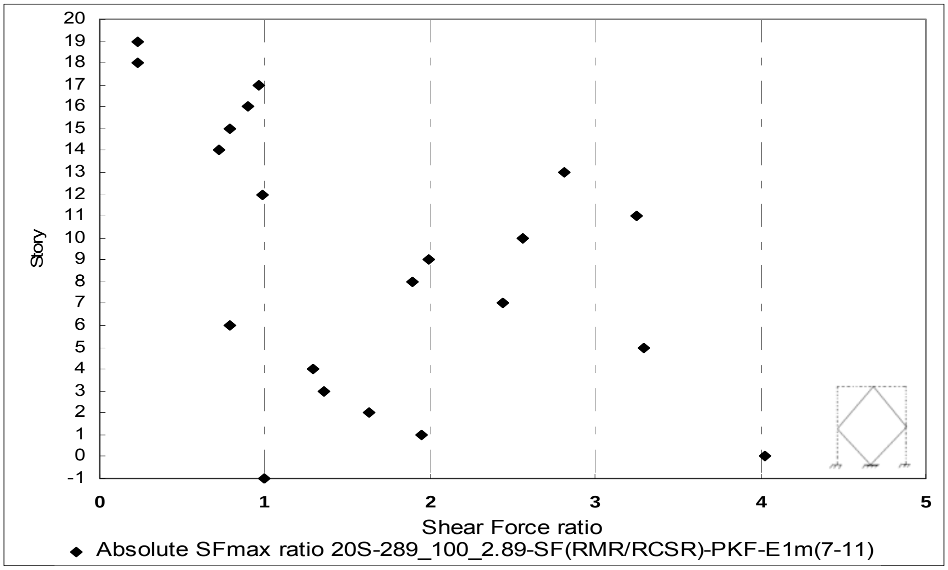

a)

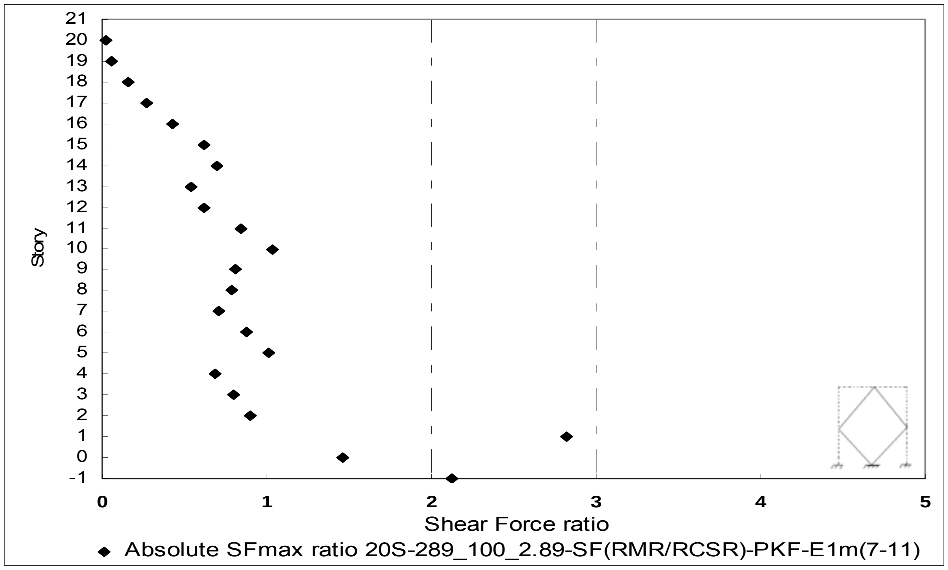

b)

Figure C.31 Shear Force ratio for 20S-289_100_2.89-PKF
a)Beams, b)Columns

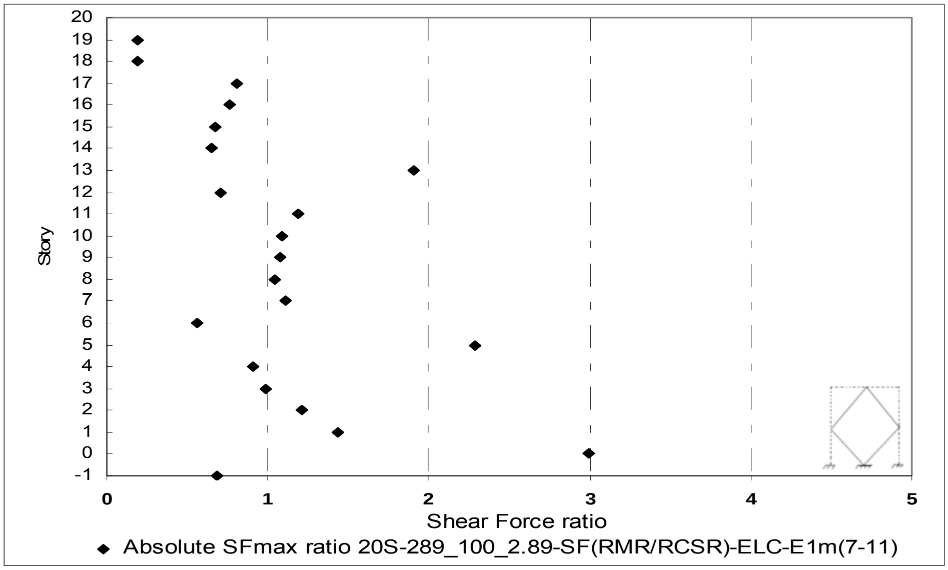

a)

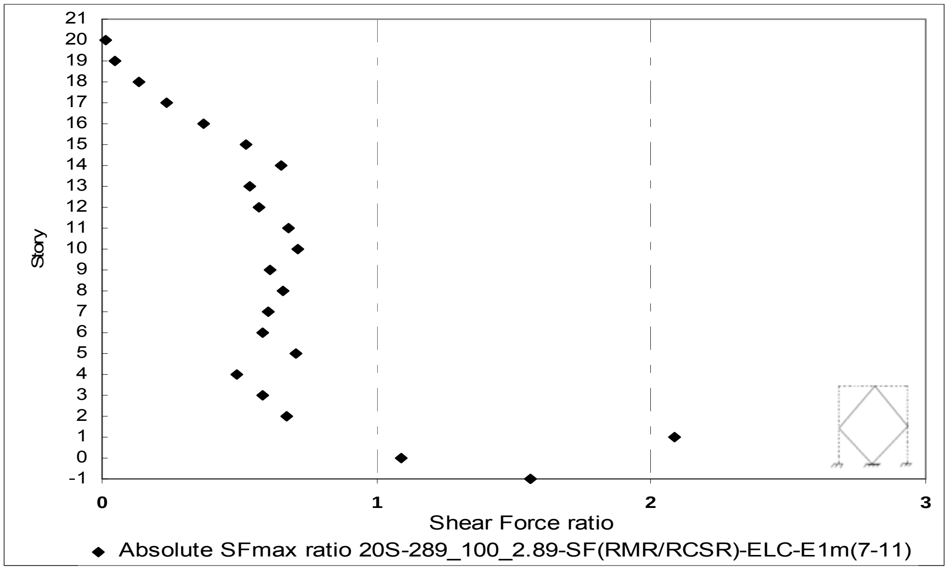

b)

Figure C.32 Shear Force ratio for 20S-289_100_2.89-ELC
a)Beams, b)Columns

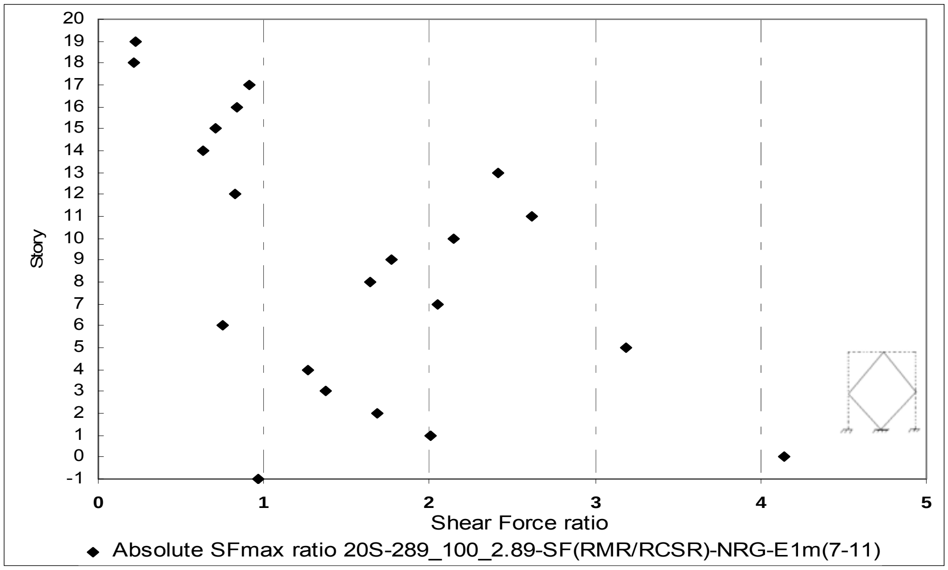

a)

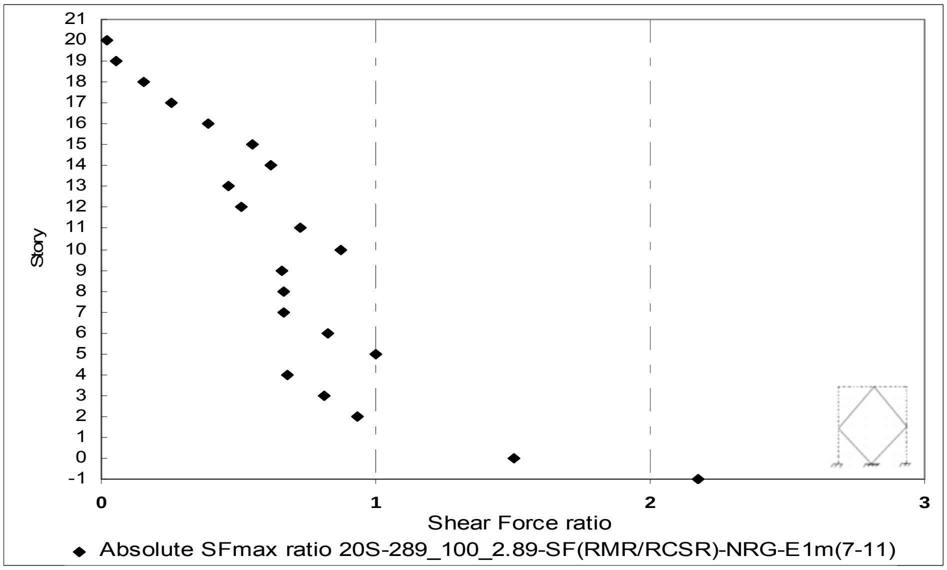

b)

Figure C.33 Shear Force ratio for 20S-289_100_2.89-NRG
a)Beams, b)Columns

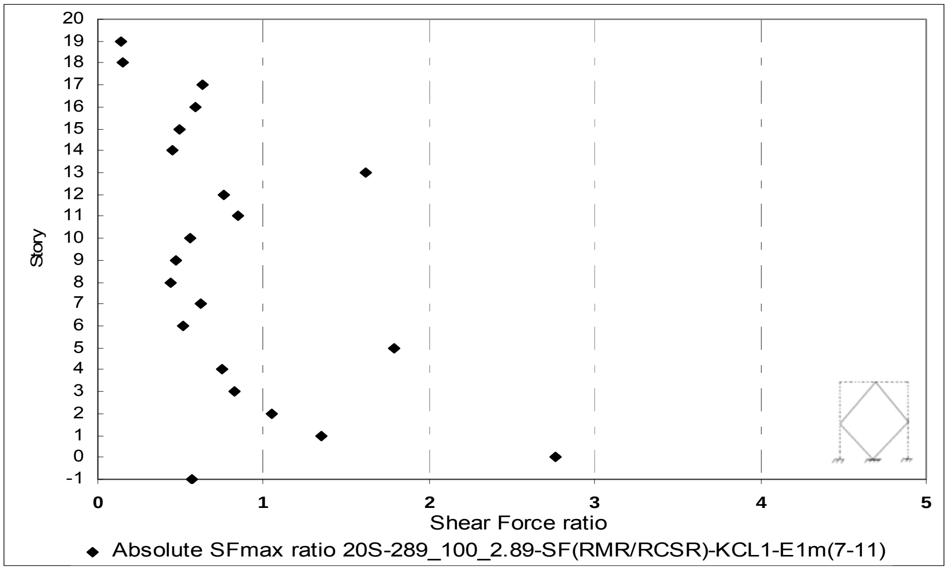

a)

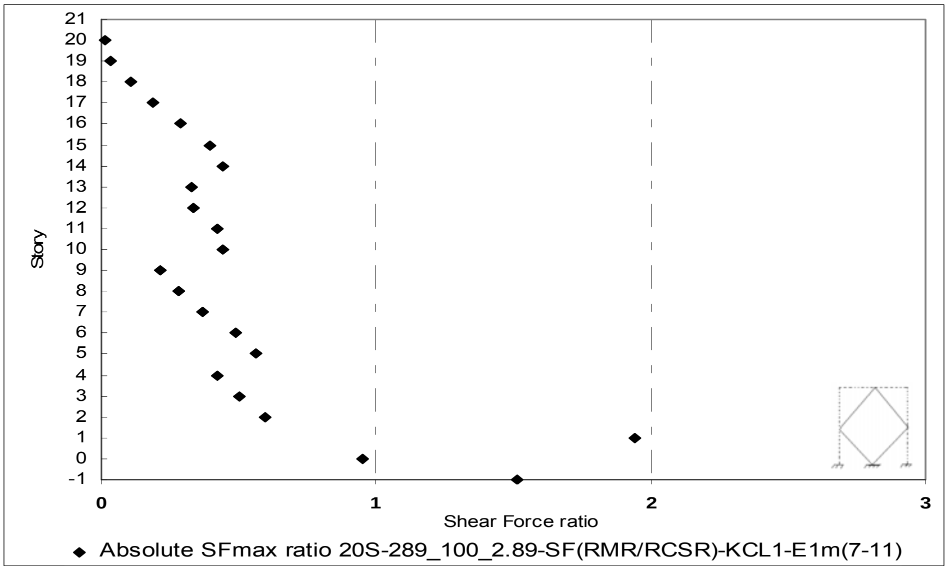

b)

Figure C.34 Shear Force ratio for 20S-289_100_2.89-KCL1
a)Beams, b)Columns

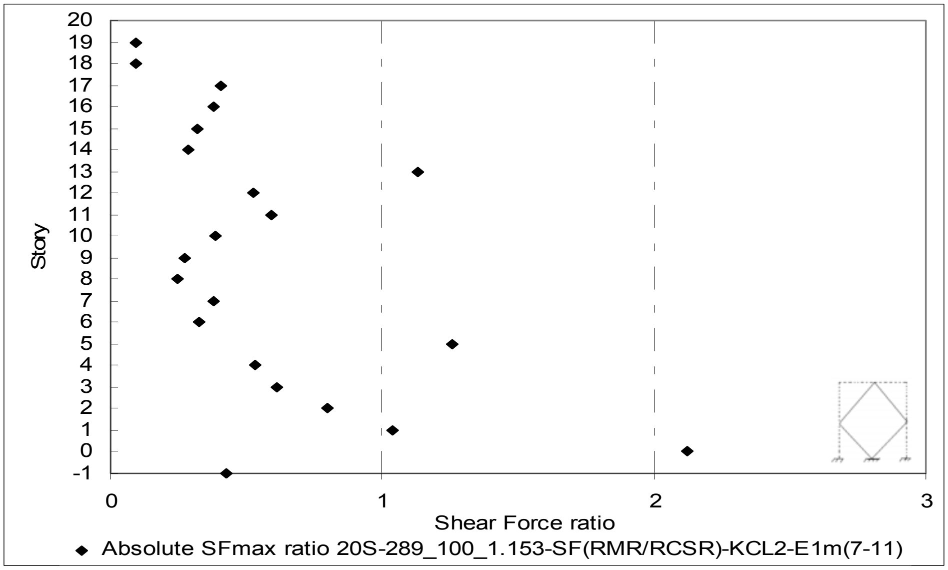

a)

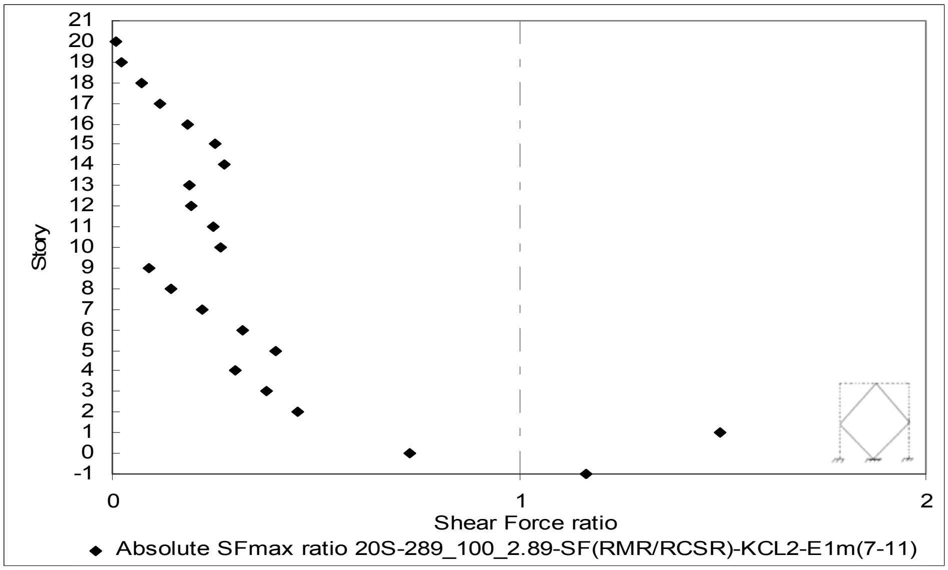

b)

Figure C.35 Shear Force ratio for 20S-289_100_2.89-KCL2
a)Beams, b)Columns

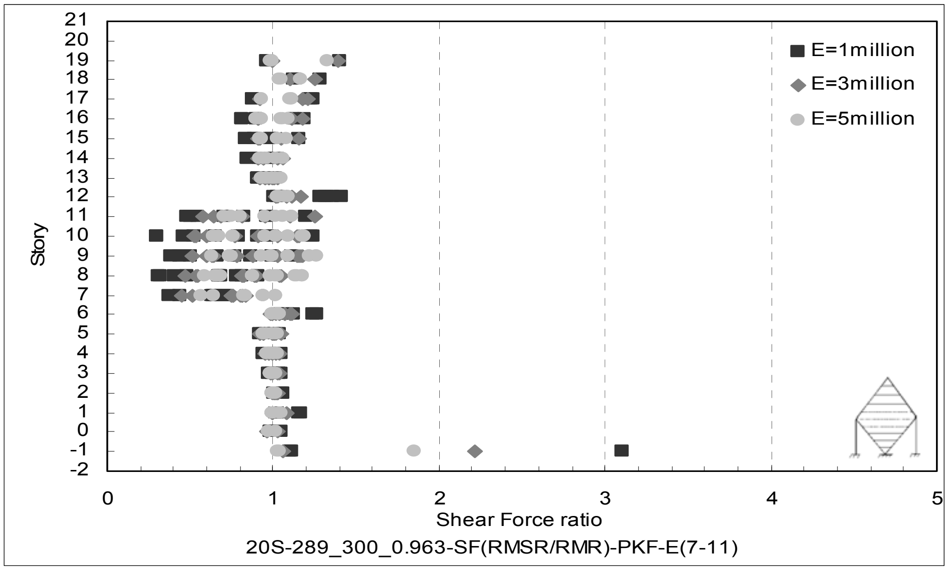

a)

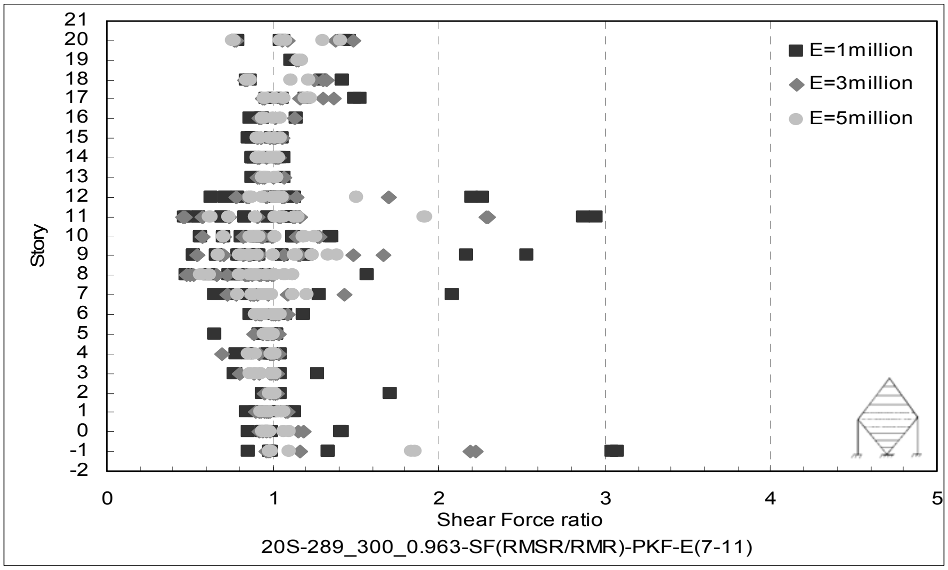

b)

Figure C.36 Shear Force ratio for 20S-289_300_0.963-PKF
a)Beams, b)Columns

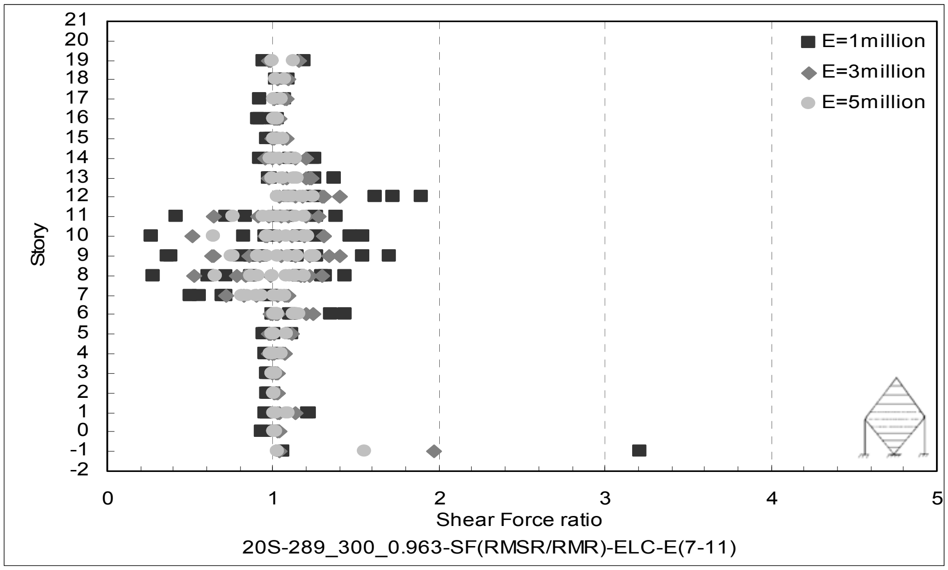

a)

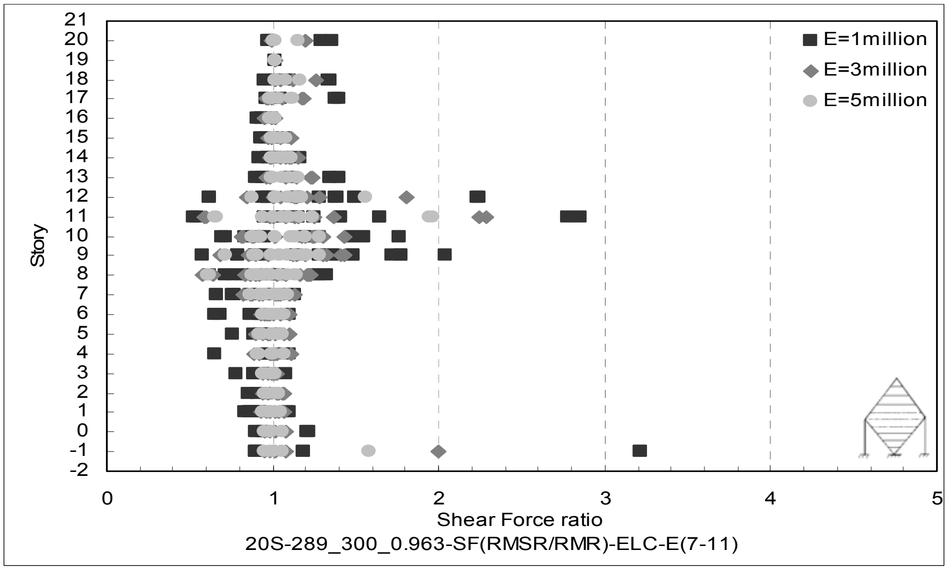

b)

Figure C.37 Shear Force ratio for 20S-289_300_0.963-ELC
a)Beams, b)Columns

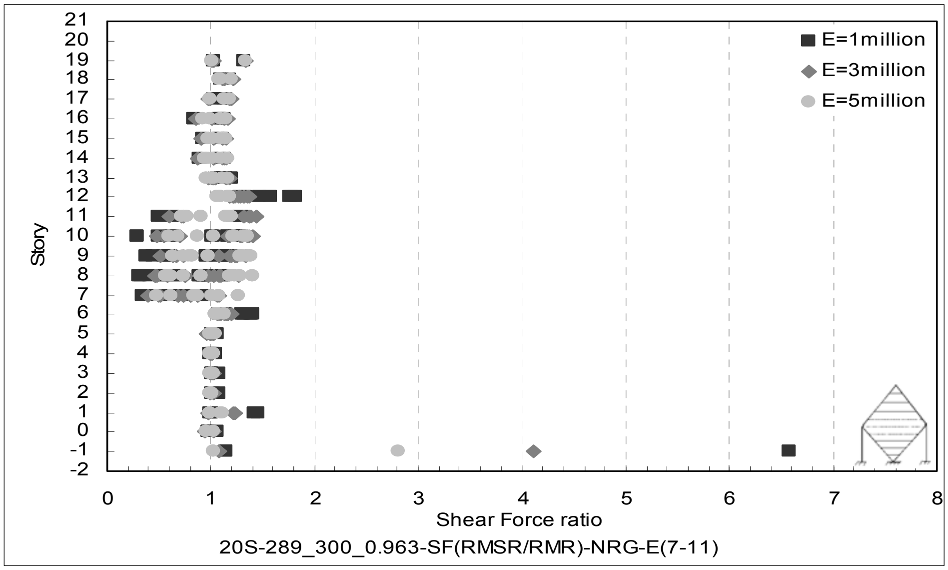

a)

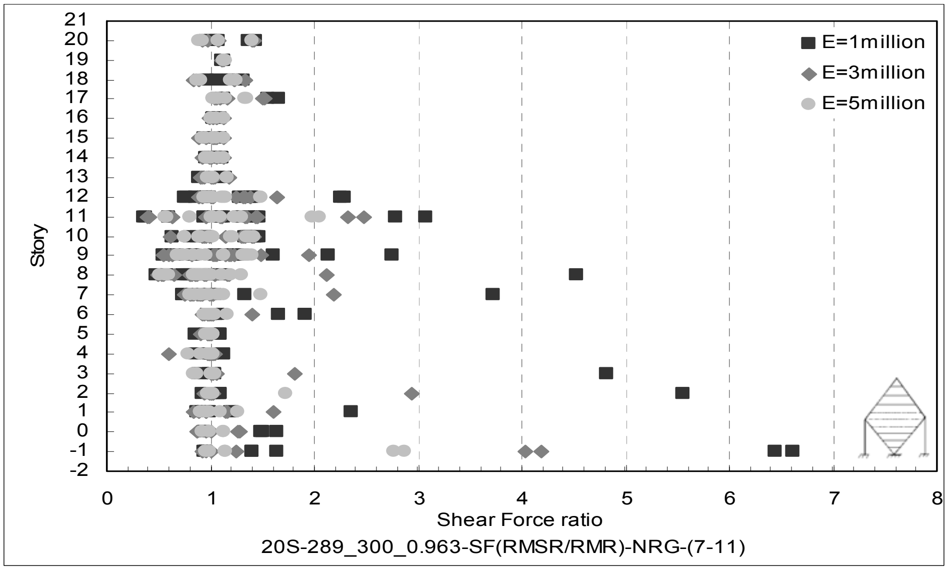

b)

Figure C.38 Shear Force ratio for20S-289_300_0.963-NRG
a)Beams, b)Columns

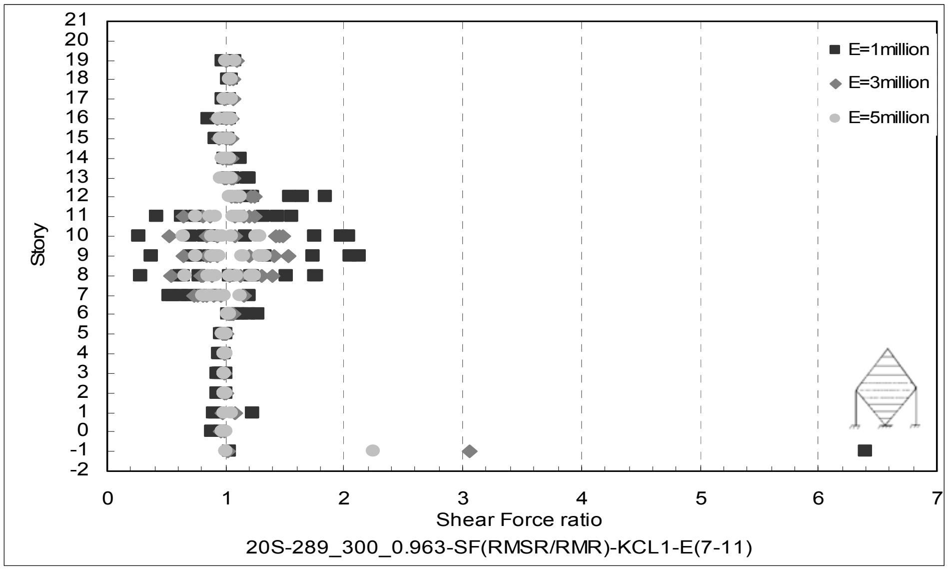

a)

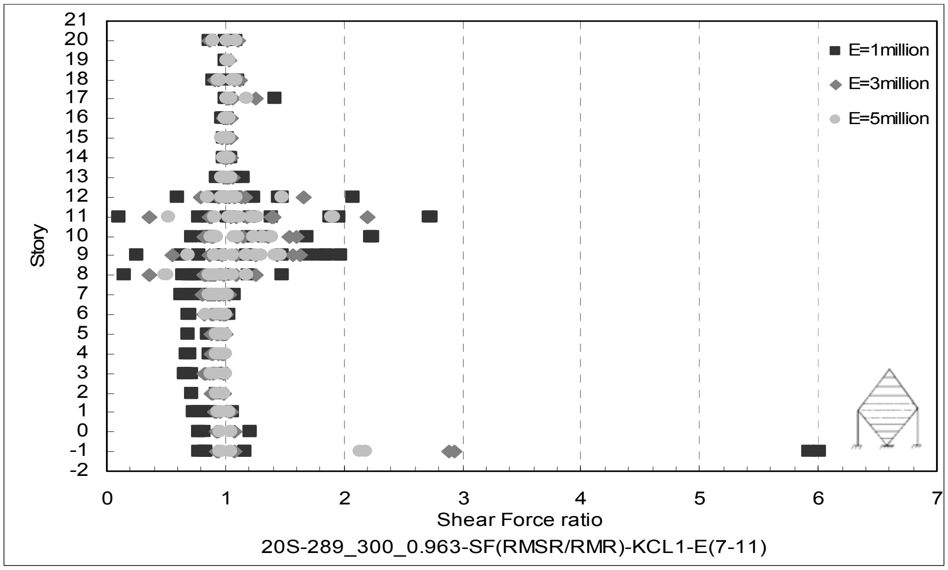

b)

Figure C.39 Shear Force ratio for20S-289_300_0.963-KCL1
a)Beams, b)Columns

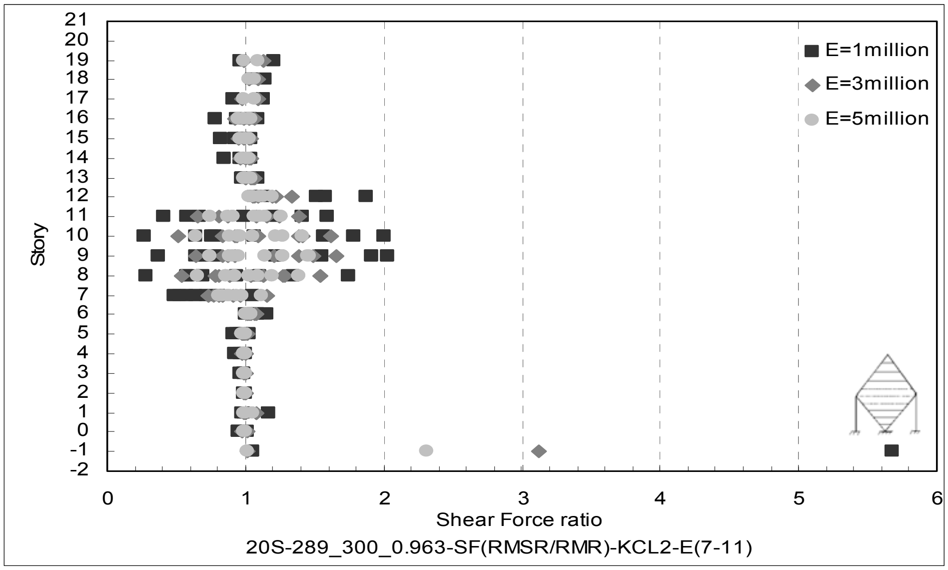

a)

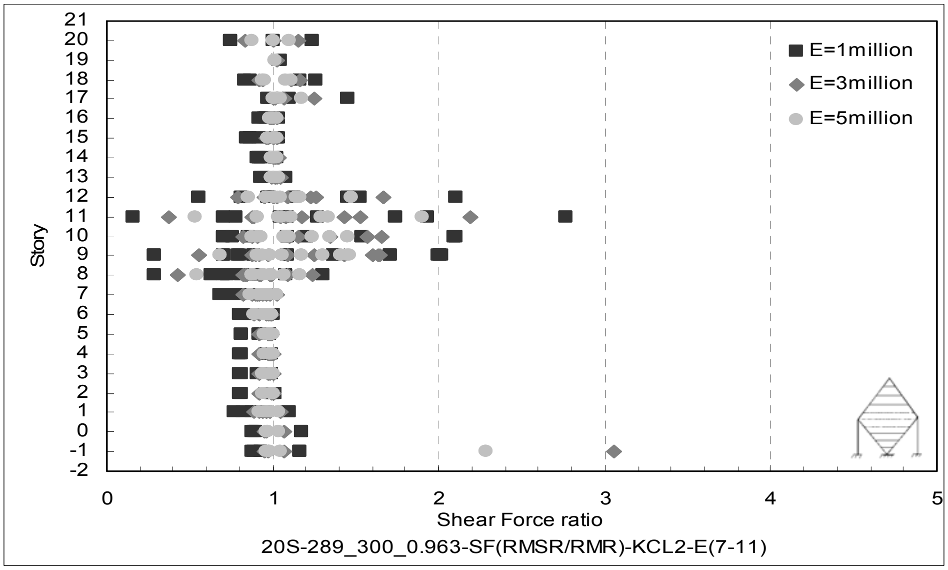

b)

Figure C.40 Shear Force ratio for 20S-289_300_0.963-KCL2
a)Beams, b)Columns

APPENDIX D

BENDING MOMENTS IN THE FRAME ELEMENTS

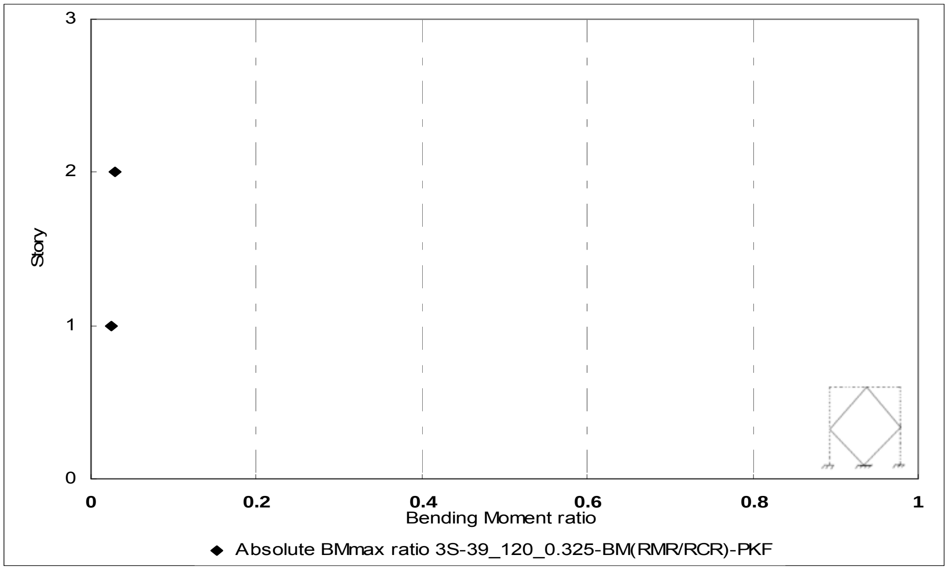

a)

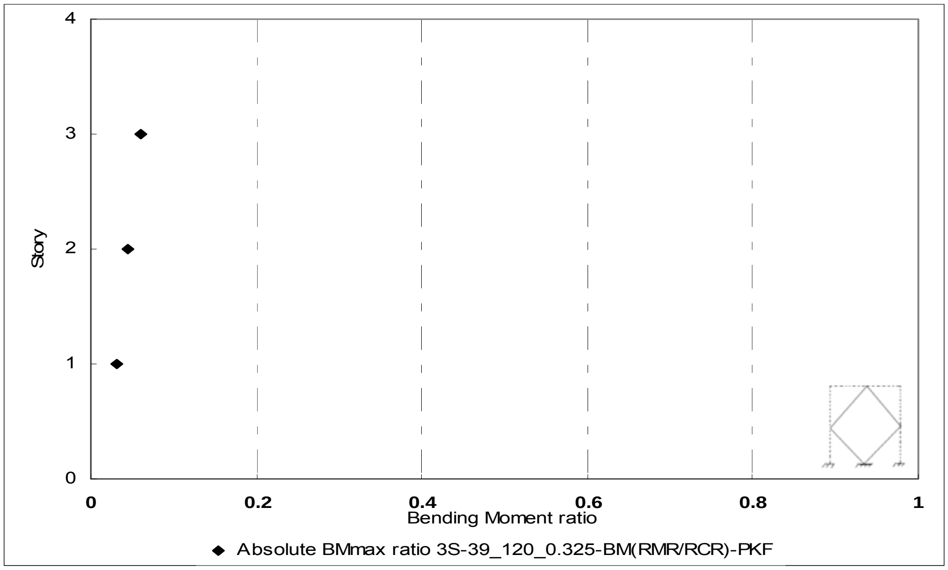

b)

Figure D.1 Bending Moment ratio for 3S-39_120_0.325-PKF
a)Beams, b)Columns

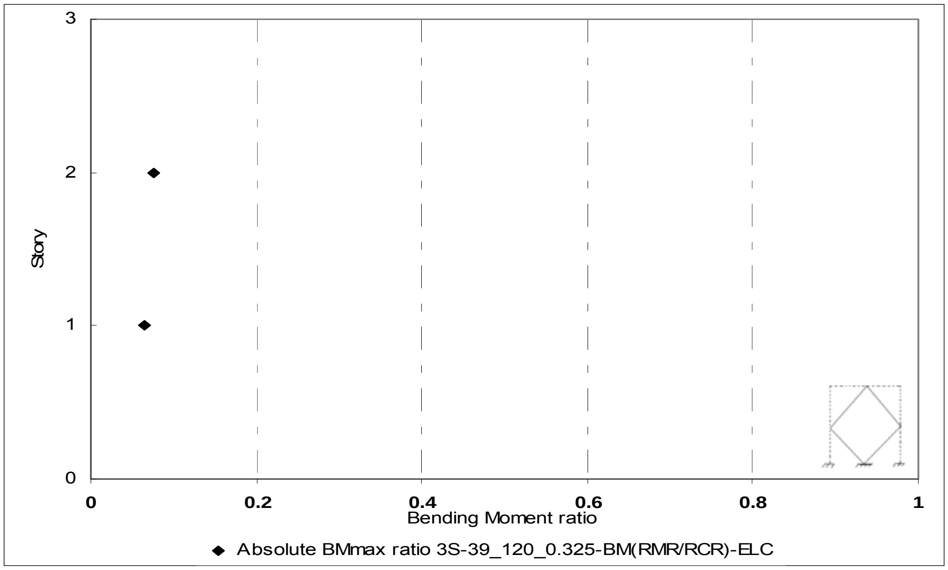

a)

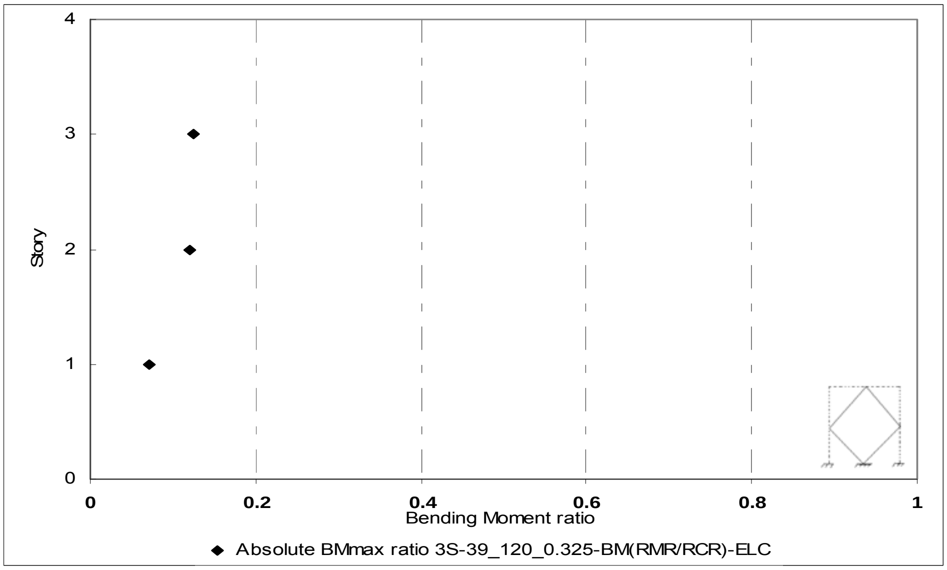

b)

Figure D.2 Bending Moment ratio for 3S-39_120_0.325-ELC
a)Beams, b)Columns

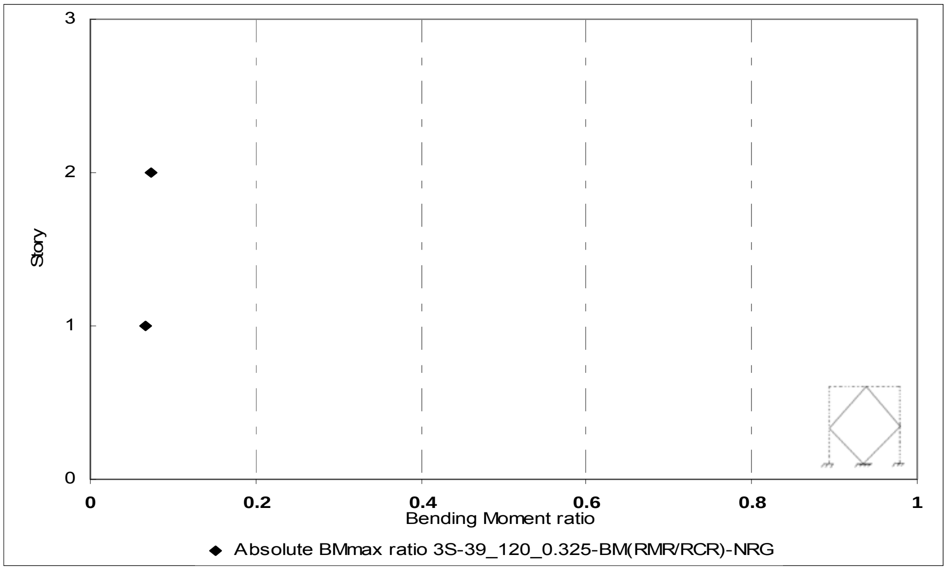

a)

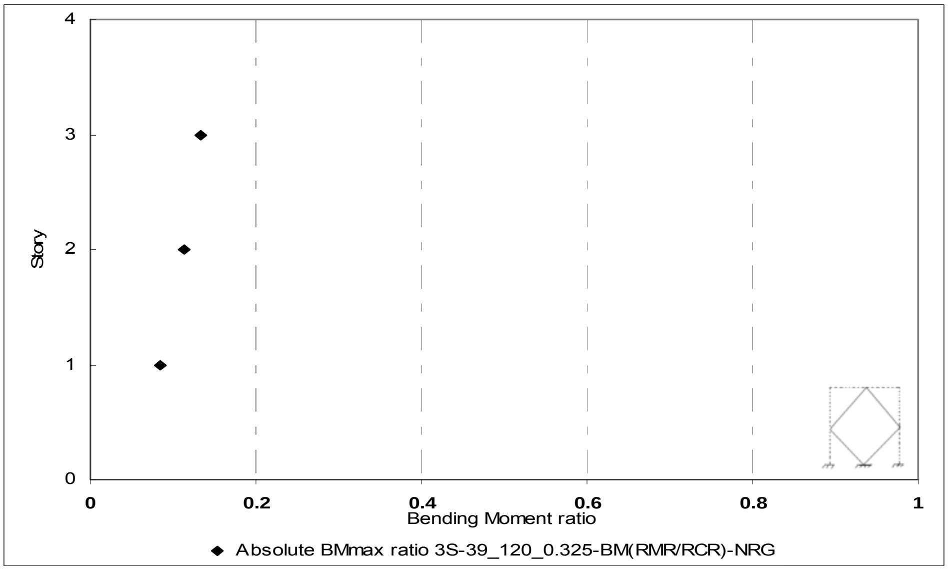

b)

Figure D.3 Bending Moment ratio for 3S-39_120_0.325-NRG
a)Beams, b)Columns

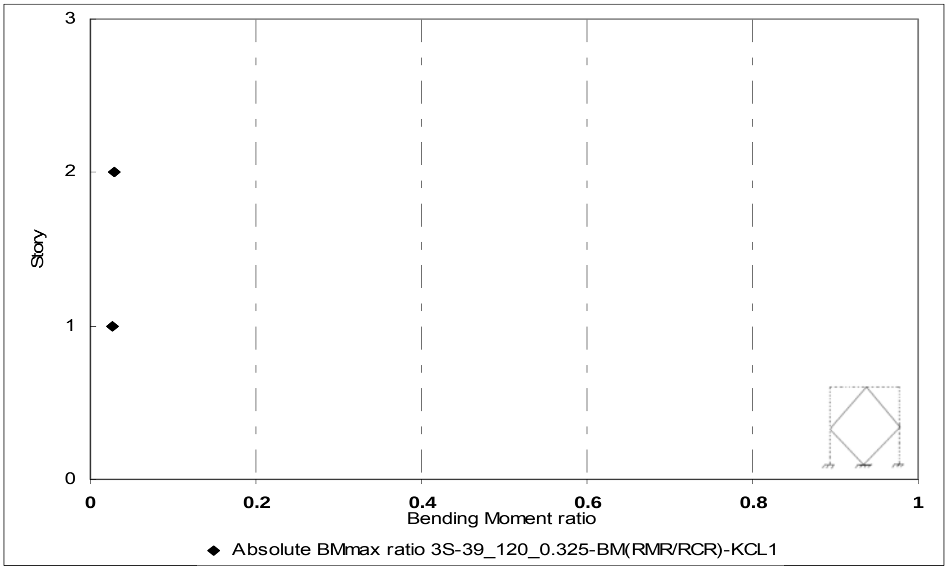

a)

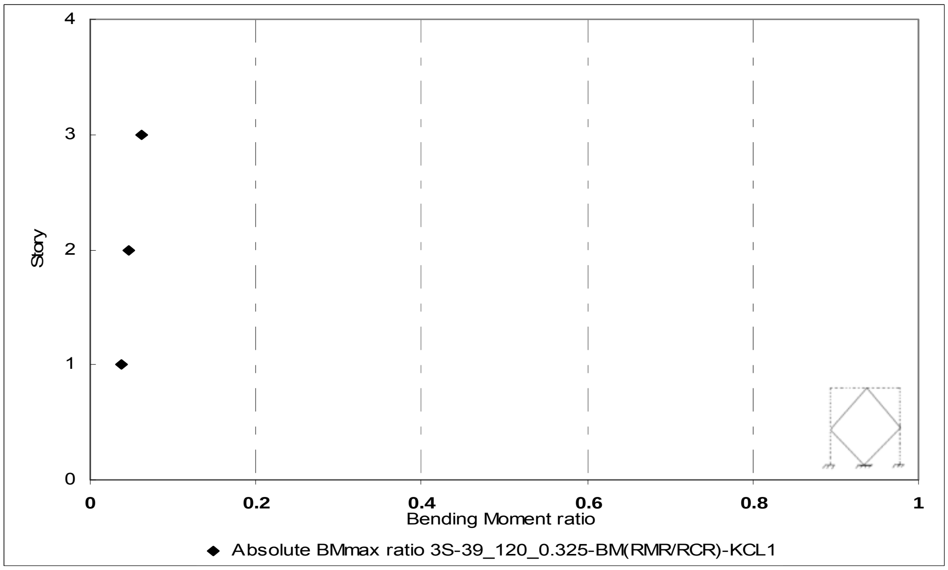

b)

Figure D.4 Bending Moment ratio for 3S-39_120_0.325-KCL1
a)Beams, b)Columns

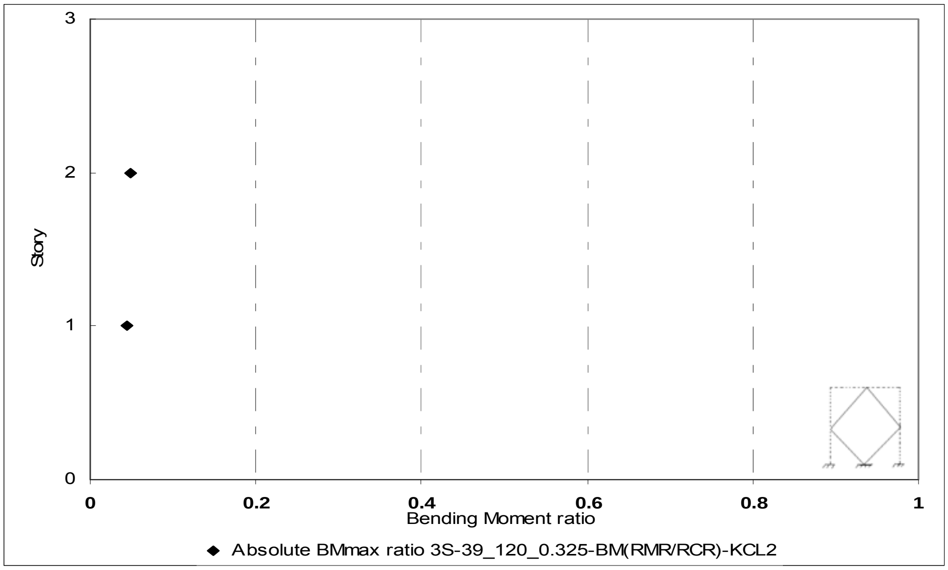

a)

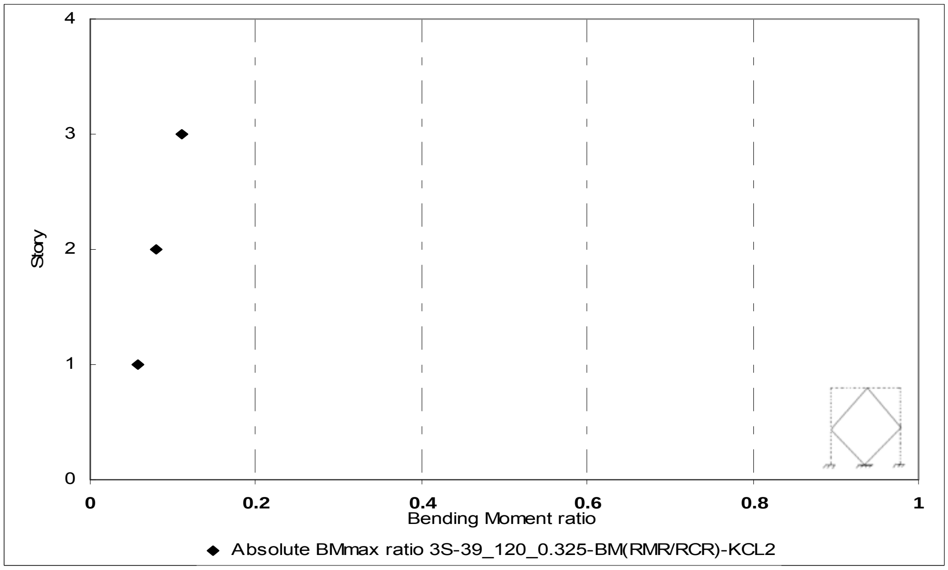

b)

Figure D.5 Bending Moment ratio for 3S-39_120_0.325-KCL2
a)Beams, b)Columns

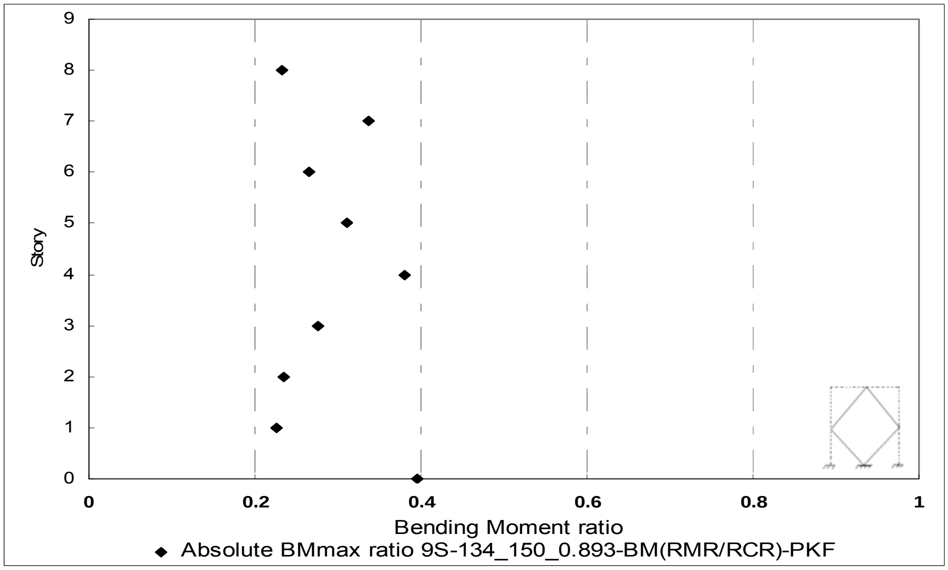

a)

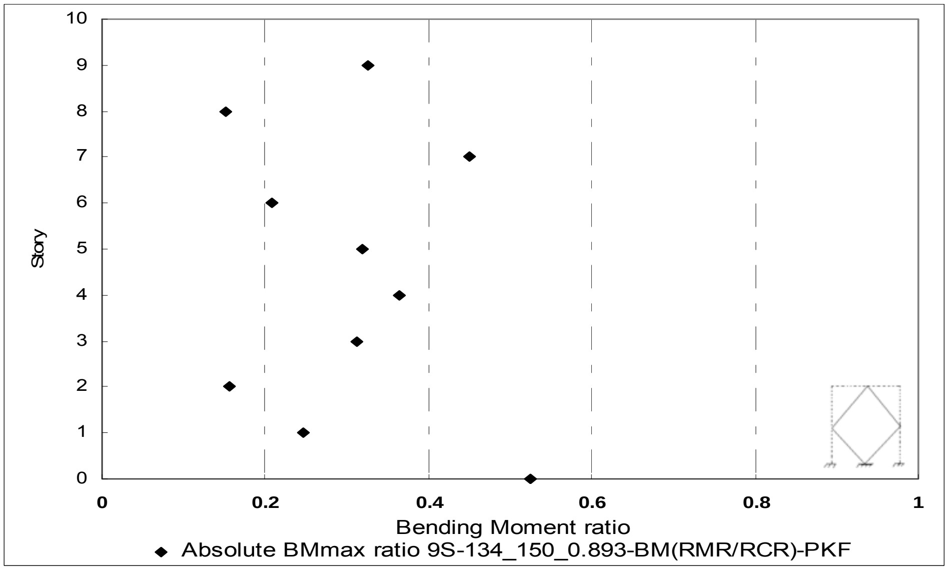

b)

Figure D.6 Bending Moment ratio for 9S-134_150_0.893-PKF
a)Beams, b)Columns

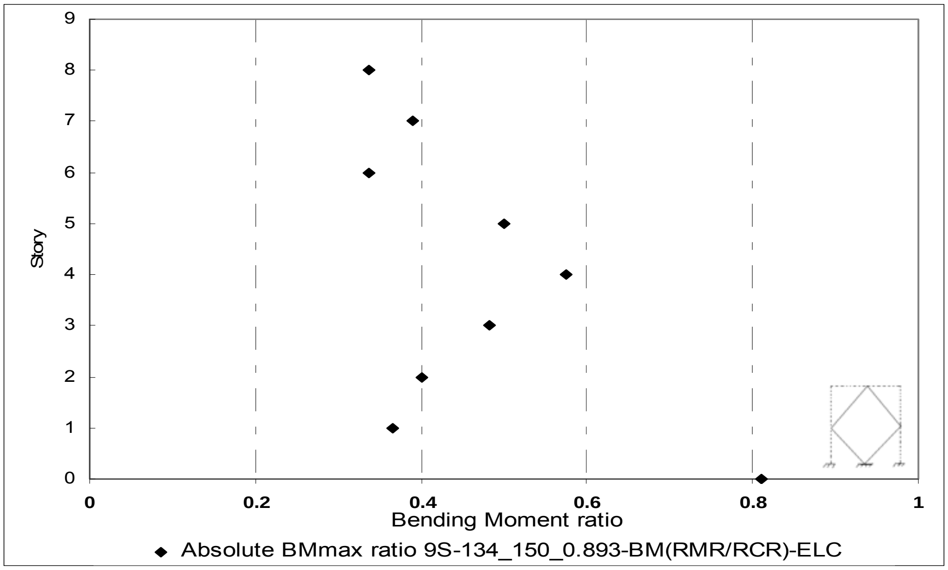

a)

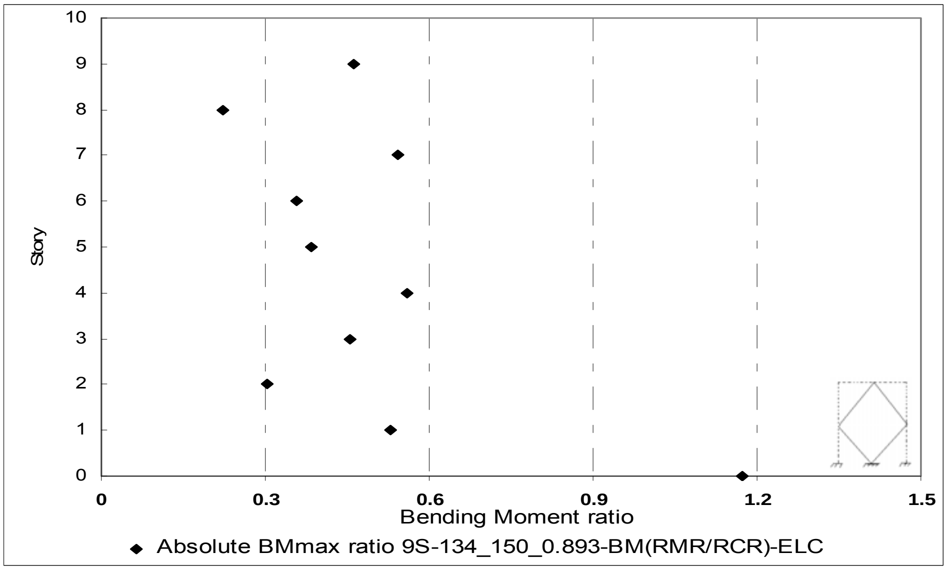

b)

Figure D.7 Bending Moment ratio for 9S-134_150_0.893-ELC
a)Beams, b)Columns

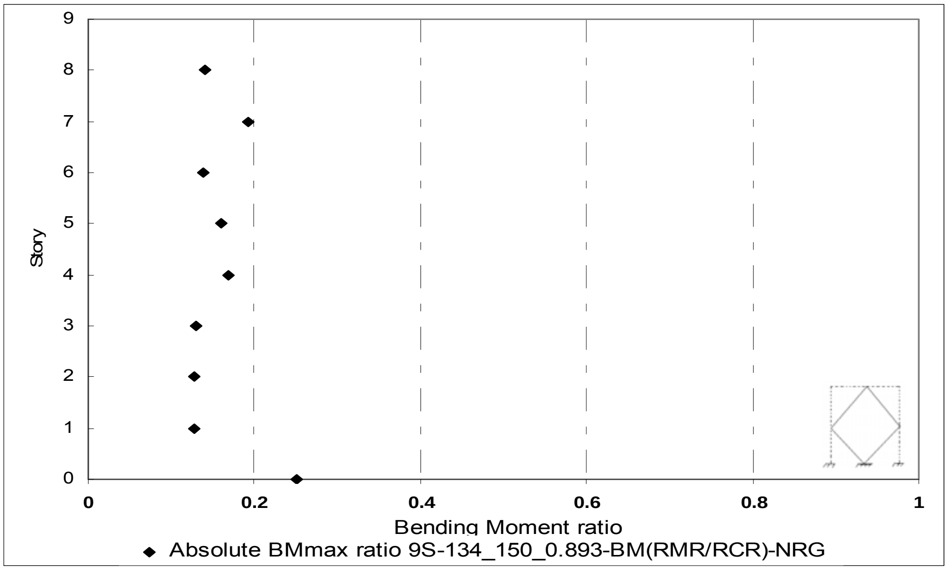

a)

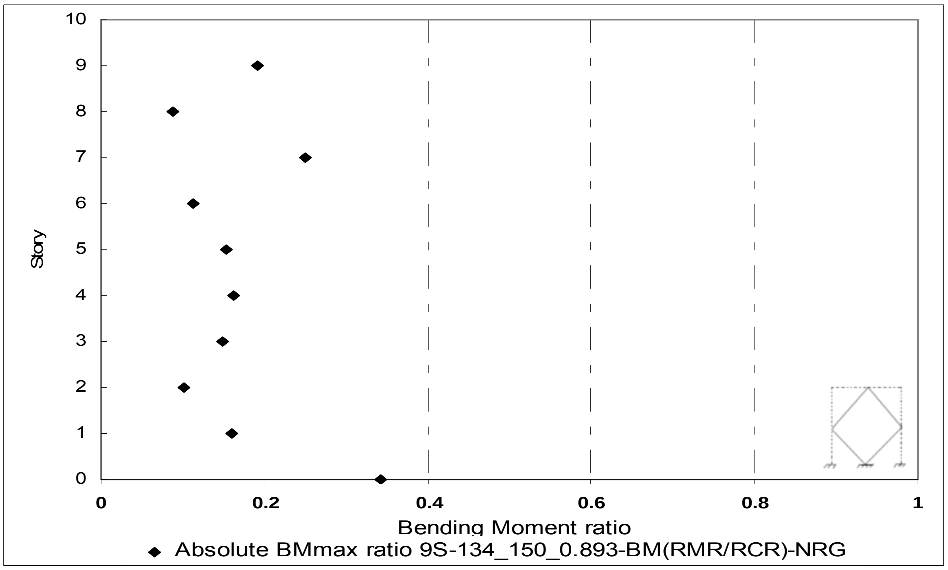

b)

Figure D.8 Bending Moment ratio for 9S-134_150_0.893-NRG
a)Beams, b)Columns

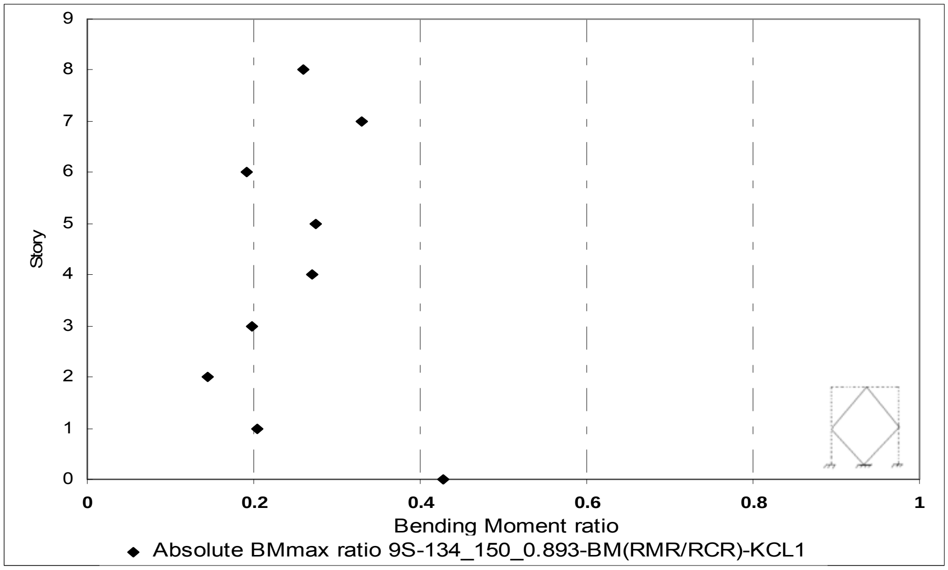

a)

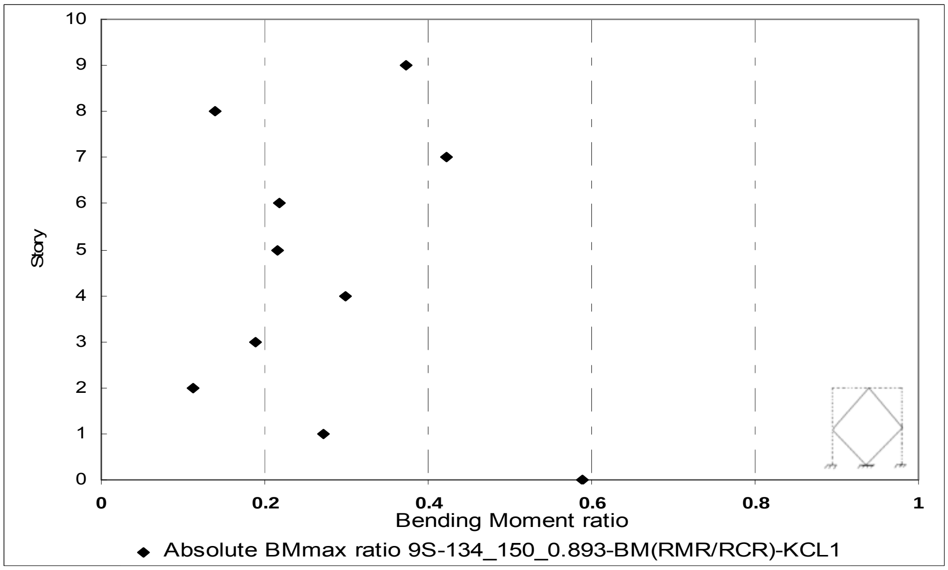

b)

Figure D.9 Bending Moment ratio for 9S-134_150_0.893-KCL1
a)Beams, b)Columns

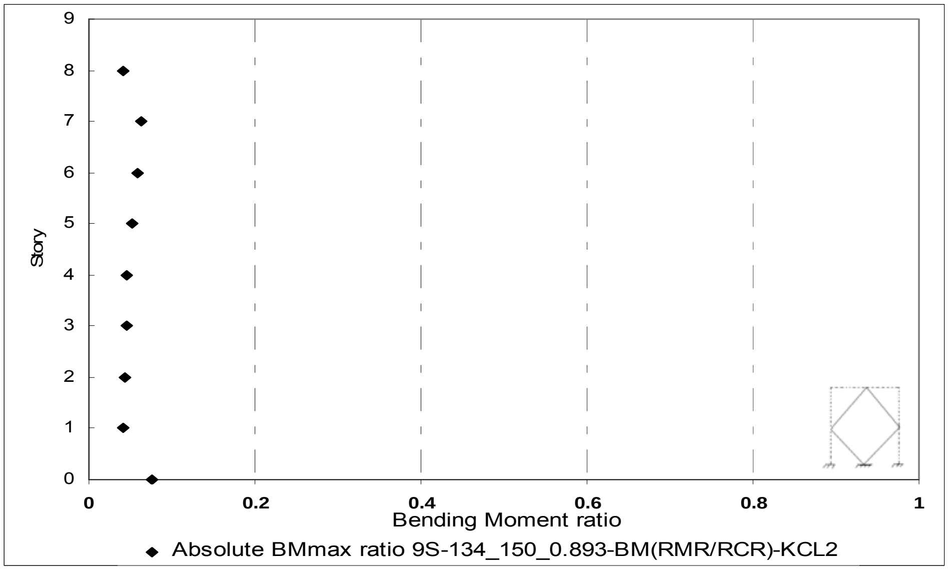

a)

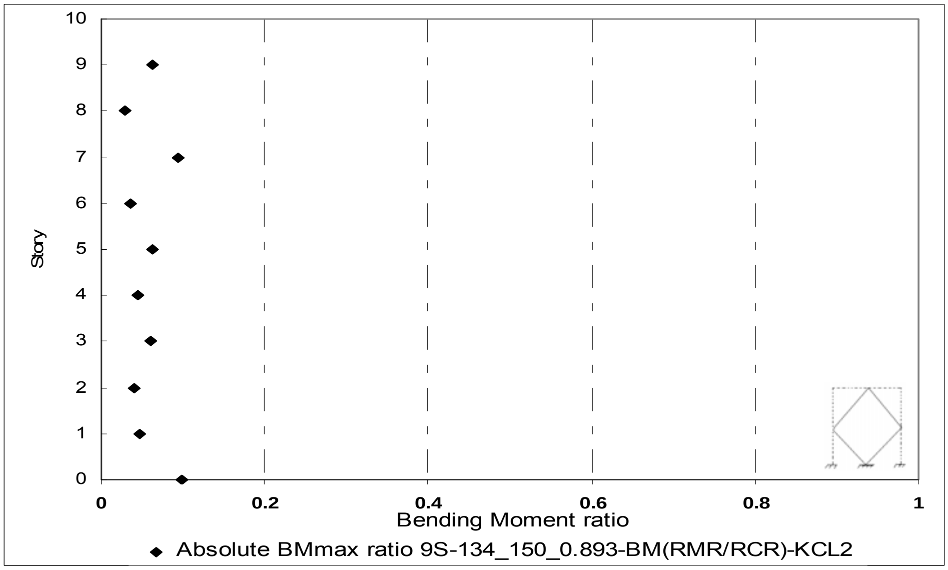

b)

Figure D.10 Bending Moment ratio for 9S-134_150_0.893-KCL2
a)Beams, b)Columns

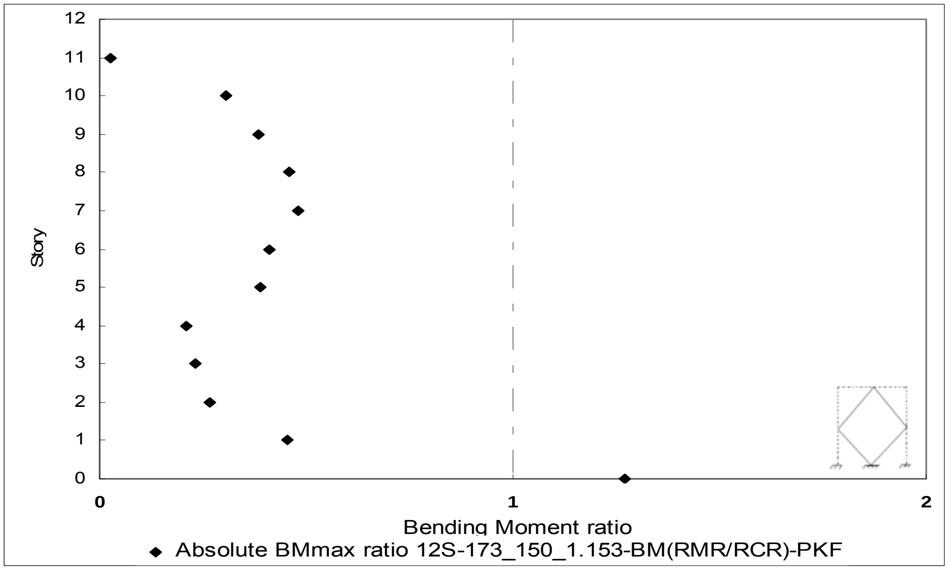

a)

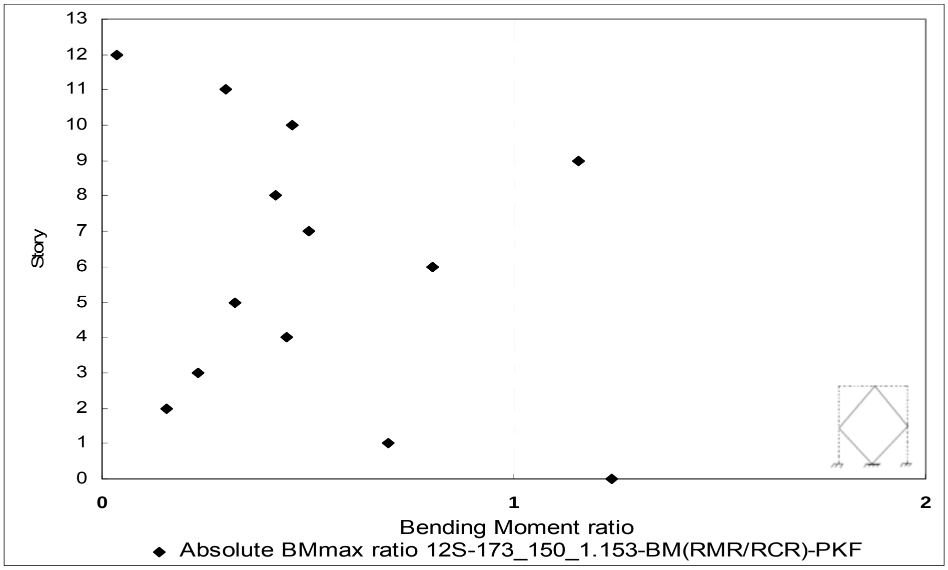

b)

Figure D.11 Bending Moment ratio for 12S-173_150_1.153-PKF
a)Beams, b)Columns

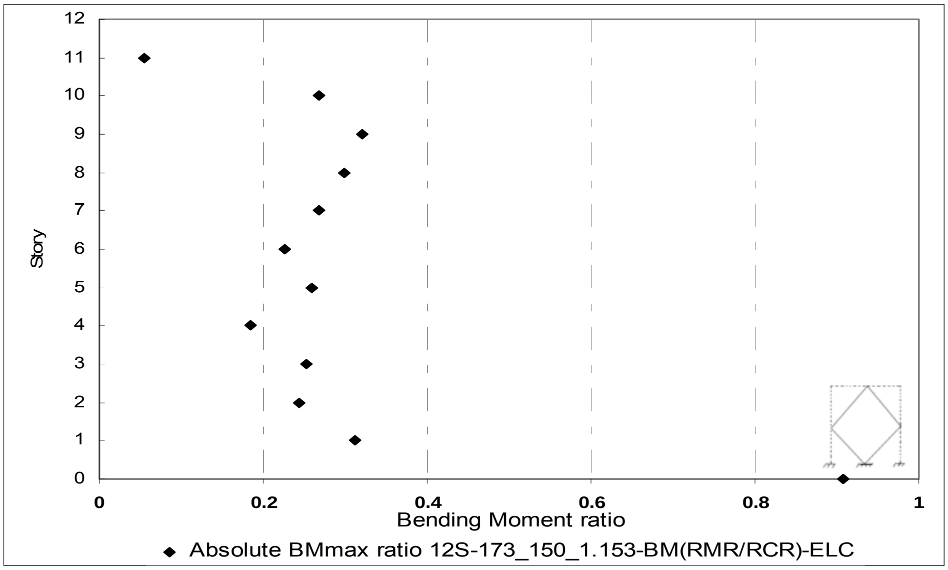

a)

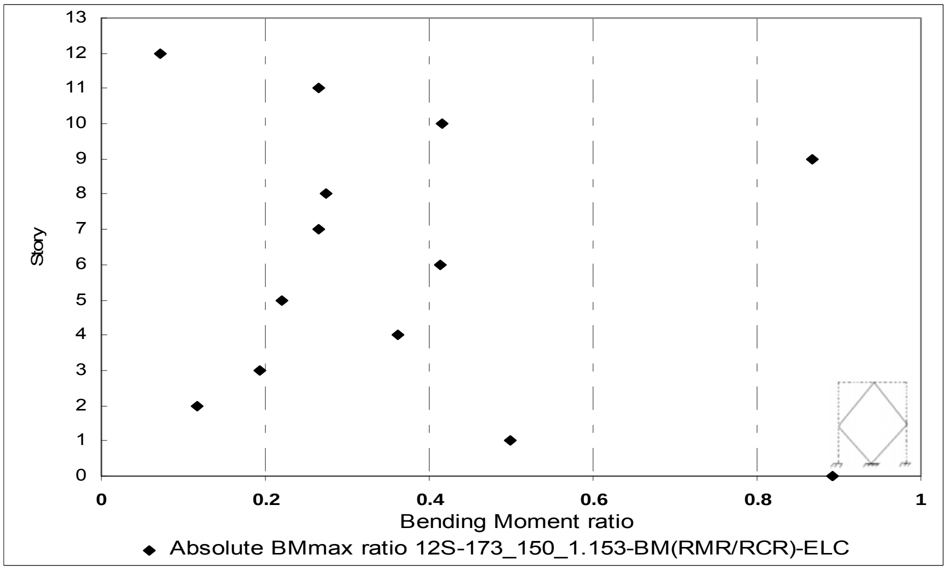

b)

Figure D.12 Bending Moment ratio for 12S-173_150_1.153-ELC
a)Beams, b)Columns

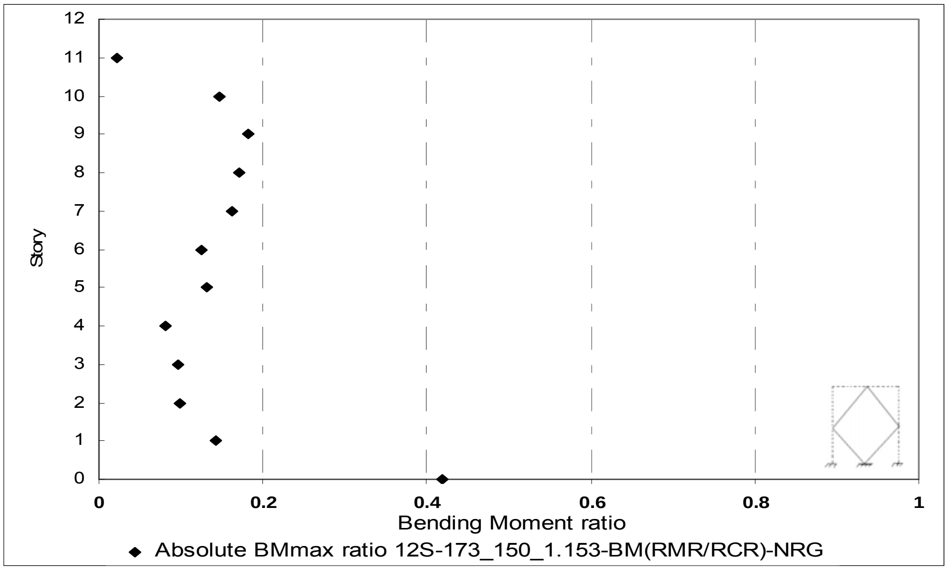

a)

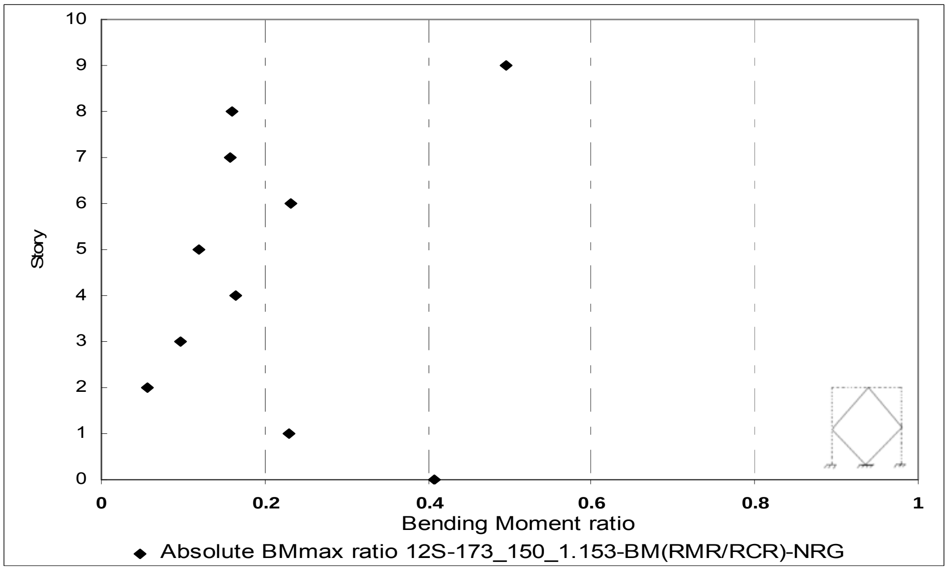

b)

Figure D.13 Bending Moment ratio for 12S-173_150_1.153-NRG
a)Beams, b)Columns

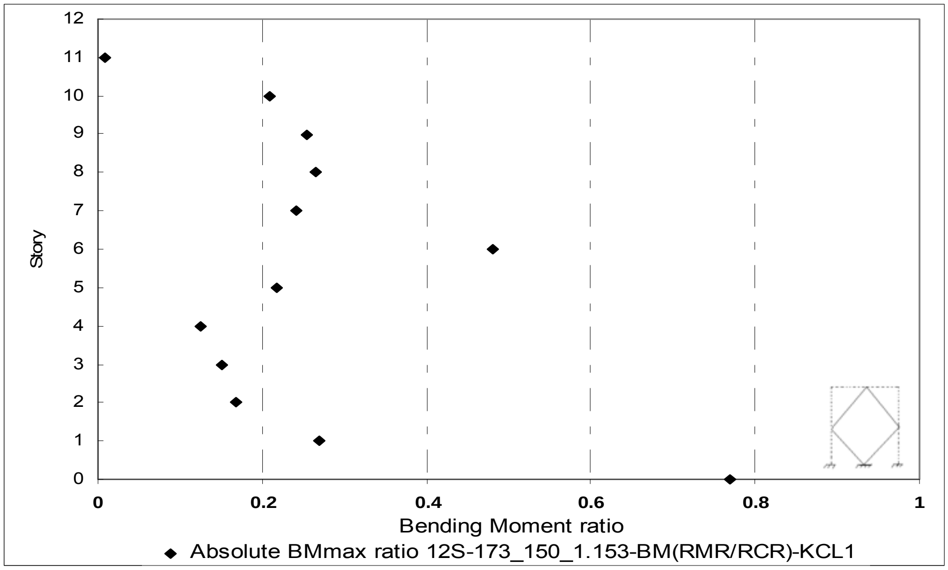

a)

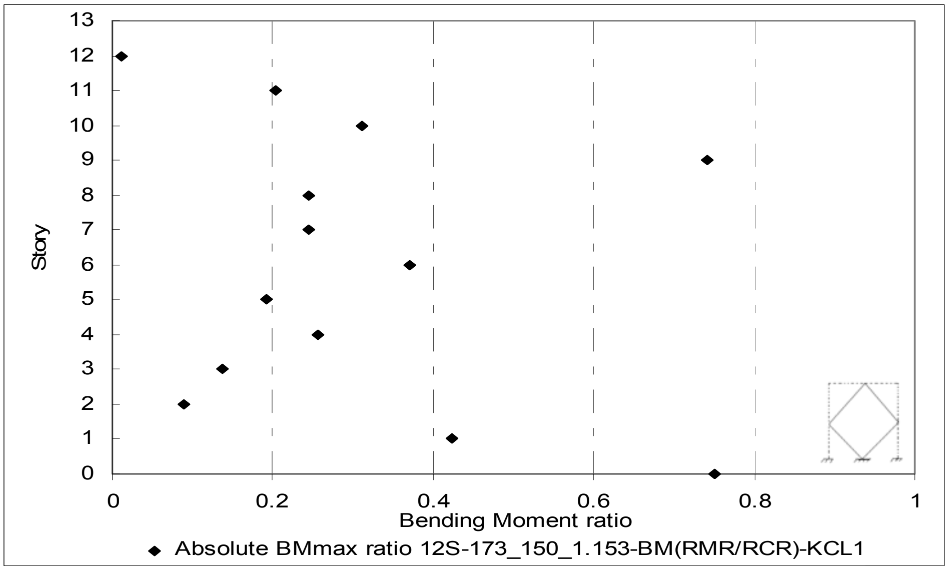

b)

Figure D.14 Bending Moment ratio for 12S-173_150_1.153-KCL1
a)Beams, b)Columns

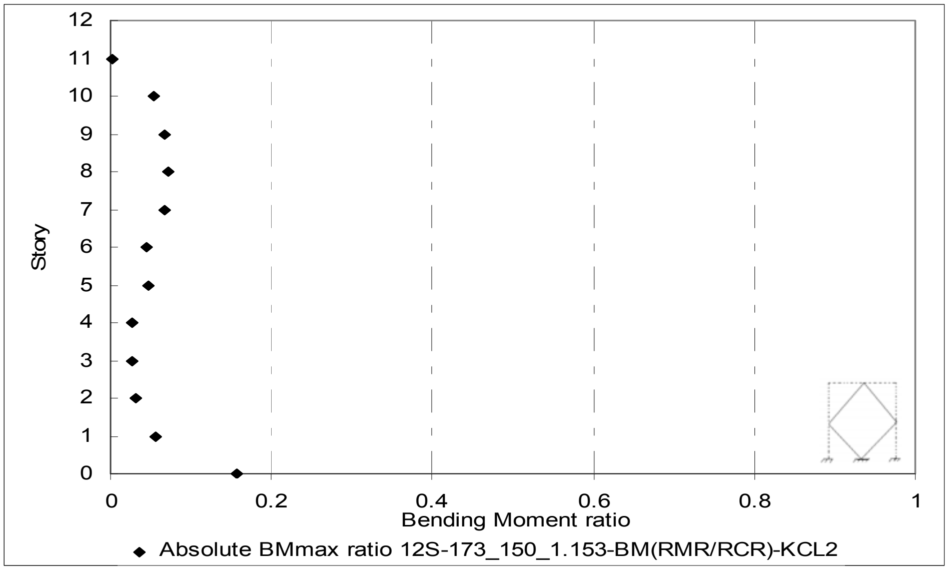

a)

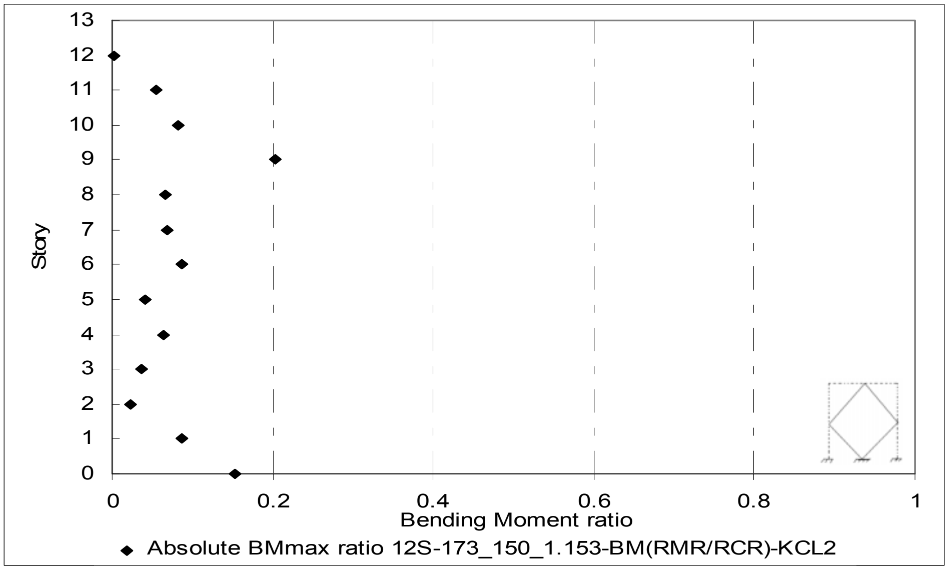

b)

Figure D.15 Bending Moment ratio for 12S-173_150_1.153-KCL2
a)Beams, b)Columns

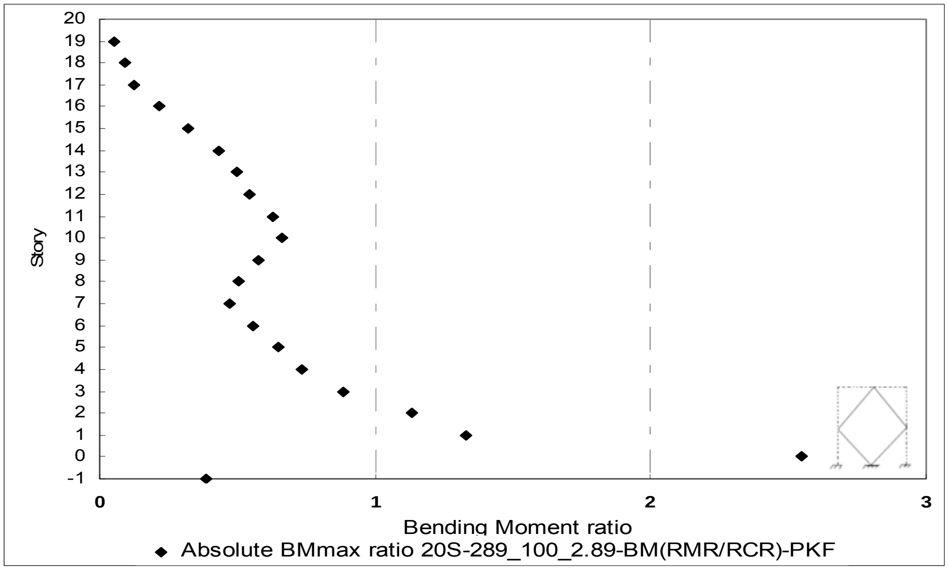

a)

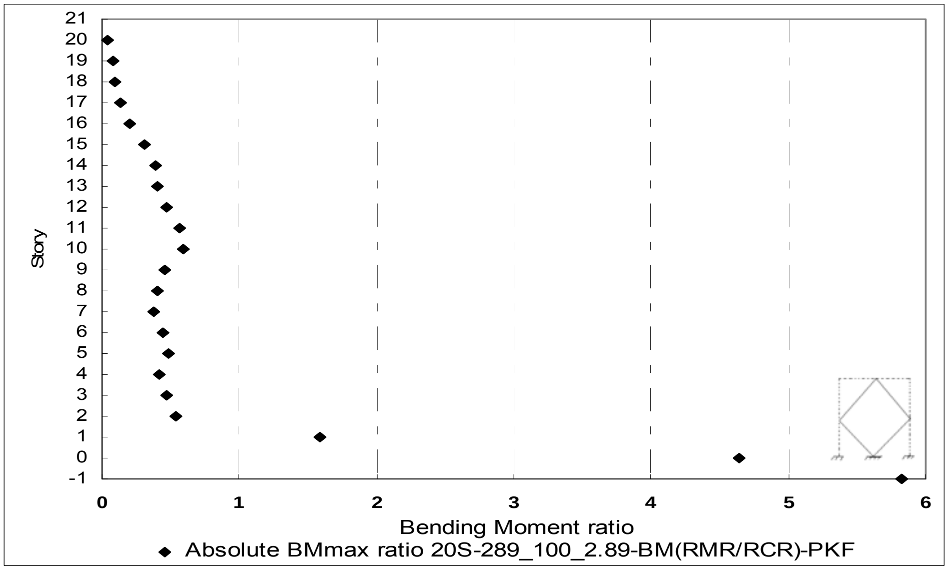

b)

Figure D.16 Bending Moment ratio for 20S-289_100_2.89-PKF
a)Beams, b)Columns

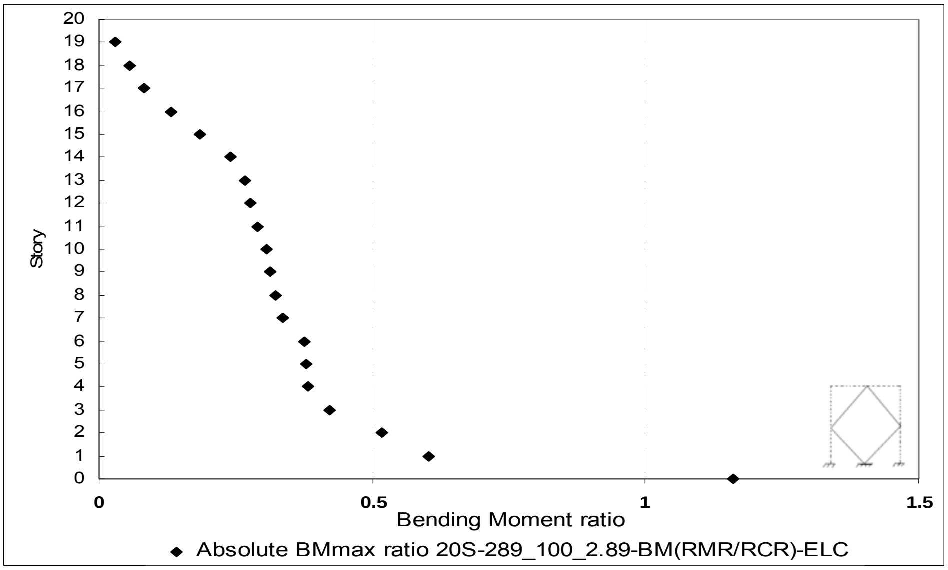

a)

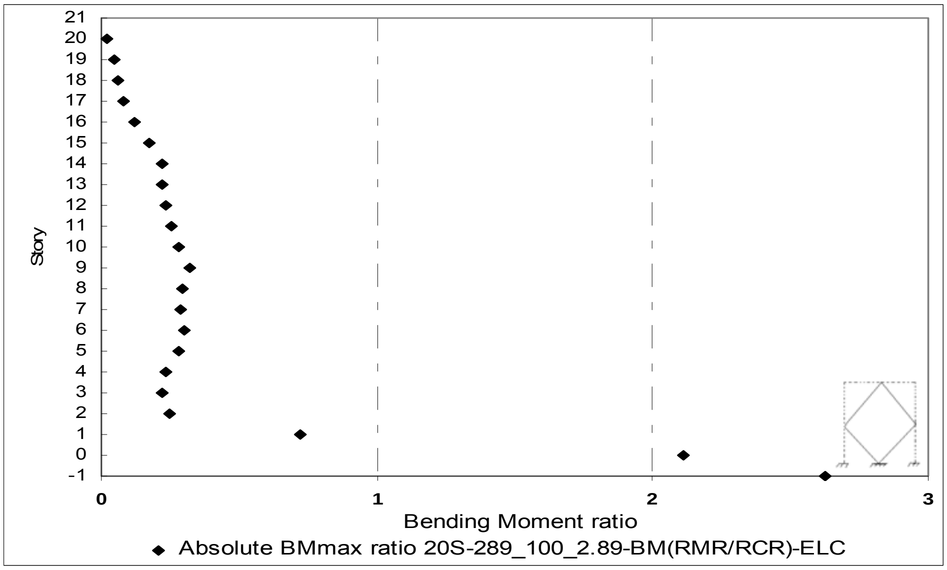

b)

Figure D.17 Bending Moment ratio for 20S-289_100_2.89-ELC
a)Beams, b)Columns

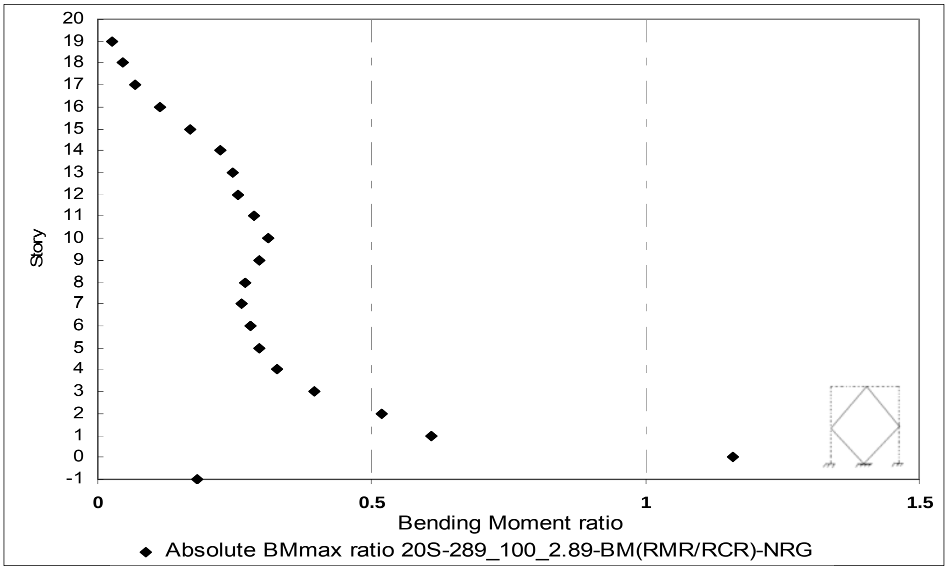

a)

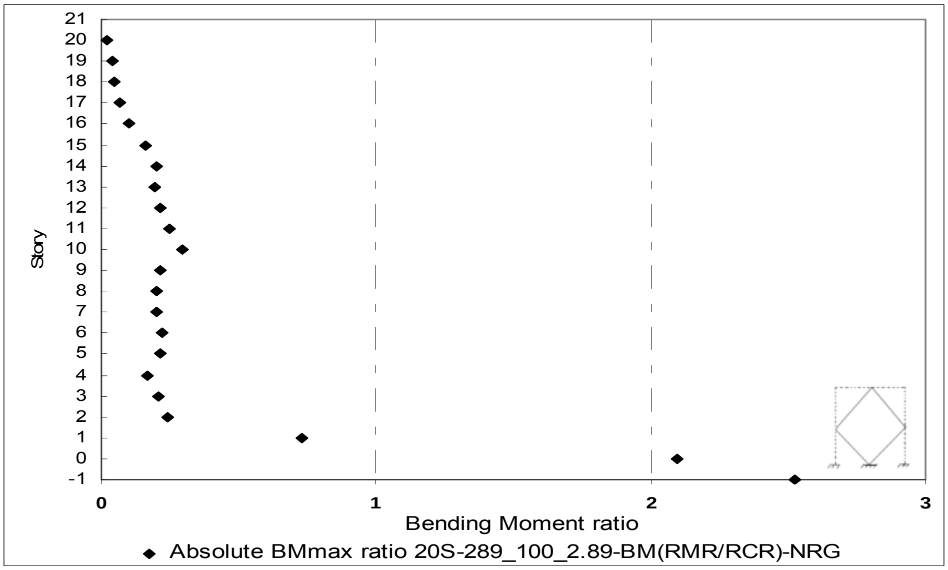

b)

Figure D.18 Bending Moment ratio for 20S-289_100_2.89-NRG
a)Beams, b)Columns

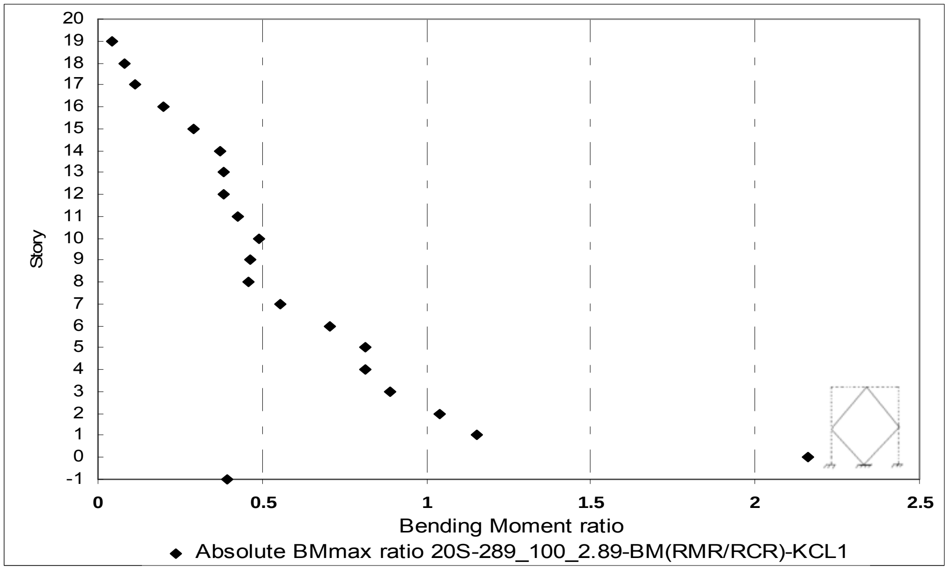

a)

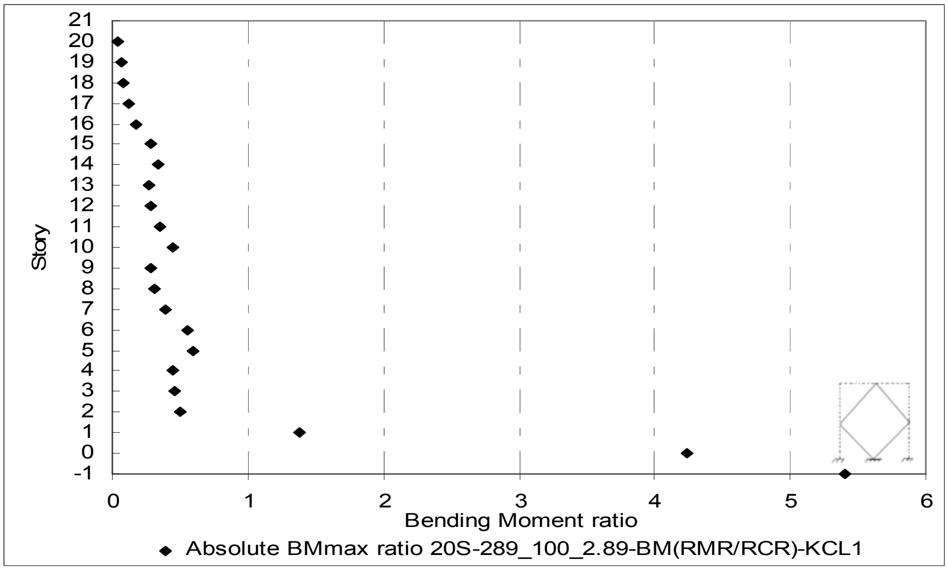

b)

Figure D.19 Bending Moment ratio for 20S-289_100_2.89-KCL1
a)Beams, b)Columns

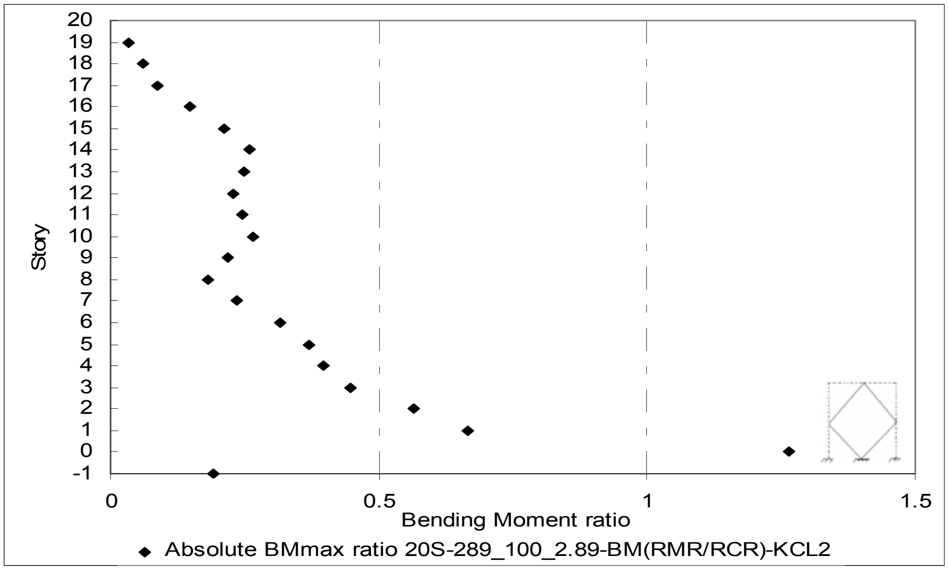

a)

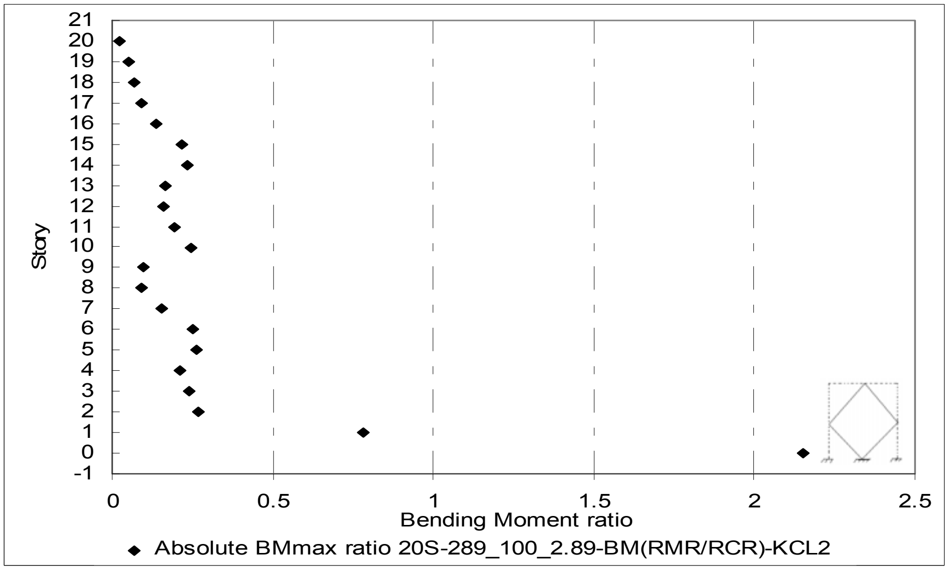

b)

Figure D.20 Bending Moment ratio for 20S-289_100_2.89-KCL2
a)Beams, b)Columns

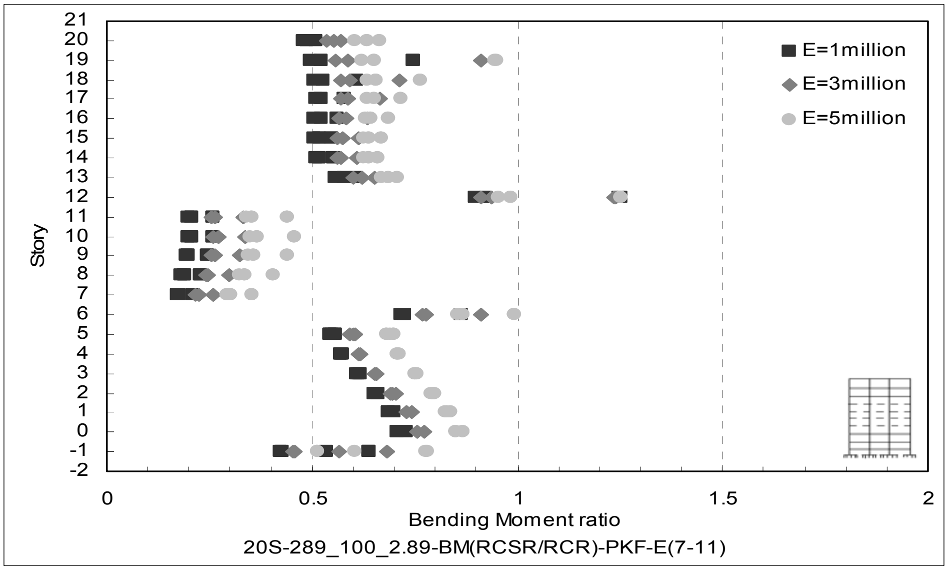

a)

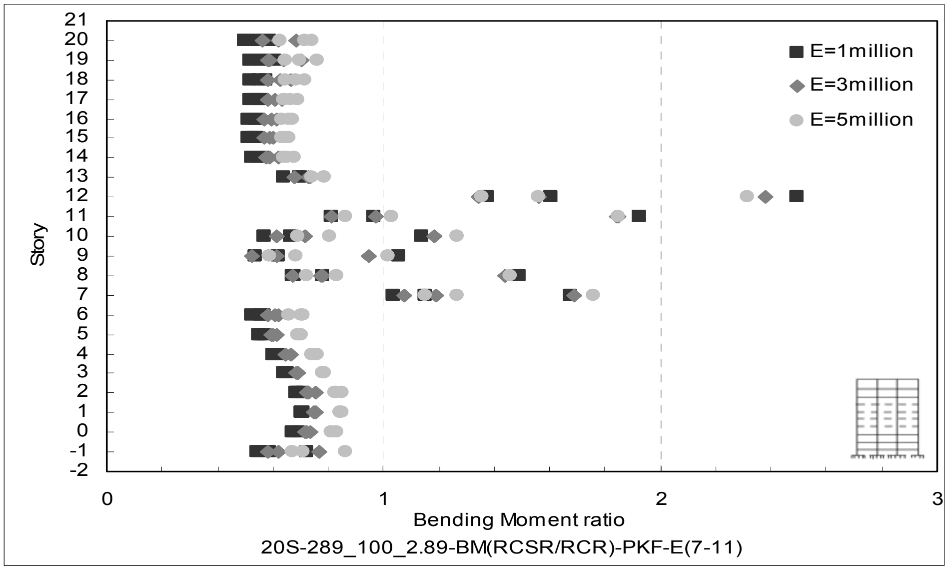

b)

Figure D.21 Bending Moment ratio for 20S-289_100_2.89-PKF
a)Beams, b)Columns

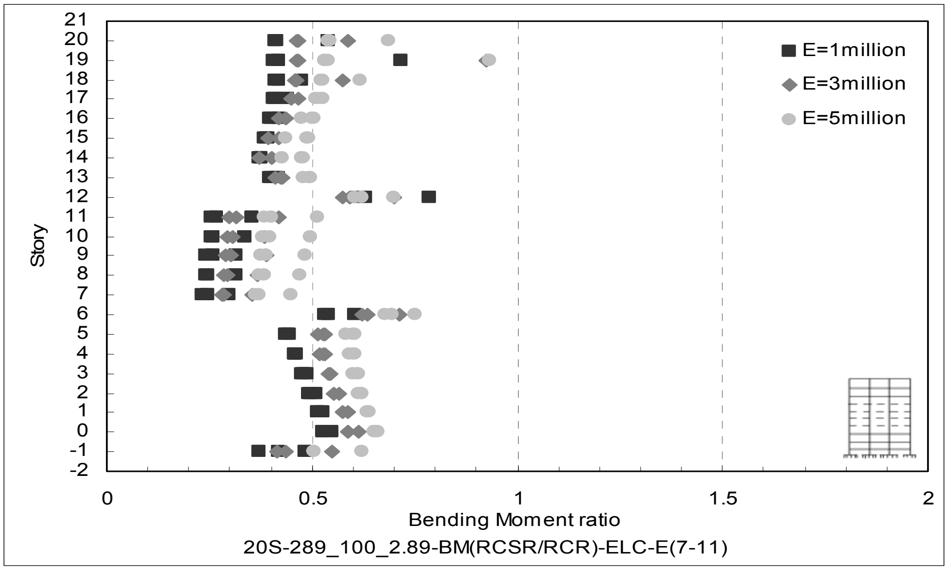

a)

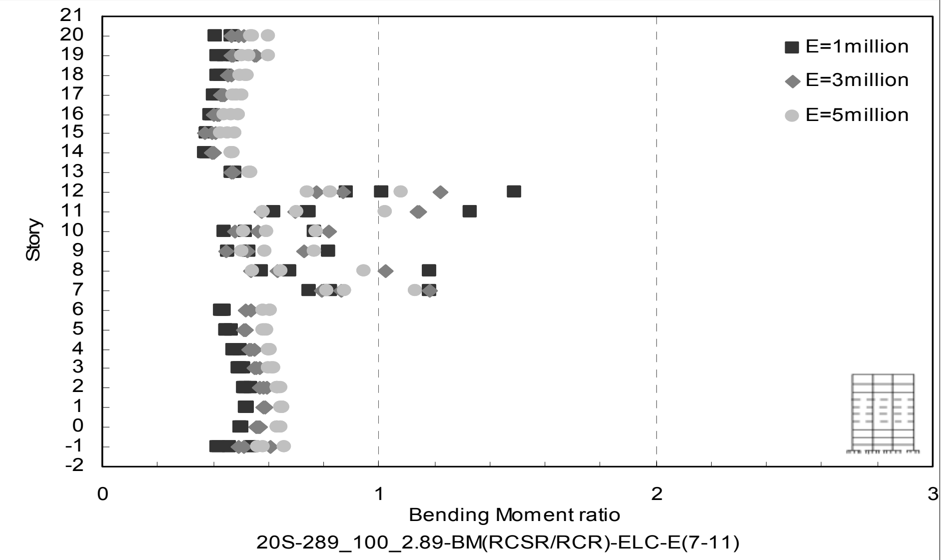

b)

Figure D.22 Bending Moment ratio for 20S-289_100_2.89-ELC
a)Beams, b)Columns

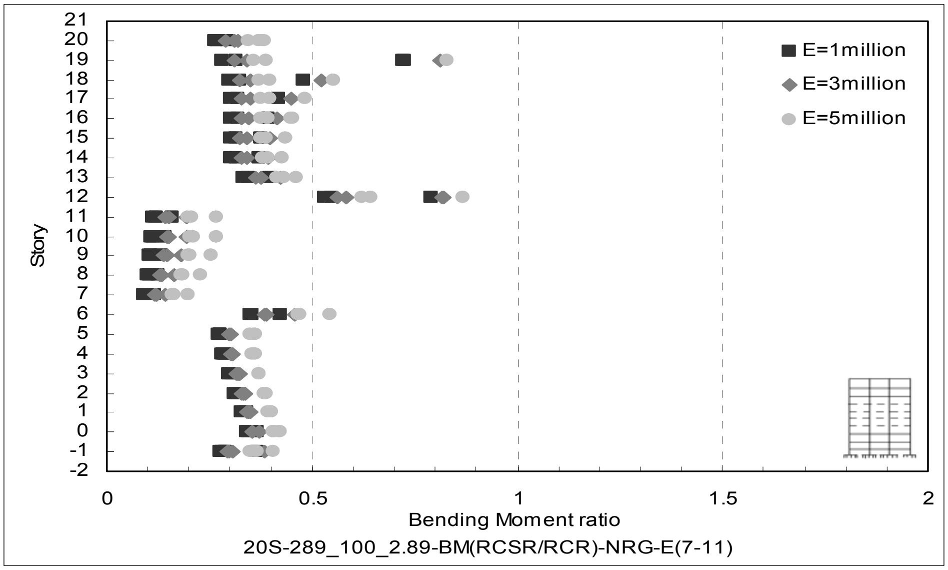

a)

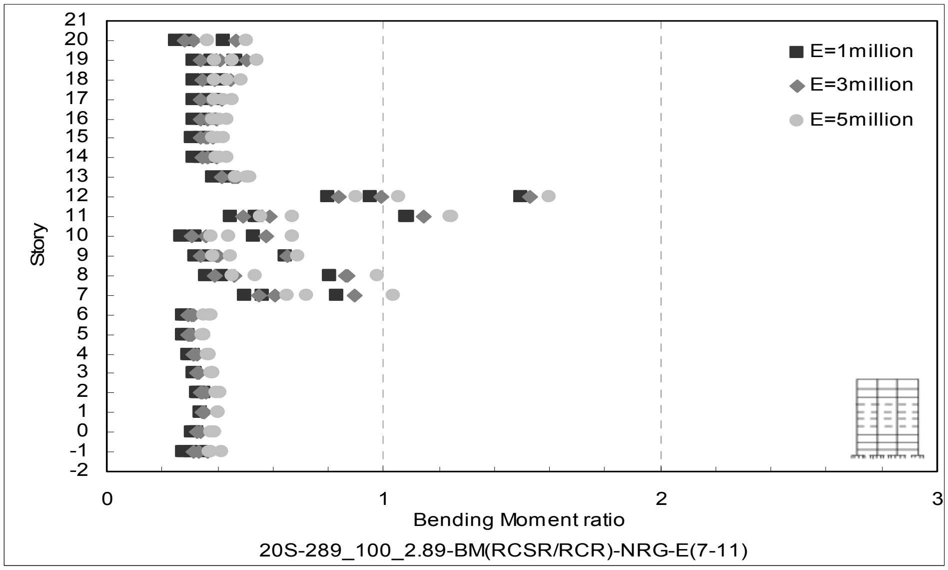

b)

Figure D.23 Bending Moment ratio for 20S-289_100_2.89-NRG
a)Beams, b)Columns

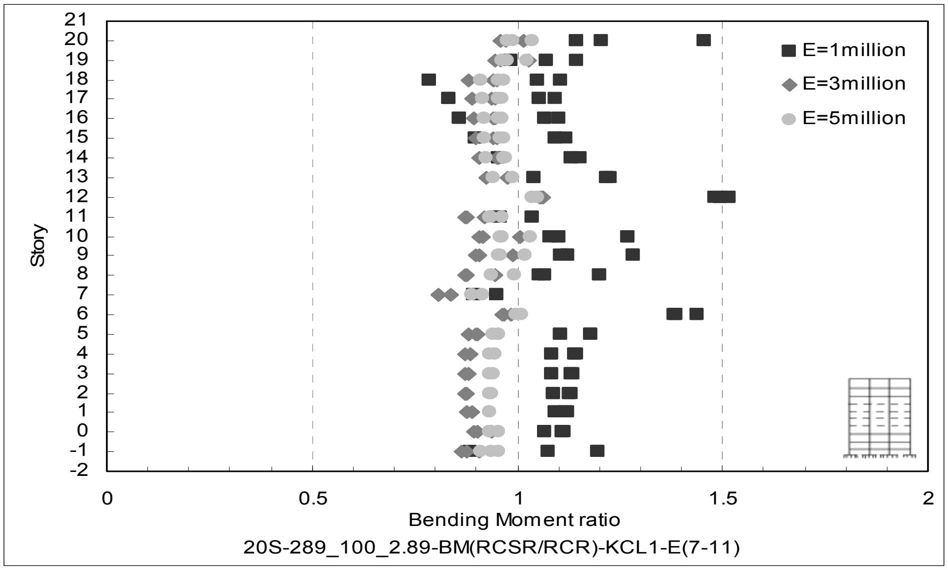

a)

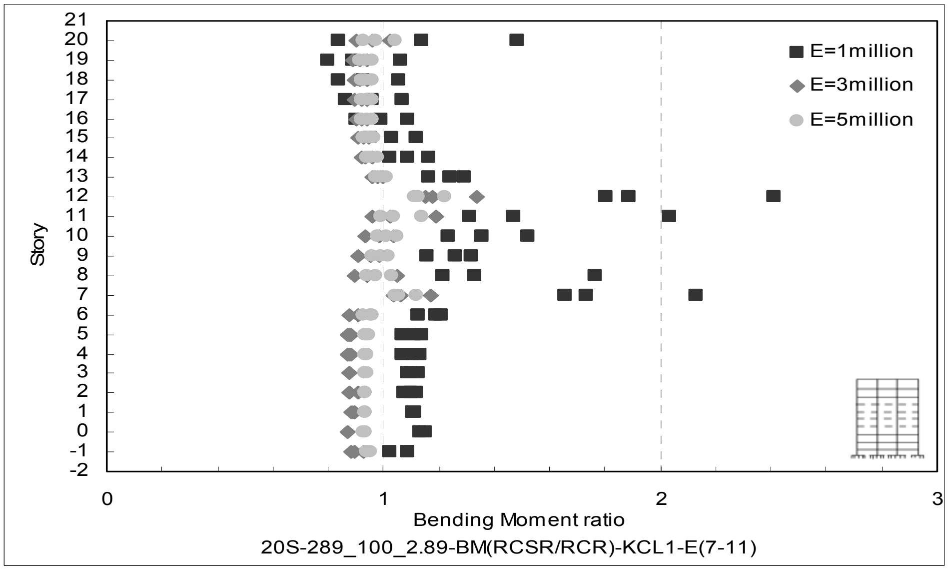

b)

Figure D.24 Bending Moment ratio for 20S-289_100_2.89-KCL1
a)Beams, b)Columns

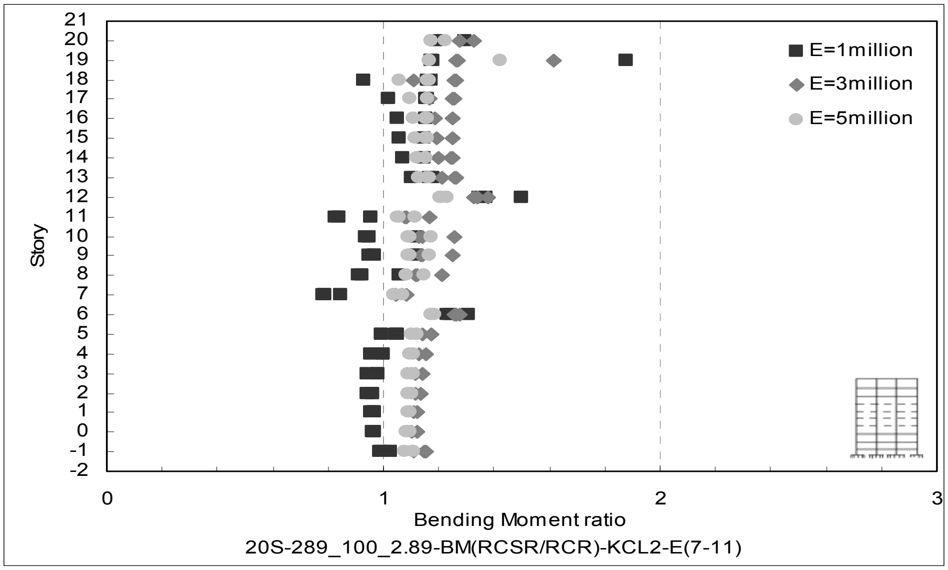

a)

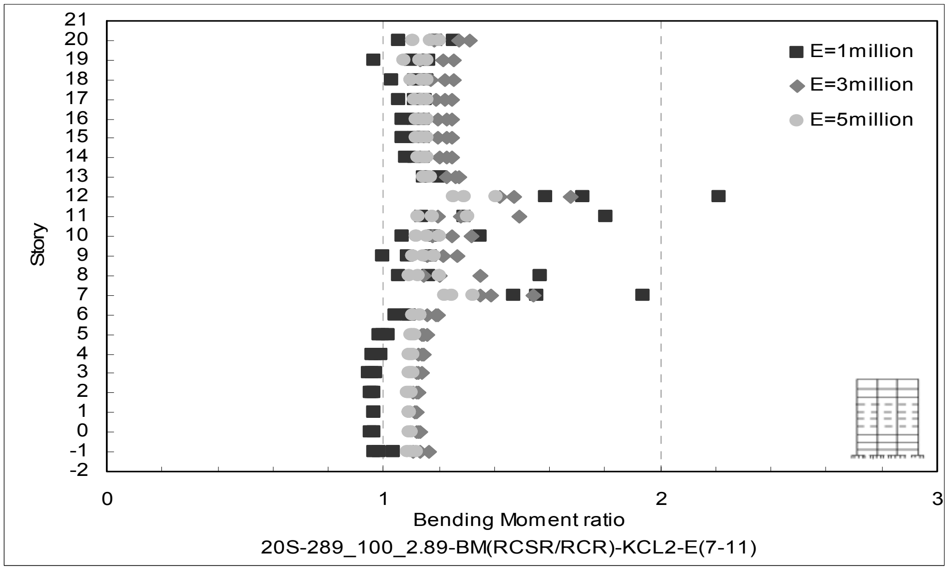

b)

Figure D.25 Bending Moment ratio for 20S-289_100_2.89-KCL2
a)Beams, b)Columns

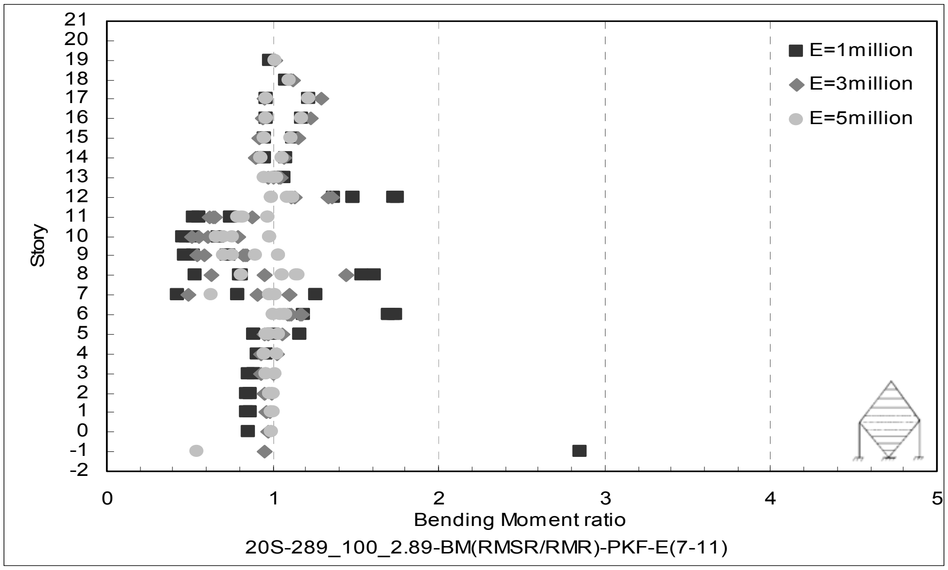

a)

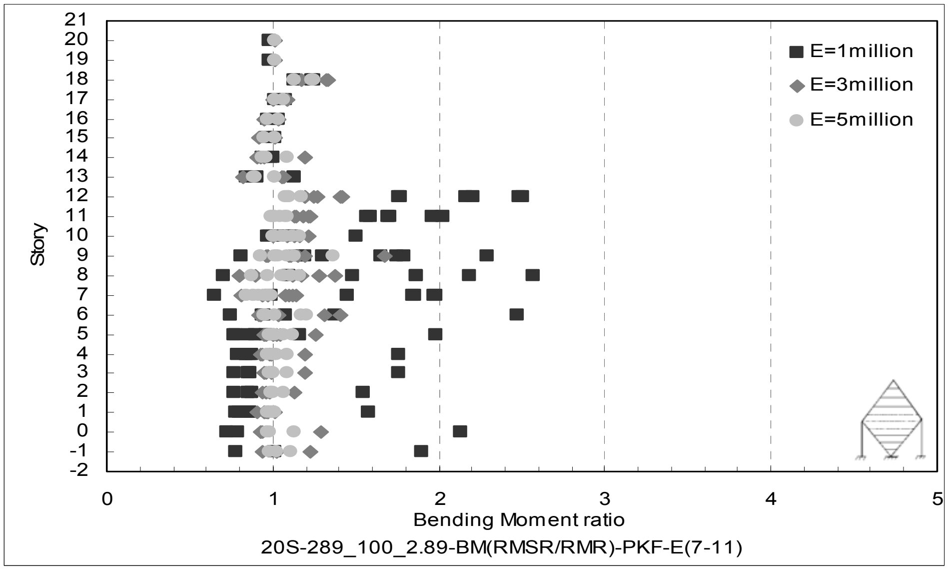

b)

Figure D.26 Bending Moment ratio for 20S-289_100_2.89-PKF
a)Beams, b)Columns

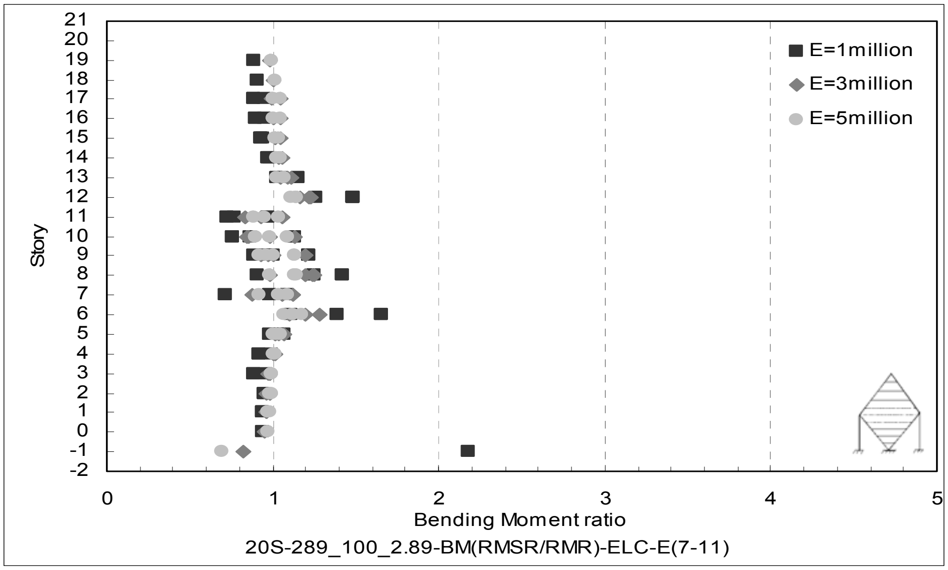

a)

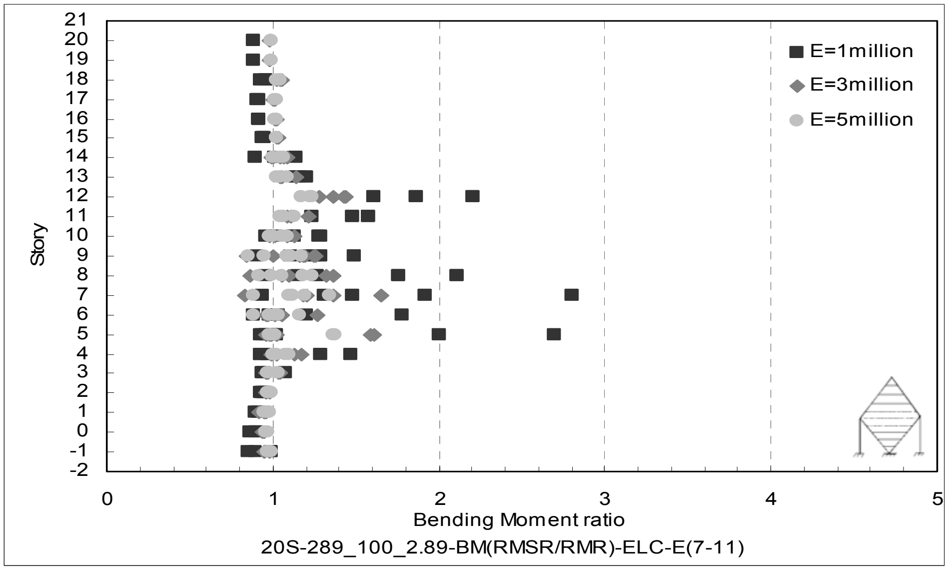

b)

Figure D.27 Bending Moment ratio for 20S-289_100_2.89-ELC
a)Beams, b)Columns

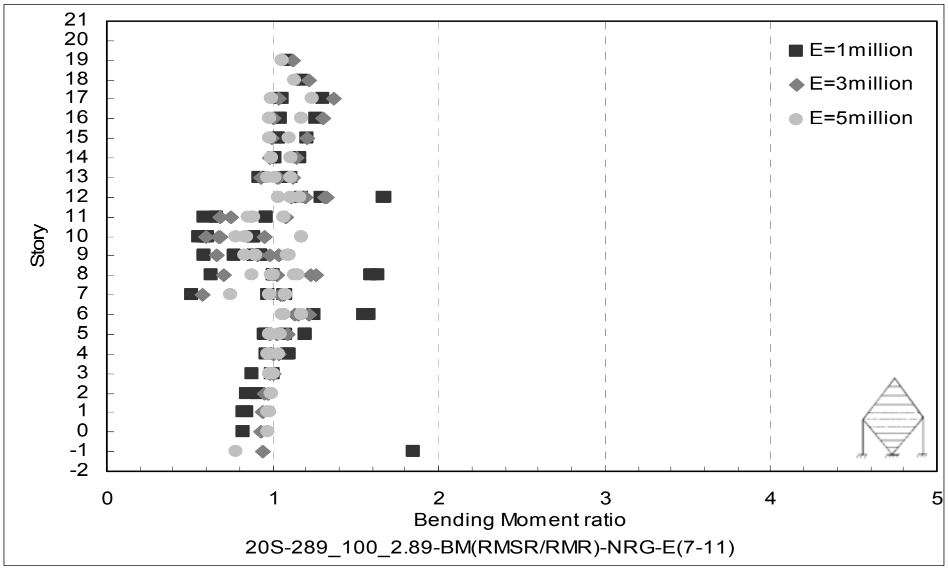

a)

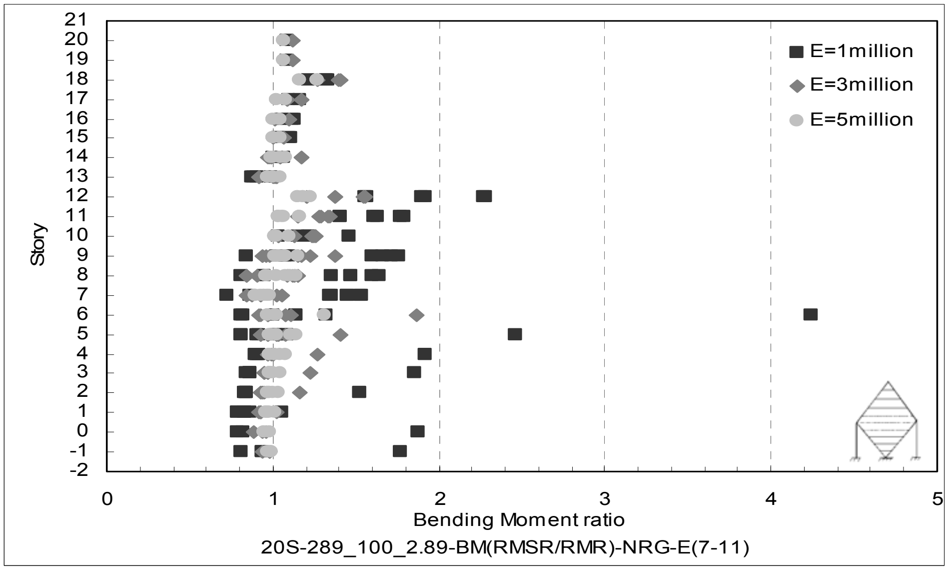

b)

Figure D.28 Bending Moment ratio for 20S-289_100_2.89-NRG
a)Beams, b)Columns

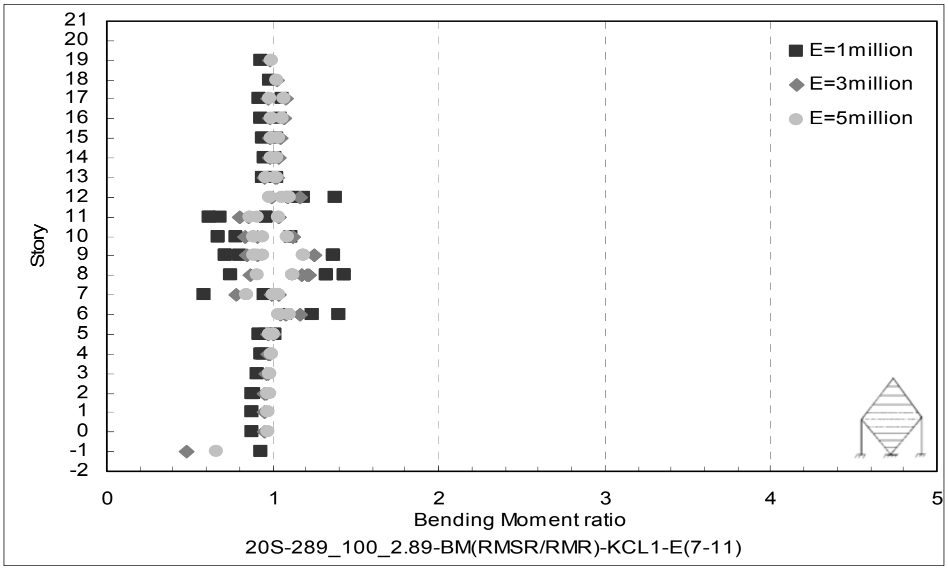

a)

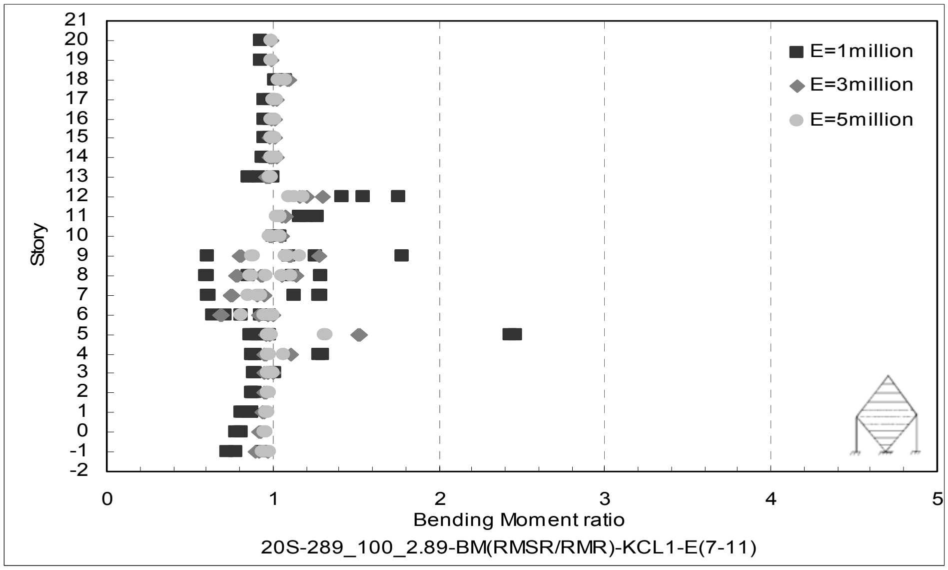

b)

Figure D.29 Bending Moment ratio for 20S-289_100_2.89-KCL1
a)Beams, b)Columns

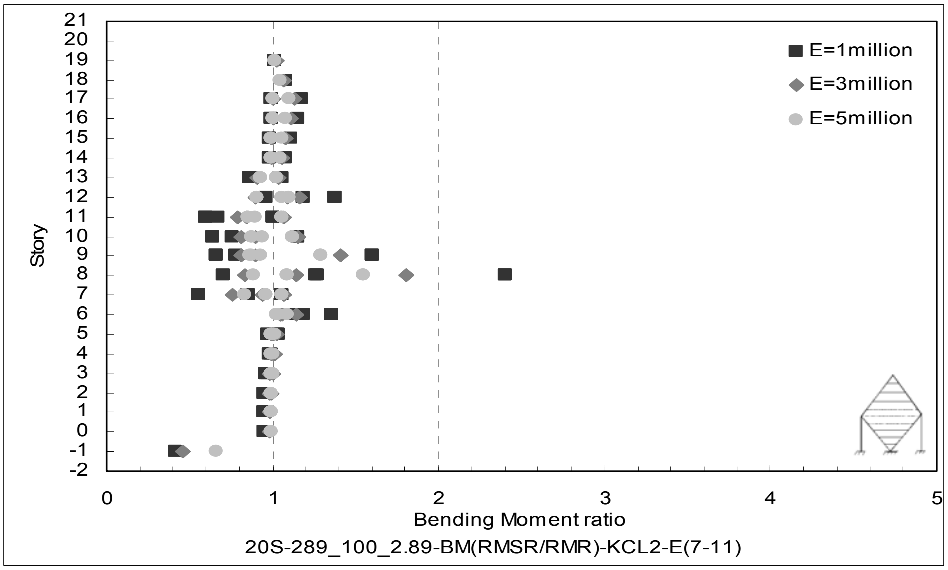

a)

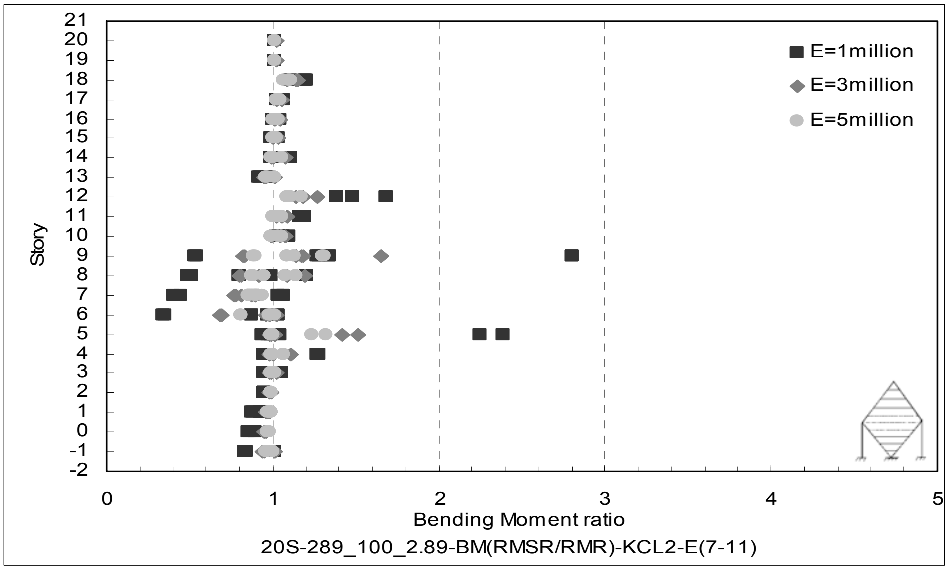

b)

Figure D.30 Bending Moment ratio for 20S-289_100_2.89-KCL2
a)Beams, b)Columns

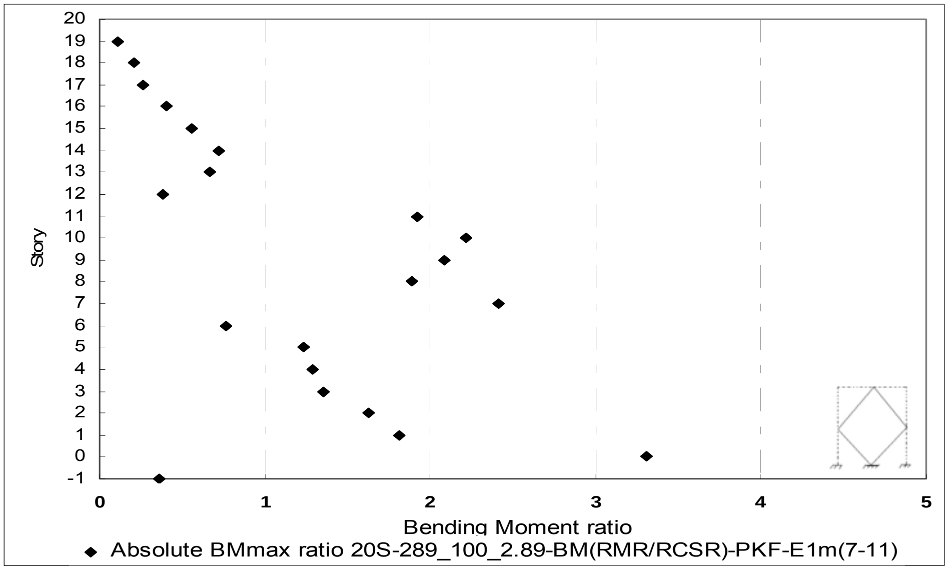

a)

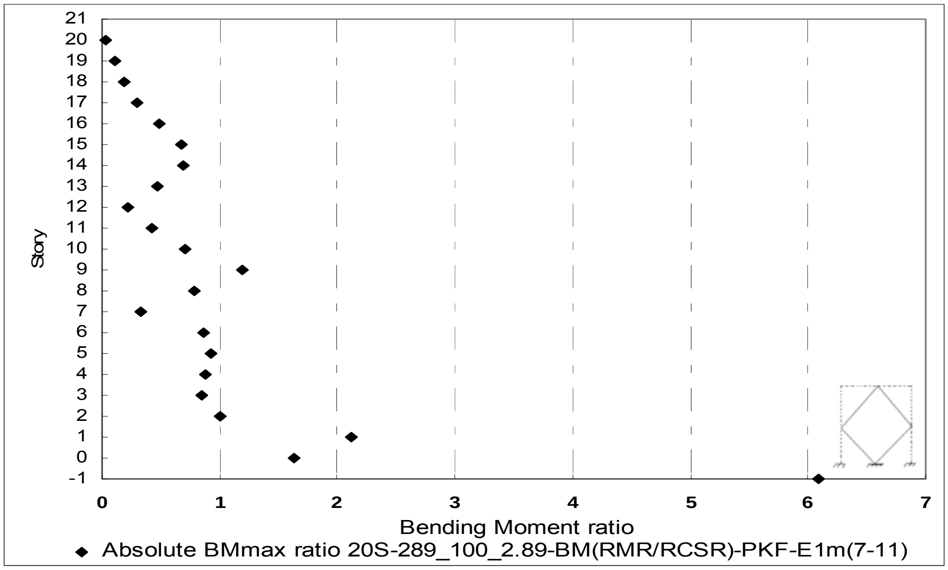

b)

Figure D.31 Bending Moment ratio for 20S-289_100_2.89-PKF
a)Beams, b)Columns

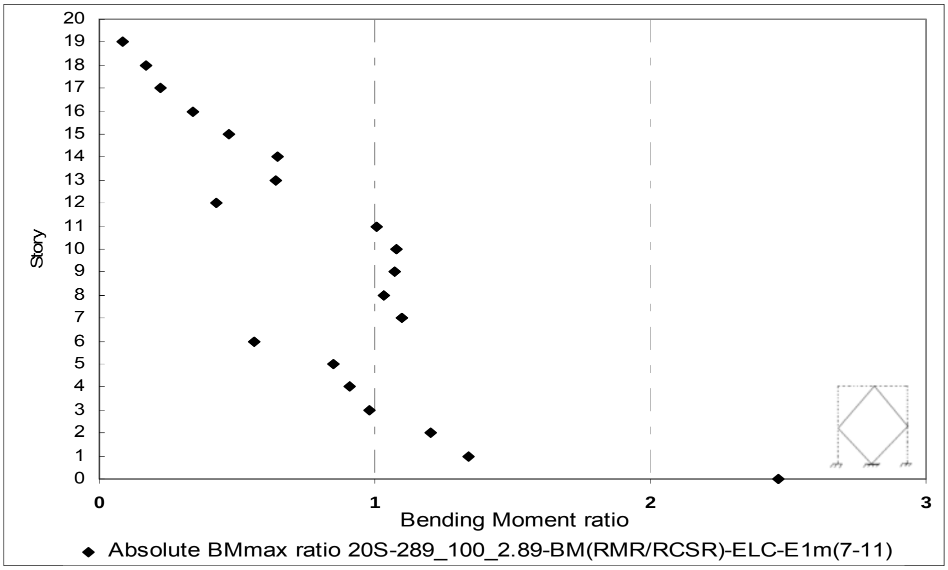

a)

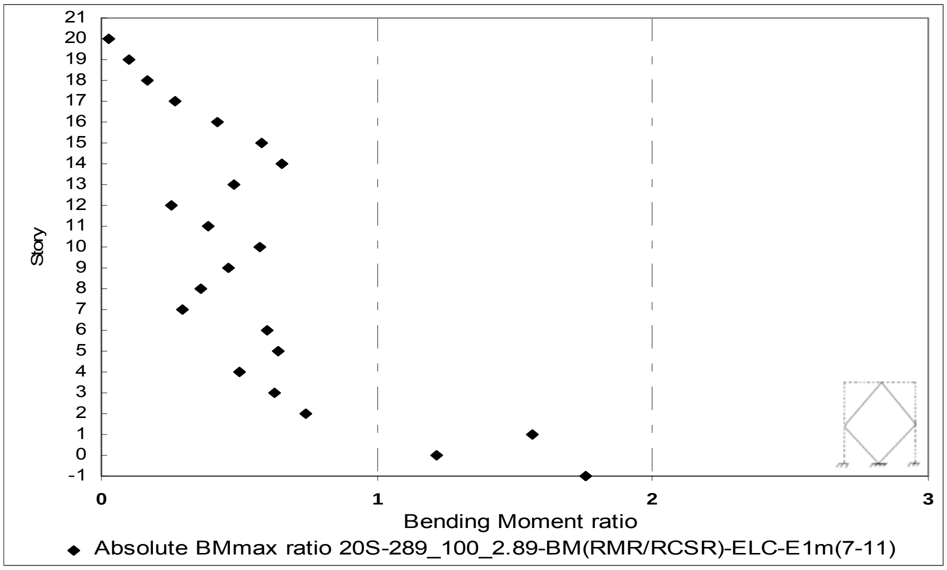

b)

Figure D.32 Bending Moment ratio for 20S-289_100_2.89-ELC
a)Beams, b)Columns

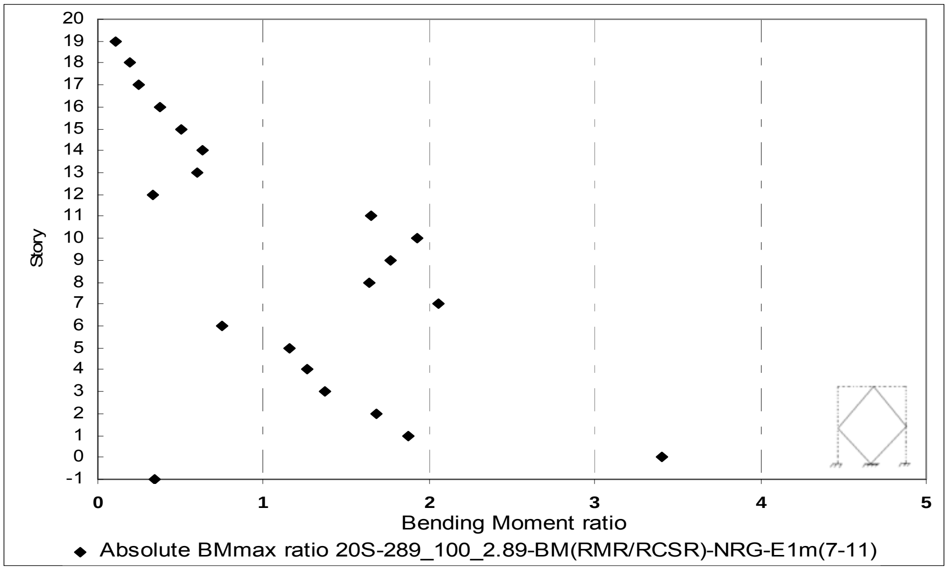

a)

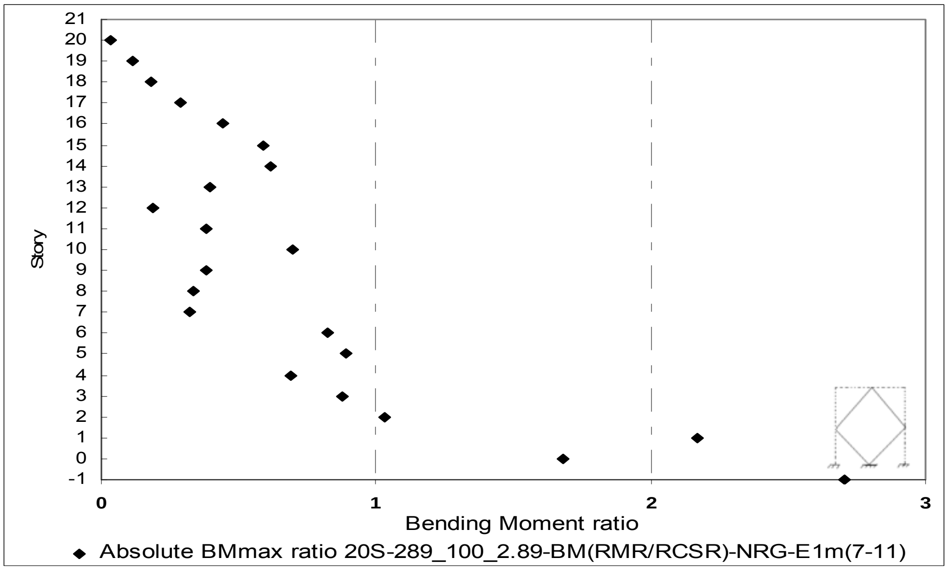

b)

Figure D.33 Bending Moment ratio for 20S-289_100_2.89-NRG
a)Beams, b)Columns

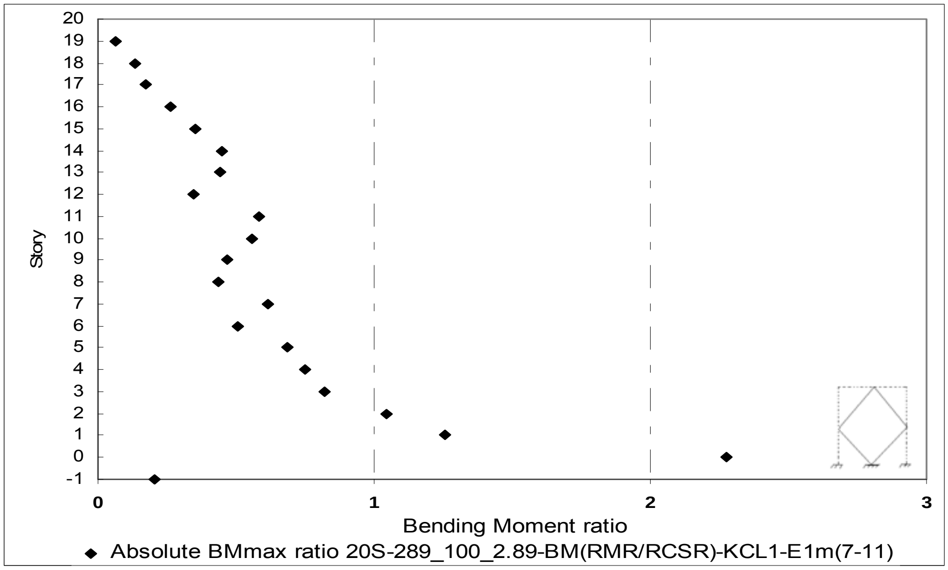

a)

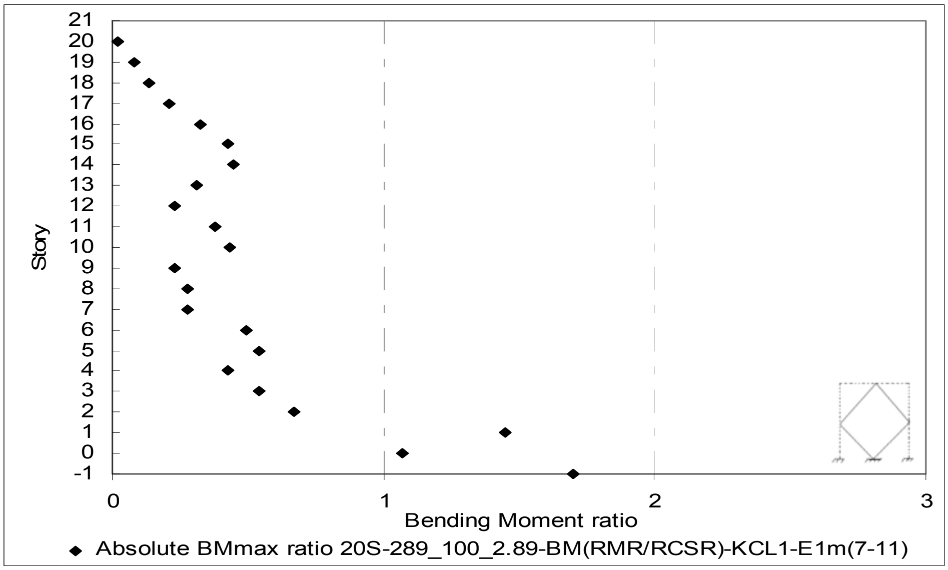

b)

Figure D.34 Bending Moment ratio for 20S-289_100_2.89-KCL1
a)Beams, b)Columns

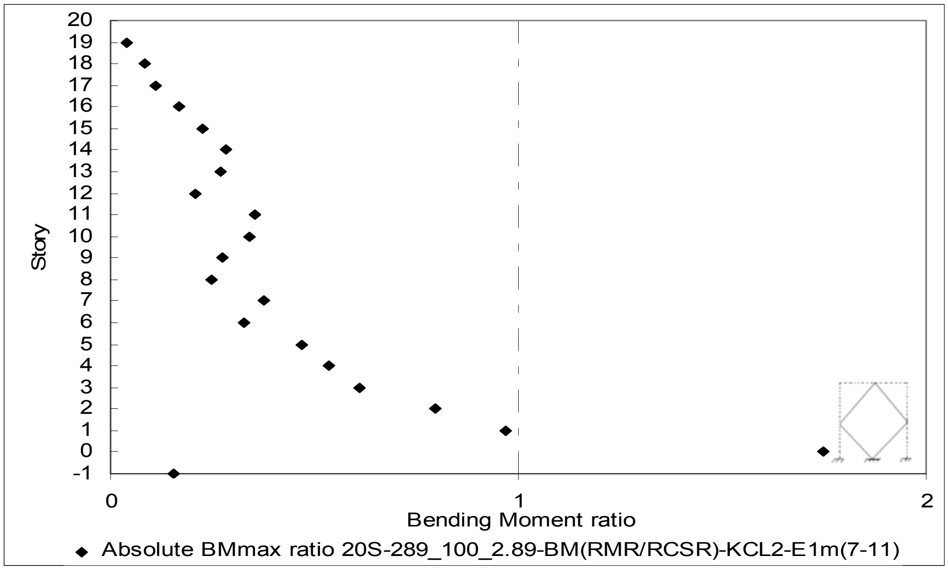

a)

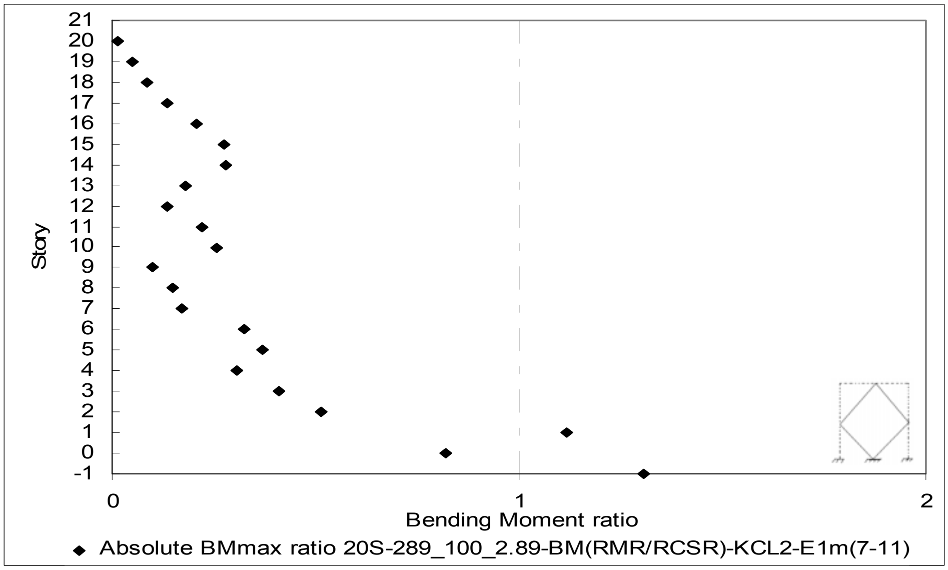

b)

Figure D.35 Bending Moment ratio for 20S-289_100_2.89-KCL2
a)Beams, b)Columns

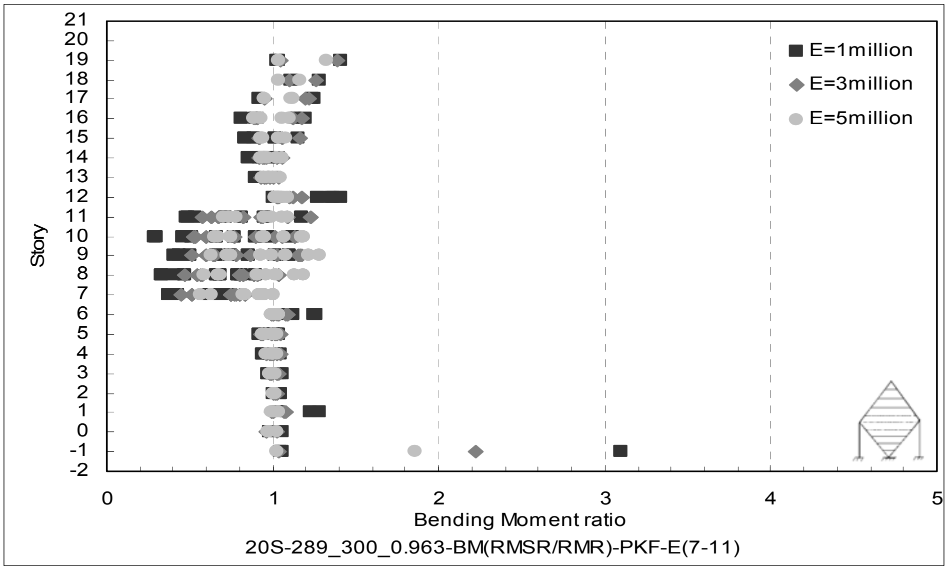

a)

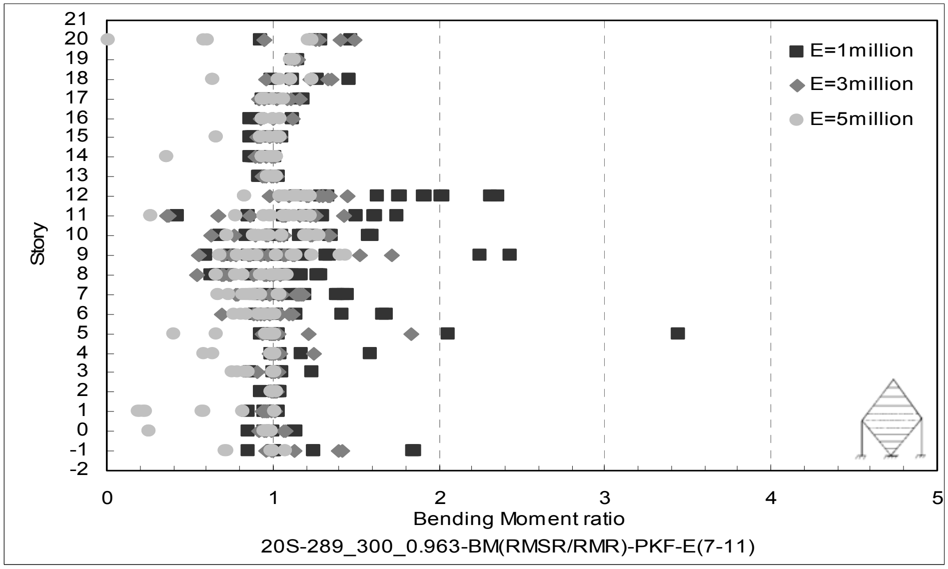

b)

Figure D.36 Bending Moment ratio for 20S-289_300_0.963-PKF
a)Beams, b)Columns

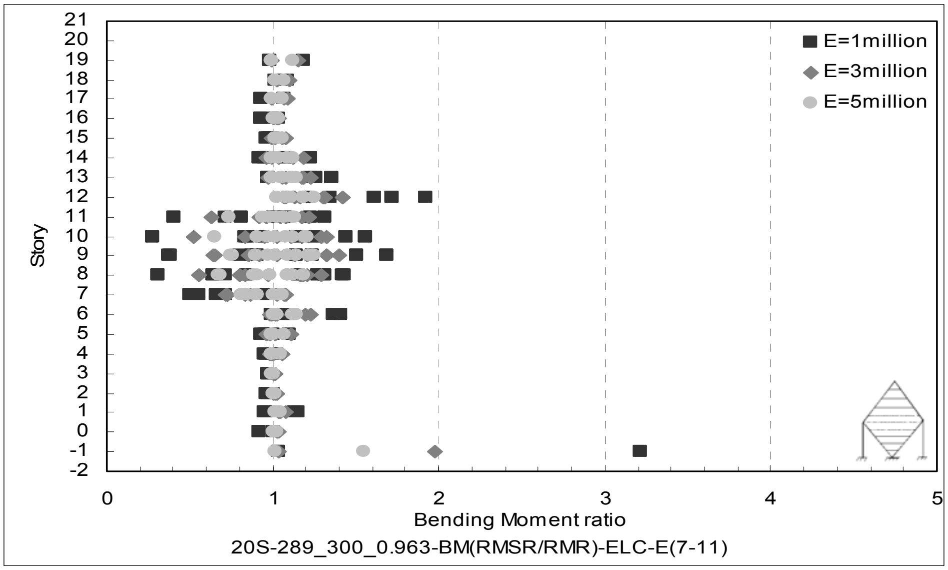

a)

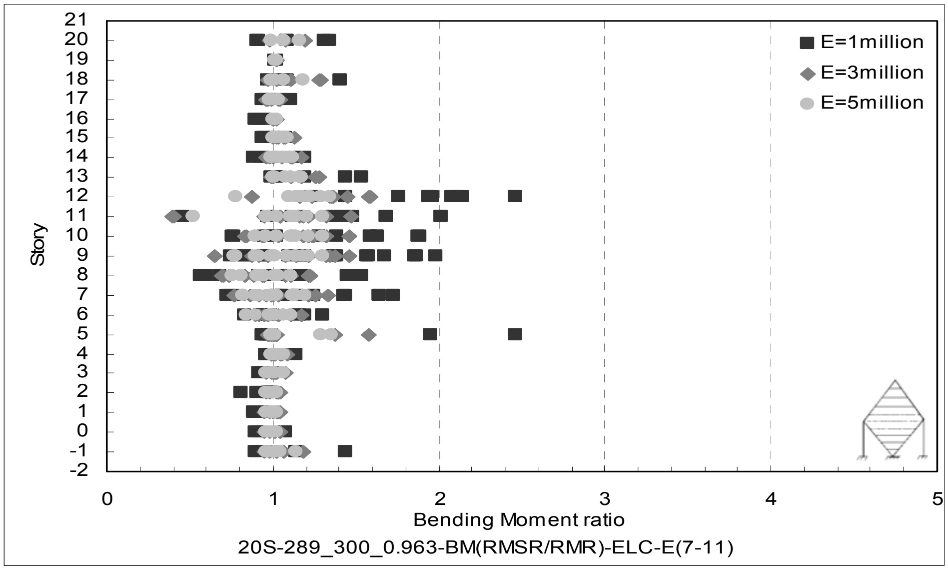

b)

Figure D.37 Bending Moment ratio for 20S-289_300_0.963-ELC
a)Beams, b)Columns

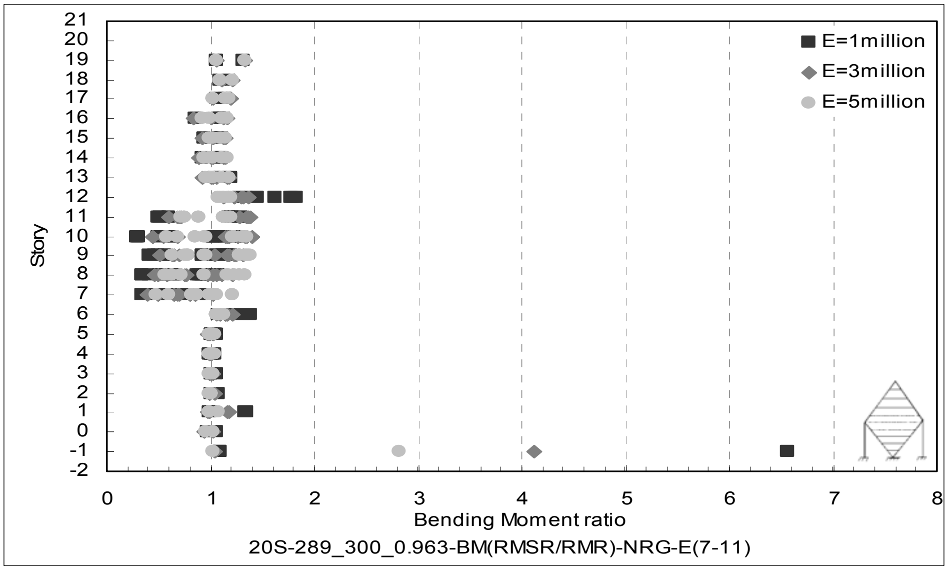

a)

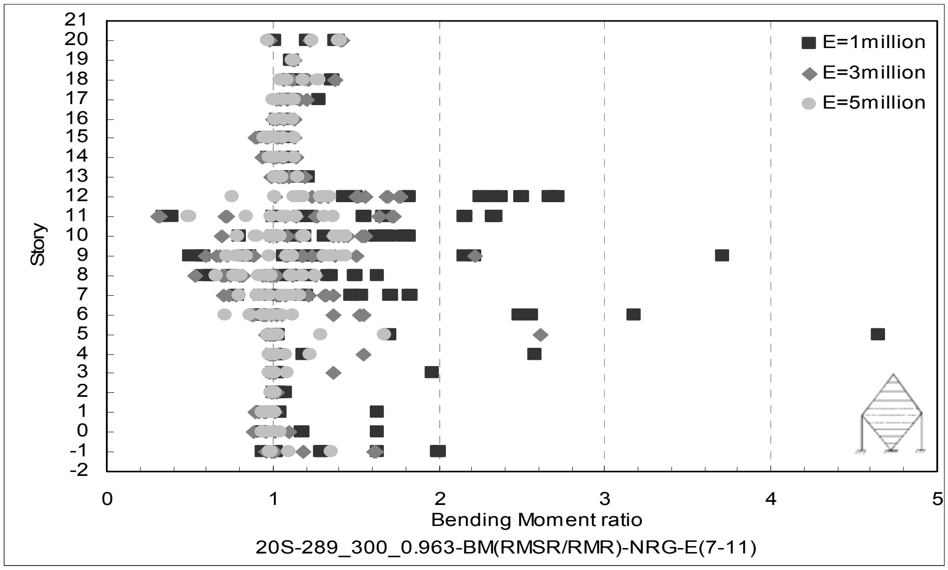

b)

Figure D.38 Bending Moment ratio for 20S-289_300_0.963-NRG
a)Beams, b)Columns

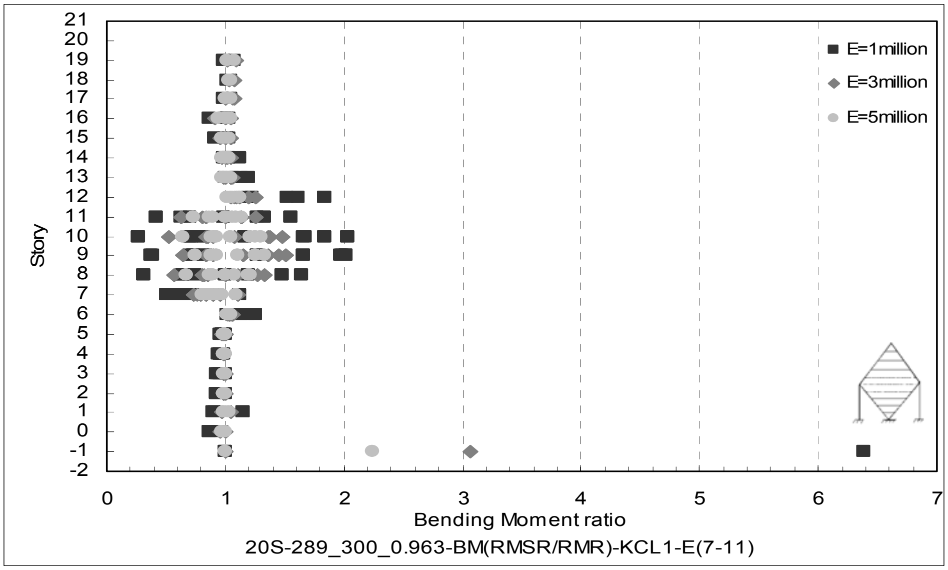

a)

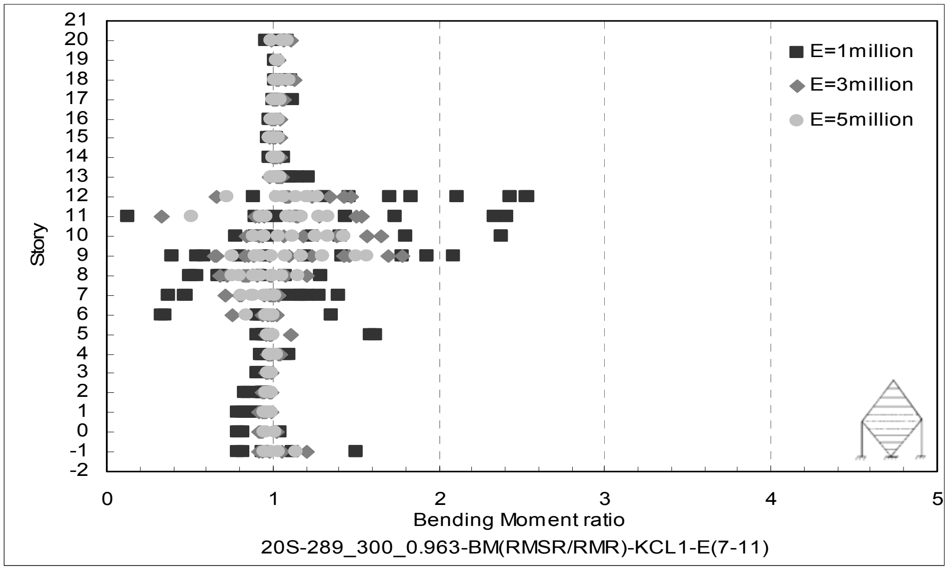

b)

Figure D.39 Bending Moment ratio for 20S-289_300_0.963-KCL1
a)Beams, b)Columns

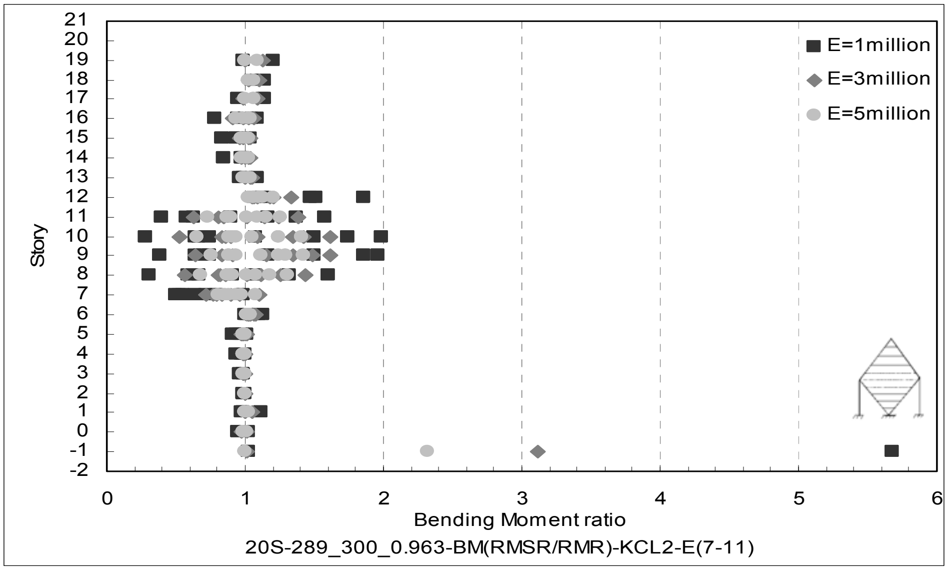

a)

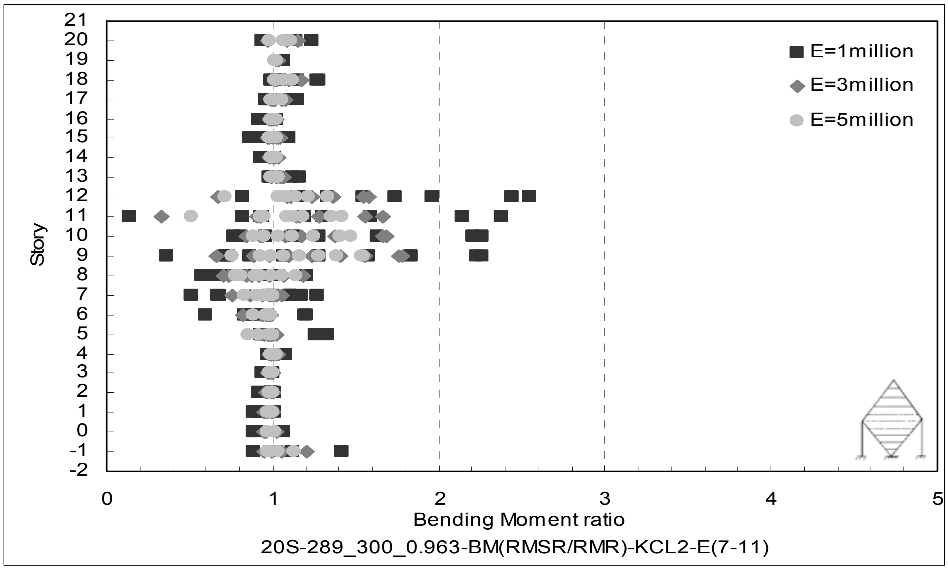

b)

Figure D.40 Bending Moment ratio for 20S-289_300_0.963-KCL2
a)Beams, b)Columns

APPENDIX E

MAXIMUM LATERAL DISPLACEMENT PROFILE

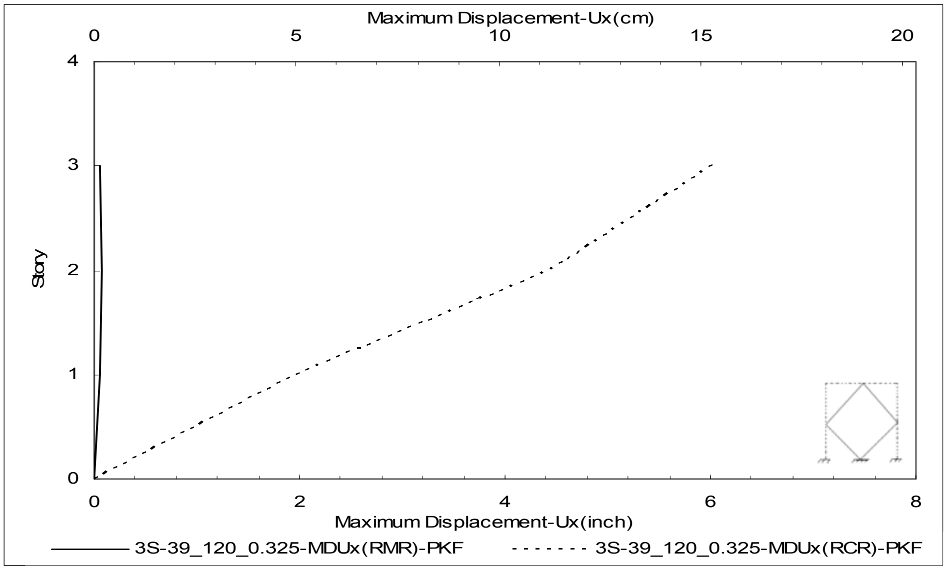

Figure E.1 Maximum lateral displacement for 3S-39_120_0.325-PKF

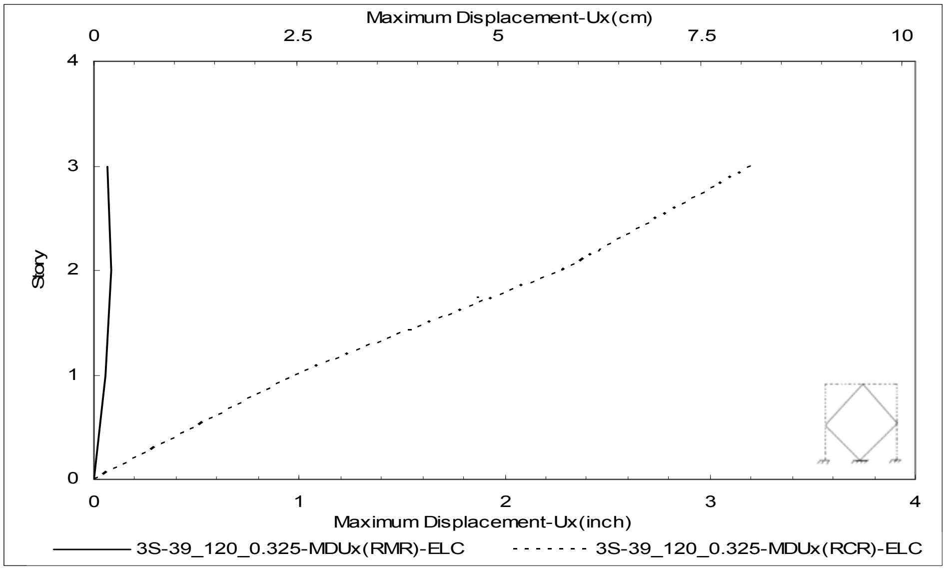

Figure E.2 Maximum lateral displacement for 3S-39_120_0.325-ELC

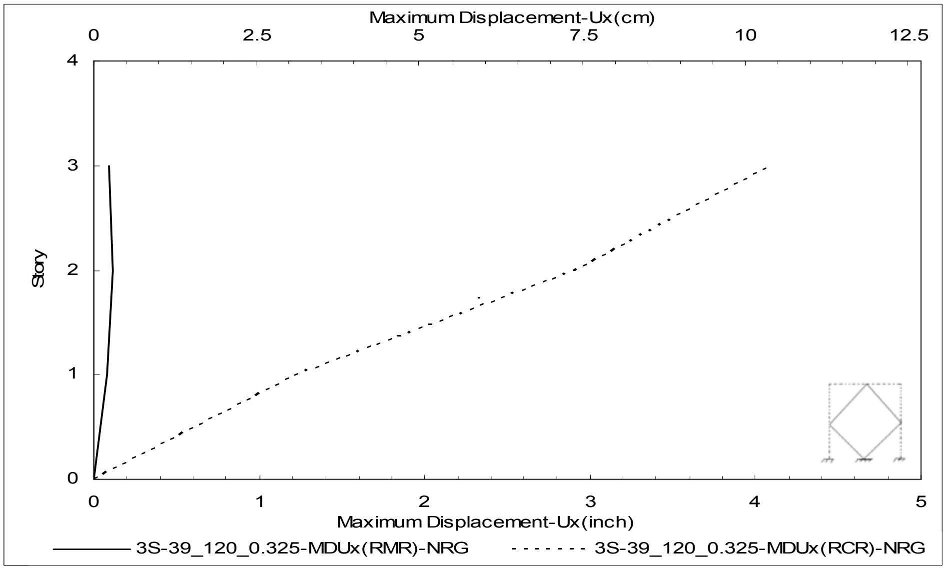

Figure E.3 Maximum lateral displacement for 3S-39_120_0.325-NRG

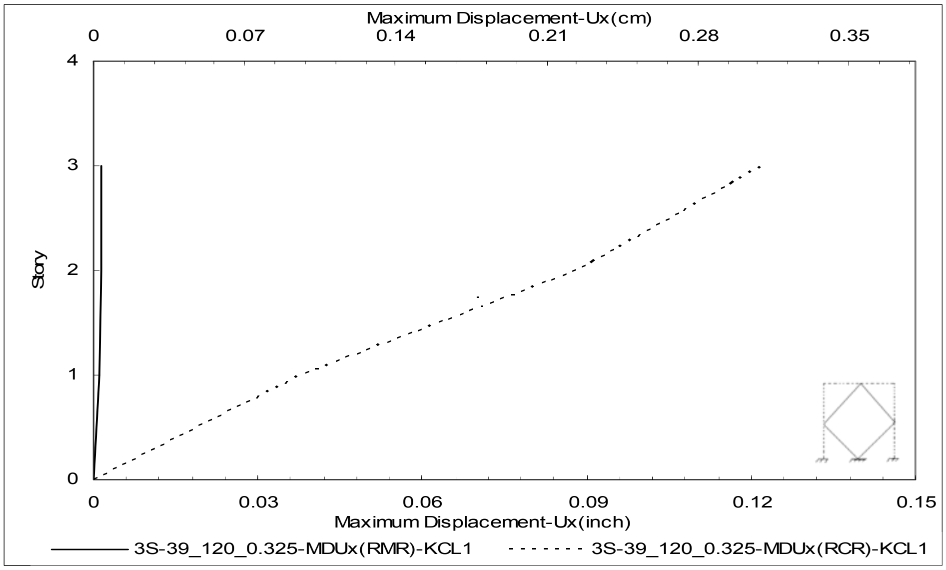

Figure E.4 Maximum lateral displacement for 3S-39_120_0.325-KCL1

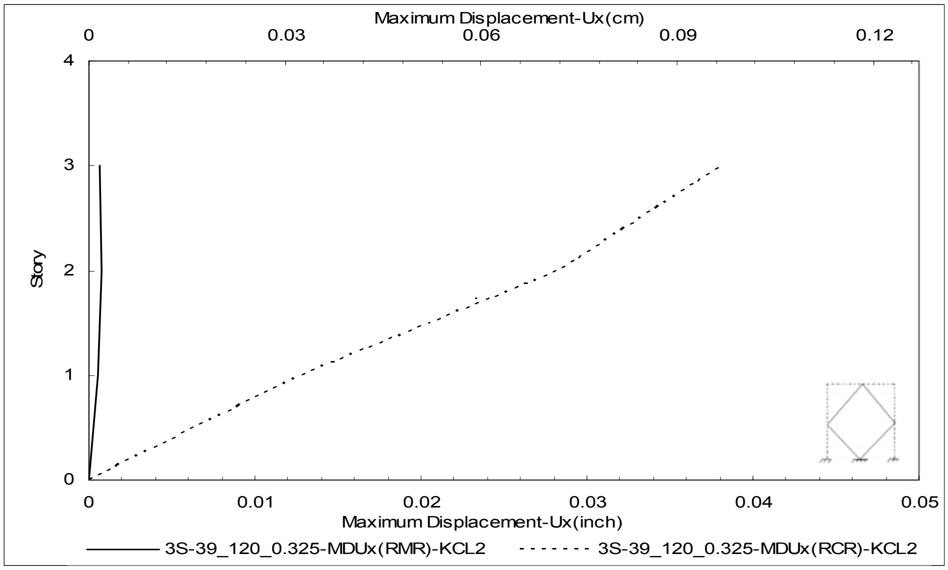

Figure E.5 Maximum lateral displacement for 3S-39_120_0.325-KCL2

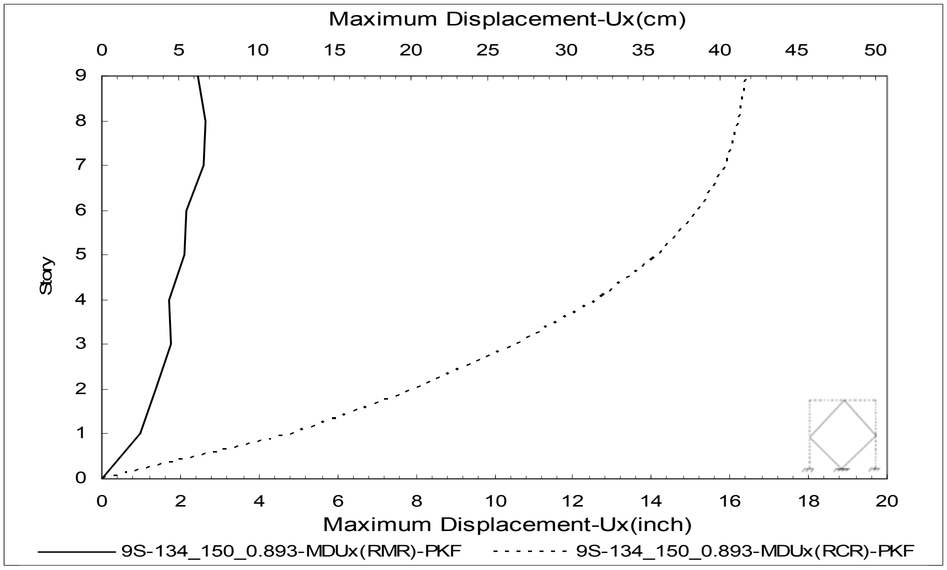

Figure E.6 Maximum lateral displacement for 9S-134_150_0.893-PKF

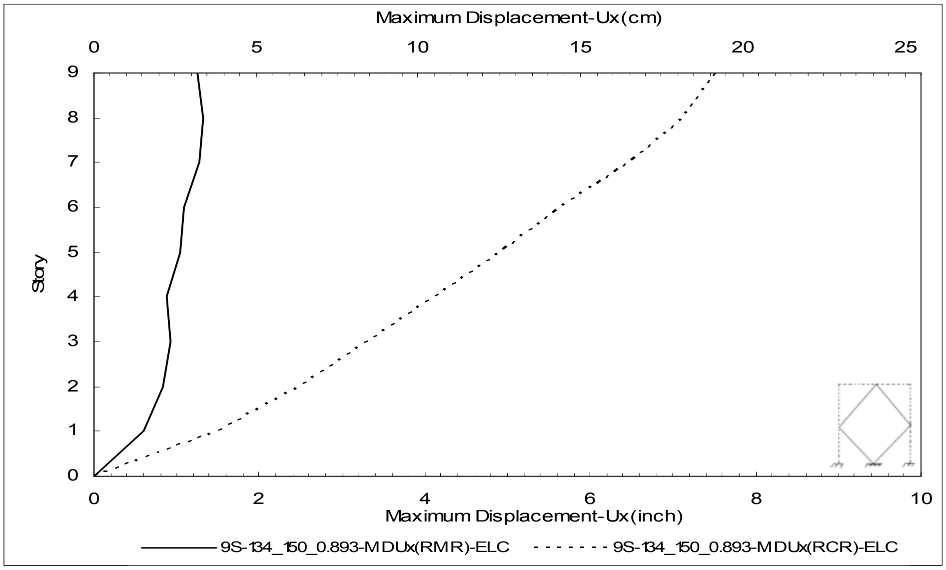

Figure E.7 Maximum lateral displacement for 9S-134_150_0.893-ELC

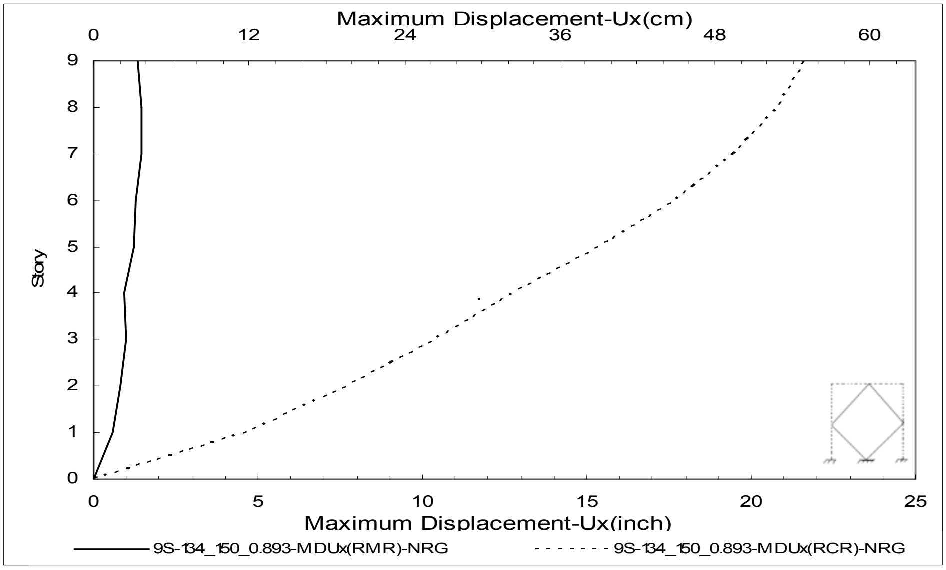

Figure E.8 Maximum lateral displacement for 9S-134_150_0.893-NRG

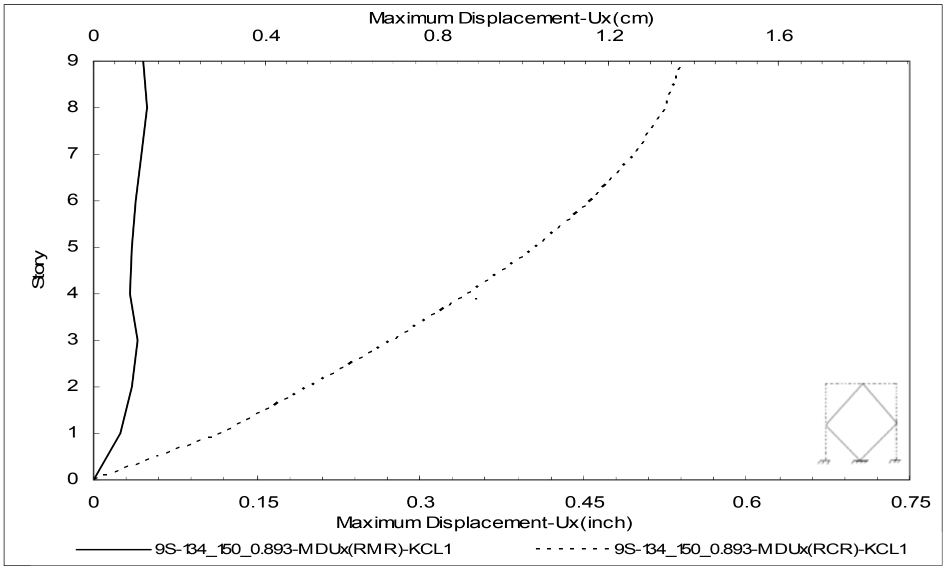

Figure E.9 Maximum lateral displacement for 9S-134_150_0.893-KCL1

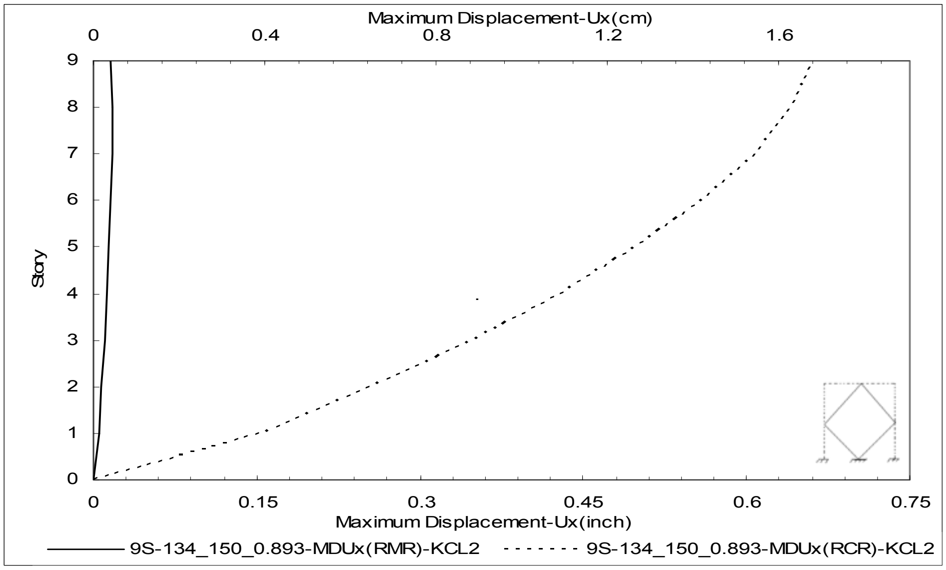

Figure E.10 Maximum lateral displacement for 9S-134_150_0.893-KCL2

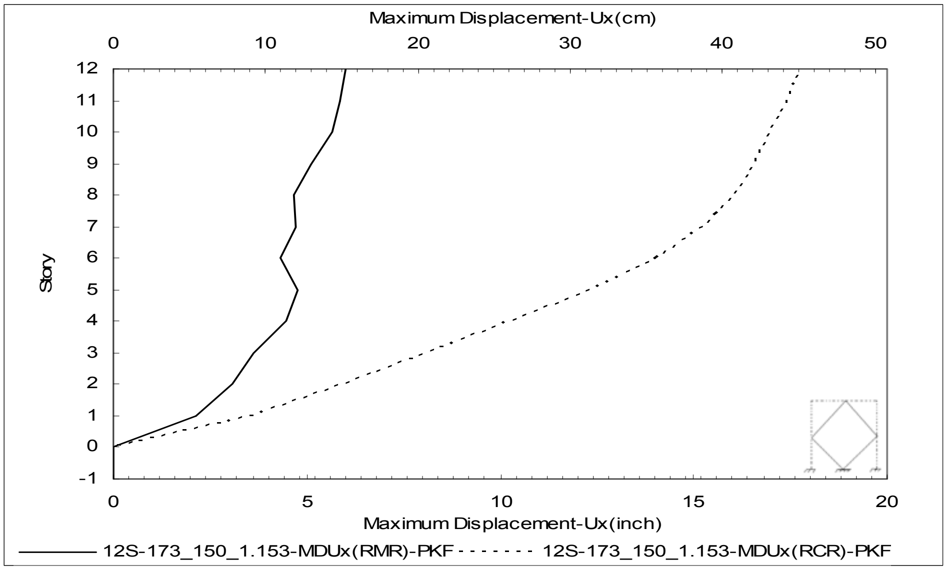

Figure E.11 Maximum lateral displacement for 12S-173_150_1.153-PKF

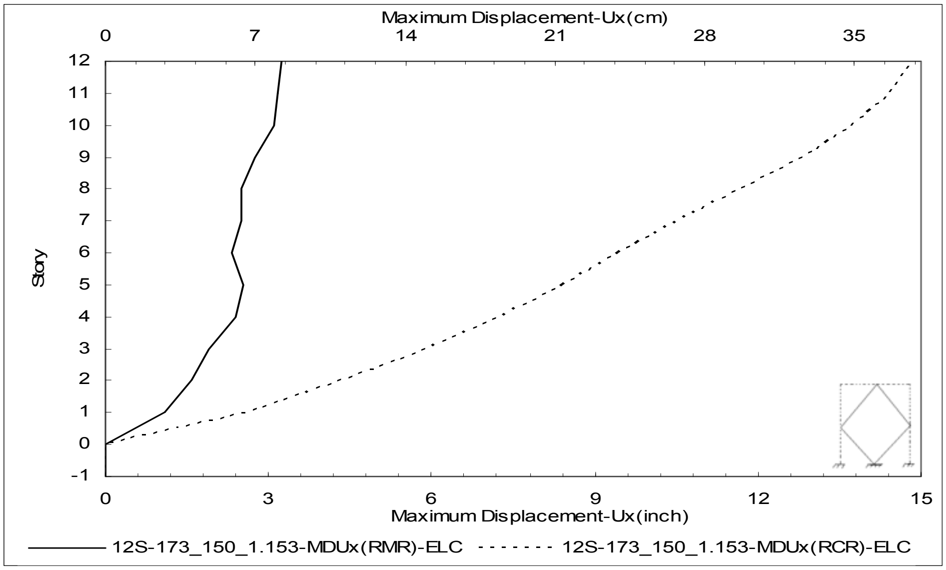

Figure E.12 Maximum lateral displacement for 12S-173_150_1.153-ELC

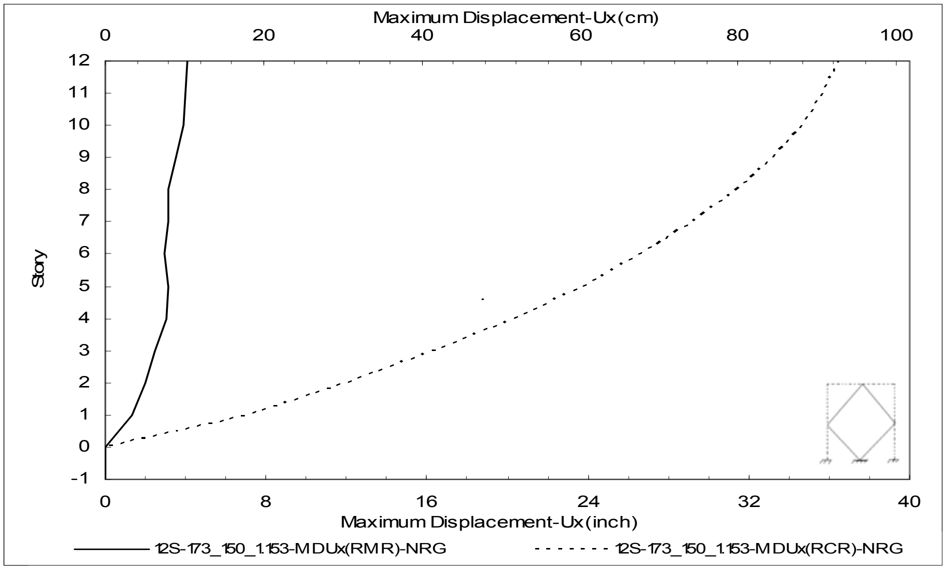

Figure E.13 Maximum lateral displacement for 12S-173_150_1.153-NRG

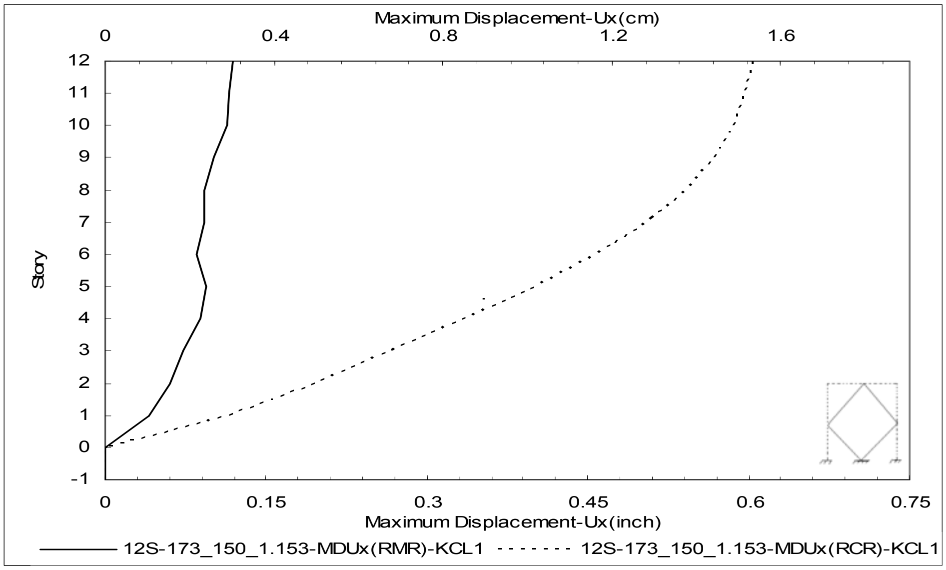

Figure E.14 Maximum lateral displacement for 12S-173_150_1.153-KCL1

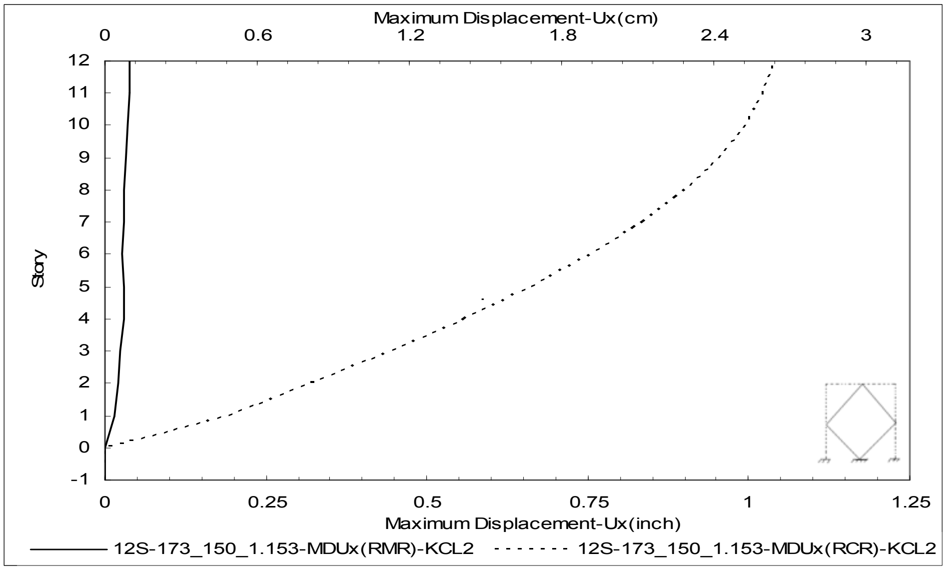

Figure E.15 Maximum lateral displacement for 12S-173_150_1.153-KCL2

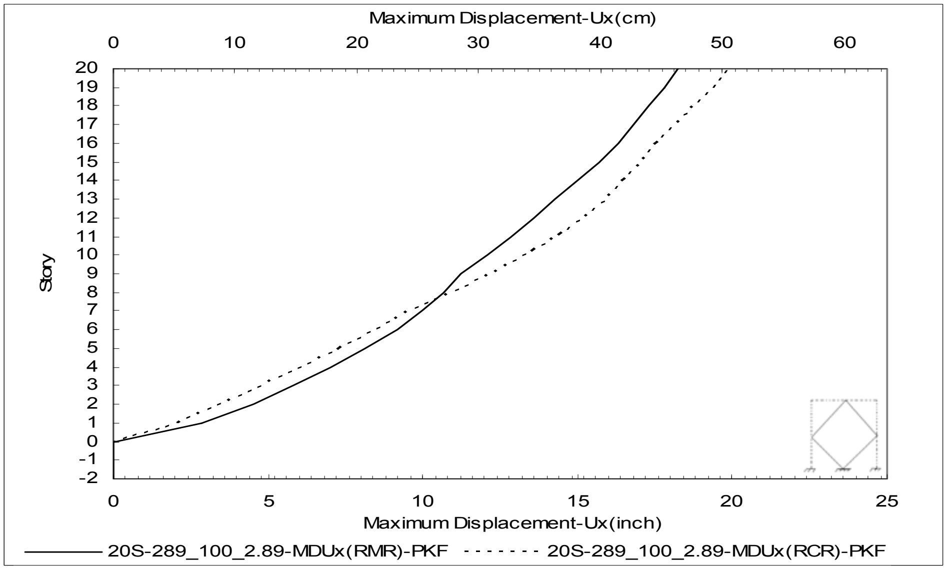

Figure E.16 Maximum lateral displacement for 20S-289_100_2.89-PKF

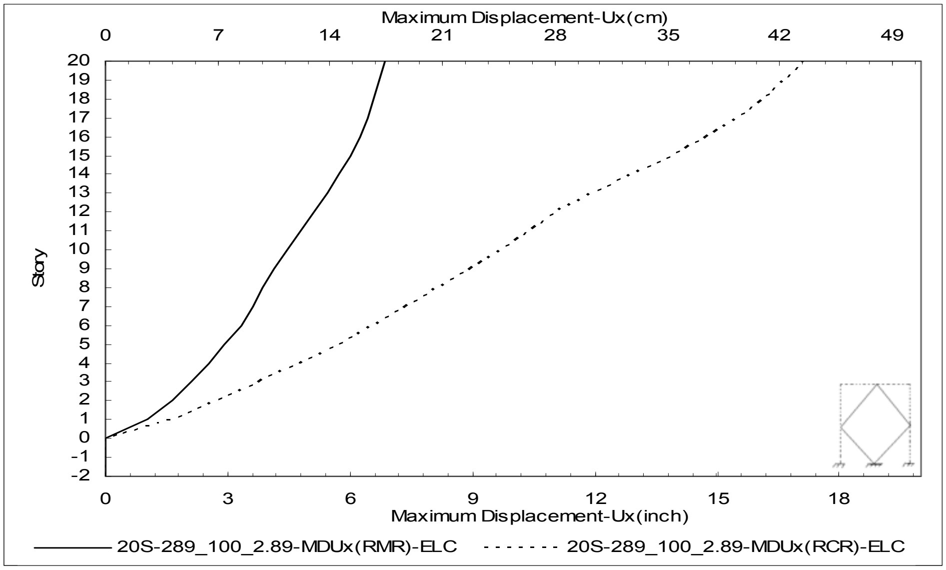

Figure E.17 Maximum lateral displacement for 20S-289_100_2.89-ELC

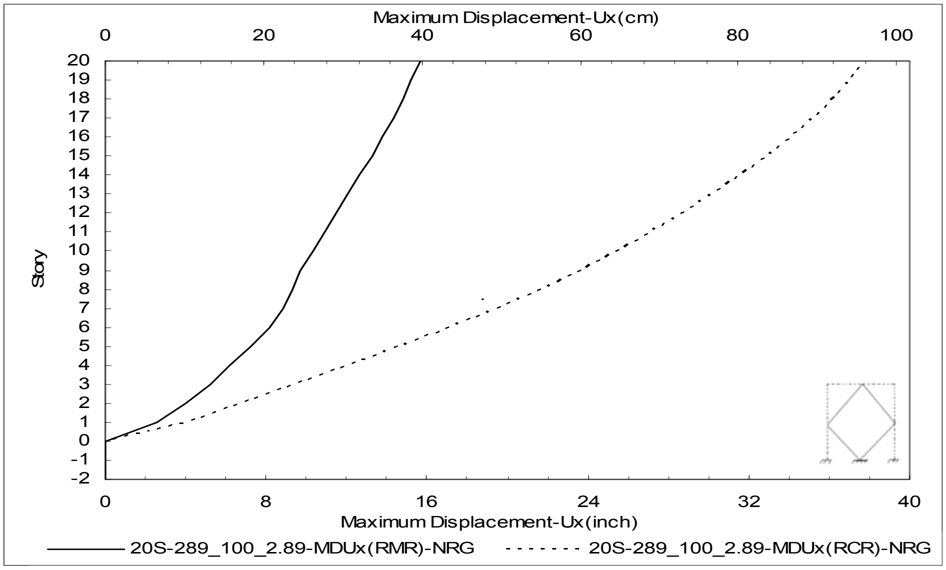

Figure E.18 Maximum lateral displacement for 20S-289_100_2.89-NRG

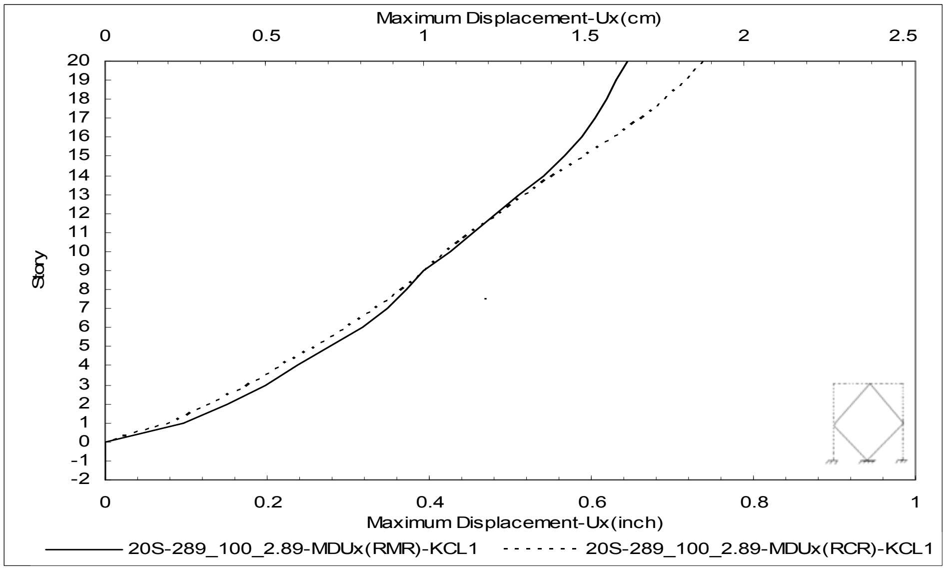

Figure E.19 Maximum lateral displacement for 20S-289_100_2.89-KCL1

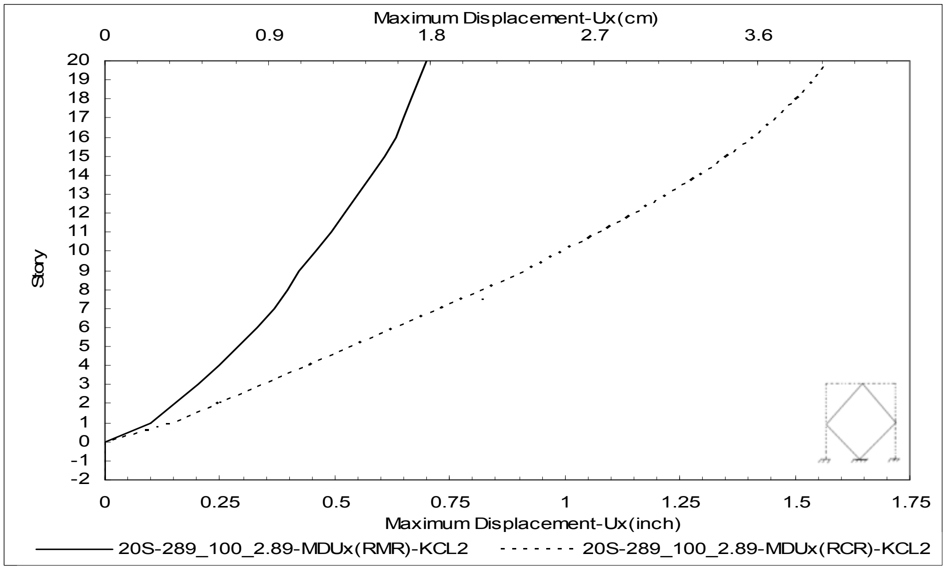

Figure E.20 Maximum lateral displacement for 20S-289_100_2.89-KCL2

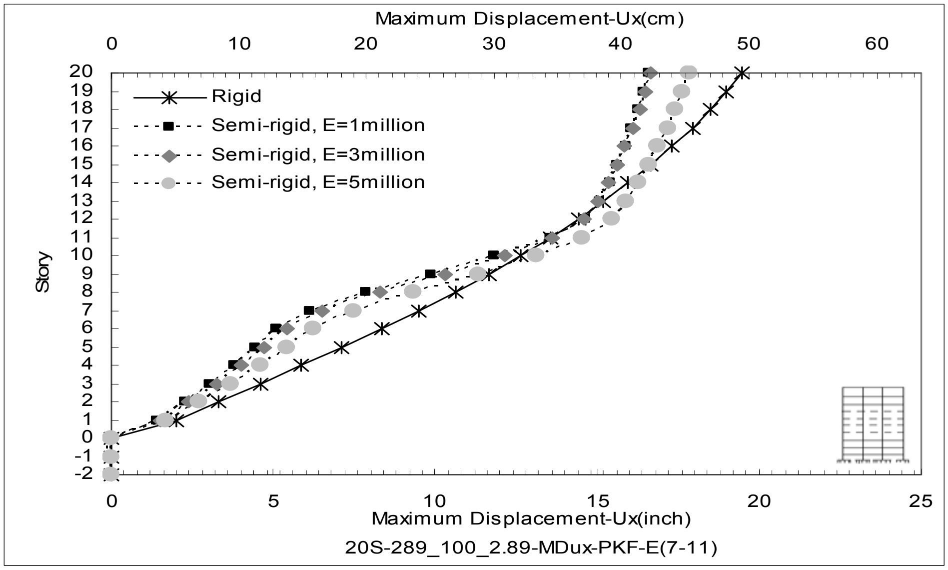

Figure E.21 Maximum lateral displacement for 20S-289_100_2.89-PKF

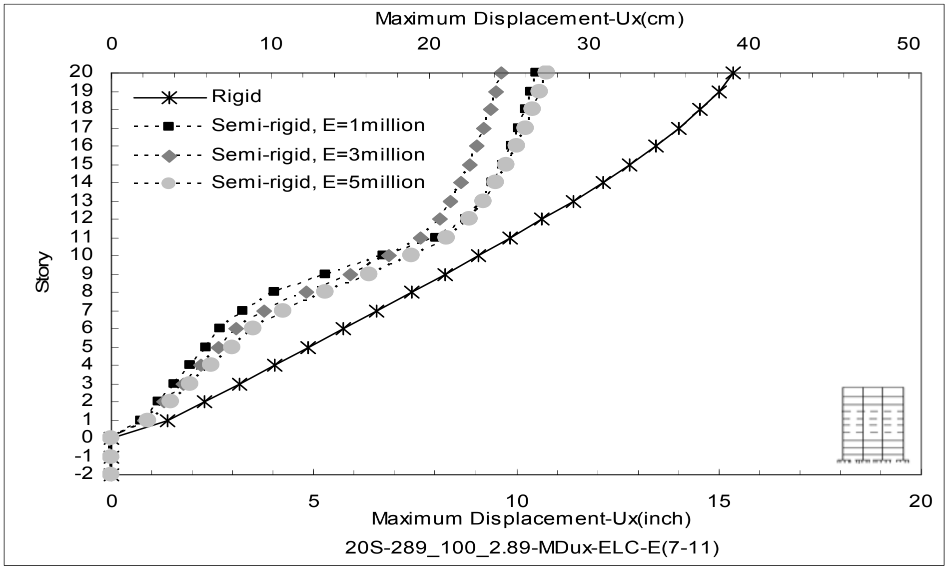

Figure E.22 Maximum lateral displacement for 20S-289_100_2.89-ELC

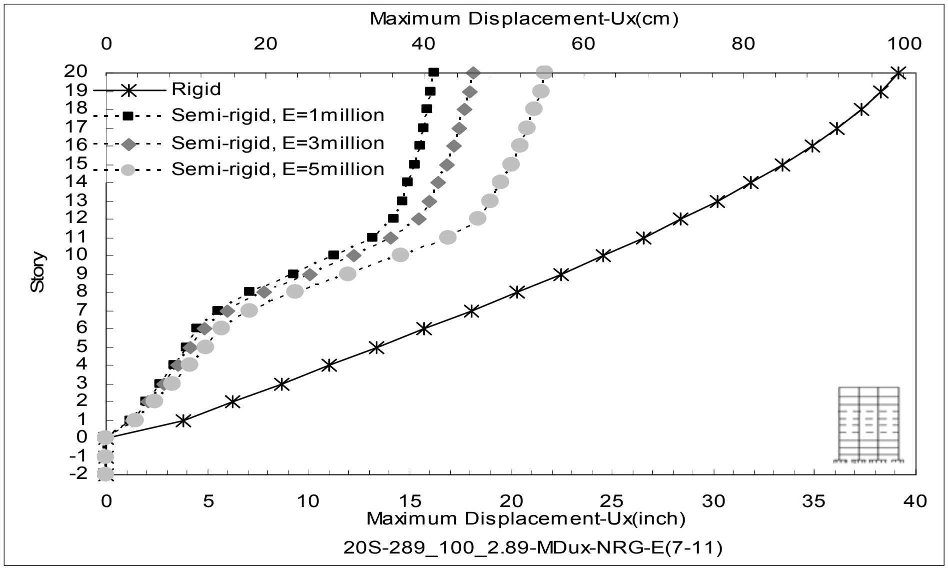

Figure E.23 Maximum lateral displacement for 20S-289_100_2.89-NRG

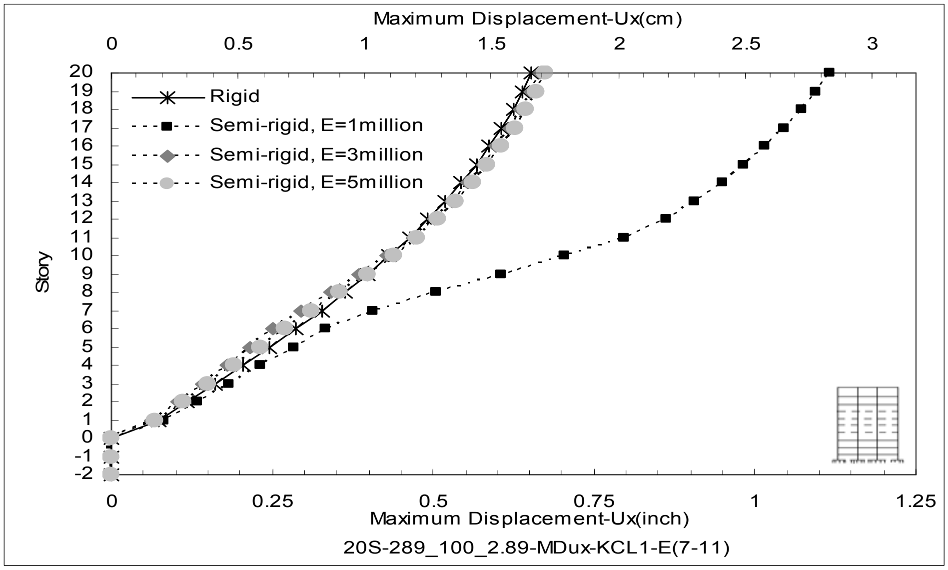

Figure E.24 Maximum lateral displacement for 20S-289_100_2.89-KCL1

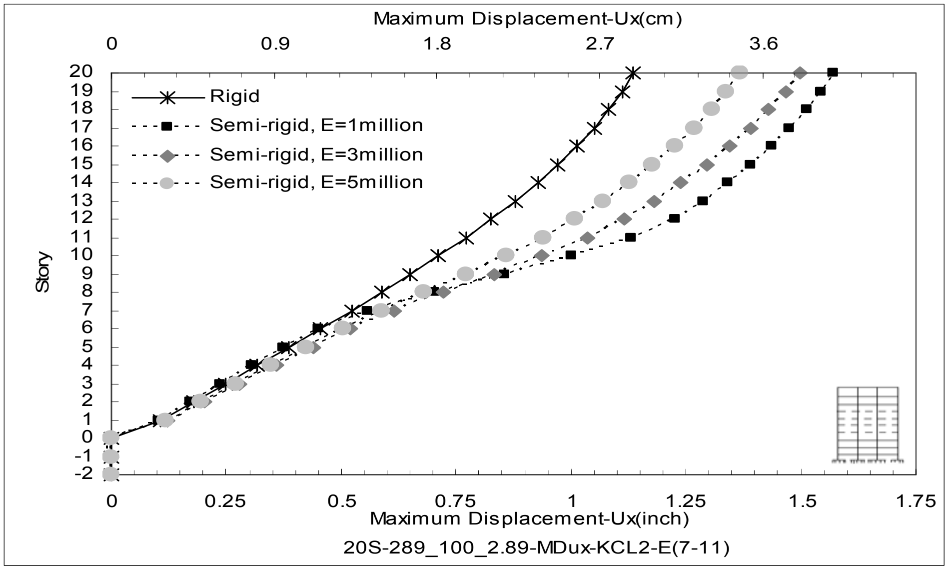

Figure E.25 Maximum lateral displacement for 20S-289_100_2.89-KCL2

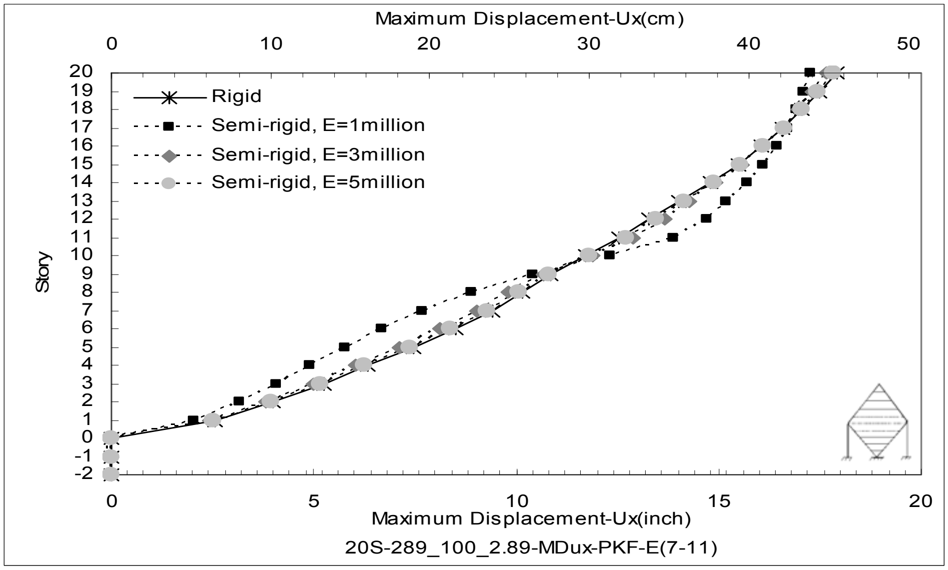

Figure E.26 Maximum lateral displacement for 20S-289_100_2.89-PKF

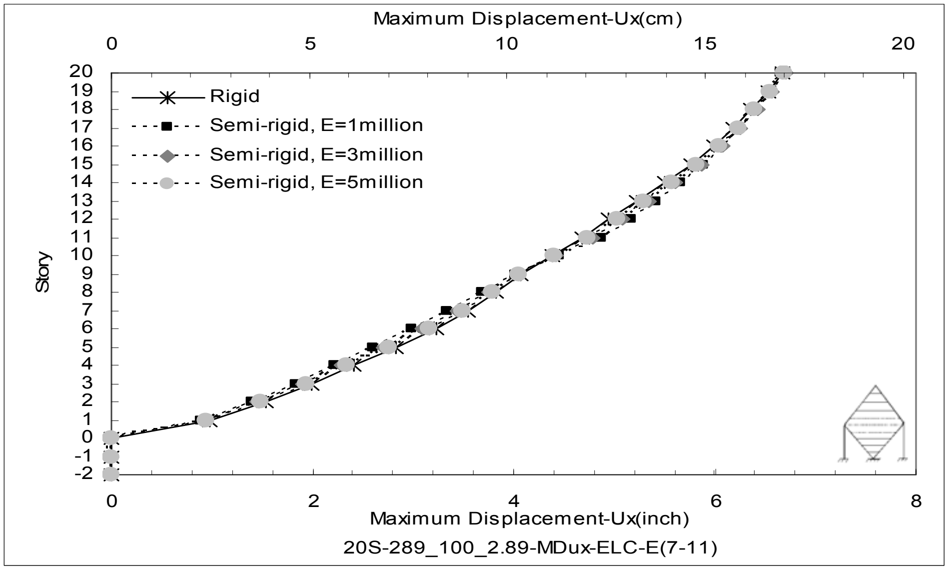

Figure E.27 Maximum lateral displacement for 20S-289_100_2.89-ELC

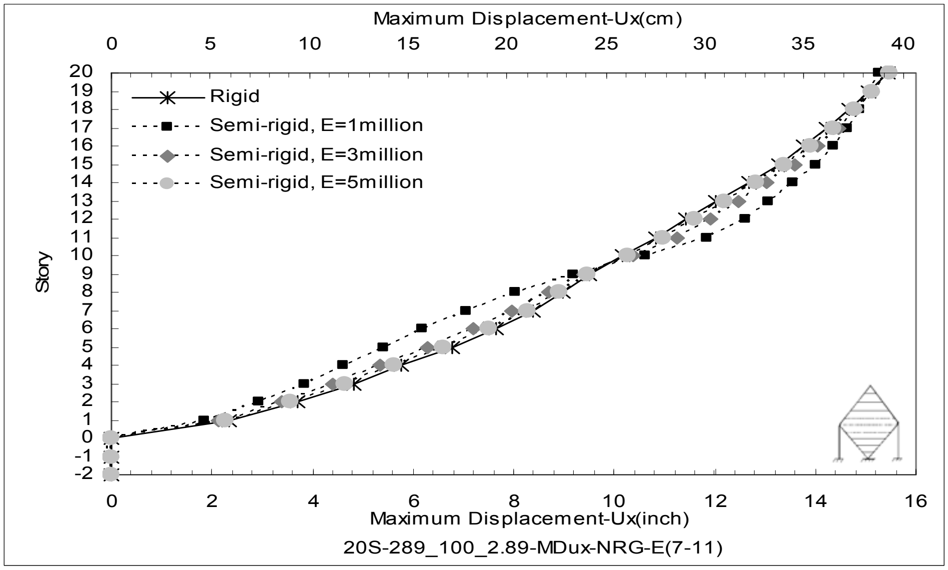

Figure E.28 Maximum lateral displacement for 20S-289_100_2.89-NRG

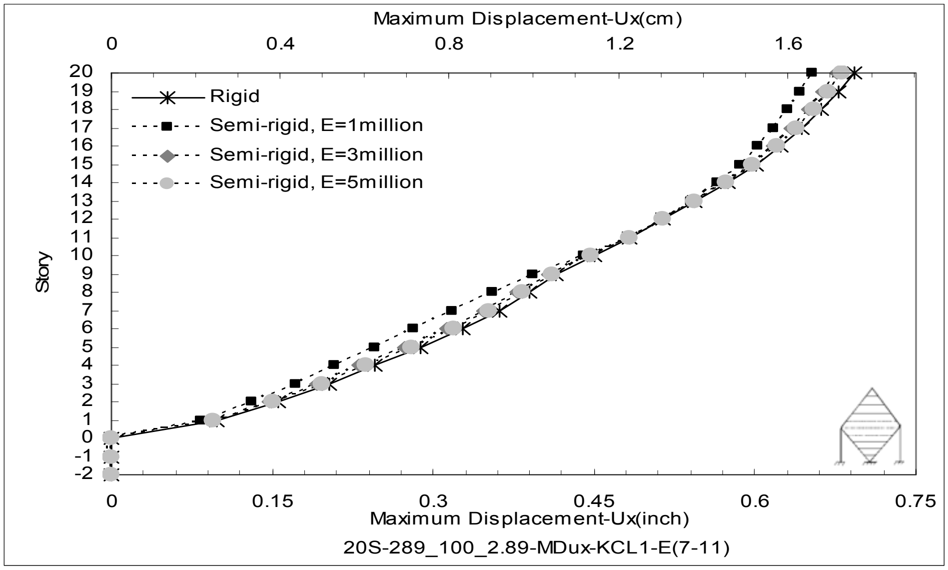

Figure E.29 Maximum lateral displacement for 20S-289_100_2.89-KCL1

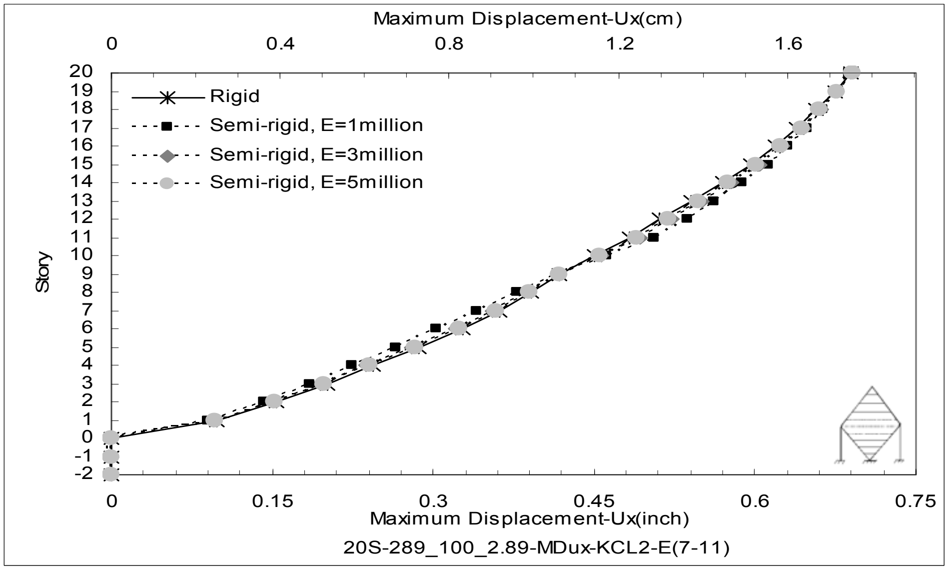

Figure E.30 Maximum lateral displacement for 20S-289_100_2.89-KCL2

APPENDIX F

LATERAL INTER STORY DRIFT

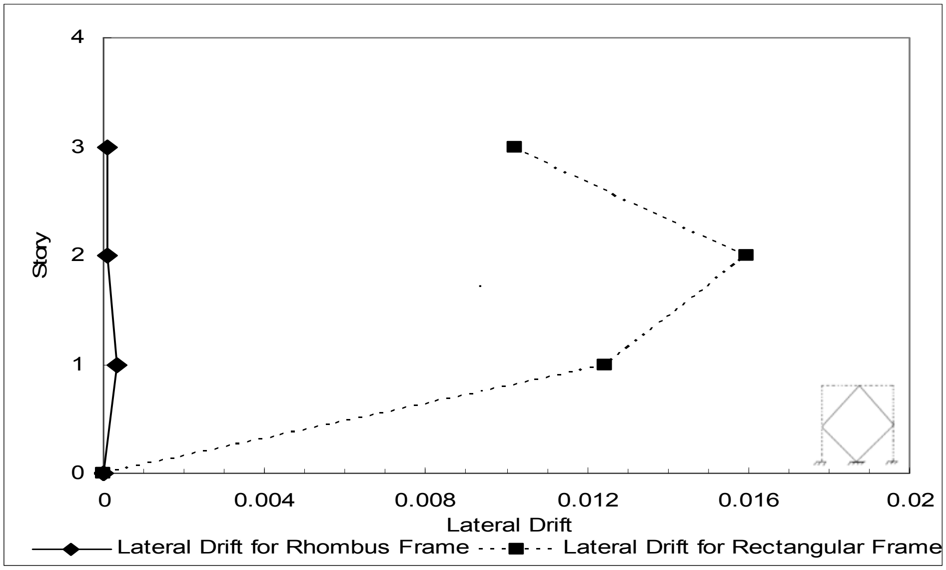

Figure F.1 Inter Story Drift for 3S-39_120_0.325-PKF

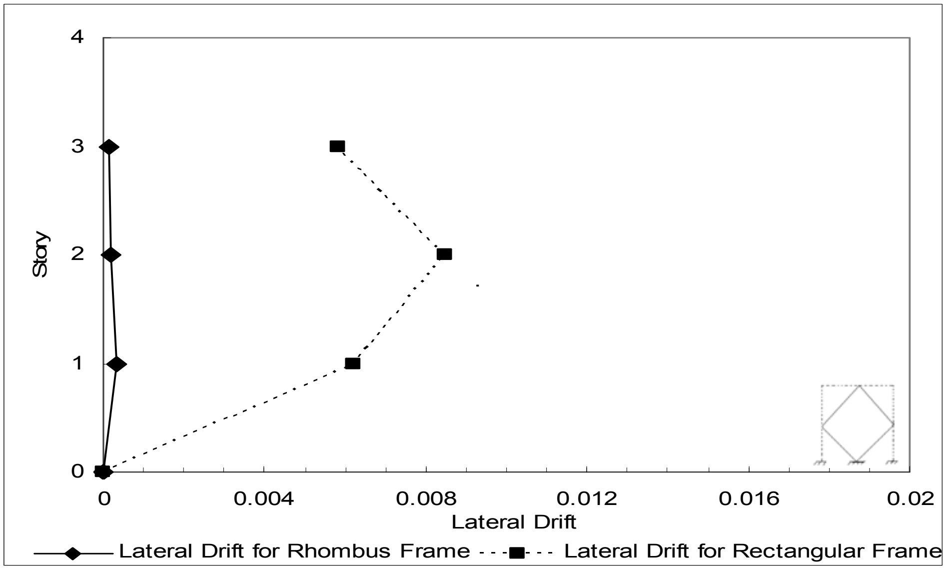

Figure F.2 Inter Story Drift for 3S-39_120_0.325-ELC

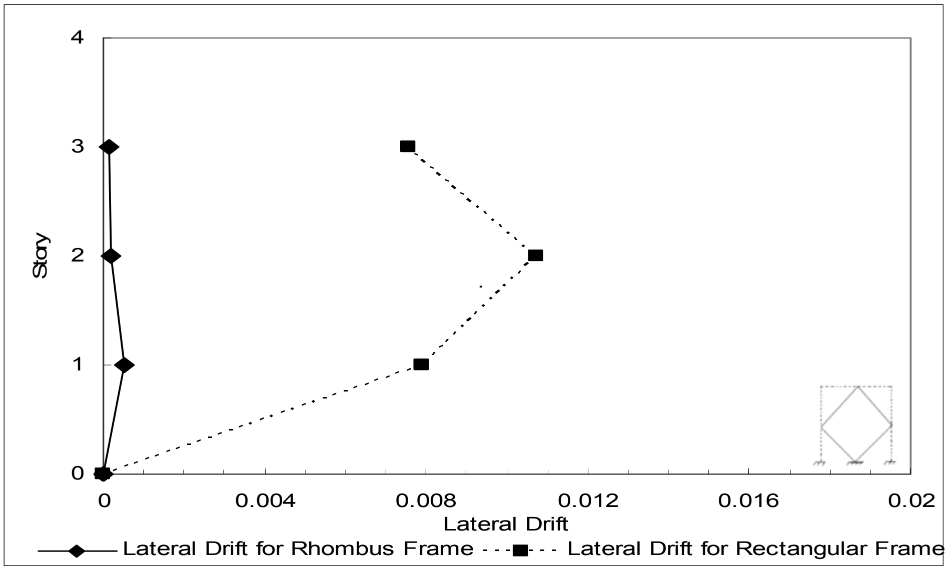

Figure F.3 Inter Story Drift for 3S-39_120_0.325-NRG

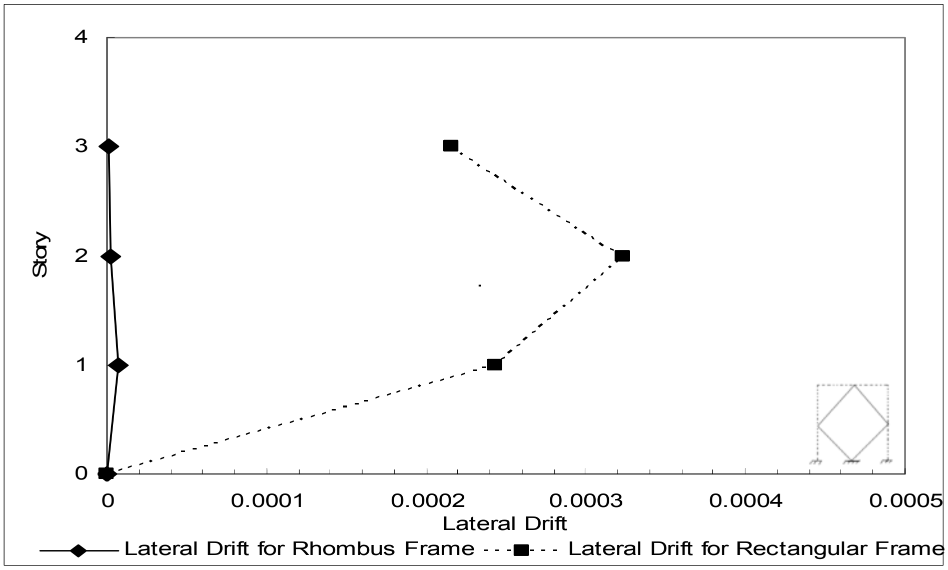

Figure F.4 Inter Story Drift for 3S-39_120_0.325-KCL1

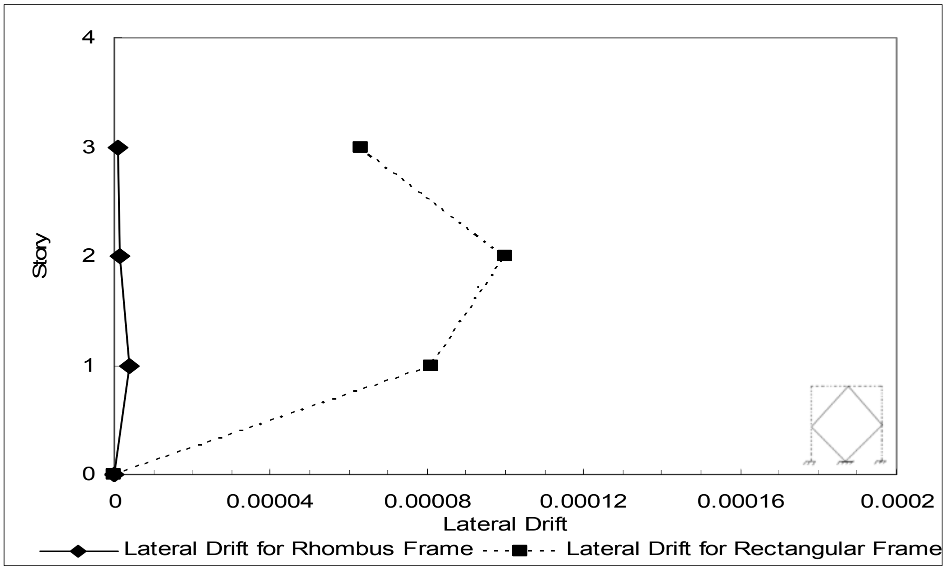

Figure F.5 Inter Story Drift for 3S-39_120_0.325-KCL2

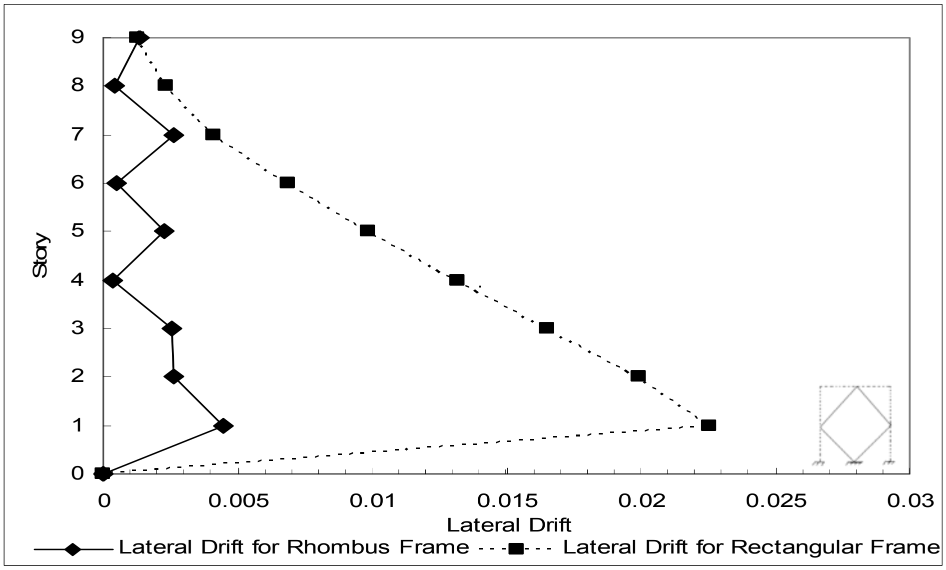

Figure F.6 Inter Story Drift for 9S-134_150_0.893-PKF

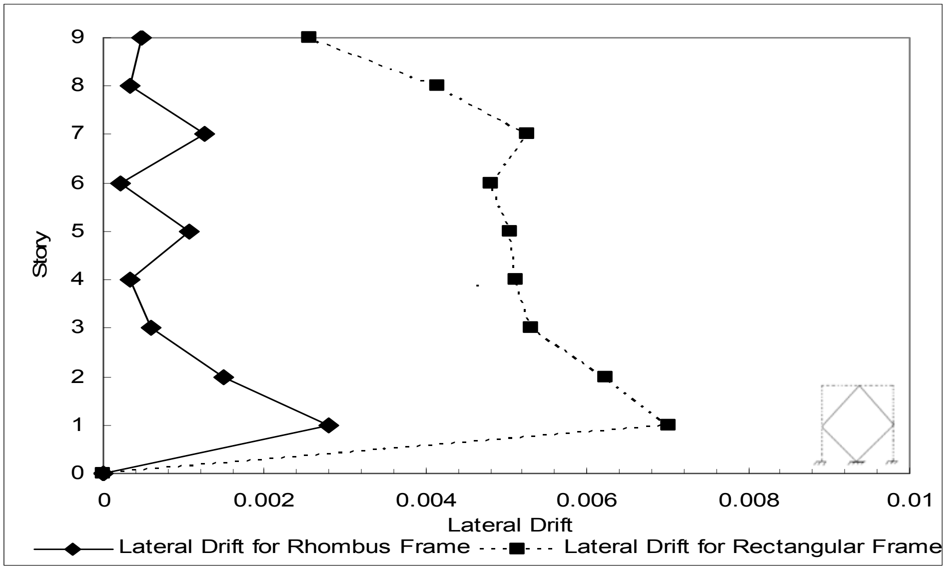

Figure F.7 Inter Story Drift for 9S-134_150_0.893-ELC

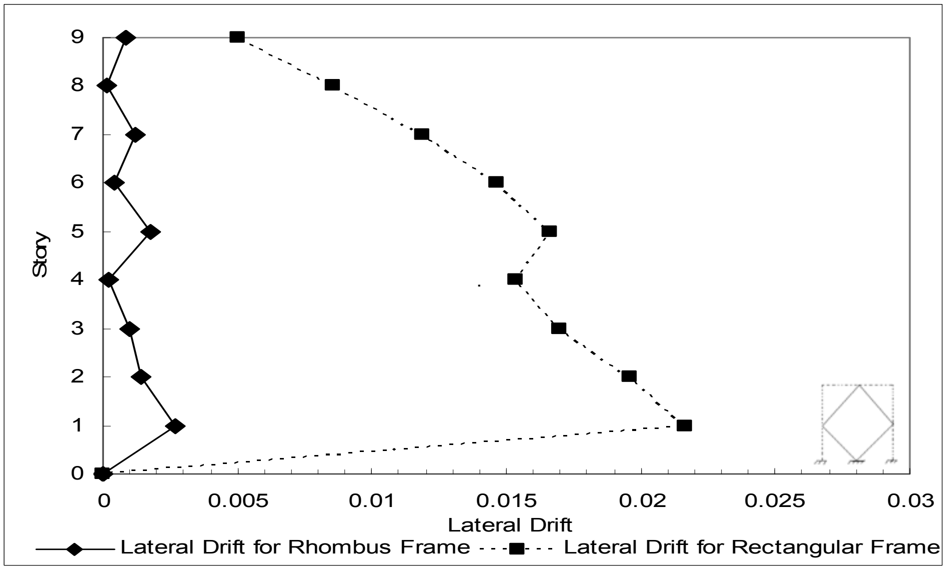

Figure F.8 Inter Story Drift for 9S-134_150_0.893-NRG

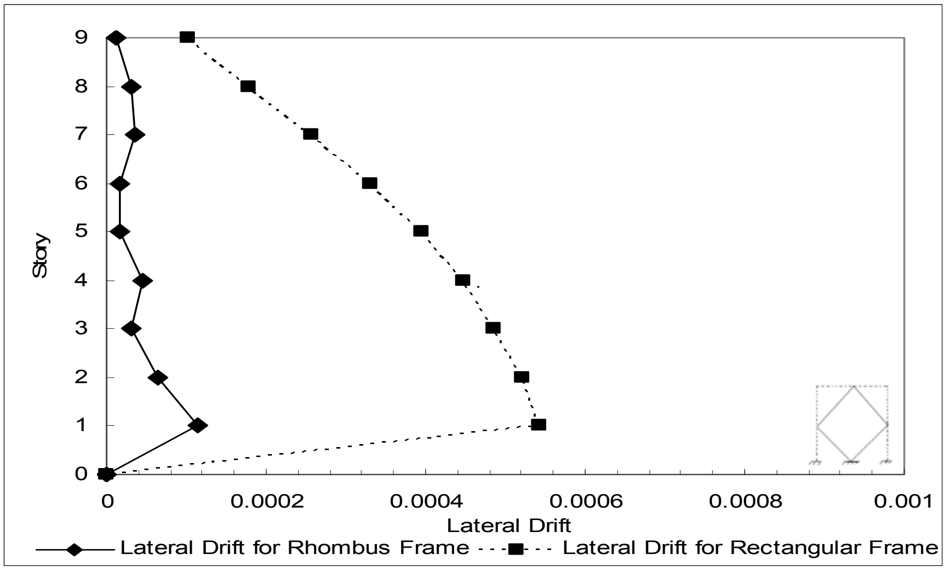

Figure F.9 Inter Story Drift for 9S-134_150_0.893-KCL1

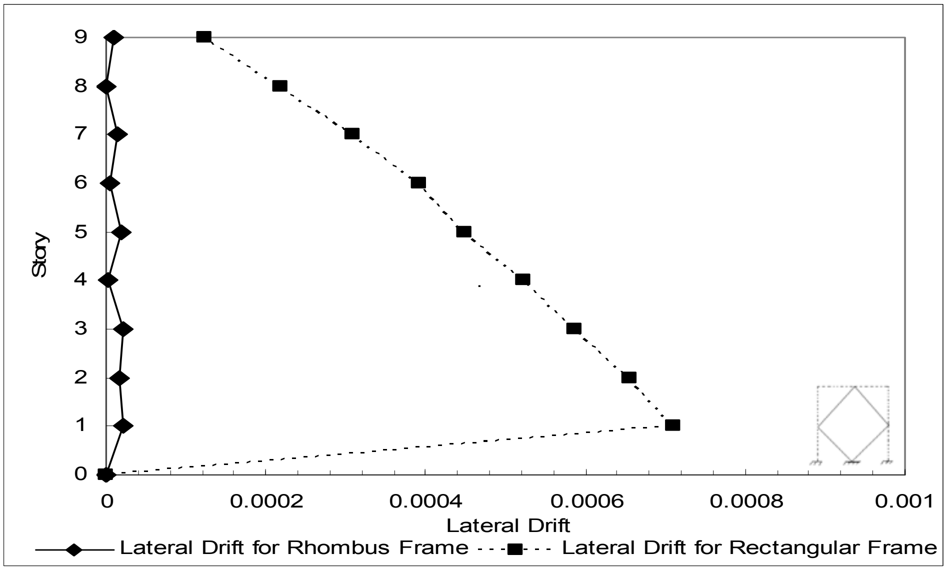

Figure F.10 Inter Story Drift for 9S-134_150_0.893-KCL2

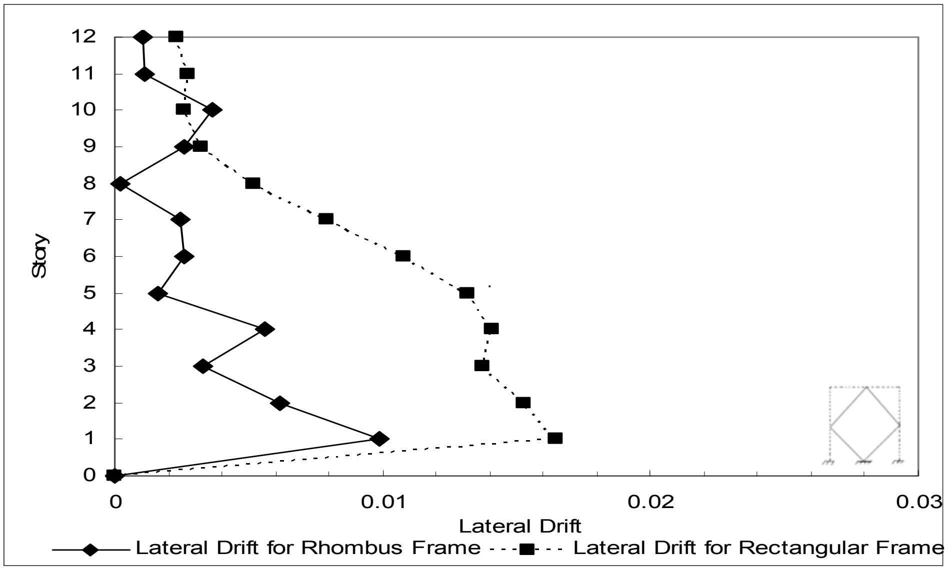

Figure F.11 Inter Story Drift for 12S-173_150_1.153-PKF

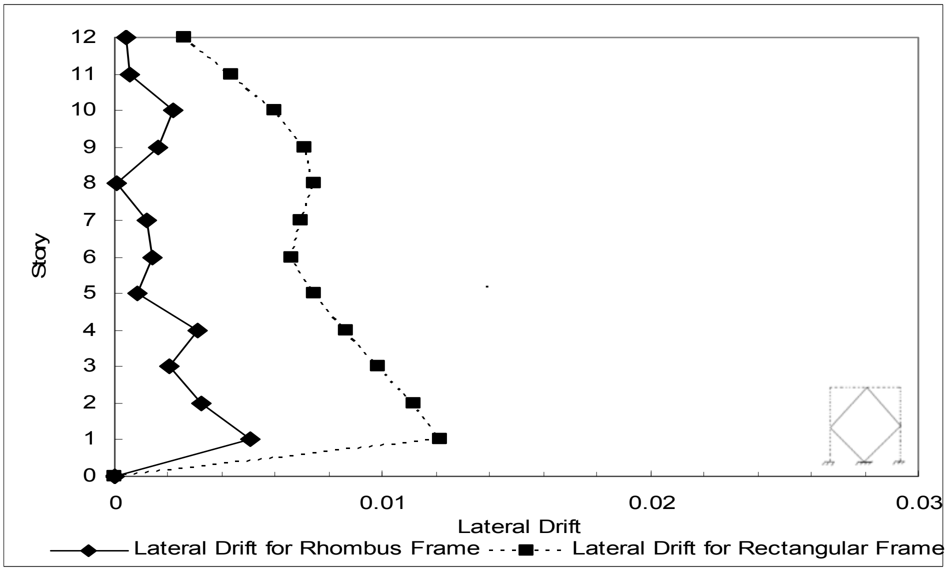

Figure F.12 Inter Story Drift for 12S-173_150_1.153-ELC

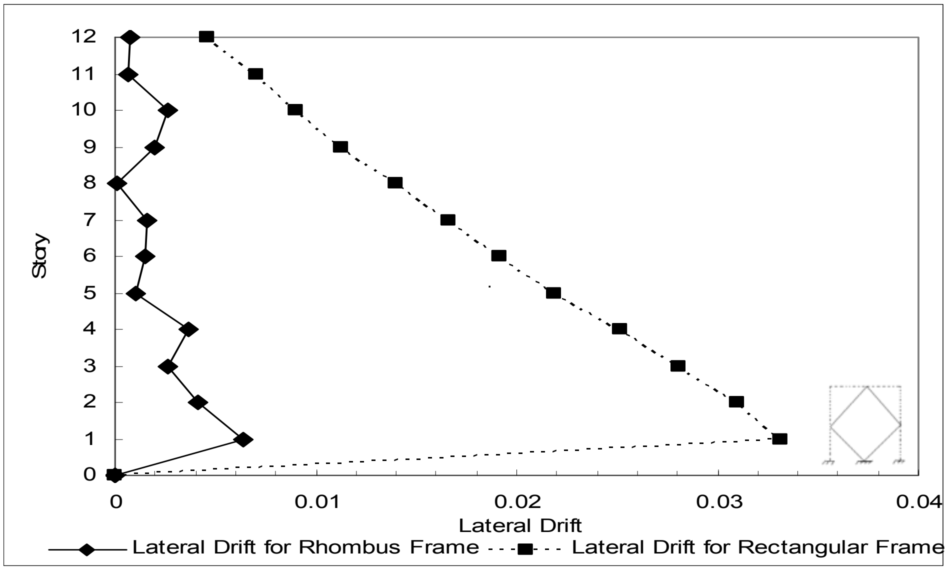

Figure F.13 Inter Story Drift for 12S-173_150_1.153-NRG

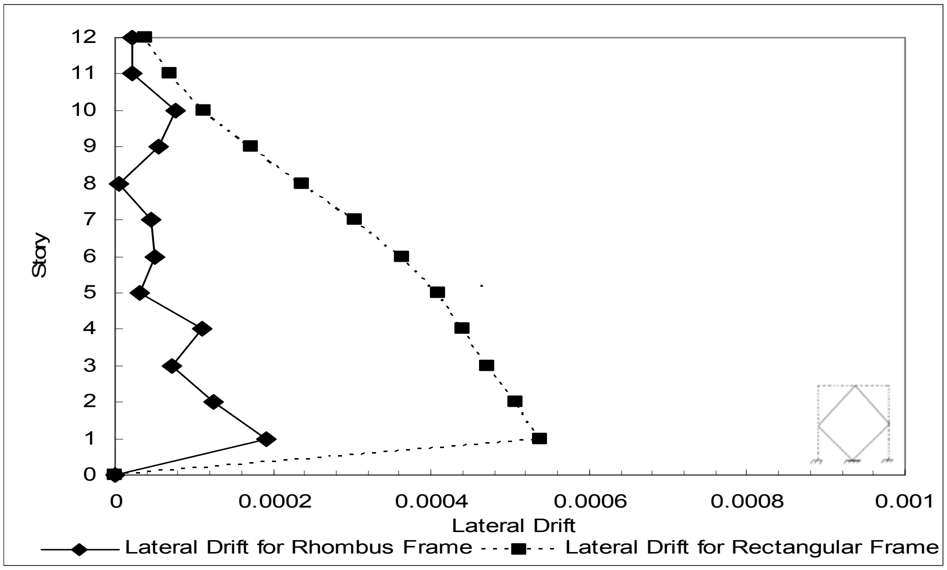

Figure F.14 Inter Story Drift for 12S-173_150_1.153-KCL1

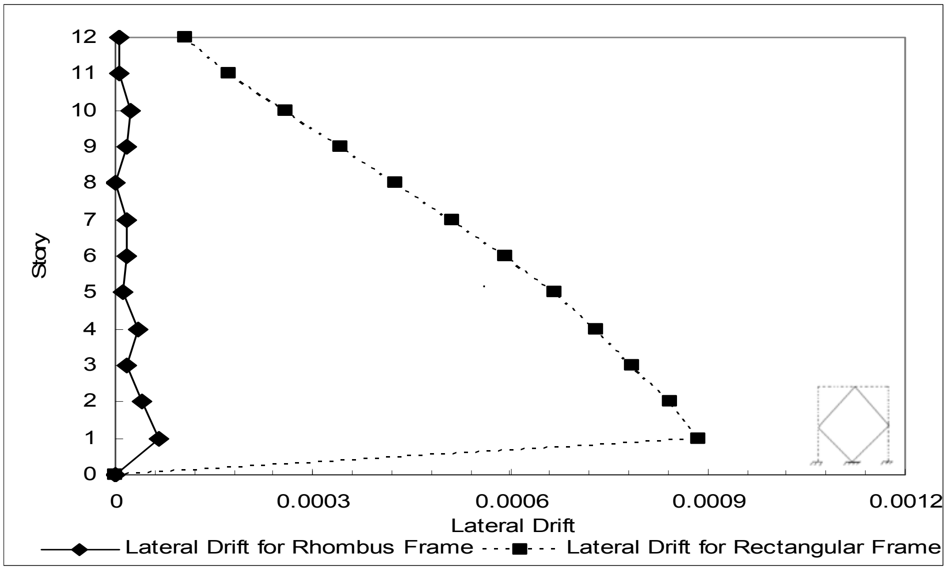

Figure F.15 Inter Story Drift for 12S-173_150_1.153-KCL2

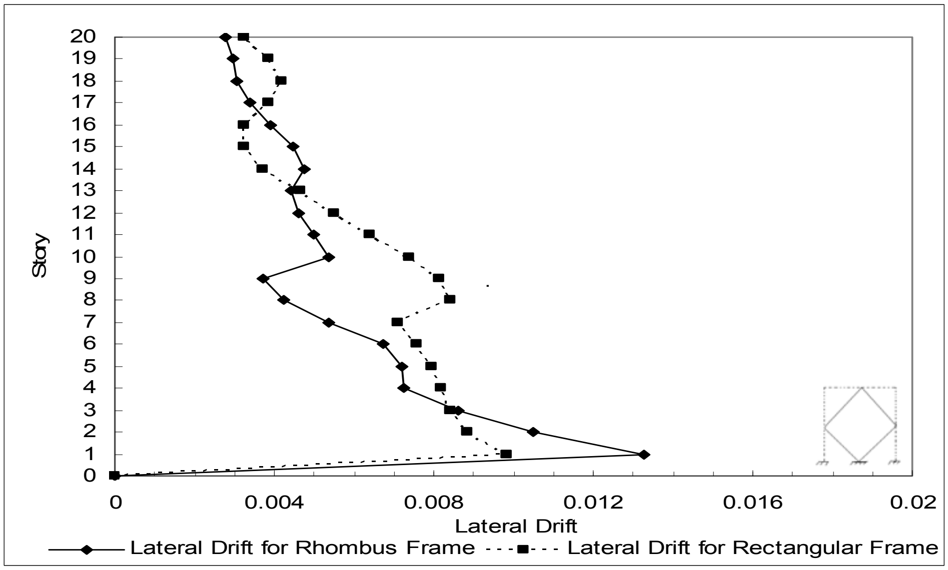

Figure F.16 Inter Story Drift for 20S-289_100_2.89-PKF

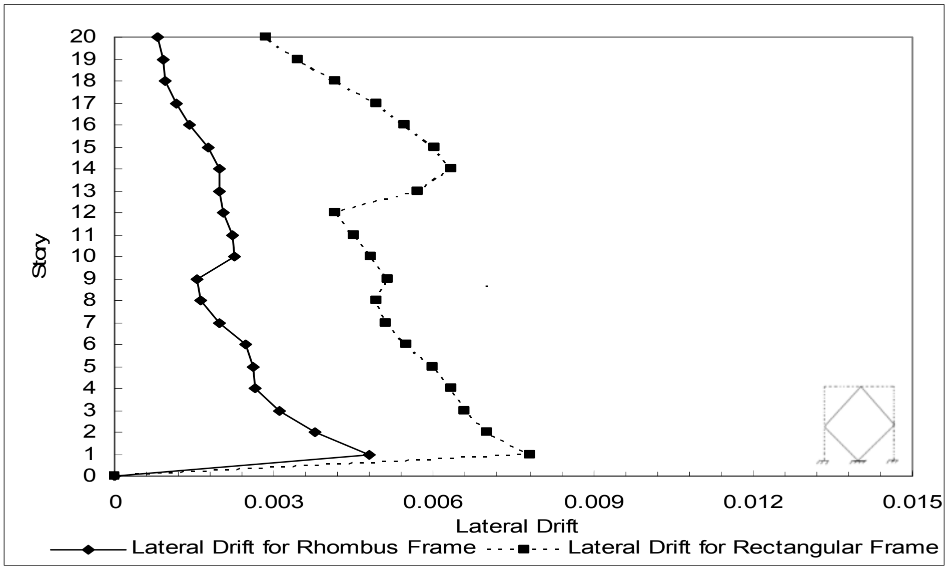

Figure F.17 Inter Story Drift for 20S-289_100_2.89-ELC

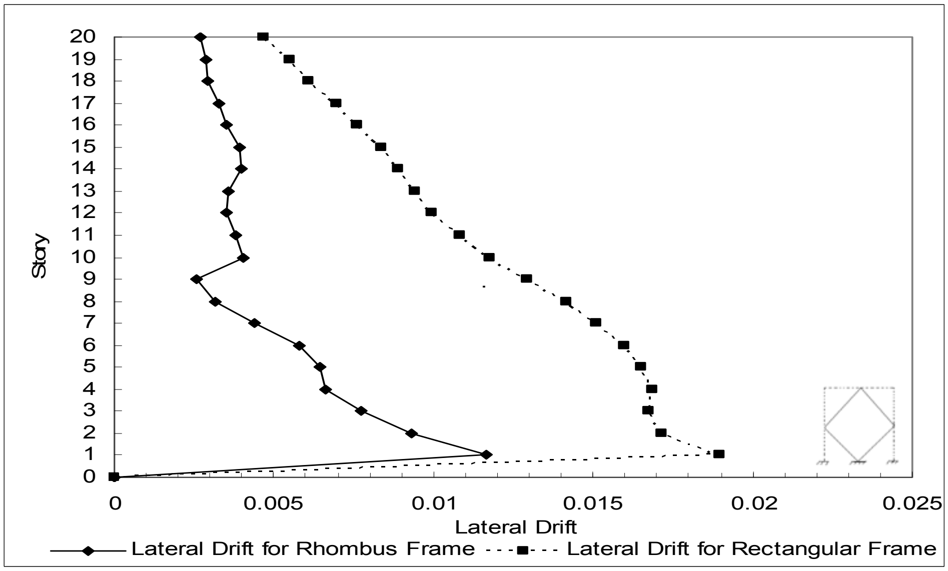

Figure F.18 Inter Story Drift for 20S-289_100_2.89-NRG

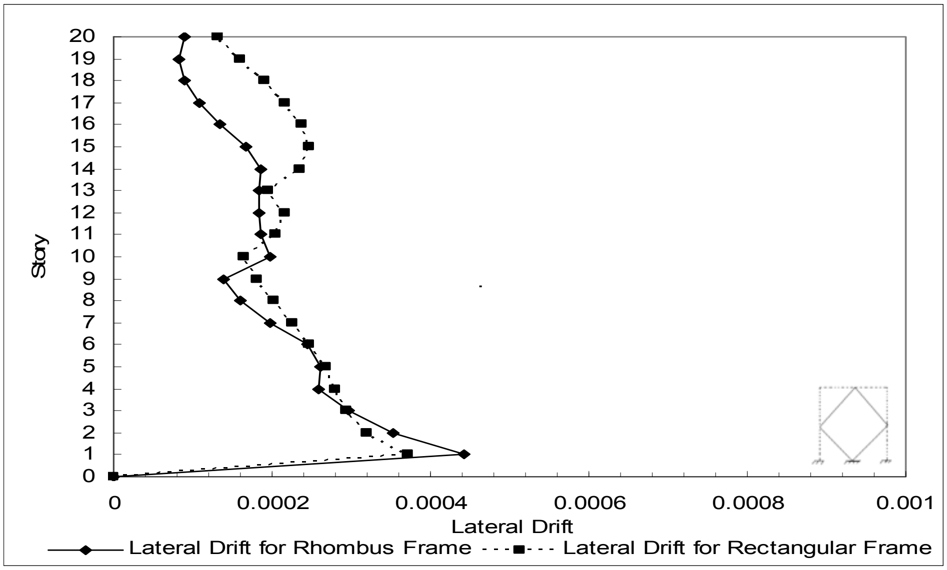

Figure F.19 Inter Story Drift for 20S-289_100_2.89-KCL1

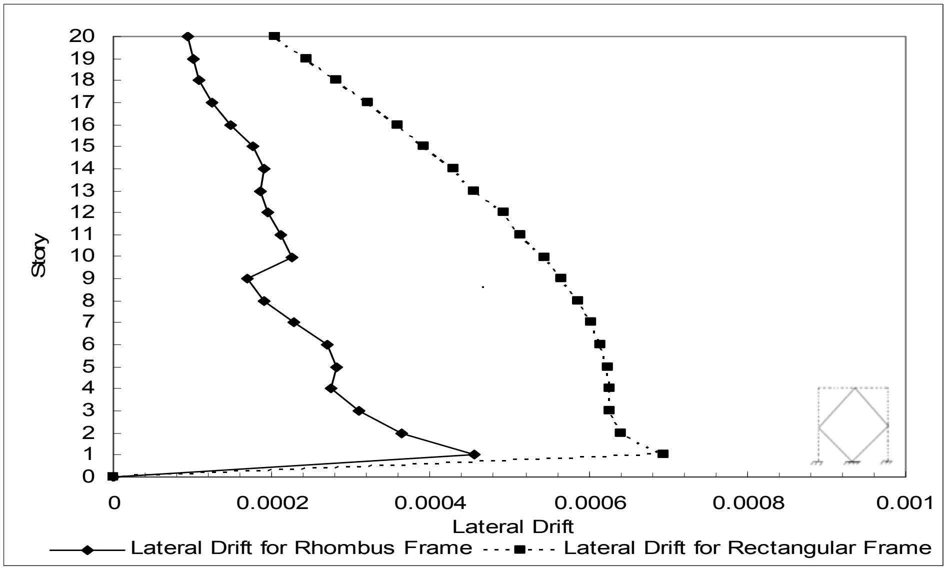

Figure F.20 Inter Story Drift for 20S-289_100_2.89-KCL2

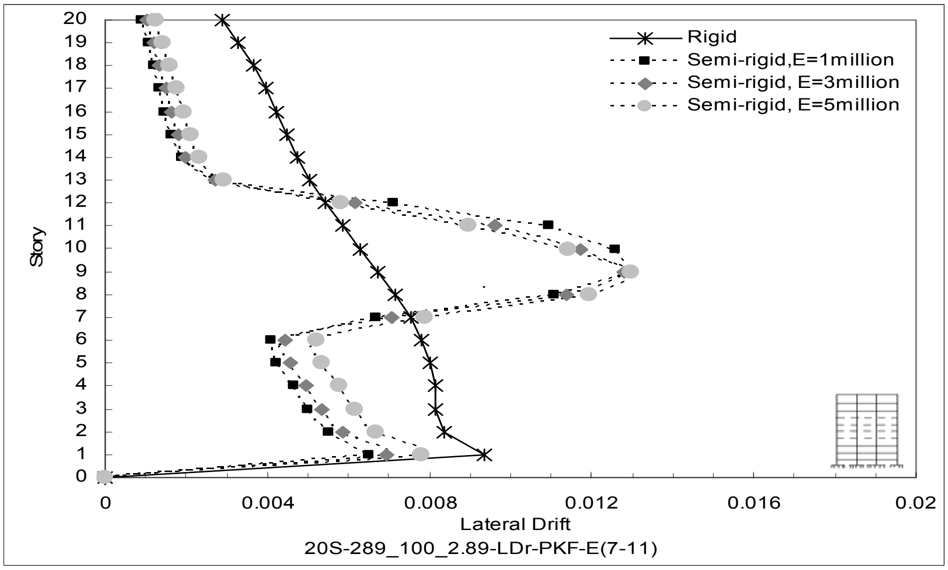

Figure F.21 Inter Story Drift for 20S-289_100_2.89-PKF

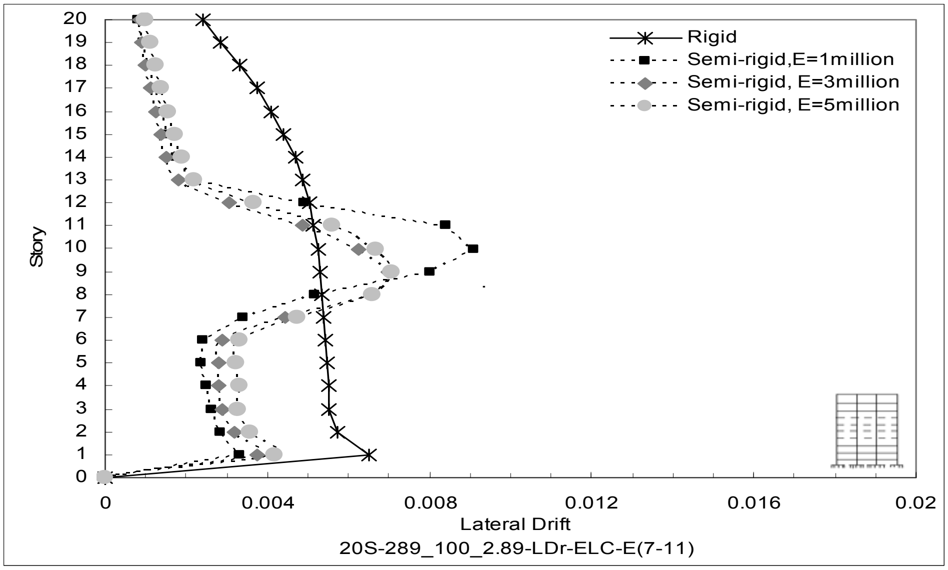

Figure F.22 Inter Story Drift for 20S-289_100_2.89-ELC

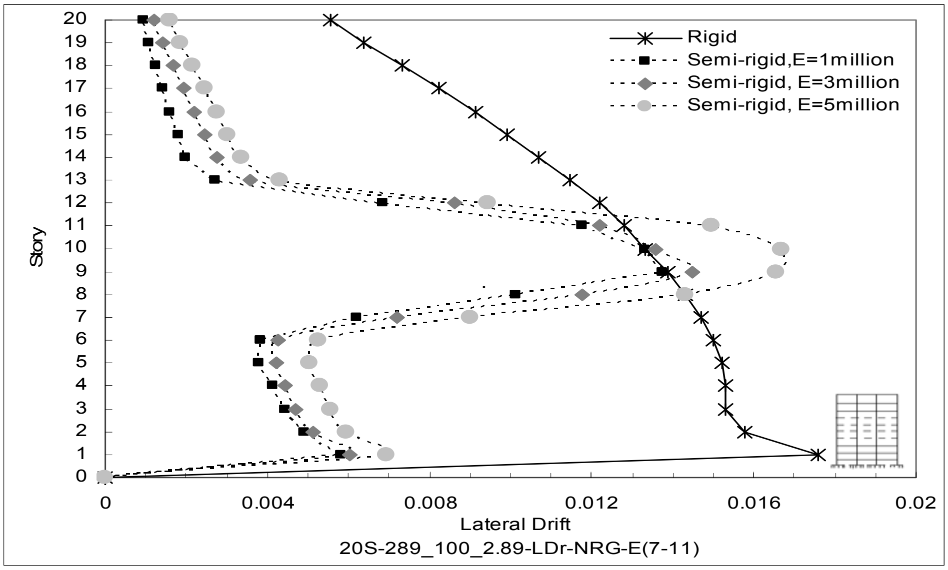

Figure F.23 Inter Story Drift for 20S-289_100_2.89-NRG

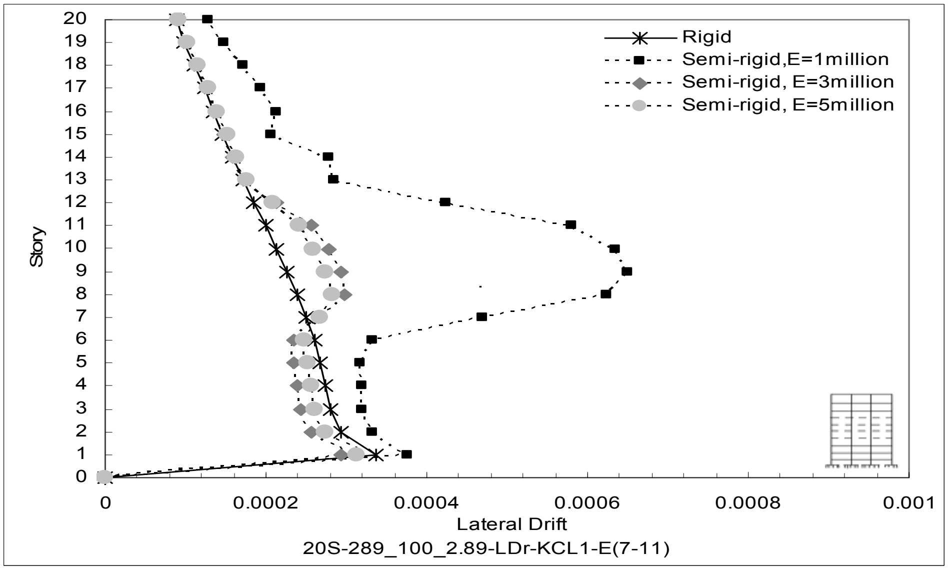

Figure F.24 Inter Story Drift for 20S-289_100_2.89-KCL1

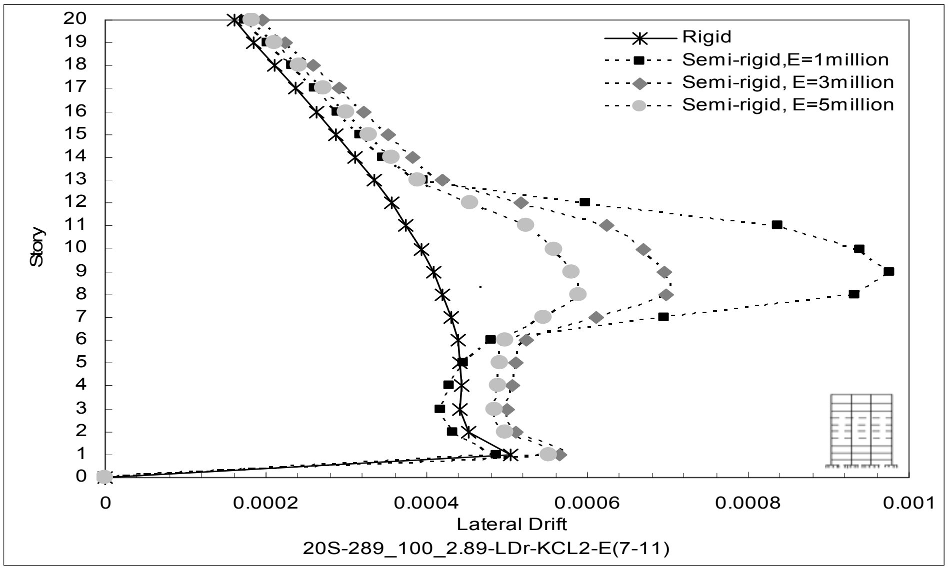

Figure F.25 Inter Story Drift for 20S-289_100_2.89-KCL2

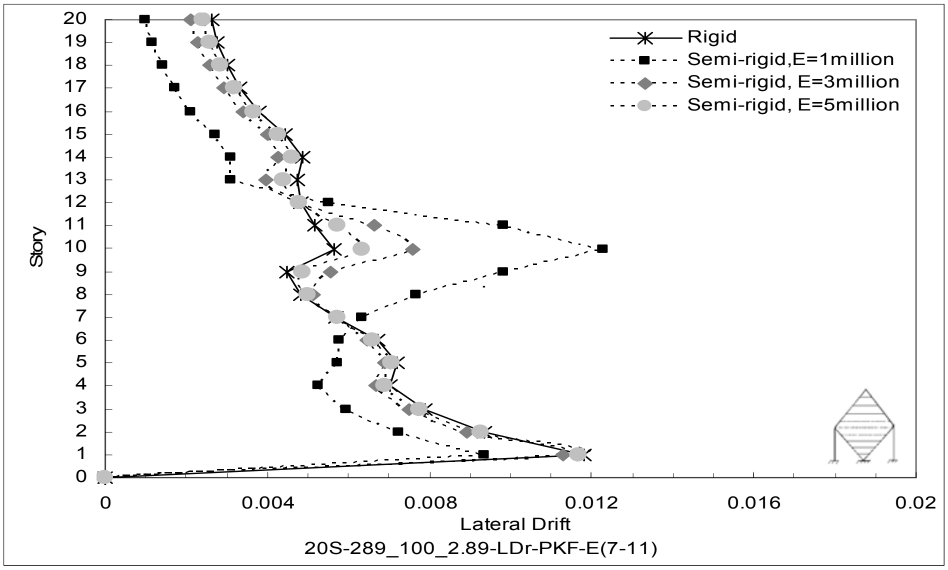

Figure F.26 Inter Story Drift for 20S-289_100_2.89-PKF

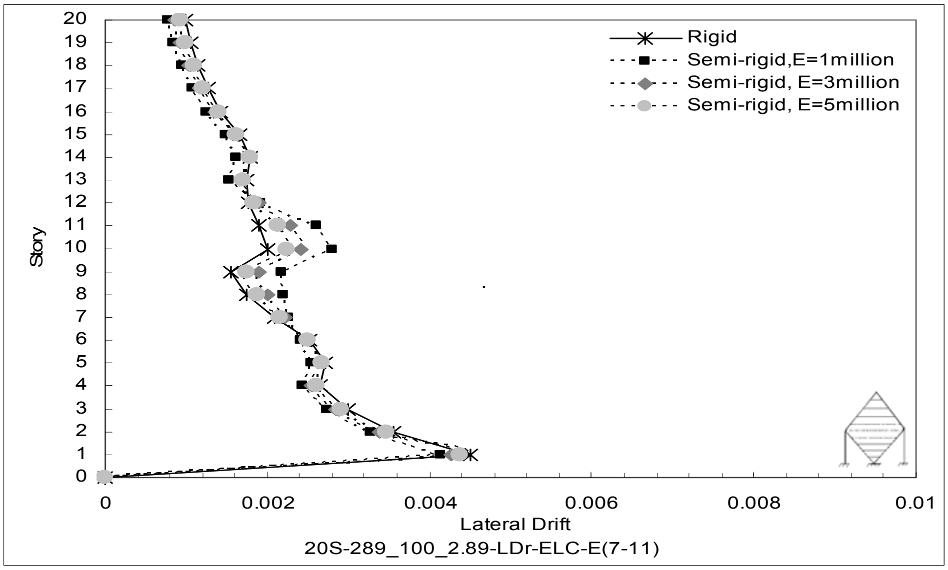

Figure F.27 Inter Story Drift for 20S-289_100_2.89-ELC

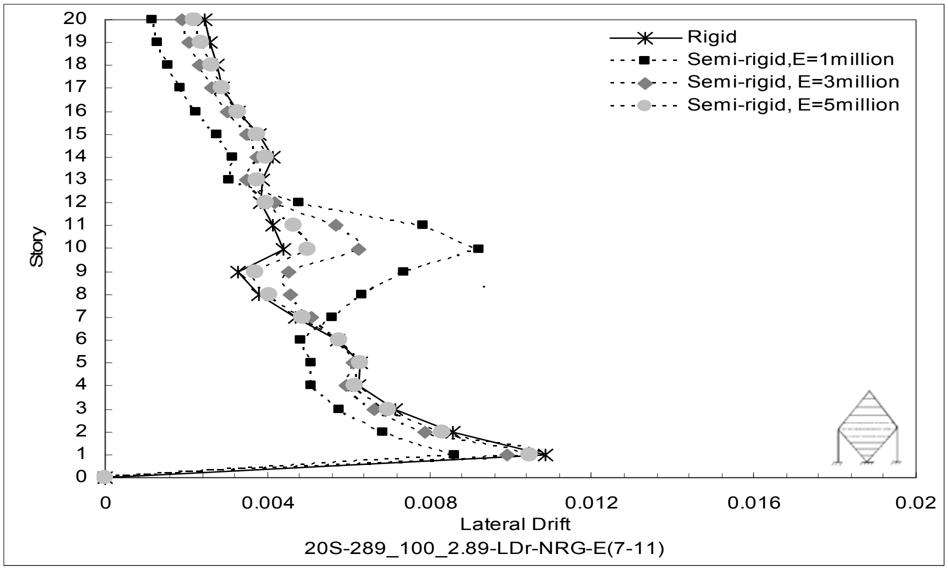

Figure F.28 Inter Story Drift for 20S-289_100_2.89-NRG

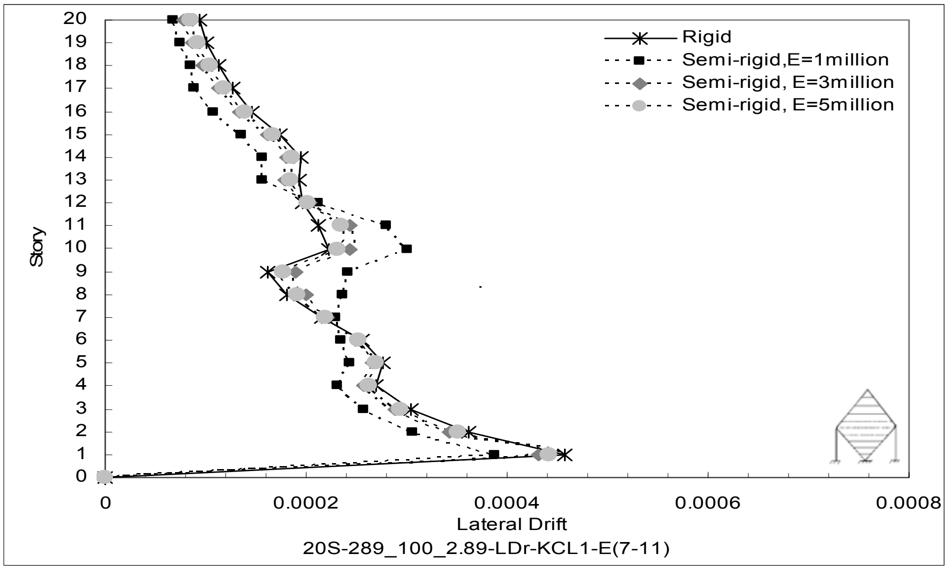

Figure F.29 Inter Story Drift for 20S-289_100_2.89-KCL1

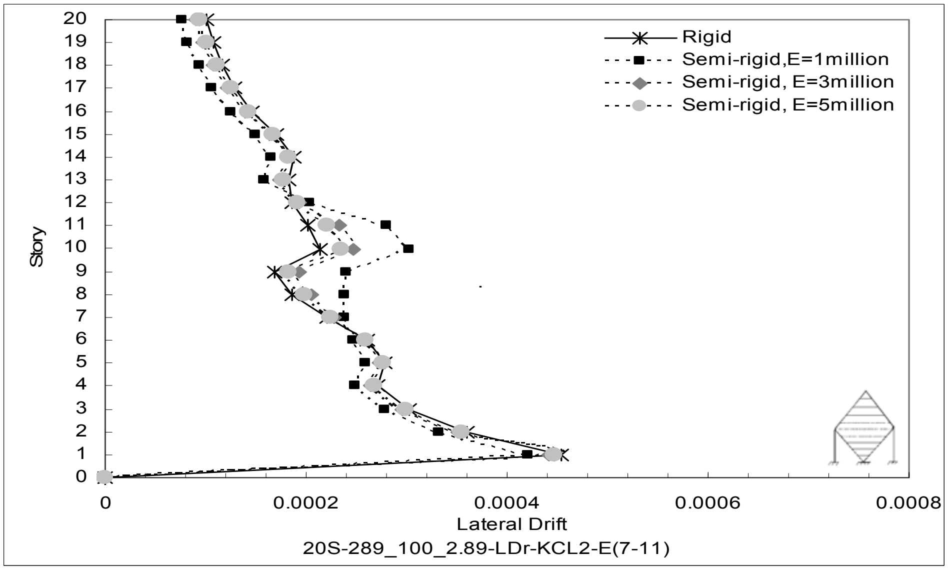

Figure F.30 Inter Story Drift for 20S-289_100_2.89-KCL2

APPENDIX G

LOAD CALCULATION

Load calculations for this study follow ASCE (American Society of Civil Engineers) standards. For dead load, a 4 inch slab thickness is considered with a super imposed dead load of 30 psf. Other dead loads are considered as per Table C3-1, ASCE 7-05.

Self weight of slab = 50 psf
Super imposed dead load = 40 psf
Mechanical duct allowance = 4 psf (Table C3-1, ASCE 7-05)
Plaster = 5 psf (Table C3-1, ASCE 7-05)
Floor finish = 32 psf (Table C3-1, ASCE 7-05)
Exterior stud walls = 48 psf (Table C3-1, ASCE 7-05)
i.e. Total dead load = 179 ≈ 180 psf

For live load calculation, residential building is considered. As per Section 4.2.2 of the ASCE 7-05, 30 psf live load for partition wall is considered. Minimum distributed live load for residential building is 40 psf as per Table 4-1, ASCE 7-05.
i.e. Total live load = 70 psf.

For effective seismic load, total dead load and 25 percentage of live load are considered as per Section 12.7.2, ASCE 7-05.

i.e. total effective seismic load = 180 + 0.25 X 70 = 197.5 psf. This load will contribute to the mass source.

For, 20- story three dimensional building; each slab dimension is 20 ft by 20 ft. For each beam, tributary area is equal to 100 ft^2, which leads to a uniformly distributed load on all beams $= \frac{197.5 \times 100}{20 \times 1000} = 0.9875 kip/ft$. Other tributary area will contribute to the point load at beam ends.

Point loads for outer nodes = $\frac{0.9875 \times 20}{2} = 9.875 kip$

Point loads for inner nodes = 19.75 kip

For 3-, 9-, 12- story three dimensional buildings, each slab dimension is 30 ft by 30 ft. For each beam, tributary area is equal to 225 ft^2, which leads to an uniformly distributed load $= \frac{197.5 \times 225}{20 \times 1000} = 1.481 kip/ft$.

Point loads for outer nodes = $\frac{1.481 \times 30}{2} = 22.215 kip$

Point loads for inner nodes = 44.43 kip

REFERENCES

Abolmaali, Ali, Ardavan Motahari, and Mehdi Ghassemieh. "Energy Dissipation Characteristics of Semi-Rigid Connections." *Journal of Construction Steel Research* (2008).

AISC. 2005a. ANSI/AISC 341-05: *Seismic Provisions for Structural Steel Buildings*. Chicago: American Institute of Steel Construction.

Al-Mashary, F. and Chen, W.F., “Simplified second-order inelastic analysis for steel frames.” *Structural Engineer,* (1991): 69(23), 395-399.

ASCE. 2005. SEI/ASCE 7-05: *Minimum Design Loads for Buildings and Other Structures.* Reston, VA: American Society of Civil Engineers.

ATC, 1997a, *NEHRP Guidelines for the Seismic Rehabilitation of Buildings*, FEMA-273, prepared by the Applied Technology Council, Redwood City, California, for the Building Seismic Safety Council, published by the Federal Emergency Management Agency, Washington, DC.

ATC, 1997b, NEHRP *Commentary on the Guidelines for the Seismic Rehabilitation of Buildings*, FEMA-274, prepared by the Applied Technology Council, Redwood City, California, for the Building Seismic Safety Council, published by the Federal Emergency Management Agency, Washington, DC.

ATC, 1992, *Development of Guidelines for Seismic Rehabilitation of Buildings, Phase I: Issues Identification and Resolution*, developed by the Applied Technology Council (Report No. ATC-28) for the Federal Emergency Management Agency (Report No. FEMA 237), Washington, D.C.

Bhatti, M. A., Hingtgen, James D., "Effects of Connection Stiffness and Plasticity on the Service Load Behavior of Unbraced Steel Frames." *Engineering Journal,* First quarter (1995): 21-33.

Bonowitz, D., "SAC Database of WSMF Connection Tests." Contractor's report submitted to the SAC Joint Venture,1999(a).

Bruneau, Michel, Uang, Chia-Ming, Whittaker. Andrew, *Ductile Design of Steel Structures engineering*. McGraw-Hill, 1998.

Chan, S.L., Chui, P.P.T., *Non-Linear Static and Cyclic Analysis of Steel Frames with Semi-Rigid Connections*, Elsevier, Netherlands, 2000.

Chen, W.F., Lui, E.M., *Stability Design of Steel Frames*. CRC Press, Boca Raton, FL 1991.

Chopra, Anil K., *Dynamics of structures theory and applications to earthquake engineering*. Ed. Prentice Hall. 3rd ed. Upper Saddle River, N.J: Pearson/Prentice Hall, 2007.

Engelhardt, M.D., and Husain, A.S, "Cyclic Loading Performance of Welded Flange-Bolted Web Connections." *Journal of Structural Engineering,* American Society of Civil Engineers, (1993): Vol. 119, No. 12: 3537-3550.

FEMA-273, 1997a, *NEHRP Guidelines for the Seismic Rehabilitation of Buildings*, prepared by the Applied Technology Council, Redwood City, California, for the Building Seismic Safety Council, published by the Federal Emergency Management Agency, Washington, DC.

FEMA-355C, 2000, *State of the Art Report on Systems Performance of Steel Moment Frames Subject to Earthquake Ground Shaking*, prepared by the SAC Joint Venture for the Federal Emergency Management Agency, Washington, DC.

FEMA-355D, 2000, *State of the Art Report on Connection Performance*, prepared by the SAC Joint Venture for the Federal Emergency Management Agency, Washington, DC.

FEMA-355E, 2000, *State of the Art Report on Past Performance of Steel Moment-Frame Buildings in Earthquakes*, prepared by the SAC Joint Venture for the Federal Emergency Management Agency, Washington, DC.

FEMA-355F, 2000, *State of the Art Report on Performance Prediction and Evaluation of Steel Moment-Frame Buildings*, prepared by the SAC Joint Venture for the Federal Emergency Management Agency, Washington, DC.

FEMA-356, 2000, *Prestandard and Commentary for the Seismic Rehabilitation of Buildings*, prepared by American Society of Civil Engineers for the Federal Emergency Management Agency, Washington, DC.

Goel, Subhash C., Chao, Shih-Ho, *Performance-Based Plastic Design Earthquake Resistant Steel Structures*, International Code Council, 2008.

Maison, B.F., and K. Kasai, "*Seismic Performance of 3 and 9 Story Partially Restrained Moment Frame Buildings*," *SAC/BD-99/16*, (1999).

Newmark, N.M., "A Method of Computation for Structural Dynamics," *Journal of the Engineering Mechanics Division, ASCE,* 85 (1959): pp. 67-94.

Open System for Earthquake Engineering Simulation - Home Page. Web. 1 Feb. 2008. <http://opensees.berkeley.edu/index.php>.

"PEER Strong Motion Database: Introduction." *Welcome to Pacific Earthquake Engineering Research Center - PEER*. Web. 15 Mar. 2008. <http://peer.berkeley.edu/smcat/>.

Popov, E.P., and Pinkney, R.B., "Cyclic Yield Reversals on Steel Building Connections," *Journal of the Structural Division,* ASCE, (1969): Vol. 95, No. 3.

Popov, E.P., and Stephen, RM., "*Cyclic Loading of Full-Size Steel Connections.*" Earthquake Engineering Research Center Report UCB/EERC-70-3, University of California, Berkeley, 1970.

Popov, E.P., and Stephen, RM, "*Cyclic Loading of Full-Size Steel Connections.*" American Iron and Steel Institute. Bulletin No. 21. New York, 1972.

Popov, E.P., Amin, N.R., Louie, J.J.C., and Stephen, R.M., "Cyclic Behavior of LargeBeam-Column Assemblies," *Earthquake Spectra*, Earthquake Engineering Research Institute, (1985).

Radulova, Dobrinka, *Nonlinear Dynamic Analysis of Hybrid Frames*, Masters Thesis, Department of Civil Engineering, The University of Texas at Arlington, Arlington, Texas, 2009.

Roeder, C.W., and Foutch, D.A., "Experimental Results for Seismic Resistant Steel Moment Frame Connections." *Journal of Structural Engineering.* American Society of Civil Engineers, (1995): Vol. 122, No.6: 581-588.

Roeder, C.W. and Foutch, D.A., "Experimental Results for Seismic Resistant Steel Moment Frame Connections," *Journal of Structural Engineering*. (1996).

Sabelli, R., FEMA/EERI report: " Research on Improving the Design and Analysis of Earthquake Resistant Steel Braced Frames." Washington, D.C.,2000: FEMA/EERI

SAC, 1995, *Interim Guidelines, Inspection, Evaluation, Repair, Upgrade and Design of Welded Moment Resisting Steel Structures*, FEMA-267, prepared by the SAC Joint Venture for the Federal Emergency Management Agency, Washington, DC. Superseded b FEMA 350.

SEAOC Vision 2000 Committee, 1995, *A Framework for Performance Based Design,* Volumes I, II, and III, Structural Engineers Association of California (SEAOC), Sacramento, California.

"SeismoSoft - SeismoSignal." *SeismoSoft - Home*. Web. 27 Aug. 2009. <http://www.seismosoft.com/en/SeismoSignal.aspx>.

Steel Construction Manual, 13th Edition (Book). New York: American Institute of Steel Construction, 2006.

Structural Analysis Program, SAP2000, Advanced 11.0.2, Computers and Structures, Inc., Berkeley CA.

Tsai, K.C. and Popov, E.P., "*Steel Beam-Column Joints in Seismic Moment Resisting Frames.*" (UCB/EERC-88/19), Earthquake Engineering Research Center, Richmond, California, 1988.

Yau, C.Y. and Chan, S.L., "Inelastic and stability analysis of flexibly connected steel frames by springs-in-series model." *Journal of Structural Engineering.* American Society of Civil Engineers, (1994): Vol. 120, No. 10 : 2803-2819.

BIOGRAPHICAL INFORMATION

S. M. Ashfaqul Hoq was born on 23rd May, 1984 in Dhaka, Bangladesh. He received his Bachelor's degree in Civil Engineering from Bangladesh University of Engineering and Technology, Dhaka, Bangladesh in June 2007. After his graduation, he started working in "Dalan-Kotha Limited", a construction firm. He worked as a Project Engineer from July 2007 to June 2008. His job responsibilities include supervision and management of different construction projects, mainly for apartment complex. Later on, Hoq started his graduate studies at the University of Texas at Arlington in Fall 2008. He was awarded with the prestigious Graduate Dean Masters Fellowship scholarship. The author worked under the guidance of Dr. Ali Abolmaali to propose a frame shape, which will improve building performance under earthquake excitations. His Masters thesis is substantially based on this research work.